Global Boundary Stratotype Section and Point (GSSP) for the Anthropocene Series: Where and how to look for potential candidates.

Colin N. Waters[1], Jan Zalasiewicz[1], Colin Summerhayes[2], Ian J. Fairchild[3], Neil L. Rose[4], Neil J. Loader[5], William Shotyk[6], Alejandro Cearreta[7], Martin J. Head[8], James P.M. Syvitski[9], Mark Williams[1], Michael Wagreich[10], Anthony D. Barnosky[11], An Zhisheng[12], Reinhold Leinfelder[13], Catherine Jeandel[14], Agnieszka Gałuszka[15], Juliana A. Ivar do Sul[16], Felix Gradstein[17], Will Steffen[18], John R. McNeill[19], Scott Wing[20], Clément Poirier[21], Matt Edgeworth[22]

[1]School of Geography, Geology and the Environment, University of Leicester, University Road, Leicester LE1 7RH, UK.

[2]Scott Polar Research Institute, Cambridge University, Lensfield Road, Cambridge CB2 1ER, UK.

[3]School of Geography, Earth and Environmental Sciences, University of Birmingham, Birmingham B15 2TT, UK.

[4]Environmental Change Research Centre, Department of Geography, University College London, Gower Street, London WC1E 6BT, UK.

[5]Department of Geography, Swansea University, Singleton Park, Swansea SA2 8PP, Wales, UK.

[6]Department of Renewable Resources, University of Alberta, 348B South Academic Building, Edmonton, Alberta T6G 2H1 CANADA.

[7]Departamento de Estratigrafía y Paleontología, Facultad de Ciencia y Tecnología, Universidad del País Vasco UPV/EHU, Apartado 644, 48080 Bilbao, Spain.

[8]Department of Earth Sciences, Brock University, 1812 Sir Isaac Brock Way, St. Catharines, ON, L2S 3A1 Canada.

[9]University of Colorado-Boulder Campus, Box 545, Boulder CO, 80309-0545, USA.

26   ^{10}*Department of Geodynamics and Sedimentology, University of Vienna, A-1090 Vienna, Austria.*

27   ^{11}*Jasper Ridge Biological Preserve, Stanford University, Stanford, CA 94305, USA.*

28   ^{12}*State Key Laboratory of Loess and Quaternary Geology, Institute of Earth Environment, Chinese*

29   *Academy of Sciences, Xi'an 710061, China.*

30   ^{13}*Department of Geological Sciences, Freie Universität Berlin, Malteserstr. 74-100/D, 12249 Berlin,*

31   *Germany.*

32   ^{14}*LEGOS, Université de Toulouse, CNRS/CNES/IRD/UPS), 14 avenue Edouard Belin, 31400 Toulouse,*

33   *France.*

34   ^{15}*Geochemistry and the Environment Division, Institute of Chemistry, Jan Kochanowski University,*

35   *15G Świętokrzyska St, 25-406 Kielce, Poland.*

36   ^{16}*Leibniz Institute for Baltic Sea Research Warnemüende (IOW), Biological Oceanography Section,*

37   *Seestrasse 15, 18119 Rostock - Germany.*

38   ^{17}*Natural History Museum, Postboks 1172, Blindern, 0318 Oslo, Norway.*

39   ^{18}*The Australian National University, Canberra ACT 0200, Australia.*

40   ^{19}*Georgetown University, Washington DC, USA.*

41   ^{20}*Smithsonian Institution, Washington DC, 20013 USA.*

42   ^{21}*Morphodynamique Continentale et Côtière, Université de Caen Normandie, CNRS; 24 rue des*

43   *Tilleuls, F-14000 Caen, France.*

44   ^{22}*School of Archaeology and Ancient History, University of Leicester, University Road, Leicester LE1*

45   *7RH, UK.*

46

47   Corresponding author: Colin N Waters

48   School of Geography, Geology and the Environment, University of Leicester, University Road,

49   Leicester LE1 7RH, UK. cw398@leicester.ac.uk

ABSTRACT

The Anthropocene as a potential new unit of the International Chronostratigraphic Chart (which serves as the basis of the Geological Time Scale) is assessed in terms of the stratigraphic markers and approximate boundary levels available to define the base of the unit. The task of assessing and selecting potential Global Boundary Stratotype Section and Point (GSSP) candidate sections, a required part of the process in seeking formalisation of the term, is now being actively pursued. Here, we review the suitability of different stratified palaeoenvironmental settings and facies as potential hosts for a candidate GSSP and auxiliary sections, and the relevant stratigraphical markers for correlation. Published examples are evaluated for their strengths and weaknesses in this respect. A marked upturn in abundance of radioisotopes of ^{239}Pu or ^{14}C, approximately in 1952 and 1954 CE respectively, broadly coincident with a downturn in δ^{13}C values, is applicable across most environments. Principal palaeoenvironments examined include: settings associated with accumulations of anthropogenic material, marine anoxic basins, coral reefs, estuaries and deltas, lakes at various latitudes, peat bogs, snow/ice layers, speleothems and trees. Together, many of these geographically diverse palaeoenvironments offer annual/subannual laminae that can be counted and independently dated radiometrically (e.g. by ^{210}Pb). Examples of possible sections offer the possibility of correlation with annual/seasonal resolution. From among such examples, a small number of potentially representative sites require the acquisition of more systematic and comprehensive datasets, with correlation established between sections, to allow selection of a candidate GSSP and auxiliary stratotypes. The assessments in this paper will help find the optimal locations for these sections.

Contents

Figures

Figure 1. [B&W] Primary and some secondary markers for the 65 GSSPs that have been ratified currently by IUGS. The four in the Cenozoic that deal with stable isotope events (base Eocene, Quaternary, Calabrian and Holocene) and the iridium anomaly (base Paleocene) provide models for choosing markers for the base of the Anthropocene.

Figure 2. [B&W] Cores through the Gorrondatxe-Tunelboca beachrock, Spain. A natural high-energy open beach sand deposit, pre-dating the discharges of iron slag, is overlain by cemented sandy and coarse beach deposits that are commonly conglomeratic with abundant slag clasts and incorporating littoral foraminifera. Three distinct foraminiferal assemblages are recognised (ranges for assemblages 1. 2 and 3 marked by arrows) Modified from Martínez-García et al. (2013).

Figure 3. [Colour] Location of marine dead zones (from NASA Earth Observatory https://earthobservatory.nasa.gov/IOTD/view.php?id=44677; Aquatic Dead Zones generated 17th July 2010). Red circles show the location and size of the dead zones. Black dots show where dead zones of unknown size have been observed. The distribution commonly occurs adjacent to populous land areas (shown by the brown scale), but not to upwelling zones (shown by concentration of particulate organic carbon, in blue scale).

Figure 4. [B&W] Key signals in marine cores from the Santa Barbara Basin, with a) Pu signal (Koide et al. 1975), b) variations in sedimentation rates (Krishnaswami et al. 1973), c) selected heavy metals (Schmidt and Reimers 1991) and d) planktonic foraminifera (Field et al. 2006).

Figure 5. [Colour] a) Distribution of shallow-water framework-building coral reefs (from NOAA: Where Are Reef Building Corals Found http://oceanservice.noaa.gov/education/tutorial_corals/coral05_distribution.html) and cold-water corals (from Freiwald et al. 2017) and b) the inventory of anthropogenic CO_2 (μmol CO_2/kg) in surface waters (from Swart et al. 2010).

158   Figure 6. [Colour] a) Changes in δ^{13}C with respect to age for corals from the Atlantic and the

159   Pacific/Indian oceans compared to published data from sclerosponges, averaged after removing the

160   mean δ^{13}C value of the coral skeleton from 1900 CE to the present day and shown as a five-year

161   running mean (Swart et al. 2010). This is compared with δ^{13}C data from Law Dome ice core (Rubino

162   et al. 2013) which show a ~1955 CE inflection; b) $^{240+239}$Pu concentrations in annual growth bands

163   from *Porites lobata* in Guam (Lindahl et al. 2011) and *Orbicella (Montastrea) annularis* in the U.S.

164   Virgin Islands (Benninger and Dodge 1986); dpm kg^{-1} = decays per minute per kilogram; mBq kg^{-1} =

165   millibecquerel per kilogram.

166   Figure 7. [Colour] a) Plot of Δ^{14}C vs age for 7 different colonies of the deep-sea gorgonian coral

167   *Primnoa resedaeformis* with spline fit through the data (Sherwood et al. 2005a), and for the bivalve

168   *Arctica islandica* (Weidman and Jones 1993); b) δ^{15}N-AA depletion in deep-sea gorgonian corals

169   the NW Atlantic (Sherwood et al. 2011) © (2011) National Academy of Sciences; c) Pb concentration;

170   and d) ^{206}Pb/^{207}Pb in Bermuda corals (Kelly et al. 2009).

171   Figure 8. [Colour] Distribution of deltas and estuaries (from Tessler et al. 2015), major mud deposits

172   (from Hanebuth et al. 2015) and areas where neobiota amenable to fossilization have recognizably

173   altered coastal ecosystems (from: Major pathways and origins of invasive species infestations in the

174   marine environment In UNEP/GRID-Arendal Maps and Graphics Library http://www.international-

175   marine.com/invasivespecies/PublishingImages/invasive_vectors_001.png).

176   Figure 9. [B&W] Example of data from a single core from the Clyde Estuary showing a) Pb

177   concentrations and $^{207/206}$Pb isotope ratios, and b) PAH, TPH and PCB organic chemical signatures

178   (Vane et al. 2011).

179   Figure 10. [Colour] Metal concentrations (Cu, Ni, Pb, Zn) versus foraminiferal density in the Urola

180   estuary (northern Spain). FA1–FA3 represent three distinct foraminiferal assemblages referred to in

181   the text. Modified from Goffard (2016).

182   Figure 11. [B&W] Chronology of selected invasive mollusc species into San Francisco Bay (for dates of

183   invasion see: Carlton et al. 1990; Cohen 2004, 2011; Committee on Non-native Oysters in the

184   Chesapeake Bay, Fofonoff et al. 2017, National Research Council 2004), and terrestrial invasive

185   species in the Maha'ulepu sinkhole succession of Kauai, Hawaii (Burney et al. 2001). In both

186   successions, cultural human changes are indicated by the lefthand column, and neobiota in the

187   righthand column. Although the two successions developed nearly 4000 km apart, and in tropical and

188   warm temperate zones respectively, by the mid-19th century some taxa present on the California

189   coast (e.g. the bivalve *Crassostrea virginica*, see DeFelice et al. 2001) were also present in Hawaii,

190   suggesting the possibility of correlation between remote successions.

191   Figure 12. [Colour] Location of the 365 sites recording lake hypoxia (Jenny et al. 2016). Recent

192   hypoxia records onset of varves after 1700 CE, whereas naturally hypoxic lakes were taken to be

193   those in which laminations persisted for at least 300 years.

194   Figure 13. [B&W] Radiogenic signature from Lake Victoria, Australia (Hancock et al. 2011). Profiles of

195   ^{137}Cs (closed squares), $^{239+240}$Pu (open circles) and ^{238}Pu/$^{239+240}$Pu (triangles).

196   Figure 14. [Colour] Sediment δ^{15}N profiles from Northern Hemisphere lakes (from Holtgrieve et al.

197   2011). Lake ecotypes include: temperate/boreal (green circles), alpine (blue circles), and arctic (red

198   circles), and the Greenland Summit ice core is indicated with a yellow circle. The solid lines are the

199   median posterior fits to the observed data using the most parsimonious model, and the dotted lines

200   are the 2.5 and 97.5% credible limits.

201   Figure 15. [B&W] Replacement of Holocene diatom assemblages by *Asterionella formosa* and/or

202   *Fragilaria crotonensis* mainly in lake cores from US high-altitude sites, since ~1950 CE (Saros et al.

203   2005). Location of lakes shown on Figure 14.

204   Figure 16. [Colour] Stratigraphic signals of the last millennium in Crawford Lake, Canada. The

205   horizontal red line near the top is the ~1950 CE level, marked by both lithological and

206   biostratigraphic changes in available data. From Zalasiewicz et al. (2017a), modified after Ekdahl et

207   al. (2004). DAR is diatom accumulation rate.

208   Figure 17. [Colour] Contamination record in Lochnagar sediments (Scotland) demonstrating

209   appearances as post-mid-20th century markers: (a) Spheroidal carbonaceous particles (SCPs) (from

210   Yang et al. 2002a); (b) Hg and Pb (from Yang et al. 2002a); (c) δ^{15}N (from Curtis and Simpson 2011);

211   (d) the chlorinated pesticides DDT and toxaphene from core collected in 1997 CE related to emission

212 data (from Muir and Rose 2007); (e) chlorobenzenes (from Muir and Rose 2007); (f) total PCBs

213 related to global emissions (from Muir and Rose 2007); and (g) PDBEs related to UK emissions (from

214 Muir and Rose 2007).

215 Figure 18. [B&W] Physical, chemical and biological trends from Lilla Öresjön (SW Sweden), a high-

216 sulphate deposition area (from Renberg and Battarbee 1990).

217 Figure 19. [Colour] Historical variations of concentrations and mass accumulation rates (MARs) of

218 black carbon (BC), char, and soot, parent-PAHs, oxygenated PAHs (OPAHs), and azaarenes (AZAs) in

219 the Huguangyan Maar Lake (from Han et al. 2016).

220 Figure 20. [Colour] Global map of peatland regions with basal peat ages (black <8 ka, red 8-12 ka, and

221 blue >12 ka) (from Yu et al. 2010).

222 Figure 21. [B&W] Core from Etang de la Gruère, Switzerland collected in 1991 CE: A) Pb Enrichment

223 Factor (EF) calculated as the ratio of Pb/Sc in the peats, normalized to the background value (from

224 Shotyk et al. 1998); B) Pb isotopic values (from Shotyk et al. 1998); C) ΣPCBs (from Berset et al. 2001);

225 D) ΣPAHs (from Berset et al. 2001); E) [137]Cs (from Appleby et al. 1997). Succession dated using [210]Pb

226 to 35 cm depth (Appleby et al. 1997) and ^{14}C yr BP from 35 cm to base (Shotyk et al. 1998).

227 Figure 22. [B&W] Spheroidal carbonaceous (fly ash) particles (SCPs), lead and iron concentrations

228 from Malham Tarn Moss, England (from Swindles et al. 2015).

229 Figure 23. [Colour] Distribution of ice caps and glaciers (blue) and ice sheets (white) from NASA Earth

230 Observatory Randall Glacier Inventory in 2014 CE http://earthobservatory.nasa.gov/IOTD/

231 view.php?id=83918 (acquired 7th May 2014; produced by Jesse Allen and Robert Simmon). Inset

232 maps showing the main polar drilling sites in Antarctica and Greenland mentioned in the text.

233 Figure 24. [Colour] δ^{18}O, δD and accumulation rates for the North Greenland Eemian Ice Drilling site

234 (NEEM) (Masson-Delmotte et al. 2015).

235 Figure 25. [Colour] Ice core signals since 1700 CE (from Wolff 2014). CH_4 and CO_2 ice-core data (blue

236 dots) are from Law Dome, Antarctica (MacFarling Meure et al. 2006), and recent atmospheric data

237 (red lines) from Mauna Loa (CO_2) and Cape Grim (CH_4) observatories. The horizontal dashed lines are

238 the highest values observed in ice cores of the last 800,000 years prior to the period shown. Beta

radioactivity is from Coats Land, Antarctica (Wolff et al. 1999). Sulphate and nitrate are shown for two cores from Greenland: B16 (dashed red) and B21 (solid blue) (Fischer et al. 1998). The 18th- and 19th-century spikes in sulphate are signals of volcanic eruptions.

Figure 26. [B&W] Concentrations (5-year running means) in Greenland ACT2 ice core from 1772 to 2003 CE of sulphur (NssS), thallium (Tl), cadmium (Cd) and lead (Pb), compared to black carbon (BC), from McConnell and Edwards (2008). Sulphur peaks in 1817 and 1883 CE relate to the Tambora and Krakatoa volcanic eruptions, respectively. © (2008) National Academy of Sciences, U.S.A.

Figure 27. [Colour] a) Law Dome ice core and firn records for CO_2 concentration and $\delta^{13}C$ for atmospheric CO_2 for the past 1000 years (from Rubino et al. 2013); b) Law Dome ice core and firn records for CH_4 concentration and $\delta^{13}C$ for atmospheric CH_4 for the past 1000 years (from Ferretti et al. 2005); c) N_2O concentrations in the Law Dome ice core over the past 2000 years and 200 years (Wolff 2013).

Figure 28. [Colour] Extent of carbonate outcrops present across global landmass by Ulrichstill https://commons.wikimedia.org/w/index.php?curid=9412430 Created 6th February 2010. Karst landscapes and speleothems occur within these regions, and locations mentioned in the text are indicated.

Figure 29. [Colour] Ernesto Cave, Italy: a) Age model based on lamina counting related to local mean air temperature (Frisia et al. 2003); b) $\delta^{18}O$ and $\delta^{13}C$ profiles (Scholz et al. 2012); c) Radiocarbon profile and comparable European atmospheric emissions (Fohlmeister et al. 2011); d) S concentration and $\delta^{34}S$ (Frisia et al. 2005, Wynn et al. 2010).

Figure 30. [Colour] Forest map of the world with key locations mentioned in the text. © (2006) FAO.

Figure 31. [Colour] a) The 20-year smoothed Northern Hemisphere extratropics reconstruction of radial stem productivity in high elevation and high latitude forest environments since 800 CE (black) and two-tailed 95% bootstrap confidence intervals (blue) (from Esper et al. 2002); b) $\delta^{13}C$ variability from Loader et al. (2013) for the period 1500-2008 CE measured in tree-ring cellulose for a composite tree-ring stable isotope chronology developed using *Pinus sylvestris* trees from northern Fennoscandia. Fine line represents annually-resolved $\delta^{13}C$ variability, thick solid line presents the

annual data smoothed with a centrally-weighted 51-year moving average. Dashed line represents the mean δ^{13}C value for the "pre-industrial" period 1500-1799 CE. Mean annual replication for the record is >13 trees. Analytical precision σ_{n-1} = 0.12 per mille n=951 which compares favourably with the analytical precision of the method typically reported (σ_{n-1} = 0.10 n=10) (Boettger et al. 2007, McCarroll and Loader 2004, Loader et al. 2013a).

Figure 32. [Colour] a) Tree rings (*Pinus sylvestris*) samples from 1960 to 2003 CE at Niepołomice (Poland) showing changes of radiocarbon concentration (from Rakowski et al. 2013) compared with Northern Hemisphere (Zone 1) atmospheric values (from Hua and Barbetti 2004); b) European S emissions; c) S concentrations; and d) δ^{34}S in *Abies alba* from NE Italy compared with European S emissions (Wynn et al. 2014).

Tables

Table 1. Requirements for establishing a Global Boundary Stratotype Section and Point (GSSP). Table modified from Gradstein et al. (2012, Table 2.1, p. 36), revised from Remane et al. (1996) according to current procedures and recommendations of the ICS.

Table 2. Potential palaeoenvironmental archives and facies and their stratigraphic markers for a candidate GSSP. ? – uncertain suitability of the specified signal.

Table 3. Reasons for and against using an anthropogenic deposit as a potential host for a GSSP.

Table 4. Reasons for and against using a marine anoxic basin deposit as a potential host for a GSSP.

Table 5. Reasons for and against using a coral or bivalve shell as a potential host for a GSSP.

Table 6. Reasons for and against using an estuarine or deltaic deposit as a potential host for a GSSP.

Table 7. Reasons for and against using a lake deposit as a potential host for a GSSP.

Table 8. Selected examples of the use of proxies for various types of atmospherically sourced environmental change.

Table 9. Reasons for and against using a peat deposit as a potential host for a GSSP.

290   Table 10. Reasons for and against using an ice core as a potential host for a GSSP.

291   Table 11. Reasons for and against using a speleothem as a potential host for a GSSP.

292   Table 12. Reasons for and against using a tree ring as a potential host for a GSSP.

293   Table 13. Summary of key mid-20th century proxy signals and potential palaeoenvironments for a

294   GSSP. The initial date represents the marked onset of the signal; the peak signal is shown in brackets.

295   Reference numbers relate to main geographical locations mentioned in the text: (1) Santa Barbara,

296   USA; (2) Caribbean; (3) Nova Scotia, Canada; (4) Clyde Estuary, Scotland; (5) Urola Estuary, Spain; (6)

297   Lake Victoria, Australia; (7) North America; (8) China; (9) Lochnagar, Scotland; (10) Lilla Öresjön,

298   Sweden; (11) Northern England; (12) Switzerland; (13) Antarctica; (14) Greenland; (15) Ernesto Cave,

299   Italy; (16) Fenno-Scandinavia; (17) Poland; (18) Ontario, Canada.

300

1. INTRODUCTION

The Anthropocene Working Group (AWG), a working group of the Subcommission on

Quaternary Stratigraphy (SQS) of the International Commission on Stratigraphy (ICS), is

facilitating the process that will lead to the submission of formal proposals to define the

Anthropocene as a chronostratigraphic unit. Such a unit comprises a body of strata formed

during a specific interval of geological time. Units of the International Chronostratigraphic

Chart (upon which the Geological Time Scale is based) are chronostratigraphic units, and

each is defined by a synchronous base. The AWG is working towards a definition of the

geological Anthropocene based on "the first appearance of a clear synchronous signal of the

transformative influence of humans on key physical, chemical, and biological processes at

the planetary scale. As such, it stands in contrast to various local or diachronous inscriptions

of human influences on the Holocene stratigraphic record" (Zalasiewicz et al. 2017c). This

working definition most closely aligns with the mid-20th century "Great Acceleration" in

human population, resource consumption, global trade and technological evolution, proxy

signals from which produce a distinctive stratigraphical boundary (Steffen et al. 2016). There

are alternative interpretations of the definition of the Anthropocene, but these are generally

grounded on a non-stratigraphical basis (e.g. the discussion on various geomorphological

considerations of the start of the Anthropocene by Brown et al. 2017).

Within the Phanerozoic, the current internationally agreed method for defining

chronostratigraphic boundaries is via selection of a Global Boundary Stratotype Section and

Point (GSSP) as a physical reference level for a particular, and optimally correlatable,

geological time boundary. The process of deciding on a GSSP, outlined by Remane et al.

324 (1996) and Remane (1997, 2003) and summarised by Smith et al. (2014) is a complex process

325 that normally requires: 1) an initial selection of a boundary level characterized by a marker

326 event (the primary marker event) of optimal global correlation potential; 2) selection of a

327 stratotype section from a number of potential sections, with the chosen stratotype section

328 containing the best possible record of the primary marker event as well as other marker

329 events that support global correlation, 3) ideally the selection of some auxiliary stratotypes

330 in which the same level is represented by similar or other proxy signals in different parts of

331 the world (Walker et al. 2009, in defining the Holocene Series, provided five auxiliary

332 stratotypes as well as the GSSP); and, 4) definition of the precise point within stratified rock

333 or sediment (or glacial ice in the case of the Holocene) that fixes the chronostratigraphic

334 boundary with a precise moment of time. Formalisation of a GSSP is a careful procedure as,

335 once ratified, it normally cannot be subsequently revised for at least ten years (Remane et

336 al. 1996).

337

338 Table 1 provides a formal and comprehensive listing of the reasonable requirements for

339 establishment of a GSSP, most of which will pertain also to a formal basis for the

340 Anthropocene. It includes the requirement for stratigraphical completeness across the GSSP

341 level, with adequate thickness of strata both above and below the boundary in order to

342 demonstrate the transition. Therefore, the presence of an unconformity, marking a

343 discontinuous succession, at or near the proposed boundary, would render it unsuitable. The

344 selected section should also be accessible for subsequent investigations, ideally with

345 provision for conservation and protection of the site.

346

347 The rank currently preferred by the AWG for the Anthropocene is that of series/epoch

348 (Zalasiewicz et al. 2017c). The procedure leading to official acceptance of a GSSP for the

349 Anthropocene Series/Epoch and its corresponding Age/Stage would require: 1) the selection

350 by the AWG of a single GSSP candidate from one or more potential candidates, based on

351 proposals submitted to it; 2) the recommendation of that proposal by the SQS; 3) its

352 approval by the voting membership of the ICS; and 4) ratification by the Executive

353 Committee of the International Union of Geological Sciences (IUGS). All voting within the ICS,

354 and its constituent subcommissions and their working groups, requires a supermajority of

355 60% or more for a proposal to be approved.

356

1. Name and stratigraphic rank of the boundary Including concise statement of GSSP definition
2. GSSP geographic and physical geology • Geographic location, including map coordinates • Geological setting (lithostratigraphy, sedimentology, palaeobathymetry, post-depositional tectonics, etc.) • Precise location and stratigraphic position of GSSP level and specific point • Stratigraphic completeness across the GSSP level • Adequate thickness and stratigraphic extent of section above and below • Accessibility, including logistics, national politics and property rights • Provisions for conservation and protection
3. Primary and secondary markers • Primary correlation marker (event) at GSSP level • Secondary markers – biostratigraphy, magnetostratigraphy, chemical stratigraphy, sequence stratigraphy, cycle stratigraphy, other event stratigraphy, marine–land correlation potential • Potential age dating from volcanic ash and/or orbital tuning • Demonstration of regional and global correlation
4. Summary of selection process • Relation of the GSSP to historical usage • References to historical background and adjacent (stage) units • Selected publications • Other candidates and reasons for rejection • Summary of votes and received comments • Other useful reference sections
5. Official publication • Summary for official documentation in IUGS journal *Episodes* • Digital stratigraphy (litho-, palaeo-, magneto-, and chemo-stratigraphic) images and graphic files submitted to ICS for public archive • Full publication in an appropriate journal

357 **Table 1.** Requirements for establishing a Global Boundary Stratotype Section and Point (GSSP). Table

358 modified from Gradstein et al. (2012, Table 2.1, p. 36), revised from Remane et al. (1996) according

359 to current procedures and recommendations of the ICS.

360

361 Here we offer a preliminary assessment of palaeoenvironments and their depositional facies

362 where potential GSSP candidate sections for defining the lower boundary of the

363 Anthropocene may be located, based on the published literature. Few of these example

364 sections were chosen with the specific purpose of defining the Anthropocene as a

365 chronostratigraphic unit. Rather they show a range of proxy signals, analysed in published

366 studies for varied (non-ICS) purposes. The palaeoenvironmental research illustrated in this

367 review demonstrates the timing and processes through which these signals have been

368 imprinted in strata, and the extent to which they allow stratigraphic correlation worldwide.

369 Even with this considerable caveat, the possibilities of correlation are clearly demonstrated,

370 and help constrain the range of potential targets for Anthropocene-specific ICS studies.

371

372 2. KEY STRATIGRAPHIC MARKERS

373 The aim – not always achieved – is for GSSPs to have many guiding criteria to support the

374 primary marker (Remane et al. 1996, Smith et al. 2014) to permit both regional and global

375 correlation. This has been the early focus of the AWG, with the description of potentially

376 suitable markers summarised by Waters et al. (2016), whose recommendations this study

377 follows, and as reported by Zalasiewicz et al. (2017c), concludes that the primary marker for

378 the Holocene–Anthropocene boundary should be selected and identified in strata with a

379 mid-20th century age. Such a definition makes the Anthropocene so recent that there are

380 more potential archives available to it than for most, if not all, earlier GSSPs.
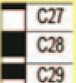
2.1 Key markers

382   The lower boundary of a chronostratigraphic unit, at the rank of Stage/Age and above, is

383   defined by a GSSP and is recognized globally by a primary marker within the stratotype

384   section that should be close to or coincident with the GSSP itself. Historically, most

385   chronostratigraphic units use biotic signals, namely the highest or (preferably) lowest

386   occurrence of a single fossil species, as the primary marker (Figure 1). More recent

387   approaches incorporate physico-chemical markers such as magnetic reversals, isotope

388   excursions and cyclostratigraphy, especially for the Cenozoic (Miller and Wright 2017).

389   Although not a requirement, the means for numerically dating the succession is considered a

390   strong site advantage.

391

392   Of the 65 GSSPs presently ratified by IUGS, all occur within strata deposited in marine

393   sedimentary environments, with the exception of the Holocene GSSP that is placed within a

394   Greenland ice core (Walker et al. 2009). This reflects the fact that marine fossils have proven

395   better for long-distance correlation than non-marine ones; and more generally that proxy

396   signals are readily preserved and continuously recorded in marine environments. However, a

397   primary marker ideally is traceable globally in marine and non-marine stratigraphic settings,

398   thereby allowing secondary markers to be chosen that will assist correlation in either setting,

399   especially when the primary marker is not detected. These secondary markers should

400   approximate closely to that the stratigraphic position of the primary marker. In an

401   Anthropocene context, the choice of markers should not be to provide an indication of the

402   start of anthropogenically driven effects, but to provide the most pragmatic marker that will

403   allow global correlation of the chosen boundary, being geographically extensive, temporally

404   abrupt and providing a permanent record. Such primary and secondary markers do not need

405   to be symptomatic of the environmental changes across the Holocene–Anthropocene

boundary, rather they need to be amenable to widespread correlation in deposits representing different palaeoenvironments. Key signals considered here are mainly anthropogenic in origin, either being entirely novel, such as the production of novel anthropogenic mineral-like compounds, artificial radionuclides, organic and inorganic chemical species, or through perturbations of natural signals associated with, for example, the carbon and nitrogen cycles, and changes to climate proxies or biotic assemblages (Table 2). However, markers of any kind, including ones with little or no human influence (e.g. palaeomagnetic signals or volcanic ash layers) may serve just as well to help correlation. These markers are discussed by Waters et al. (2016), and are summarised below in the context of their likely presence in potential candidate palaeoenvironments.

Figure 1. Primary and some secondary markers for the 65 GSSPs that have been ratified currently by

418 IUGS. The four in the Cenozoic that deal with stable isotope events (base Eocene, Quaternary,

419 Calabrian and Holocene) and the iridium anomaly (base Paleocene) provide models for choosing

420 markers for the base of the Anthropocene.

2.1.1 Novel materials

422 Synthetic solids such as metal alloys, glass, carbide abrasives, gemstones, laser crystals,

423 piezoelectric compounds, semiconductors and cement have proliferated in the environment

424 in recent decades (Hazen et al. 2017), being present in novel "metamorphic rocks" such as

425 porcelain, brick and concrete, the latter being the most abundant novel rock on the planet,

426 with over 90% of the ~500 Gt (gigatonnes or 10^{15} grams) produced since the mid-20th

427 century. Complex additives to cement help to chemically and petrographically fingerprint

428 modern concrete (Waters and Zalasiewicz, 2017). These novel anthropogenic mineral-like

429 compounds and rocks often accumulate directly within terrestrial anthropogenic deposits

430 such as landfill sites and road networks. Through subsequent erosion of the widespread

431 human-built landscape, these materials may be reworked and deposited in fluvial, lacustrine,

432 coastal and marine sediments, with a variable time lag between formation and

433 accumulation.

434

435 Synthetic organic compounds have become abundant, including plastics that are

436 exceptionally mobile and durable within river and ocean currents. Plastics have, since ~1950

437 CE, become increasingly widely dispersed, including as abundant microfibres and

438 microbeads, forming signals found extensively in lake, estuarine and marine sediments, even

439 within remote abyssal environments (Zalasiewicz et al. 2016a). Most are the effluents from

440 waste water treatment works and transported through river systems to accumulate in lakes

441 or oceans. The recent recognition of synthetic microfibre fallout accumulations in urban

19

442   Paris (Dris et al. 2016) raises the possibility of rapid and widespread airborne dispersal across

443   environments.

444

445   The first development (in effect first occurrence) and annual production figures of novel

446   anthropogenic mineral-like compounds and organic polymers are known from historical

447   records. However, few studies have investigated them in their stratigraphic context, in order

448   to determine the pattern of their accumulation in sedimentary environments. Matsugama et

449   al. (2017) record the first influx of microplastics into canal sediments in Tokyo in the 1950s,

450   whereas in the Gulf of Thailand a significant increase in abundance occurs in the 1990s; in all

451   cases there is an upward increase in microplastic abundance and polymer types. Because of

452   their novelty, little is known of the longevity and potential fragmentation of plastics in

453   buried sediments. Also of significance in lakes and marine settings is the settling rate within

454   the water column. In the case of microplastic organic polymers (<5 mm diameter) sinking

455   velocities have been estimated as 6–91 mm s^{-1}, which is more rapid than the settling of clay

456   minerals and organic-rich aggregates (Kowalski et al. 2016). Particle density (variable

457   between distinct polymers) and shape, fluid density (with slower settling in saline water),

458   temperature and ingestion by microplankton all can influence settling rates, and these

459   parameters have different effects on different polymers (Kowalski et al. 2016).

460

461   Fly ash, the unburned particulates sourced from fossil fuel combustion, includes inorganic

462   ash spheres (IAS), mainly residues from coal burning, and spheroidal carbonaceous particles

463   (SCPs) principally from both coal burning and oil combustion. These particulates are

464   disseminated aerially, and typically show a marked upturn in abundance from about 1950 CE

465   (Oldfield 2014, Rose 2015, Swindles et al. 2015). The upturn in abundance of SCPs should

466   serve as a likely permanent stratigraphic marker for the Anthropocene in lake sediments

467   across all continents. Work is ongoing to assess their likely presence in other environments,

468   such as glacial ice, peat sequences, marine basin sediment and terrestrial anthropogenic

469   deposits such as industrial dumps and landfills. Black carbon (BC), present as char or soot, is

470   generated from both anthropogenic combustion and natural biomass burning (Bond et al.

471   2007, Han et al. 2017). BC is commonly identified in soil, lacustrine and marine sediments,

472   and glacial ice (Xu et al. 2009).

473   ## 2.1.2 Geochemical markers

474   Oxygen and hydrogen isotopes and dust signals are important climate change proxies and

475   hence tools for Quaternary correlation. All three proxies are recognised in glacial ice, within

476   the ice fraction, and complement the air bubble record. Deuterium (^{2}H or D) is an important

477   isotopic tracer for precipitation, and the relationship between δD and δ^{18}O signatures

478   defines a "deuterium excess" marker that is a proxy for sea surface temperature. The

479   deuterium excess ratio is used as the primary marker for the base of the Holocene Series in

480   an ice core GSSP (Walker et al. 2009), where a 2–3‰ decrease in the ratio is associated with

481   a rapid ocean surface temperature decline of 2–4°C. An abrupt dip in δD and deuterium

482   excess reflecting cooling is also seen in a Greenland ice core at 8.2 ka (Walker et al. 2012),

483   and suggested to mark the base of the proposed Middle Holocene Subseries and

484   Northgrippian Stage. Cold stages are commonly associated with increased aeolian dust

485   deposition in ice cores. Decreases in δ^{18}O mark cooling events, and in Greenland ice the

486   overall trend since the Middle to Late Holocene has been of gradual cooling culminating in

487   the Little Ice Age from about 1200 to 1850 CE. The shift to warming induced by increased

488   anthropogenic greenhouse gases emissions is first indicated by a slight change to less

489   negative δ^{18}O values in Greenland ice from ~1850 through to the 1870s CE and again from

490   1979 to 2007 CE (Masson-Delmotte et al. 2015; see Figure 24 below), although the

491 magnitude of enrichment is small compared with variations across the Pleistocene–

492 Holocene boundary. Warming is also apparent in the Antarctic Peninsula from about 1950

493 CE, e.g. on James Ross Island (Abram et al. 2013), with lakes on Signy Island from the South

494 Orkney Islands having experienced some of the most rapid air temperature increases of 2^oC

495 since the mid-20th century, with concomitant marked responses by lake biota and increased

496 nutrient levels, linked to deglaciation and reductions in lake snow and ice cover (Quayle et

497 al. 2002). Variations in $\delta^{18}O$ are observable in carbonate and phosphate minerals in

498 speleothems, shells, corals, teeth, and bones and also in tree rings. They can be used as a

499 palaeotemperature proxy in marine settings or within terrestrial environments, primarily as

500 a proxy for $\delta^{18}O$ composition in atmospheric precipitation.

501

502 About 50% of anthropogenic carbon dioxide emissions, the major product of fossil-fuel

503 combustion, have accumulated in the atmosphere, with the lifetime of much of the

504 atmospheric fossil-fuel-derived CO_2 being ~200 to 2000 years (Archer et al. 2009). The

505 remainder is absorbed approximately equally by land and ocean sinks (Le Quéré et al. 2016).

506 The atmospheric CO_2 record from ~7 ka shows a very slow rise to ~280 ppm by ~1850 CE.

507 Subsequently, the CO_2 concentration shows a marked rate increase (Etheridge et al. 1996,

508 MacFarling-Meure et al. 2006, Rubino et al. 2013), attaining ~310 ppm by 1950 CE and with a

509 further sharp acceleration to its current mean value of >400 ppm, reached in 2015 CE. The

510 rate of increase between 1950 and 2015 CE is ~100 times greater than that of the Late

511 Pleistocene to Early Holocene rise, itself considered rapid in geological terms (Wolff 2014).

512

513 Anthropogenic methane emissions arise primarily from agriculture (wet rice cultivation and

514 ruminants), with a smaller fraction from biomass burning and fossil fuel combustion. Some

515 large terrestrial anthropogenic deposits in the form of landfills also emit significant amounts

of methane. Unlike CO_2, methane is chemically reactive in the atmosphere, with the dominant sink being oxidation by OH radicals. This process removes about 90% of all emissions of CH_4 each year, or about 9% of the total burden of CH_4 – the atmospheric lifetime is 7–11 years (Ciais et al. 2013). Throughout the Quaternary Period, CH_4 concentrations range from ~400 to 800 ppb, with the higher values marking interglacials. In marked contrast, from 1875 CE there has been a sharp climb to the current levels of ~1800 ppb (Nisbet et al. 2016).

Both CO_2 and CH_4 provide a direct stratigraphic marker where they are preserved within air bubbles in glacial ice, and an indirect record via carbon isotope variations. $\delta^{13}C$ values in CO_2 from ice cores varied by less than 0.4‰ over the duration of the pre-industrial Holocene, with the principal change being a slow enrichment in ^{13}C during the Early Holocene. The subsequent combustion of hydrocarbons, which are depleted in the ^{13}C isotope, has resulted in a sharp reduction in $\delta^{13}C$ values in atmospheric CO_2 of about 2‰ since the late 18th century, with a pronounced inflection at about 1960 CE (Rubino et al. 2013). This Suess effect is recorded in diverse materials, including plants (tree rings), shells, bones, limestones, corals, and in the atmospheric composition of air bubbles trapped in ice, although speleothems are comparatively insensitive to this signal. An abrupt shift towards less negative $\delta^{13}C$ values in atmospheric CH_4 of ~2.5‰ since ~1875 CE in response to these pyrogenic emissions (Ferretti et al. 2005) has been succeeded over the last 12 years by a shift of −0.17‰ of $\delta^{13}C$ in the increasing volume of atmospheric CH_4, attributed to an expansion of tropical wetlands (Nisbet et al. 2016).

Nitrate concentrations have been perturbed mainly through the production of agricultural fertilizers, initially through mined nitrate deposits in the 19th century, but most notably

23

541 through the industrial production of ammonia from atmospheric nitrogen by the Haber-

542 Bosch process, which started in 1913 CE (Fowler et al. 2013). The nitrate associated with

543 artificial fertilizers shows global airborne distribution. $\delta^{15}N$ values have been acquired from

544 sediment organic matter, commonly from lake deposits, although determinations from

545 anthropogenic deposits, marine anoxic basins, estuaries, deltas, tree rings, and amino acids

546 in corals are also available. Nitrogen compounds and isotopes are not typically recorded in

547 carbonates, including speleothems. Nitrate, total nitrogen oxides (NO_x) and $\delta^{15}N$ values are

548 determined from solid ice in ice cores, providing data at the time of snow accumulation.

549 Both Northern Hemisphere lake sediments (Holtgrieve et al. 2011, Wolfe et al. 2013) and

550 glacial ice (Hastings et al. 2009) show elevated nitrate concentrations and a fall in $\delta^{15}N$,

551 which start towards the end of the 19th century but become appreciably more pronounced

552 during the mid-20th century. A marked increase in NO_x sourced from elevated combustion of

553 hydrocarbons, particularly automobiles and power stations, is also evident in Greenland ice

554 sheets from the mid-20th century (Erisman et al. 2013).

555

556 Natural sources of sulphate include volcanic eruptions that produce high-magnitude, short-

557 duration spikes evident in glacial ice over past millennia. There has been an overall trend of

558 increased sulphate content in glacial ice, trees and speleothems since the start of the

559 Industrial Revolution, peaking in the mid- to late-20th century, reflecting patterns of coal

560 consumption; sulphate has widely declined over recent decades, most likely due to

561 legislation requiring the fitting of sulphur scrubbers to power station chimneys to combat

562 acid rain. The signals tend to be associated with local-to-regional industrial changes rather

563 than representing global signals. Stable sulphur isotopes show lower $\delta^{34}S$ ratios in tree rings

564 (e.g. Fairchild et al. 2009, Wynn et al. 2014) and speleothems (e.g. Frisia et al. 2005, Wynn et

565 al. 2010) during the second half of the 20th century.

566

567 Pure metals such as gold, silver, lead, copper and iron have a long history of extraction (and

568 blending to obtain alloys) to produce tools or ornaments. The early historical mining of these

569 metals provides local and highly diachronous signals evident in lakes, estuaries, peats, sea-

570 floor sediments, and carbonates including corals and speleothems, and they are also present

571 in glacial ice records. The heavy metals are either air-borne as aerosols, dissolved in water,

572 or carried as water-transported particulates. Mercury (Hg) is also transported in gaseous

573 form (RGM – reactive gaseous Hg; GEM – gaseous elemental Hg) (Yang et al. 2010). Within

574 sediments, metal compounds are commonly stabilized by being adsorbed to clay mineral

575 surfaces or organic matter; locally they may be diagenetically mobilized as conditions

576 become reducing with burial, and redeposited in overlying oxidizing environments, thus

577 decreasing their effectiveness as stratigraphic markers. Elevated heavy metal concentrations

578 in tree rings have been suggested as unsuitable for temporal studies of pollution events

579 (Bindler et al. 2004). For most metals and their compounds, the 20th century environmental

580 signals continue to be localised, related to production from local industries. Some metals,

581 such as elemental aluminium and many trace elements, have seen marked upturns in

582 production in the second half of the 20th century as new uses are found for them, and these

583 may be expected to leave signals in sediments. For at least two millennia prior to the

584 Industrial Revolution, Pb concentration in sediments increased and Pb isotope ratios

585 declined as a result of European metallurgy (Renberg et al. 2000). Perhaps the most

586 widespread and abrupt signal is that associated with Pb isotope ratios related to the use of

587 tetraethyl-lead in gasoline from the 1920s, although the isotopic fingerprint reflects the

588 sources of lead used to manufacture this additive, which differ between countries (Reuer

589 and Weiss 2002). Current global atmospheric concentrations of Hg are about two to four

590 times higher than pre-industrial levels as a result of refining ore and burning coal and waste

591 (Lindberg et al. 2007, Yang et al. 2010). Hg has an atmospheric lifetime of 0.75 years so can

592 be dispersed globally before deposition, whereas the larger and more slowly cycling marine

593 reservoir can produce a lagged response of 1 to 2 centuries (Lindberg et al. 2007).

594

595 A huge variety of novel organic compounds have been generated and used in industrial

596 processes. Persistent organic pollutants (POPs), those recalcitrant to decomposition, which

597 readily adsorb onto clay and organic particles and are poorly soluble, provide potentially

598 suitable signals. Key potential POP signals include those from organochlorine pesticides

599 (OCPs) such as DDT, aldrin and dieldrin, and various polychlorinated biphenyls (PCBs), along

600 with brominated flame retardants (e.g. polybrominated diphenyl ethers, PBDEs). Most of

601 these have only been generated on industrial scales and released into the environment in

602 notable quantities since the mid-20th century, particularly concentrating in sediments in

603 lakes (Muir and Rose 2005, 2007), estuaries (Vane et al. 2011) and canyons on continental

604 shelf margins (Paull et al. 2006).

605

606 Large amounts of anthropogenically-sourced radionuclides have been released by 543

607 atmospheric nuclear weapons tests, with a total yield of about 440 Mt (i.e. energy released

608 in TNT equivalent), and subsequent fallout (UNSCEAR 2000). Although atmospheric tests and

609 military use began in 1945 CE, it was only with the testing of the large thermonuclear

610 (hydrogen) devices from 1952 CE that fallout was dispersed globally and became recorded in

611 most environments. The signal is almost instantaneous in geological terms, with residence

612 times in the stratosphere of some 15 to 18 months following thermonuclear detonations.

613 Typically, the Pu signal shows an abrupt rise in 1952 CE, a peak in 1963–1964 CE and rapid

614 decline since 1963 CE in response to a Partial Test Ban Treaty, which resulted in most testing

615 moving underground (Waters et al. 2015). Radionuclides that are absent or rare in nature,

26

616 such as plutonium-239 (^{239}Pu), americium-241 (^{241}Am), caesium-137 (^{137}Cs) and strontium-90

617 (^{90}Sr) show clear signals in soils, peats, lake and sea-bed deposits, coral and tree rings, and

618 glacial ice. However, the caesium and strontium isotopes have half-lives of about 30 years,

619 so their sedimentary signal is short-lived, while caesium and plutonium may be mobile in

620 anoxic conditions (Jeandel 1981). Additional brief spikes of certain isotopes can be used to

621 aid correlation. For instance, an artificial satellite re-entry in 1964 CE provided a distinctive

622 global ^{238}Pu signal, and, more regionally, the Chernobyl and Fukushima reactor accidents

623 produced spikes in 1986 and 2011 CE, respectively. The common natural radioisotope ^{14}C

624 shows greatly elevated values associated with nuclear tests and provides a further clear and

625 long-lasting signal in most growing organic matter such as wood, bone and carbonates

626 including corals, speleothems and also in glacial ice. ^{239}Pu, because of its longevity (half-life

627 of 24,110 years), is a strong candidate as a primary marker of radionuclide deposition as it

628 will remain detectable for ~100 000 years (Hancock et al. 2014) and beyond as the decay

629 product ^{235}U. Alpha-spectrometry carried out during early studies does not differentiate

630 between ^{239}Pu and ^{240}Pu (itself not an issue, as the combined signal is clearly expressed), but

631 is only applicable where Pu concentrations are high – the detection limit is approximately

632 0.05 mBq of $^{239+240}$Pu (Hancock et al. 2014). Modern ICP-MS techniques can discriminate

633 between these isotopes, although it is necessary to remove interferences from ^{238}UH$^+$ and

634 other species, and can be used at low Pu concentrations – the absolute limit of

635 quantification is 0.2 µBq and 0.9 µBq for ^{239}Pu and ^{240}Pu respectively (Lindahl et al. 2011).

636 Other mass spectrometric methods, such as Accelerator Mass Spectrometry (AMS) and

637 Thermal Ionisation Mass Spectrometry (TIMS) also allow the simultaneous determination of

638 ^{239}Pu and ^{240}Pu.

2.1.3 Biotic markers

Changes in fossil assemblages are used to demarcate most chronostratigraphic boundaries in the Phanerozoic, mainly through recognition of the lowest stratigraphic occurrence of a fossil taxon, which may approximate to its evolutionary origin, although within any individual stratal section the stratigraphic appearance of a taxon more specifically reflects its local immigration to that place. Such stratigraphic appearances (and commonly disappearances too) provide a widely effective tool for correlation. In the Quaternary Period (and especially for the Anthropocene) the time scales involved are generally too short for many evolutionary appearances and disappearances to have taken place, and so immigration/emigration patterns are widely used for biostratigraphic correlation. Prominent Anthropocene biostratigraphic signals are expressed in recently forming sedimentary deposits by the appearance of unique terrestrial and marine species associations of the neobiota ('invasive species'), the result of human transport of tens of thousands of species around the globe. Recent neobiota include examples among common microplankton such as foraminifera, coccoliths, dinoflagellates and radiolarians in the marine realm, of the kind commonly used as microfossils to recognise stage boundaries in pre-Anthropocene deposits of the Cenozoic (Figure 1). These organisms, as well as macroinvertebrates, such as molluscs, vertebrates and plants (both macroplant remains and pollen) can form useful biostratigraphic tools for correlation because of their geologically preservable hard parts such as skeletons, frustules, shells, or phytoliths.

Human-driven extinctions and local extirpations have become increasingly common over the last 500 years, particularly in island faunas (Ceballos et al. 2015). So far, island floras have been more resilient to extinction than island faunas in spite of the high abundance of introduced plant species in many environments (Ellis et al. 2012), but an accumulating

664　extinction debt is likely (Sax and Gaines 2008). Their provincial nature and low abundances

665　mean that island floras provide regional rather than global stratigraphic markers. Selective

666　breeding of domesticated floras and faunas tends to be associated with rapid changes to

667　morphology, in effect forming distinct morphospecies that can be preserved in sedimentary

668　successions. Moreover, species beneficial to humans, such as domestic maize or chickens,

669　tend to be abundant and geographically widespread. The development of factory farming

670　led to massive increases in amounts of faunal remains of domesticated species being

671　deposited in landfills and other terrestrial stratigraphic contexts from the mid-20th century

672　on.

673

674　Another extensive stratigraphic signature over recent centuries, but especially since the mid-

675　20th century, reflects neobiota reaching far beyond their original geographical ranges,

676　through deliberate or accidental human actions. Local arrival of these neobiota is well

677　documented through observation, and is often linked with the extinction or extirpation of

678　local fauna and flora, as observed on Kauai, Hawaii (see section 3.5.5), or among benthic

679　foraminifera preserved in the coastal sedimentary record (McGann et al. 2000, Calvo-

680　Marcilese and Langer 2010).

681

682　Biostratigraphic signals may also relate to ecological degradation (Willis et al. 2010, Dearing

683　et al. 2012). In marine environments, a long lead-in of low-level and provincialized ecological

684　degradation gave way to accelerating global change in the early 1950s (Wilkinson et al.

685　2014). The driver was expansion of industrial pollution, expanding human populations

686　associated with increased raw sewage dispersal offshore, and increased use of fertilisers

687　during agricultural intensification. In Northern Hemisphere lakes, an increase in reactive

688　nitrogen from artificial fertilisers has been well-documented (Holtgrieve et al. 2011, Wolfe et

689 al. 2013), giving rise to increases in primary productivity and marked changes to diatom

690 populations and species assemblages, with surface water acidification as an additional

691 factor. The stratigraphic records collated by Smol (2008) commonly show clear mid-20th

692 century inflections in such lacustrine proxies. Runoff contaminated with these fertilisers has

693 also resulted in seasonally oxygen-starved 'dead zones' in lakes and coastal seas, causing –

694 to take just one example - increases in hypoxia-tolerant benthic foraminifera (Wilkinson et

695 al. 2014). Environmental legislation has locally led to a phase of recovery from pollution

696 stressors in the late-20th and early-21st centuries, but increasingly climate change is imposing

697 pole-ward shifts in species distributions and confounding recovery from acidification (e.g.

698 Battarbee et al. 2014).

699 *2.2 Independent dating techniques*

700 Direct numerical dating of a GSSP is not a prerequisite in the selection of a site, but is

701 beneficial. For the Anthropocene, annual resolution for any proposed boundary section is

702 highly desirable, giving a level of precision not available for any other boundary within the

703 Geological Time Scale. The best time resolution for previous GSSPs is for that of the

704 Holocene, with a 2σ uncertainty of ±99 years (Walker et al. 2009).

705

706 Counting annual sedimentary laminae in presently accumulating successions, or annual

707 growth layers in living organisms (that are demonstrably complete), is one means of

708 establishing the numerical age, expressed in years, of an Anthropocene base. The age so

709 determined may be additionally constrained by ^{210}Pb, sourced from the atmosphere or

710 directly from sediments (Noller 2000). This isotope is rapidly scavenged from sea and

711 freshwater onto organic detritus, but is not mobile in the sediment. It has a useful dating

712 range of up to 150 years (the half-life is 22.3 years) with a measurement error of about 10%,

713 and is typically used to determine accumulation rates in organic lake, coastal or marine

714 sediments, peats or glacial ice; it is fixed in living plants and corals, too, and so can determine

715 their growth rates.

716

717 Other short-lived radioisotopes include ^{234}Th, with a half-life of 24 days, which can be used to

718 date changes in speleothems and corals over periods as short as 3 months, but it has little

719 value for laminae straddling the Holocene–Anthropocene boundary. Radiocarbon (^{14}C) has a

720 half-life of ~5600 years and has limited use as a chronometer from the mid-20th century, but

721 along with ^{137}Cs (half-life 30 years) and ^{90}Sr (half-life ~28 years), it can help to identify

722 specific episodes, such as the 1963–1964 CE peak in atmospheric nuclear tests (the 'bomb-

723 spike') and the 1986 CE Chernobyl accident recorded in sediments, ice, tree rings and corals.

724

725 Anthropogenic materials present possibilities for absolute and relative dating not available in
726 earlier geological successions. For example, the date of manufacture of artefacts
727 (technofossils) found as inclusions in strata can often be ascertained with high resolution
728 through the use of type series, and sometimes the precise date is even stamped, moulded,
729 cast, or indelibly imprinted on objects. Such evidence could be immensely valuable in
730 supplementing more traditional dating methods. More generally, the value of using
731 archaeological techniques for relative dating of stratigraphic sequences of terrestrial
732 anthropogenic ground, in conjunction with geological methods, should be considered.

| Environment | Annual laminae | Novel materials | | Geochemical markers | | | | | | | | | Biotic markers |
		Plastics	Fly ash	$\delta^{18}O$	Deuterium &/or dust	CO_2 & CH_4	$\delta^{13}C$	NO_3^- & $\delta^{15}N$	S & SO_4^{2-}	Heavy metals	Organic compounds	Radiogenics	Extinctions/ neobiota
Anthropogenic deposits		✓	✓				✓	✓		✓	✓	✓	✓
Marine anoxic basin deposits	✓	✓	✓	✓			✓	✓		✓	✓	✓	✓
Coral bioherms & marine bivalve shells	✓	✓	?	✓			✓	✓		✓	✓	✓	
Estuarine & deltaic deposits	✓	✓	✓	✓			✓	✓		✓	✓	✓	✓
Lake depositss	✓	✓	✓	✓			✓	✓		✓	✓	✓	✓
Peat & peatlands (mires)			✓		✓		✓	✓	✓	✓	✓	✓	✓
Ice	✓		?	✓	✓	✓	✓	✓	✓	✓	✓	✓	
Speleothems	✓			✓						✓	✓	✓	
Tree	✓			✓	✓		✓	✓	✓	✓		✓	

733

Table 2. Potential palaeoenvironmental archives and facies and their stratigraphic markers for a candidate GSSP. ? – uncertain suitability of the specified signal.

3. SUITABILITY OF PALAEOENVIRONMENTAL ARCHIVES FOR HOSTING POTENTIAL GSSP CANDIDATES

There is a wide range of sedimentary and biological records within which a GSSP is feasible. For any candidate section, high-precision dating is needed, if only to provide confidence that there are no missing surfaces in successions that are merely decades to centuries long. Such high-precision dating, potentially to annual resolution, can be achieved in seasonally layered sediments in anoxic marine basins and hypoxic lakes, in glacially influenced or hypersaline lakes and sinking marine deltas, in seasonally layered ice and annual growth layers in corals, bivalves, and in speleothems and trees. Non-layered strata, including anthropogenic deposits and peats provide additional environments in which the Holocene–Anthropocene transition may be observed. In this section these key potential archives are discussed in turn, describing their global extent and continuity, and the arguments for or against their potential for hosting a candidate GSSP. Examples are provided to show how key signals are recorded.

3.1 Anthropogenic deposits

This category includes sedimentary successions that have accumulated through direct human deposition (artificial ground) or by human influence on natural systems (Ford et al. 2014). Artificial ground can show a continuum from entirely natural through to entirely anthropogenic materials, but with the key requirement that they have been deposited through human action. Conversely, few "natural" systems are these days free from human modification (Barnosky et al. 2017), whether via construction of dams influencing sediment flux in fluvial systems (Syvitski and Kettner 2011), or trawler fishing disturbing the upper decimetres of sediments on the continental shelf and slope (Martin et al. 2015).

759 Zalasiewicz et al. (2017b) estimated the spatial extent of human modification of the

760 landscape at about 82 x 10^6 km^2, or about 16% of the total Earth's surface or 55% of the

761 terrestrial land surface, providing many sections that could be investigated as potential

762 GSSPs. Road surfaces alone, with a mass estimated at 1.3% of the physical technosphere

763 (*sensu* Zalasiewicz et al. 2017b), comprise an extensive boundary layer in temperate and

764 tropical climates. Anthropogenic deposits may show remarkably high accumulation rates,

765 locally in excess of one metre per year, and rapidly incorporate novel anthropogenic

766 signatures, which may be lithological, geochemical or biotic. This provides a highly resolvable

767 succession in which artefacts and novel materials can be constrained to decadal resolution

768 (Zalasiewicz et al. 2014a).

769

770 A potential Anthropocene Series, which would be defined in a unit of strata, and would

771 represent an equivalent Epoch of geological time, is not synonymous with anthropogenic

772 impact. The lower boundary of anthropogenically-modified deposits (or archaeosphere in an

773 archaeological context) may commonly be a marked unconformity, with the overlying first

774 expression of the archaeosphere often being markedly diachronous over millennia

775 (Edgeworth et al. 2015). Such deposits represent a lithostratigraphic – and when one

776 considers technofossils – also a biostratigraphic unit, but not a chronostratigraphic

777 subdivision with a necessarily isochronous basal boundary. The Anthropocene, if it is to be

778 distinguished within these deposits, requires continuous stratiform accumulation of

779 sediments within which a clear signal can be recognised that can distinguish Anthropocene

780 anthropogenic deposits from underlying Holocene anthropogenic deposits. Although such

781 distinguishing signals can be readily found within these deposits, e.g. novel minerals,

782 aluminium, concrete, plastics, organic compounds (Waters et al. 2016, Zalasiewicz et al.

783 2016a and references therein), the successions overall are typically marked by numerous

784   internal erosion/hiatus surfaces; anthropogenic deposits are mainly formed by intermittent

785   depositional events, lack simple vertical accretionary patterns, and are commonly disturbed

786   by 'anthroturbation'. The pattern of such complex erosional/non-depositional surfaces is of

787   great value for local correlation, and also for correlation over wider areas where exact

788   synchronicity is not required, but hinders precise regional to global correlation (Edgeworth

789   et al. 2015). The typical stratigraphic incompleteness of these deposits also makes them

790   generally unsuitable for hosting a GSSP. Furthermore, they are also mostly terrestrial

791   (although increasingly they are also becoming a feature of the marine realm), making some

792   of them prone to erosion. However, artificial deposits have potential for direct preservation

793   over geological time scales when located on subsiding environments such as major deltas

794   (see section 3.4) and within subsurface excavations (Zalasiewicz et al. 2014b).

795

796   Table 3 summarises the key advantages and disadvantages of using anthropogenic deposits

797   and examples of these extraordinarily diverse successions are provided: the Fresh Kills

798   Landfill (New York), Teufelsberg (Berlin) and in Vienna, all of which are examples of artificial

799   ground; and the Gorrondatxe-Tunelboca beachrock (northern Spain), a naturally formed

800   succession comprising mainly artificial materials (Figure 2).

For:	Against:
• Abundant, mainly terrestrial and notably in urban settings • Comparatively thick; rapid accumulation • Independent dating using ^{210}Pb and ^{14}C and historical and archaeological context • Highly resolvable technofossil stratigraphy • Rapid incorporation of novel materials and geochemical signals	• No annual lamination • Limited extent in oceans • Limited lateral continuity • Highly variable deposition rates • Numerous omission surfaces • Prone to erosion and organic degradation • No guarantee of principle of superposition

801   **Table 3**. Reasons for and against using an anthropogenic deposit as a potential host for a GSSP.

3.1.1 Fresh Kills Landfill, New York

Fresh Kills Landfill on Staten Island (USA) is a former repository for New York City refuse. Covering some 8.9 million m^2, up to 70 m high, and containing ~150 million tons of municipal waste, it may be the largest human-engineered formation in the world (Melosi 2016). It was opened in 1948 CE (Melosi 2016), with a peak influx of garbage reaching 29,000 tons per day (Nagle 2008) and closed in 2002 CE, the last debris being from the 9/11 event in 2001 CE. The deposit rests upon Holocene estuarine marsh deposits, with few intervening pre-mid-20th century anthropogenic deposits, has complex internal patterns, having accreted laterally as the site expanded, and may even have been overturned in places. Its internal complexity precludes it from hosting a functional GSSP.

3.1.2 Teufelsberg, Berlin

Rubble generated in Berlin during World War II was later redistributed in mounds within the city boundary, the largest being the Teufelsberg. The rubble, including concrete, brick, clinker, rock, fly ash, slag and solid chemical waste, was deposited between 1950 and 1972 CE and is up to 80 m thick, with an area of 1.1 million m^2, and an original rubble volume of 26.2 million m^3 (Mielke 2011, Cocroft and Schofield 2012). The Teufelsberg deposit mainly rests unconformably upon Upper Pleistocene sand and till, and these areas would be unsuitable for hosting a GSSP for that reason. But locally, thin Holocene deposits occur between the two units, and here the placing of a GSSP might be considered. The Teufelsberg comprises a distinct, mappable lithostratigraphic unit with a base approximating to that of the Anthropocene, which also extends lens-like across other rubble heaps of the Berlin area (cf. Zalasiewicz et al. 2016a), and these can be correlated through technofossil and novel material inclusions with other such deposits elsewhere. Similar lens-like post-World War II

825 rubble heaps in Germany occur also at Cologne, Dresden, Frankfurt am Main, Hannover,

826 Leipzig, Stuttgart and Munich, and in England in heavily bombed cities such as Coventry.

3.1.3 Vienna, Austria

828 In the 19th century, Eduard Suess (1862, 1897) mapped urban strata in Vienna as a geological

829 unit (Schuttdecke), which comprised anthropogenic strata formed during development of

830 the Ringstrasse. The deposits typically range from 4 to 5 m in thickness, locally reaching 10–

831 12 m where infilling the former 17th century city moat, and include brick fragments, broken

832 glass, coins, clay jars, and bones of humans and domestic animals. Subsequently, these

833 artificial deposits extended laterally and aggraded vertically, with the newer Anthropocene

834 materials being of distinctively different composition to those described by Suess. The

835 succession of anthropogenic strata below Vienna dates back to the Neolithic, and has been

836 more or less continuous since Roman times, but many unconformities and much reworking

837 make them typically unsuitable for hosting a GSSP.

3.1.4 Gorrondatxe-Tunelboca beachrock, Spain

839 The Gorrondatxe-Tunelboca beachrock (Figure 2) comprises 1 million tonnes of sediments

840 accumulated since the 1940s. Its source is the 30 million tonnes of blast furnace waste that

841 was tipped offshore between 1902 and 1995 CE (Irabien et al. 2015). Wave activity

842 transported the waste and it re-sedimented as a beachrock deposit about 1.8 km long and

843 50 to 100 m wide. The succession comprises up to 7 m of deposits of anthropogenic origin,

844 resting on up to 2.5 m of bioclastic beach sands (Martínez-García et al. 2013). The lowermost

845 high-energy open beach deposit pre-dates the discharges of iron slag and has a distinct

846 foraminiferal assemblage (Figure 2). This is overlain by sands with an anthropogenic

847 component, where the foraminifera decrease upwards in abundance (assemblage 2 of Fig.

848 2), and then decrease in diversity to become largely monospecific (assemblage 3). The

849 decrease in foraminiferal abundance and diversity coincides with the dumping of the iron

850 foundry deposits offshore. The upper deposits comprise a foreshore succession of cemented

851 conglomerate of furnace bricks, foundry slag with an upper sandy deposit that includes

852 plastics (Zalasiewicz et al. 2016a). Internal erosion surfaces are present throughout, as in any

853 beach deposit. Access to the section is good, the site coinciding with the existing GSSP for

854 the Lutetian Stage (Middle Eocene), while the beachrock deposits are recognised as Geosite

855 96 of the Basque Region. The supply of anthropogenic materials to the shelf ceased in the

856 1990s, and the beach deposits have started to be eroded by waves, and so have limited

857 potential for long-term preservation. The presence of internal erosion surfaces, the lack of

858 clear lateral continuity, absence of annually laminated deposition, and poor preservation

859 potential of the site make it unsuitable for hosting a candidate GSSP.

860

861
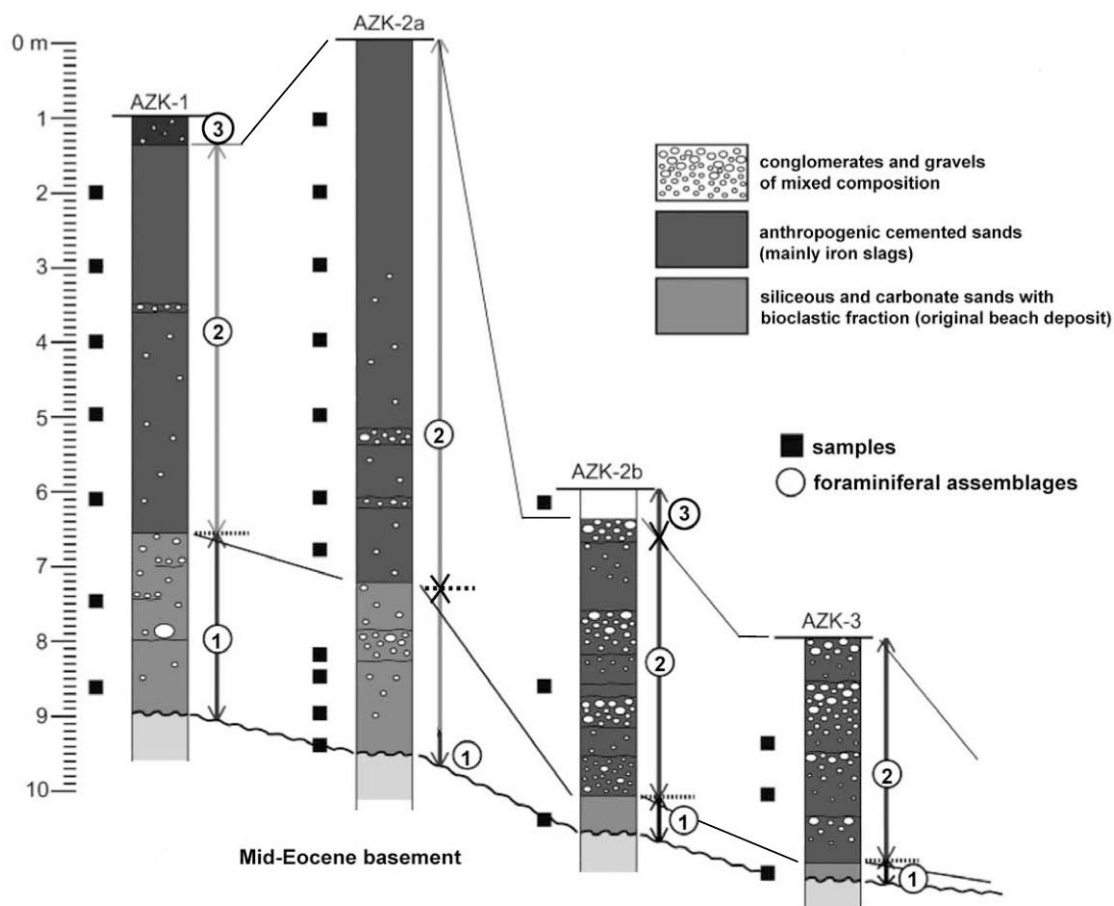
Figure 2. Cores through the Gorrondatxe-Tunelboca beachrock, Spain. A natural high-energy open beach sand deposit, pre-dating the discharges of iron slag, is overlain by cemented sandy and coarse beach deposits that are commonly conglomeratic with abundant slag clasts and incorporating littoral foraminifera. Three distinct foraminiferal assemblages are recognised (ranges for assemblages 1, 2 and 3 marked by arrows). Modified from Martínez-García et al. 2013.

3.2 Marine anoxic basin deposits

The oceans where water is >200 m deep comprise about 66% of the Earth's surface, and the sediments that accumulate there might be expected to preserve relatively complete and less disturbed successions compared with those on land or on the continental shelf. However, for deep-ocean deposits to form outcrops on land, rapid rates of uplift are needed and the prospects of such outcrops diminish with increasingly young deposits. Deep marine deposits of the Anthropocene, therefore, almost invariably need to be cored in situ. Cores are not ordinarily used for GSSPs because of their limited material and access, although exceptions were made for the base of the Holocene (Walker et al. 2009), and the proposed base of the Middle Holocene (Walker et al. 2012), both in ice cores. A case might therefore be made for an Anthropocene GSSP in a deep-ocean core. However, deep-ocean deposits often have low sedimentation rates limiting time-stratigraphic resolution, possess few terrestrial fossils, commonly show reduced preservation of calcareous microfossils, and are generally bioturbated, blurring the stratigraphic record in detail. Nevertheless, GSSPs have been located in relatively deep-water facies now preserved in terrestrial cliff sections, as in the Gelasian and Calabrian GSSPs of the Quaternary (Head and Gibbard 2015). Zalasiewicz et al. (2014c) recognised two distinct deep marine systems, the clastic wedges of turbidite fans and contourites that occur adjacent to the continents, and the slowly accumulating deep-sea oozes that lie beyond. In the modern deep ocean, both of these environments may be

887   affected by human activity, directly or indirectly. Anthropogenic modification of river

888   systems, notably through dam construction on major rivers (e.g. Syvitski and Kettner 2011),

889   and trawling on the upper continental slope (e.g. Martin et al. 2015), directly affect sediment

890   supply, as does, indirectly, global warming and resultant rising sea-level. In the abyssal

891   depths the main impacts are: litter, especially plastics (Ivar do Sul and Costa 2014,

892   Zalasiewicz et al. 2016a); organic and inorganic chemical contamination, including radiogenic

893   fallout signals; effects associated with atmospheric CO_2 increase and warming such as

894   variations in pH, dissolved oxygen content and $\delta^{13}C$; and resultant biological changes

895   (Zalasiewicz et al. 2014c, Table 2). Sediment accumulation rates in the deep oceans are

896   typically on the scale of 1–4 mm kyr^{-1} (Tyson and Pearson 1991), with the lowest rates at

897   abyssal depths farther from shore. In such distal settings, the Anthropocene would be sub-

898   millimetric in thickness, with the Holocene represented by just ~10–50 mm.

899

900   A suitable marine environment for a GSSP would include rhythmic varves associated with

901   seasonal variation in sediment input that provides exceptionally high temporal resolution

902   (Schimmelmann et al. 2016). For GSSP consideration, such varved successions would need to

903   show little or no disturbance through storm or current activity, bioturbation or trawler

904   fishing, but at the same time be characterised by sufficiently high rates of sedimentation to

905   accumulate an adequate thickness of strata to represent the Anthropocene. Marine anoxic

906   basins appear to be potentially suitable environments, where varve preservation is favoured

907   by oxygen-deficient bottom waters, associated with thermal/or chemical density

908   stratification and enhanced organic accumulation at depth through increased primary

909   productivity in the photic zone, either through coastal upwelling or eutrophication

910   (Schimmelmann et al. 2016).

911

912 Varved marine anoxic basin successions can be correlated laterally over tens to thousands of

913 kilometres and can record changes to large-scale ocean and atmospheric circulation patterns

914 (Schimmelmann et al. 2016). Marine varved successions are logistically difficult to collect and

915 as a consequence few modern records have received detailed multi-proxy studies including

916 varve counting in coordination with radiometric dating (Schimmelmann et al. 2016).

917

918 Marine anoxic/dysoxic basins are mainly semi-enclosed basins where the water mass is

919 isolated from the main shelf, typically below ~100 m and the reach of storm mixing of shelf

920 waters. This can occur in depressions on the continental shelf (e.g. the Santa Barbara and

921 Cariaco basins), in fjords, (e.g. Saanich Inlet and Saguenay Fjord) or in enclosed seas, (e.g. the

922 Black and Baltic seas), but areas with periodic anoxia can also occur on an open shelf (e.g.

923 Middle Atlantic Bight, northern Gulf of Mexico, Namibia, Peru) (Tyson and Pearson 1991,

924 Figure 3), or on a continental slope on which impinges a well-developed anoxic oxygen-

925 minimum zone (southeastern Pacific off Peru, northwestern Arabian Sea).

926

927 De-oxygenated dead zones currently occur over ~245,000 km^2 of the coastal oceans (Diaz

928 and Rosenberg 2008), or about 0.7% of the sea floor. The number of these dead zones has

929 approximately doubled each decade since the 1960s (Diaz and Rosenberg 2008). About half

930 of them are the consequence of eutrophication through runoff of fertilisers into the sea,

931 increased primary productivity and enhanced organic flux to the sea bed (Diaz and

932 Rosenberg 2008), and so they tend to occur offshore or downriver from populated areas

933 (Figure 3). Most dead zones are currently seasonal, tending to occur in the summer after

934 spring blooms, when the water is warmest and stratification is strongest (Diaz and

935 Rosenberg 2008). Autumn storms bring a temporary return of benthos, disrupting seabed

936 stratification. Only ~8% of dead zones are persistent (Diaz and Rosenberg 2008), these areas

937 experiencing the least sediment bioturbation, though in open oceans these seem not yet to

938 have developed varves. Sediments of modern dead zones are a local expression of

939 Anthropocene-related conditions, and identifiable by changes in geochemical character and

940 fauna (Diaz and Rosenberg 2008), but they seem unlikely to provide good potential for

941 candidate GSSPs, as they typically rest on the bioturbated deposits of the earlier more

942 consistently oxygenated sea floor.

943
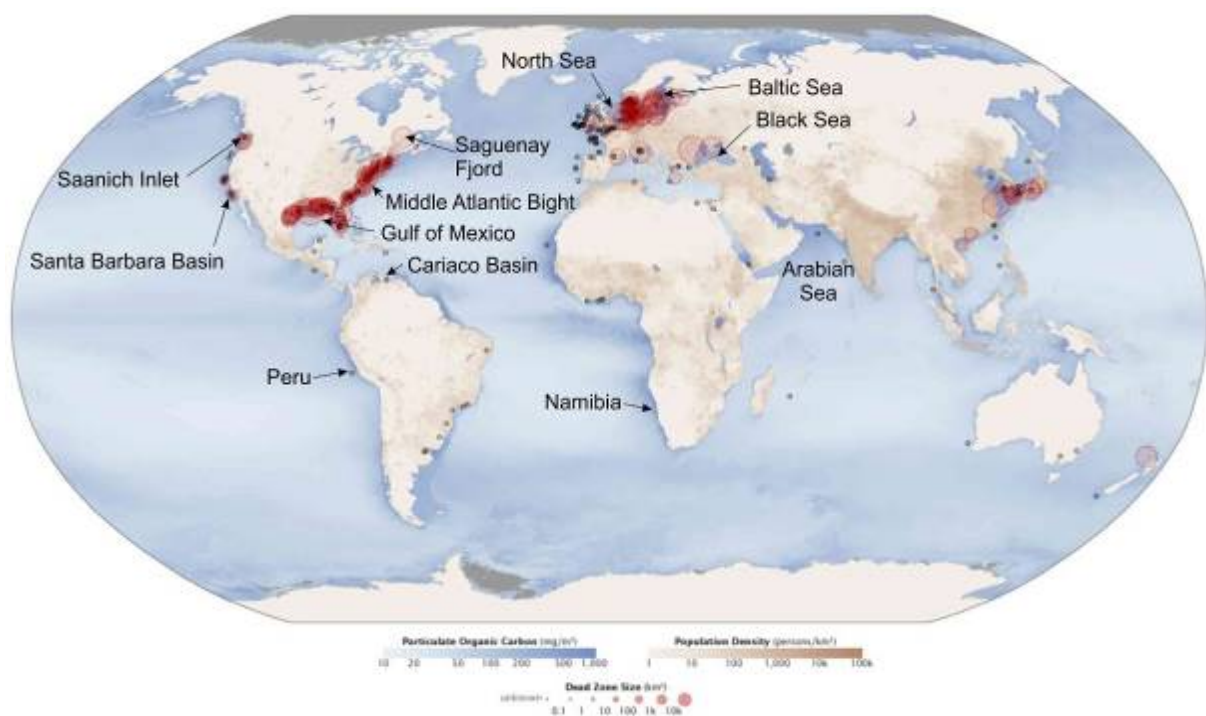
944

945 **Figure 3.** Location of marine dead zones (from NASA Earth Observatory

946 https://earthobservatory.nasa.gov/IOTD/view.php?id=44677; Aquatic Dead Zones generated 17th

947 July 2010). Red circles show the location and size of the dead zones. Black dots show where dead

948 zones of unknown size have been observed. The distribution commonly occurs adjacent to populous

949 land areas (shown by the brown scale), but not to upwelling zones (shown by concentration of

950 particulate organic carbon, in blue scale).

951

952 Litter from ships is now seen in most sea floor surveys (Ramirez-Llodra et al. 2011). Clinker,

953 from coal burnt to power steam-ships, was extensively dumped on the sea floor from ~1800

954   to ~1950 CE (Ramirez-Llodra et al. 2011), and may form a useful signal for latest Holocene

955   strata. Much power station fly-ash and clinker has also been dumped at sea, e.g. Blyth power

956   station ash into the North Sea, UK (Bamber 1980). Plastics and aluminium largely date from

957   after 1950 CE, with land-derived microplastic beads and plastic fibres now a near-universal

958   component of low-energy modern marine sediments (Ivar do Sul and Costa 2014,

959   Zalasiewicz et al. 2016a). With about 4.9 billion tons discarded (which is 60% of all plastics

960   produced since 1950) in geologically unstable waste dumps to uncontrolled deposition in

961   terrestrial, aquatic and marine environments (Geyer et al. 2017), the quantity of plastic

962   debris entering the oceans was estimated at 4.8–12.7 million tonnes in 2010 CE (Jambeck et

963   al. 2015) and might strongly increase in the future. However, little work has been done to

964   profile its stratigraphic distribution in marine sediment cores.

965

966   Table 4 summarises the key advantages and disadvantages of marine anoxic basin deposits

967   for hosting a potential GSSP. Well-studied examples (explored below) include the Santa

968   Barbara Basin (California), Black Sea, Saanich Inlet (Canada), Saguenay Fjord (Canada) and

969   Cariaco Basin (Venezuela).

For:	Against:
• Undisturbed laterally extensive varves (below storm base) correlatable within basins • Independent ^{210}Pb and ^{14}C dating • Anoxic/dysoxic/hypoxic, no/little benthic bio /anthroturbation • Modification of fluvial input to oceanic basins • Clinker ash from steam-powered ships ~1850-1950 CE; microplastics signal post-1950 CE • Coastal eutrophication since mid-20th century • High organic and clay components scavenge contaminants from water column e.g. metals, radionuclides and POPs • Global radionuclide signal (e.g. ^{239}Pu, ^{14}C)	• Restricted extent (~0.7% of oceans) • Possibility of missing/additional laminae in near-coastal settings due to turbidite events • Thin strata, e.g. last 75 years <20 cm for the for Santa Barbara Basin and 75 cm for Saanich Inlet • Potential decadal time delay for Pu/metal contaminants to reach sea-bed (but settling velocity of ~2000 m yr^{-1} if present as grains, see Kowalski et al. 2016) • Difficult and costly environment to collect samples without disturbance of youngest laminae

• Planktonic foraminifera and diatoms as bio/geochemical signals	

970   **Table 4.** Reasons for and against using a marine anoxic basin deposit as a potential host for a GSSP.

971   ### 3.2.1 Santa Barbara Basin, California

972   The Santa Barbara Basin lies 100 km west of Los Angeles, USA (Figure 3), at depths of up to

973   590 m. Varves comprise dark terrigenous laminae derived from greater winter river runoff

974   alternating with paler summer bloom laminae with diatoms (mainly *Chaetoceros*), planktonic

975   foraminifera, radiolaria and silicoflagellates (Koide et al. 1975, Field et al. 2006, Barron et al.

976   2015), reflecting seasonal NW winds that cause upwelling and increase biogenic productivity

977   (Barron et al. 2015). Varves have been dated using ^{210}Pb (Krishnaswami et al. 1973, Koide et

978   al. 1975) and radiocarbon AMS (Schimmelmann et al. 2013). Before 1700 CE some drought

979   years did not produce varves, with intermittent oxygenation events causing bioturbation, but

980   from the 18th century to the present the lamina have been shown to be consistently annual

981   and without gaps (Hendy et al. 2013, Schimmelmann et al. 2013). Strata below the upper ~1

982   cm are highly anaerobic so there is little bioturbation of the laminae or leaching of Pu (Koide

983   et al. 1975). A distinct 1841 CE bioturbated layer is associated with a flood and turbidite

984   event (Hendy et al. 2013). There are no flood event deposits younger than 1930 CE

985   (Krishnaswami et al. 1973), as dam construction along rivers feeding into the basin began in

986   1912 CE, limiting sediment supply. Despite this, there has been substantial sediment flux

987   since 1928 CE (Krishnaswami et al. 1973, Figure 4b), with a post-compactional thickness of

988   ~0.5–3 mm per lamina, the diatom ooze lamina component being up to 2 mm thick

989   (Schimmelmann et al. 2016).

990

991   The high organic carbon (3–5%) and clay fractions of the sediments scavenge heavy metals,

992   including Pu, from seawater. The $^{239+240}$Pu concentrations initially rise in 1945–1949 CE

varves, exceeding background values in the 1950–1954 CE varves (Figure 4a), and continuing

to rise into the 1970s (latest data available), with no sign of a distinct 1963–1964 CE bomb

spike (Koide et al. 1975), perhaps reflecting the slow settling of Pu in deep water. Radiogenic

particles settle only slowly through the water column, at 12.5 m yr^{-1} in the western Pacific

(Livingston et al. 2001). But when such particles are bound within marine snow/faecal pellet

aggregates they sink more quickly, at an estimated 74–39 m day^{-1} in the Santa Barbara Basin

(Alldredge and Gotschalk 1988), allowing rapid transmission to the sea-floor. The continued

rise of the Pu signal after the 1963–1964 CE bomb spike likely reflects reworking of

terrigenous fallout into the basin (Koide et al. 1975), suggesting the first $^{239+240}$Pu signal

above background, rather than a peak value, as a possible primary marker for the

Anthropocene (Zalasiewicz et al. 2015). An ancillary radiogenic signal of ^{238}Pu, sourced from

the Snap 9A satellite burnup in 1964 CE, does show a 1964 CE peak (Koide et al. 1975, Figure

4a), suggesting both little mobility of Pu within the sediment and little reworking of that

radioisotope.

Heavy metal signals in the basin are complex. A rise in Pb concentrations from 1931 CE

(Figure 4c) is due to airborne particulates from leaded gasoline, derived from increased

automobile use in Los Angeles, with levelling off from the 1970s representing introduction of

unleaded gasoline (Schmidt and Reimers 1991). Cu values increase notably from about 1960

CE, probably industrially sourced via sewage outfalls (Schmidt and Reimers 1991). Reduced

anthropogenic input, in the case of Cd since the 1970s, may reflect improved sewage

treatment (Schmidt and Reimers 1991).

Among organic geochemical signals, a significant oil spill from a production well in 1969 CE

increased Total Organic Carbon (TOC) values, generating a distinctive hydrocarbon signature

(Hendy et al. 2015). Polychlorinated biphenyls (PCBs) appeared in the basin sediments about

1019 1945 CE, the DDT pesticide breakdown product DDE [1,1-dichloro-2-2-bis(p-chlorophenyl)

1020 ethylene] first appearing ~1952 CE. Concentrations of both show a progressive increase

1021 through to 1967 CE (Hom et al. 1974); they may be sourced from sewage outfalls and surface

1022 runoff, while DDE can also arrive via atmospheric fallout (Hom et al. 1974).
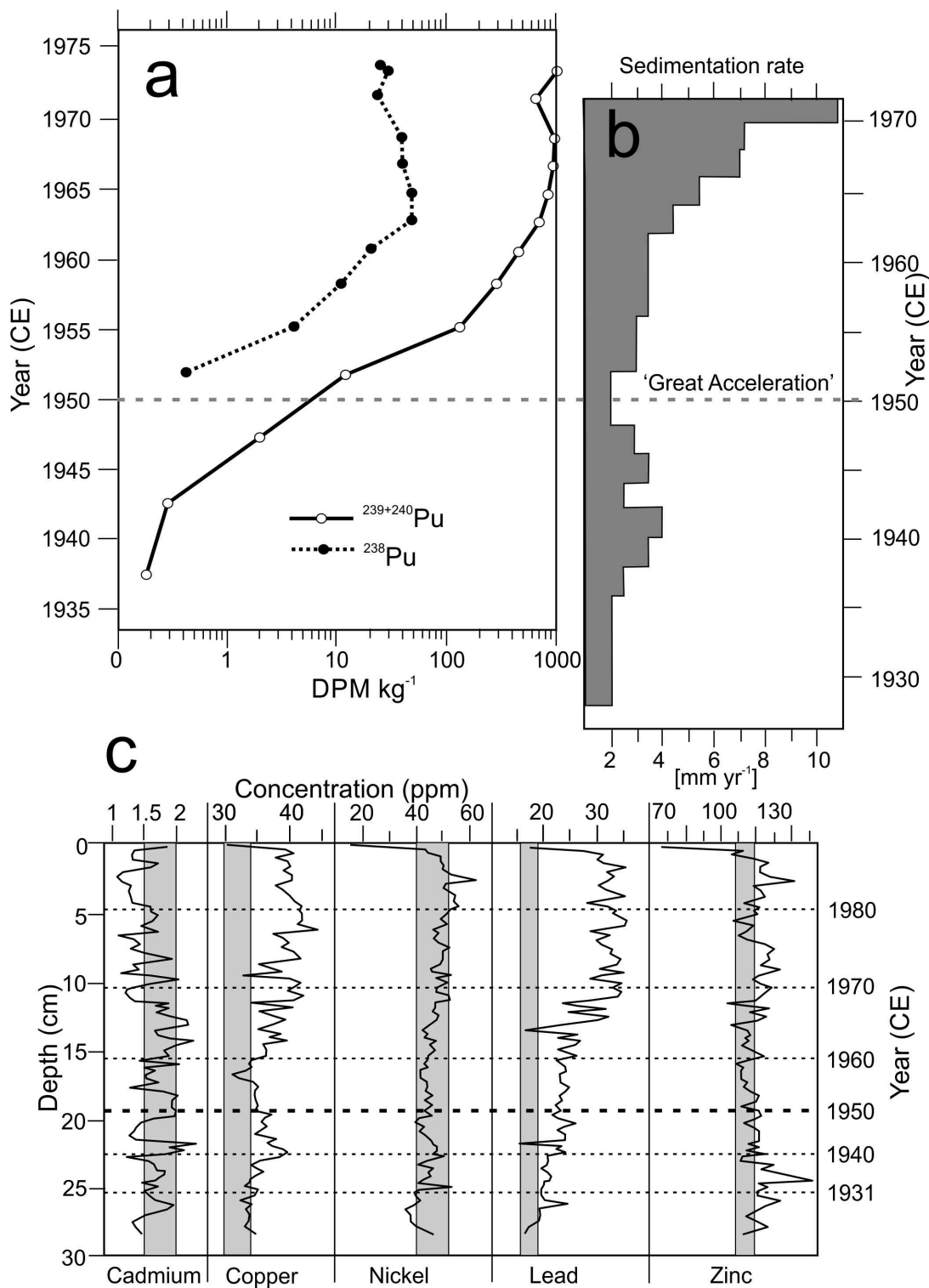

1023
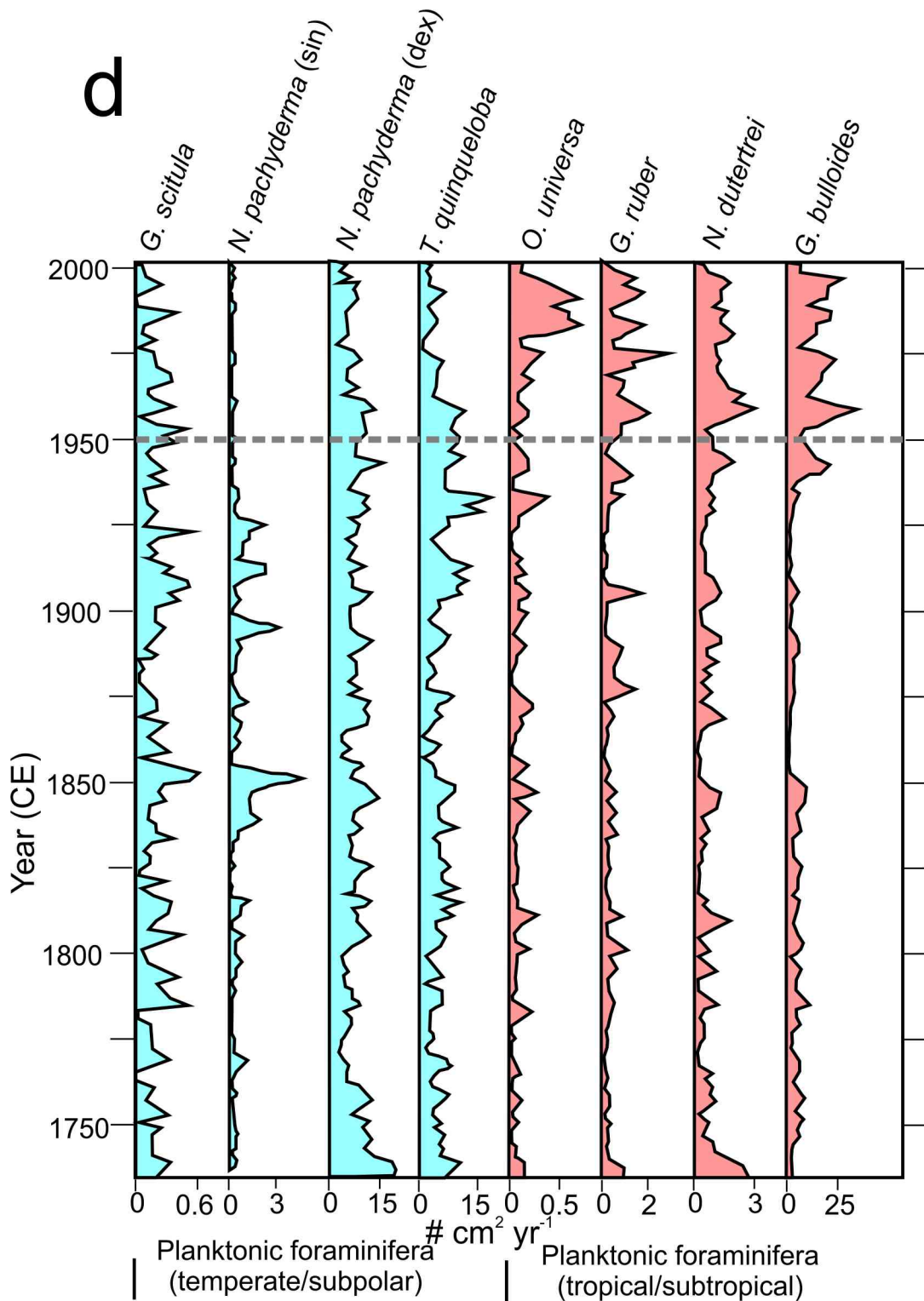
Figure 4. Key signals in marine cores from the Santa Barbara Basin, with a) Pu signal (Koide et al. 1975), b) variations in sedimentation rates (Krishnaswami et al. 1973), c) selected heavy metals (Schmidt and Reimers 1991) and d) planktonic foraminifera (Field et al. 2006).

1030 The basin is located close to the boundary between the subarctic and subtropical gyres, the

1031 planktonic foraminiferal assemblages reflecting the dominance of one or other of these

1032 gyres (Barron et al. 2015). In a 1400-year dataset, decadal-scale fluctuations (the Pacific

1033 Decadal Oscillation) dominate, the two assemblages co-varying until 1959 CE (Figure 4d),

1034 after which there is increasing abundance of tropical/subtropical species, especially after the

1035 mid-1970s (Field et al. 2006). A complementary decrease in temperate/polar species in the

1036 late-20th century indicates the penetration of deep warm waters (Field et al. 2006). Evidence

1037 of such pronounced warming is not seen earlier in the record, not even during the Medieval

1038 Climate Anomaly (Barron et al. 2015). This warming is thought to reflect widespread change

1039 in the Northern Pacific in the mid-1970s, with greater cyclonic activity of the Aleutian Low

1040 Pressure System and warming in the eastern North Pacific (Field et al. 2006). Observed

1041 decreases in algae, zooplankton (which show 80% decline between 1951 and 1993 CE), fish

1042 and seabird abundance have also been related to this temperature increase (Roemmich and

1043 McGowan 1995).

1044 ## 3.2.2 Black Sea

1045 The Black Sea is an enclosed silled basin with an area of 422,000 km^2 and a maximum depth

1046 of 2212 m (Florea et al. 2011). The water column is stratified, with the pycnocline and

1047 halocline both occurring at about 75 m depth in the centre of the basin and 200 m at the

1048 margins, and marking the boundary between oxygenated water above and euxinic, H_2S-

1049 saturated and saline deeper waters below (Arthur et al. 1994, Florea et al. 2011). At the

1050 seafloor, there is a topmost gelatinous flocculent surface layer about 2 cm thick overlying a

1051 further 2 cm of unlaminated grey/white carbonate-rich sediment (Pilskaln and Pike 2001).

1052 The underlying unit (Unit I) is 25–45 cm thick and represents 1633 ± 100 years of

1053 sedimentation, based upon varve chronology (Arthur et al. 1994). This unit, present in the

1054 deeper parts of the basin, contains varves averaging 0.2 mm thick, consisting of thicker

1055 white carbonate-rich summer/autumn laminae with abundant *Emiliania huxleyi* coccoliths

1056 alternating with thinner grey clastic-rich laminae deposited from spring and winter river

1057 runoff (Arthur et al. 1994, Pilskaln and Pike 2001, Schimmelmann et al. 2016). Black organic-

1058 rich laminae with biogenic metal sulphides occur between the carbonate and terrigenous

1059 laminae (Pilskaln and Pike 2001, Schimmelmann et al. 2016). The top flocculent layer is

1060 thought to be a permanent transition zone that hydraulically sorts particles by density

1061 (Pilskaln and Pike 2001).

1062

1063 The varves have been independently dated using ^{210}Pb, ^{137}Cs and ^{14}C AMS, although the

1064 latter commonly gives older ages due either to the presence of "dead" carbon in Black Sea

1065 sediments or missing varves (Arthur et al. 1994, Pilskaln and Pike 2001, Florea et al. 2011).

1066 Although the highest countable varves beneath the flocculent layer date to about 1918 CE

1067 (Arthur et al. 1994), Florea et al. (2011) discerned the 1986 CE Chernobyl ^{137}Cs signal at

1068 between 5 and 10 mm depth (in samples collected in 2004 CE), which agrees with a ^{210}Pb-

1069 dated accumulation rate of 0.49 ± 0.03 mm yr^{-1}. Groups of varves in Unit I have been

1070 correlated across the entire deeper basin (Arthur et al. 1994), with no sign of erosion by

1071 interbedded cm- to dm-scale fine-grained turbidite layers (Arthur et al. 1994).

1072 ### 3.2.3 Saanich Inlet, Canada

1073 Saanich Inlet is a 24 km long, up to a ~240 m deep, silled fjord in Vancouver Island, Canada,

1074 in which the water column shows stratification by density, salinity and temperature, with

1075 deep anoxic water containing hydrogen sulphide (Schimmelmann et al. 2016). Bottom water

1076 renewal is restricted to brief episodes of coastal upwelling during late summer, with H$_2$S

1077 otherwise present in water as little as 120 m deep (Anderson et al. 1989). Maximum river

1078 discharge and minimum salinity occur during summer months (McQuoid and Hobson 1997).

1079 Modern sediments include varves in which pale diatomaceous laminae (1.5–17 mm thick),

1080 with distinct seasonal assemblages, alternate with terrigenous silty clay laminae (0.5–6 mm

1081 thick) deposited in winter (Dean et al. 2001, Dean and Kemp 2004). The varves have been

1082 independently dated using ^{210}Pb, ^{137}Cs and ^{14}C (Matsumoto and Wong 1977, McQuoid and

1083 Hobson 1997). Laminated intervals during the Holocene are punctuated by massive debris

1084 flow event beds (Dean et al. 2001). Laminae dated from 1950 CE have been recognised at a

1085 depth of about 75 cm (McQuoid and Hobson 1997).

1086

1087 Biostratigraphic indicators include the invasive diatom *Rhizosolenia setigera*, abundant in

1088 autumn blooms (Dean et al. 2001), and introduced in the early 1940s through the arrival of

1089 aquaculture species and/or from ship ballast waters, both potential sources increasing in the

1090 1930s and 1940s (McQuoid and Hobson 1997). This invader partly supplanted the species

1091 *Thalassiosira gravida* and *Chaetoceros diadema*, which were more abundant prior to the

1092 1930s to 1940s, the assemblages also reflecting increased logging, farming and urbanization,

1093 especially from the 1930s (McQuoid and Hobson 1997). Sinking rates of these organisms,

1094 when present in aggregates, may reach 50 to 100 m day^{-1} (McQuoid and Hobson 1997 and

1095 references therein) meaning that the biotic signal in varves is highly responsive to seasonal

1096 changes in abundance in the surface waters. The stratigraphic record shows an abrupt

1097 regional climate shift in 1976/1977 CE, with the modern Pacific Decadal Oscillation changing

1098 to 22-year periodicity, in contrast to ~15-year periodicity recorded over the previous 2100

1099 years (Dean and Kemp 2004).

1100

1101 Heavy metal residence times in the water column of the inlet are an estimated 0.08 years for

1102 ^{210}Pb, 0.07 years for stable Pb, 0.3 years for Cu, 3 years for Cd, and 2 years for Hg

1103　(Matsumoto and Wong 1977). This indicates a near-synchronicity of the influx of Pb into the

1104　inlet and its subsequent accumulation in the sediments.

1105　3.2.4 Saguenay Fjord, Canada

1106　The Saguenay Fjord, Quebec, Canada, is a submarine valley, 93 km long and 1–6 km wide

1107　which links to the St. Lawrence Seaway via a shallow, 20 m deep sill (Gagnon et al. 1997).

1108　The fjord comprises two distinct basins with a deeper and larger landward basin up to 275 m

1109　deep and a seaward basin up to 250 m deep (Gagnon et al. 1997). The succession is dated

1110　with ^{210}Pb and ^{137}Cs (Loring et al. 1983, Smith and Levy 1990). Sediment accumulation rates

1111　in the landward basin are 0.2–0.4 cm yr^{-1} (Smith and Walton 1980). The deeper waters are

1112　generally saline, well-mixed and oxygenated with the redox boundary present a few

1113　centimetres below the sediment surface (Gagnon et al. 1997), but organic-rich effluent from

1114　pulp and paper mills produces anoxic, unbioturbated sediments at the head of the fjord

1115　(Smith and Levy 1990), making that location more suitable as a potential GSSP target locality.

1116

1117　The Saguenay Fjord has been affected by industrial and municipal waste discharges since the

1118　1930s (Loring et al. 1983, Smith and Levy 1990). Very high Hg concentrations, and significant

1119　Zn, Pb, V and Cd contamination are evident in fjord sediments dating from 1948 CE, with

1120　peak values in the early 1960s and early 1970s (Loring et al. 1983, Gagnon et al. 1997). Most

1121　of the Hg is bound to organic matter (Loring et al. 1983), limiting Hg diffusion through the

1122　sediment (Gagnon et al. 1997). The oxidized surface sediments inhibit transfer of Hg to the

1123　overlying bottom waters, although surface bioturbation may reduce the efficiency of this

1124　barrier (Gagnon et al. 1997). Sustained high Hg values suggest resuspension of the Hg by

1125　spring runoff or frequent submarine mass flow events (Gagnon et al. 1997). A time lag of a

1126 few months at the head of the fjord and 10–15 years at the seaward end (Loring et al. 1983)

1127 makes the Hg signal markedly diachronous.

1128

1129 Polycyclic aromatic hydrocarbon (PAH) concentrations gradually increase in 1926 CE above

1130 pre-industrial levels, with dramatic increases in the 1940s after major expansion of

1131 aluminium production (Smith and Levy 1990). The PAHs in sediments are mainly scavenged

1132 from the water column by organic matter (Smith and Levy 1990).

1133 ### 3.2.5 Cariaco Basin, Venezuela

1134 The Cariaco Basin off Venezuela comprises two euxinic sub-basins of >1400 m depth

1135 separated by a 900 m-deep saddle. It contains a stratified water column, with a thermocline

1136 and a chemocline between 250 and 375 m deep separating oxic waters above from anoxic

1137 waters below (Schimmelmann et al. 2016). The basin has been anoxic since about 12.6 ka BP

1138 (Hughen et al. 1996). Euxinic bottom waters are associated with sediments including varves

1139 (~0.9–3 mm thick, average 1.3 mm) of pale, biogenic (mainly diatoms) winter/spring laminae

1140 rich in planktonic opal, carbonate and organic matter accumulated during arid conditions

1141 when upwelling develops, and dark, siliciclastic summer/autumn laminae deposited during

1142 times of increased runoff, when there is enhanced input of Saharan dust and reduced

1143 upwelling (Hughen et al. 1996, Schimmelmann et al. 2016). Microbioturbation is ubiquitous,

1144 but generally only slightly disrupts the laminae (Hughen et al. 1996). The varves have been

1145 independently dated using ^{210}Pb, ^{137}Cs and ^{14}C AMS (Hughen et al. 1996). Microturbidites a

1146 few mm thick occur throughout, with two distinct turbidites dated to 1897 ± 5 and 1932 ± 4

1147 CE, likely earthquake-triggered, with the older turbidite possibly having eroded a few

1148 centimetres of underlying varves (Hughen et al. 1996, Schimmelmann et al. 2016).

1149

3.3 Coral bioherms, calcified sponges and marine bivalve shells

Shallow-water coral reefs extend over only about 0.1–0.2% of the oceans, and are limited to the tropics, but they contain a large proportion of marine biotic diversity (Figure 5a). They were first impacted by humans via decreasing diversity of large marine animals beginning around 3.5 ka BP, a trend which accelerated during the Industrial Revolution and especially since 1950 CE (Pandolfi et al. 2003, Hoegh-Guldberg 2014). Widespread bleaching of tropical coral reefs in response to rising sea temperatures started in 1979 CE and has subsequently increased in frequency and severity (Hoegh-Guldberg 2014, Hughes et al. 2017). Other significant stressors, including increased turbidity of marine waters due to increased runoff, rises in pollutants, eutrophication and acidification, and severe overfishing, including the dynamiting of reefs by fishermen, have contributed to a 50% reduction in the abundance of reef-building corals over the past 40–50 years. Over the next several decades, this may lead to the collapse of whole reef systems, as happened during mass extinction events of the geological past (Hoegh-Guldberg 2014).
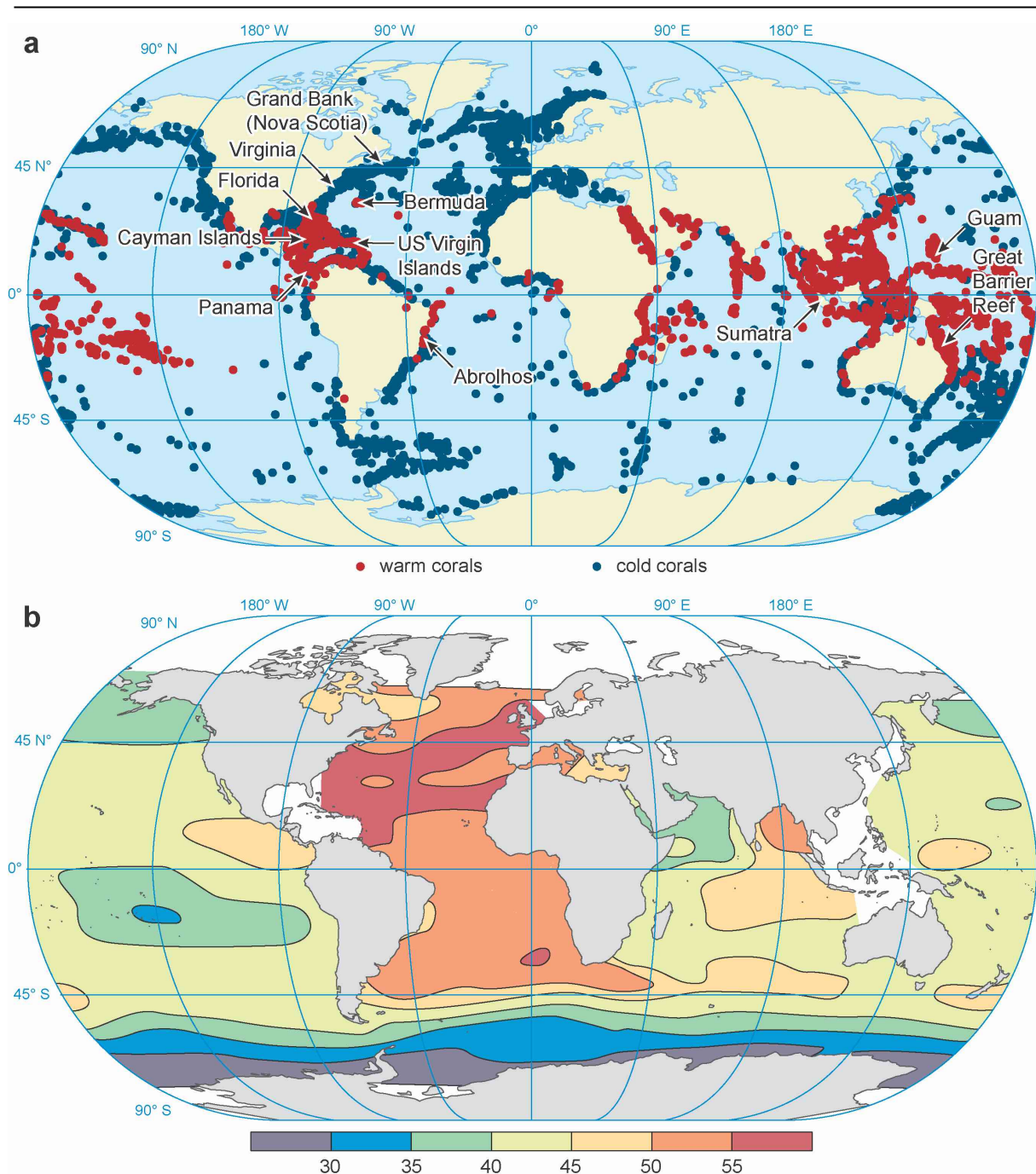
Figure 5. a) Distribution of shallow-water framework-building coral reefs (from NOAA: Where Are

Reef Building Corals Found http://oceanservice.noaa.gov/education/tutorial_corals/

coral05_distribution.html and cold-water corals (from Freiwald et al. 2017) and b) the inventory of

anthropogenic CO_2 (μmol CO_2/kg) in surface waters (from Swart et al. 2010).

Although reef systems as a whole are undergoing significant change, indicating their

importance for recognising anthropogenic impacts, individual reefs are complex and non-

stratiform. Consequently, it is not a reef as a whole that should be considered as hosting a

1174 potential GSSP, but one of the long-lived coral bioherms within it that shows annual growth

1175 bands. In the Great Barrier Reef, fluorescent banding reflects seasonal-interannual variations

1176 in fluvial discharge of organic compounds (Isdale 1984). The annual laminae can be

1177 independently dated using ^{210}Pb and ^{14}C. Key correlatory signals include Pu radionuclide

1178 fallout, the ^{13}C Suess effect and uptake of pollutants, in particular heavy metals (Figure 6a).

1179

1180 Cold-water growths of aragonitic scleractinian corals and proteinaceous corals are smaller

1181 than the tropical reefs, and occupy a range of latitudes and of water depths – from a few

1182 metres to abyssal depths (Figure 5a). Such corals also imprint the Suess effect, radiocarbon

1183 and heavy metal signals, and individual cold-water corals can be long-lived. But, those from

1184 deep waters contain banding that is not necessarily annual, and ages can only be reliably

1185 provided through radiometric dating (Lee et al. 2017). Long-lived bivalves, which also occur

1186 in cold waters, also record proxy environmental signals including water temperature and the

1187 radiocarbon fallout bomb-spike, though they occupy a smaller depth range (up to ~300 m

1188 depth, exceptionally up to 500 m) than cold-water corals.

1189

1190 Calcified sponges (or sclerosponges), found living in water depths up to 145 m, are known to

1191 provide good proxy records of water temperature and salinity, secreting their skeletons

1192 without some of the vital effects seen in corals and clearly showing the Suess effect on

1193 carbon isotopes (Figure 6a). They provide records stretching up to 1000 years, much further

1194 back in time than many corals (Swart et al. 1998). However, they are very slow growing

1195 (~0.22–0.27 mm yr^{-1}) with living tissue accounting for 3 to 4 years of growth; consequently

1196 despite some species showing growth banding, evidence that this is annual is equivocal and

1197 ^{14}C- and ^{210}Pb-dating are required to determine ages (Swart et al. 1998). As such, they seem

1198   to provide a lower resolution and hence less suitable host for a GSSP than corals or bivalves

1199   (see section 3.3.6).

1200

1201   Table 5 summarises the key advantages and disadvantages of using coral laminae in tropical

1202   reef bioherms and cold-water corals and bivalve shells for hosting a potential GSSP. Up to

1203   now, research on corals has rarely provided multi-proxy signals, so the examples provided

1204   below focus on the specific signatures where research has been done.

1205

For:	Against:
• Seasonal growth bands, with large growth rates in shallow-water corals • Independent dating using ^{210}Pb and ^{14}C • Microplastic ingestion in corals, e.g. Great Barrier Reef • Temperature recording (δ^{18}O and Sr/Ca) in corals and bivalves; bleaching events in corals beginning 1979 CE • δ^{13}C Suess effect mirrors anthropogenic CO_2 ocean inventory • Shallow water corals with rapid uptake of radionuclides and contaminants • Heavy metal enrichment is coral-species specific and more sensitive than adjacent sediments	• Shallow, warm-water corals limited to tropics; deep-water corals and bivalves provide greater geographical spread • Reefs are complex structures; signal defined on individual coral or bivalve • Deep-water corals are affected by a ~25 year lag in Δ^{14}C and Pb records compared with shallow-water corals • No GSSP precedent of using living/deceased coral or bivalve

1206   **Table 5.** Reasons for and against using a coral or bivalve shell as a potential host for a GSSP.

1207   ## 3.3.1 Caribbean ^{13}C Suess effect and heavy metal concentrations

1208   Scleractinian corals mirror changes in the anthropogenic CO_2 inventory of surface oceans

1209   (Figure 6a). In a global comparison of rates of change of δ^{13}C in coral skeletons between

1210   1800 and 2000 CE (Swart et al. 2010), 64% showed a marked decrease from the mid-20th

1211   century, attributed to the addition of anthropogenically derived CO_2 (the ^{13}C Suess effect).

1212   The decrease was greatest in areas of largest input of anthropogenic CO_2 (Figure 5b) and, in

1213 Florida and elsewhere in the Caribbean, from 1960 to 1990 CE, was comparable to the

1214 carbon isotopic decrease in atmospheric CO_2 (Swart et al. 2010, Figure 6a). A marked

1215 inflection of $\delta^{13}C$ values is seen at about 1955 CE in Atlantic corals and sclerosponges,

1216 comparable to the $\delta^{13}C$ inflection seen in Law Dome ice core from the Antarctic (Figure 6a).

1217 The rate of change is more variable and less pronounced in the Indian and Pacific oceans

1218 (Swart et al. 2010). There is an average air–sea equilibration time of about 1 year for the

1219 anthropogenically derived CO_2 (Key et al. 2004), resulting in a minimal signal lag in surface

1220 waters. However, anthropogenic CO_2 concentrations decrease with depth, and at about 1000

1221 m water depth the signal is only discernible in the North Atlantic (Key et al. 2004), suggesting

1222 either a significant lag or lack of transport to these depths. Shallow-water corals thus

1223 provide a more effectively correlatable stable carbon isotope signal than do records from

1224 deep marine environments such as deep anoxic basins.
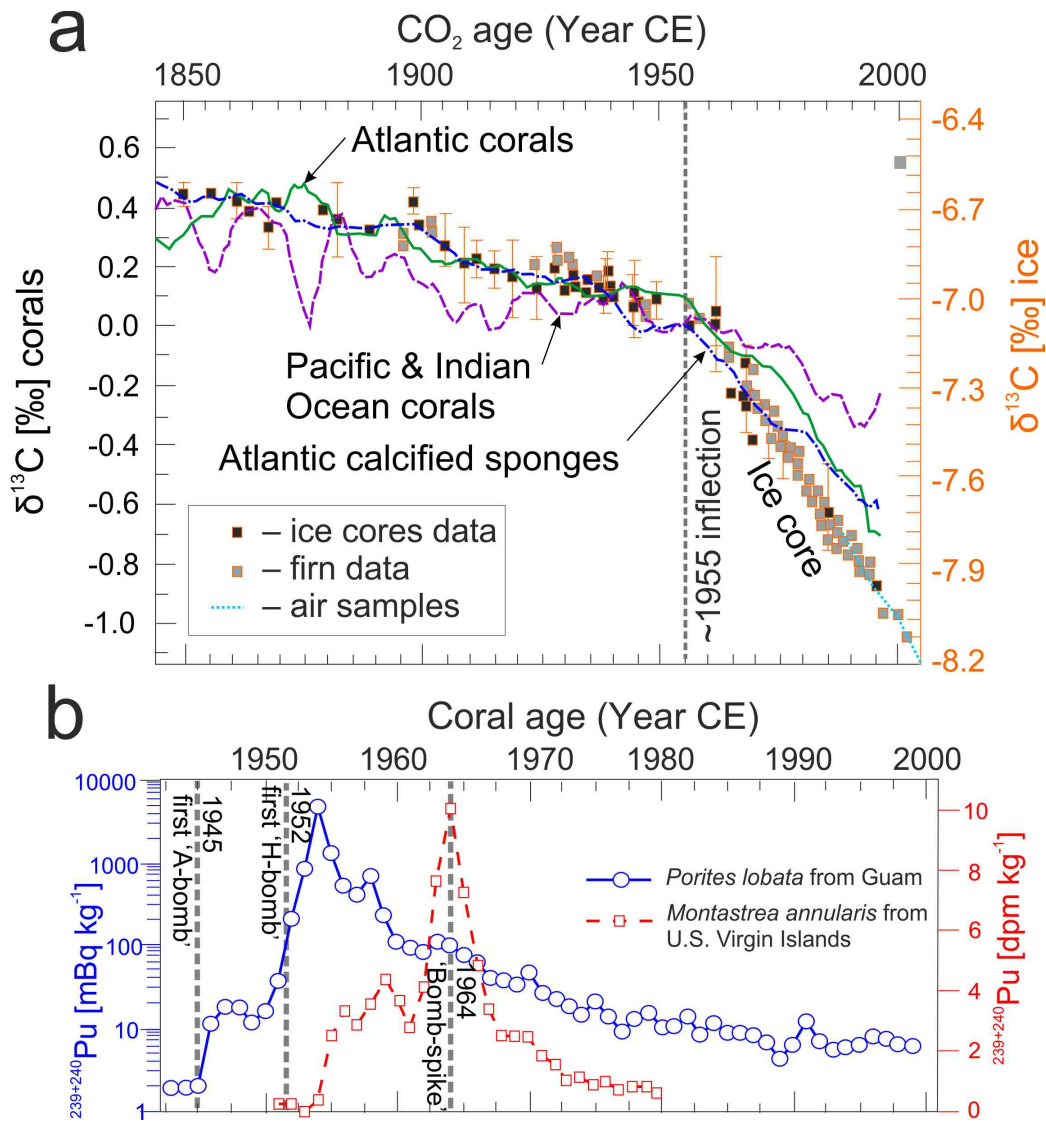
Figure 6. a) Changes in $\delta^{13}C$ with respect to age for corals from the Atlantic and the Pacific/Indian oceans compared to published data from Atlantic calcified sponges, averaged after removing the mean $\delta^{13}C$ value of the coral skeleton from 1900 CE to the present day and shown as a five-year running mean (Swart et al. 2010). This is compared with $\delta^{13}C$ data from Law Dome ice core (Rubino et al. 2013) which show a ~1955 CE inflection; b) $^{240+239}$Pu concentrations in annual growth bands from *Porites lobata* in Guam (Lindahl et al. 2011) and *Orbicella (Montastrea) annularis* in the U.S. Virgin Islands (Benninger and Dodge 1986); dpm kg^{-1} = decays per minute per kilogram; mBq kg^{-1} = millibecquerel per kilogram.

Heavy metal concentrations in Panama tend to be higher in nearshore coral reefs and also in certain species such as *Porites furcata,* and show greater concentrations than in nearby

1237 sediments (Berry et al. 2013). Humans have increased the flux of Pb by at least a factor of 10,

1238 with rapid and widespread dispersal of Pb into the atmosphere as aerosol particles, and a

1239 short residence time of two years within ocean waters (Boyle et al. 2014), which makes Pb

1240 potentially suitable as a stratigraphic marker. Of the oceans, the North Atlantic Ocean is

1241 most affected by Pb emissions from the Industrial Revolution and subsequently it is this

1242 region that has seen most research (Boyle et al. 2014). Corals in Bermuda (Kelly et al. 2009,

1243 Figure 7c) show an initial rise of Pb following exploitation of the Upper Mississippi Valley

1244 lead-zinc ore in the USA, with an initial peak in lead mining in 1840–1848 CE, followed by a

1245 clear increase that began in the late-1940s due to greater consumption of leaded gasoline,

1246 peaking in the 1970s following US environmental legislation (the US Clean Air Act of 1970,

1247 Boyle et al. 2014). Pb in gasoline from the USA typically has $^{206}Pb/^{207}Pb$ ratios >1.17 as

1248 compared to European Pb with ratios <1.15 (Boyle et al. 2014). This is expressed in the

1249 Bermuda corals, although the signal is complex, reflecting the different histories of leaded

1250 gasoline consumption and legislation in the USA and Europe (Bollhöfer and Rosman 2001).

1251 Higher $^{206}Pb/^{207}Pb$ ratios seen in Bermuda until the late-1970s (Figure 7d) are considered

1252 sourced from US gasoline, while the markedly lower ratios in the 1980s and 1990s reflect a

1253 European source (Kelly et al. 2009). Pb settles only slowly into deep oceanic waters, as seen

1254 off Bermuda (Boyle et al. 2014), but this is not a significant factor in contamination of corals

1255 at shallow water depths.

1256

1257 The Pb signal shows global heterogeneity. In the Indian Ocean, significant Pb contamination

1258 started in the western Sumatra region around the mid-1970s, with increasing Pb/Ca ratios

1259 and decreasing $^{206/207}Pb$ and $^{208/207}Pb$ ratios around that time, trends that continue into the

1260 21st century (Lee et al. 2014). Pb emissions from China and SE Asia continue to increase (in

contrast to the pattern in areas fringing the North Atlantic), sourced from coal consumption

1262 (Boyle et al. 2014).

1263
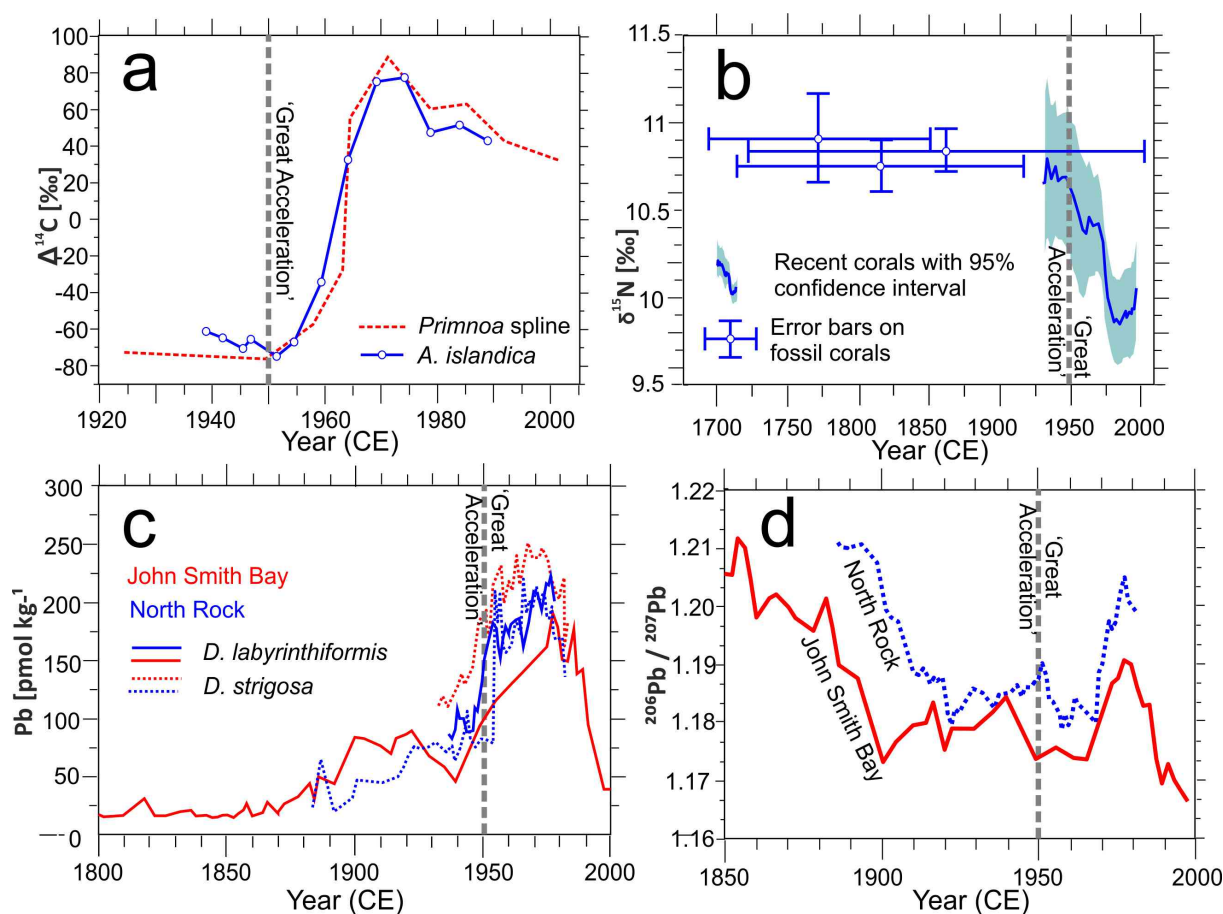
1264

Figure 7. a) Plot of Δ^{14}C vs age for 7 different colonies of the deep-sea gorgonian coral *Primnoa*

resedaeformis with spline fit through the data (Sherwood et al. 2005a), and for the bivalve *Arctica*

islandica (Weidman and Jones 1993); b) δ^{15}N-AA depletion in deep-sea gorgonian corals in the NW

Atlantic (Sherwood et al. 2011) © (2011) National Academy of Sciences; c) Pb concentration; and d)

^{206}Pb/^{207}Pb in Bermuda corals (Kelly et al. 2009).

1270

3.3.2 Guam (Pacific Ocean) .v. Caribbean Pu radionuclide signals

A natural coral archive in *Porites lobata* from Guam Island (NW Pacific Ocean), dated

independently using δ^{18}O cycles to produce a biweekly to monthly chronology between 1787

and 2000 CE, was retrieved in a 273 cm core (Lindahl et al. 2011). Between 1943 and 2000

1275 CE the average growth rate was ~15 mm yr^{-1} (Lindahl et al. 2011), significantly higher than

1276 most natural accumulation rates in marine and lacustrine basins. From 1943 to 1945 CE,

1277 ^{239}Pu (but not ^{240}Pu) was detected in small concentrations (average of 1.96 ± 0.11 mBq kg^{-1},

1278 Figure 6b), though at levels higher than would be expected from an entirely natural source

1279 at that time (Lindahl et al. 2011). This suggests some minor mobility of anthropogenic (post-

1280 1945 CE) Pu after incorporation into the coral. In 1946 CE, $^{239+240}$Pu activity concentrations

1281 increased by an order of magnitude (11.3 ± 2.4 mBq kg^{-1}, Figure 6b) and continued at low

1282 levels until 1951 CE, reflecting fallout from locally tested, low-yield, nuclear devices (Lindahl

1283 et al. 2011). A marked bomb-nuclide peak is evident from 1952 to 1960 CE, with an apex in

1284 1954 CE (4540 ± 70 mBq kg^{-1}, Figure 6b), the pattern being closely linked to that of large

1285 detonations in the local Pacific Proving Grounds (Lindahl et al. 2011). From 1961 to 1980 CE,

1286 there was an exponential decrease of $^{239+240}$Pu activity, but despite Nuclear Test Ban treaties,

1287 residual Pu remains in the sea water and continues to be incorporated into coral growth

1288 laminae, such that by 2000 CE levels were comparable to those in 1946 CE (Figure 6b).

1289

1290 The Pu signals seen in a short (30-year) duration record from the coral *Orbicella*

1291 (*Montastrea) annularis* in the U.S. Virgin Islands (Benninger and Dodge 1986), reflect a

1292 location that is distant from atmospheric nuclear detonations. That study did not analyse

1293 coral bands from 1950 CE or earlier, so it is not possible to determine if a pre-1952 CE global

1294 fallout signal is present. But it did show clear 1959 and 1964 CE peaks in $^{239+240}$Pu that closely

1295 correspond to global fallout maxima (Benninger and Dodge 1986; Figure 6b herein).

1296

1297 These data illustrate the very high-resolution Pu signal present in coral laminae, with only

1298 limited evidence of post-growth mobility of Pu. The example in Guam shows an initial rise in

1299 Pu between 1946 and 1951 CE and a peak signal in 1954 CE. Such a signal contrasts with

1300 areas distant from testing grounds which show a global Pu fallout pattern (e.g. Waters et al.

1301 2015), with an initial 1959 CE peak and a subsequent higher 1964 CE peak (e.g. Benninger

1302 and Dodge 1986). This variability in peak signals suggest the initial rise in global Pu levels

1303 would better mark the basal boundary of the Anthropocene than any of the various peak

1304 signals (cf. Zalasiewicz et al. 2015). For hosting a potential GSSP, choosing a coral that was

1305 distant from nuclear testing grounds would mean that the global atmospheric signal is

1306 resolved without local perturbations.

1307

1308 3.3.3 ^{14}C, Pb and δ^{15}N signals in deep-water Atlantic gorgonian corals

1309 Corals show a ^{14}C bomb-spike that has potential as a marker (Sherwood et al. 2005a; Figure

1310 7a herein). Compared to coral Δ^{14}C records from Florida in the North Atlantic, the inception

1311 of the Brazil (Abrolhos Archipelago) record is delayed by ~1 year during the late 1950s with

1312 peak Δ^{14}C values reached from 1970 to 1972 CE in Florida and at 1974 CE at Abrolhos

1313 (Druffel 1996), suggesting an appreciable lag for the bomb ^{14}C to transfer from the main

1314 source latitudes in the Northern Hemisphere. There is also a Δ^{14}C atmosphere–surface ocean

1315 equilibration time of approximately 10 years, with some resultant time lag in the signal (Key

1316 et al. 2004). However, analysis of growth rings in the deep-water gorgonian coral *Primnoa*

1317 *resedaeformis* at depths of 250–475 m off Nova Scotia (Canada) shows a Δ^{14}C peak around

1318 1972 CE (Sherwood et al. 2005a; Figure 7a herein), similar to that in shallow water corals in

1319 Florida (USA), suggesting rapid transfer of the radiocarbon to such moderate depths via

1320 plankton. Overall, a mid-1950s inception of the signal is evident in gorgonian corals from

1321 these environments, providing a reasonable proxy for the beginning of the Anthropocene.

1322

1323 At much greater depths, Δ^{14}C records from the coral *Enallopsammia rostrata* from 1410 m

1324 depth off Bermuda first show bomb radiocarbon at ~1980 CE (Lee et al. 2017), a delay of

1325 some 25 years compared with the atmospheric signal (Lee et al. 2017). In this record, the

1326 introduction of anthropogenic lead, evident as an increased Pb/Ca ratio and decreased

1327 ^{206}Pb/^{207}Pb and ^{208}Pb/^{207}Pb ratios, occurs in the 1990s and hence shows a similar 25-year

1328 delay, and the signal is significantly smaller compared with that from nearby shallow-water

1329 corals (Lee et al. 2017). Given the decade-scale lags for Δ^{14}C in shallow-water corals, with

1330 even greater lags in deep-water corals, Pu is here considered the preferred fallout signal in

1331 corals.

1332

1333 *Primnoa resedaeformis* from Nova Scotia (Canada) to Virginia (USA) records the Suess effect,

1334 with δ^{13}C values decreasing by at least 2‰ since around 1960 CE (Sherwood et al. 2005b).

1335 *Primnoa resedaeformis* off Nova Scotia also records a δ^{15}N signal, considered a proxy for

1336 nitrogen source, which is correlated with increasing subtropical versus subpolar slope waters

1337 over the 20th century (Sherwood et al. 2011); δ^{15}N decreased by about 1‰ over this interval,

1338 with most of the decline occurring after 1970 CE, coincident with a rise in nitrates (Sherwood

1339 et al. 2011). Such coral studies show that the persistence of a warm, nutrient-rich regime

1340 since the early 1970s is exceptional in the context of the last ~1800 years (Sherwood et al.

1341 2011, Figure 7b). Coral cores from Dongsha Atoll, western Pacific, show markedly lowered

1342 δ^{15}N values since ~2000 CE in coral skeleton-bound organic matter, probably associated with

1343 increased deposition of anthropogenic atmospheric nitrogen (Ren et al. 2017). By contrast,

1344 coral studies from some Indo-Pacific reefs affected by untreated sewage outfalls show high

1345 δ^{15}N (and δ^{13}C) signals (Heikoop et al. 2000), indicating the complex behaviour of the

1346 nitrogen stratigraphic proxy.

3.3.4 Global temperature and pH proxies from corals in the Great Barrier Reef

1347

1348 In the Great Barrier Reef, Australia, annual band thicknesses in corals equate to growth rate,

1349 which can be correlated with sea surface temperatures (SSTs) on a time scale of years to

1350 centuries (Lough and Barnes 2000). During the bleaching events associated with elevated

1351 SSTs of the late 20th century, *Porites* colonies from the Great Barrier Reef showed a decline

1352 in linear growth of 13.3% between 1990 and 2005 CE (De'ath et al. 2009), with calcification

1353 rates falling by 14.2%. Such changes are unprecedented over at least the last 400 years

1354 (De'ath et al. 2009).

1355

1356 Corals in the tropical Pacific region have shown a general decrease of $\delta^{18}O$ values from the

1357 late 20th century to the present (Cole 1996). This reflects large-scale warming in the upper

1358 layers of the ocean, or a general freshening of these waters, or a combination of both. $\delta^{18}O$

1359 signals in scleractinian coral skeletons have been used as SST proxies in other areas, some as

1360 long records (e.g. Colonna et al. 1996), or at very high resolution (e.g. Ahmad et al. 2011).

1361 However, $\delta^{18}O$ signals reflect evaporation rates as well as SST, which is why they are

1362 frequently used together with other proxies, especially Sr/Ca (e.g. Tierney et al. 2015, Zinke

1363 et al. 2016). While some locations show a pronounced temperature increase around 1950 CE

1364 (e.g. Hetzinger et al. 2010), coral proxies have also shown that tropical seas might have

1365 started to warm as early as the mid-19th century, as an effect of both natural and possibly

1366 anthropogenic drivers predating the widely recognized global warming typical of the mid-

1367 20th century (Abram et al. 2016). Although temperature reconstructions can be highly

1368 refined (DeLong et al. 2016), temperature records from coral skeletons are a mix of local and

1369 global factors, and hence better as an ancillary rather than primary marker for defining any

1370 potential coral-based GSSP.

1371

δ^{11}B isotopic records in carbonates can provide a proxy for seawater pH. Data from a *Porites* coral in the Great Barrier Reef covering an interval from 1800 to 2004 CE show a recent trend of acidification correlating positively with the δ^{13}C Suess effect, and negatively with Mg/Ca ratios (a further proxy for SSTs) from 1940 to 2004 CE, indicating a coincident warming (Wei et al. 2009). Pre-industrial boron isotope signals in the coral show 22- and 10-year cycles strongly controlled by the Pacific Decadal Oscillation (Wei et al. 2009). From 1940 to 2004 CE the δ^{11}B signal indicates a decrease in pH of about 0.2–0.3 U, but with marked annual oscillations of 0.5 U around 1940 and 1998 CE (Wei et al. 2009).

3.3.5 Plastics in the Great Barrier Reef

Macroplastics have become noticeable in coral reefs, through the snagging of fishing nets and as plastic debris generally washed into the oceans. Microplastics are increasingly found both within marine waters and in underlying sediments (Zalasiewicz et al. 2016a). These plastics adsorb heavy metals and organic compounds from water, which can bioaccumulate in worms, fish and seabirds (Ivar do Sul and Costa 2014), and zooplankton (Cole et al. 2013). Microplastic ingestion into scleractinian coral polyps has been recognised recently in the Great Barrier Reef (Hall et al. 2015). Ingestion probably occurs both via microplastic-containing zooplankton and directly from the water. It remains uncertain whether any ingested plastic is transferred into the coral skeleton, as a potentially recognizable feature of future coral growth bands.

3.3.6 North Atlantic marine bivalves

A Δ^{14}C bomb signal comparable to that in cold-water corals (Figure 7a) was recorded in a long-lived bivalve, the ocean quahog (*Arctica islandica*) collected at a depth of 75 m on Georges Bank off New England, USA (Weidman and Jones 1993), with similar records in haddock otoliths (*Melanogrammus aeglefinus*) from the Grand Banks (Campana 1997). The

1396 $\Delta^{14}C$ values measured in these and in the gorgonian coral *P. resedaeformis* (see above) (~ -80

1397 to ~ +80‰) are low compared to those in reef corals from Florida (~ -60 to ~ +160‰) where

1398 the stratified subtropical waters have a less diluted bomb signal (Sherwood et al. 2005a).

1399 *Arctica islandica* from water depths of 3–80 m across the temperate North Atlantic shows a

1400 gradient of increasing amplitude of the radiocarbon bomb-spike from Iceland southwards

1401 towards the North Sea (Scourse et al. 2012). All localities show a rapid response to the

1402 increase in atmospheric $\Delta^{14}C$ excess, with a lag within the bivalves of as little as 1–2 years,

1403 despite the equilibration time between atmosphere and ocean of 7–10 years (Scourse et al.

1404 2012). However, the bivalve data shows a slow response to the decline in the radiocarbon

1405 signal, with a diachronous peak that occurs earlier in the south (Scourse et al. 2012).

1406

1407 Annually resolved $\delta^{18}O$ signals recorded in *A. islandica* collected at a water depth of 80 m

1408 north of Iceland show gradually increasing values over the period 953–1891 CE (±18 years),

1409 after which there is a rapid transition to lower values, with the 20th century represented by

1410 values that are significantly lower than at any other time in the last 1000 years (Reynolds et

1411 al. 2016).

1412

1413 *3.4 Estuarine and deltaic deposits*

1414 River estuaries and deltas are present on all continents except Antarctica, forming the

1415 transition between the fluvial and marine realms (Figure 8) and representing the zone

1416 through which most terrestrial sediments (including those associated with human signals)

1417 are transported to the oceans. Estuaries occupy about 10 million km^2 and major deltas 1

1418 million km^2 (Syvitski and Saito 2007). Most modern estuaries and deltas developed during

1419 the Early Holocene sea-level rise, with the flooding of river or glacial valleys. Sea level during

1420 the Middle and Late Holocene was essentially stable, allowing estuaries to silt up and deltas

1421 to build seawards (Zalasiewicz et al. 2014c). In addition, early deforestation and new

1422 agricultural practices commonly resulted in increased sediment flux to estuaries and deltas

1423 (Syvitski and Kettner 2011). Current and projected absolute sea-level rises are expected to

1424 flood both estuarine and deltaic deposits as warming continues to expand ocean water and

1425 melt land ice (Giosan et al. 2014). The trapping of sediment behind major dams, constructed

1426 on nearly all major rivers in recent decades (Syvitski and Kettner 2011), has greatly reduced

1427 sediment flux to the coast since the 1950s (Walling and Fang 2003). This change will leave a

1428 clear response as a transgressive, diachronous sequence-stratigraphic system with excellent

1429 preservation potential (Poirier et al. 2011). One consequence of decreasing fluvial profiles

1430 during sea-level rise is lower rates of erosion in the proximal headwaters, resulting in rivers

1431 with slower flow regimes, transporting relatively finer sediments to estuaries and deltas and

1432 therefore to coastlines. Where rivers have been dammed, even these sediment loads will

1433 not reach the coastal ocean. Many urban centres are located on or close to deltas or

1434 estuaries, which may therefore experience substantial anthropogenic influence. Deltas and

1435 coastal deposits continue to subside under their own weight, the subsidence now being

1436 accentuated by the compaction associated with urban development and with the extraction

1437 of groundwater and hydrocarbons (Syvitski and Kettner 2011), while locally drainage has led

1438 to the wholesale removal of surface peat layers, further lowering the surface (e.g. Smith et

1439 al. 2010) and increasing flooding risk. Twenty four out of the world's 33 major deltas are

1440 subsiding, levels of subsidence having reached several metres, as on parts of the Rhine, Nile,

1441 Pearl and Yangtze River deltas (Syvitski et al. 2009).

1442
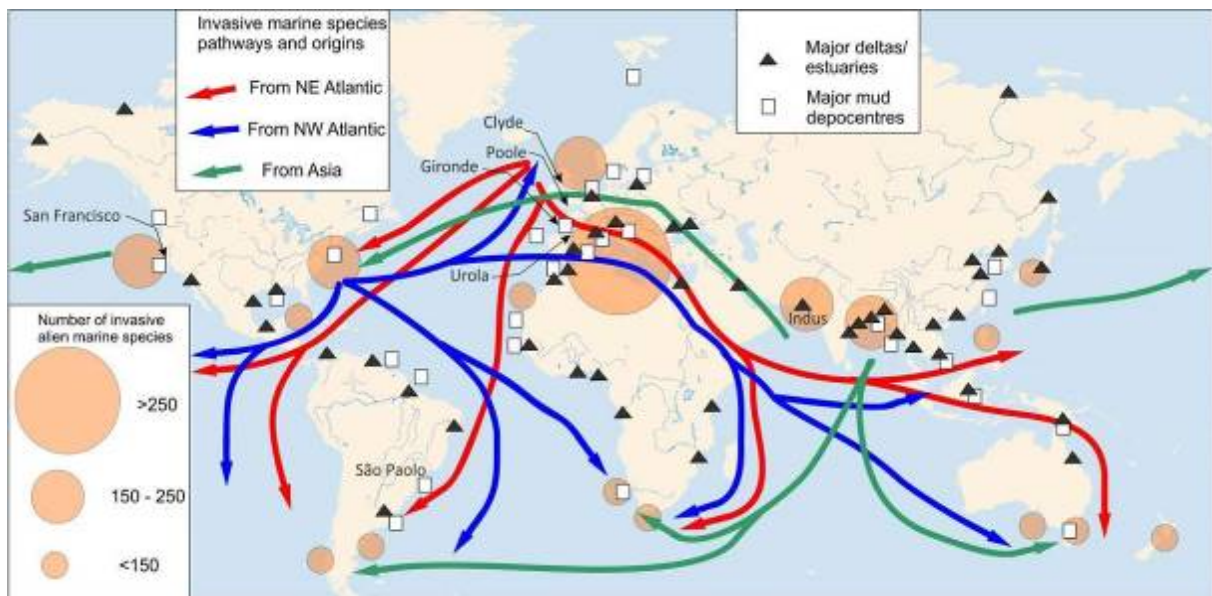
Figure 8. Distribution of deltas and estuaries (from Tessler et al. 2015), major mud depocentres (from Hanebuth et al. 2015) and areas where neobiota amenable to fossilization have recognizably altered coastal ecosystems (from: Major pathways and origins of invasive species infestations in the marine environment In UNEP/GRID-Arendal Maps and Graphics Library http://www.international-marine.com/invasivespecies/PublishingImages/invasive_vectors_001.png).

Mud deposition occurs on the continental shelves in front of major estuarine and deltaic areas (pro-deltas) around the world (Figure 8). They can also form subaqueous deltas disconnected from the source delta, or as scattered mud patches and widespread mud blankets, with a moderate sedimentation rate of 1–5 mm yr^{-1} (Hanebuth et al. 2015). They represent well-resolved palaeoenvironmental accumulations, commonly initiated during early flooding of continental shelves following deglaciation ~14 ky ago (Hanebuth et al. 2015). One example now forming a sink of anthropogenic pollution, including heavy metals and hydrocarbons, lies off the coast of São Paolo State, SE Brazil (Mahiques et al. 2016). Here, the mud deposits originate from many small river inputs and are mixed with coastal sediments. These deposits form a laterally extensive sedimentary succession, where the mid-shelf section at 50–100 m depth is prone to reworking through bioturbation, storms and

1461   anthropogenic disturbance, including trawler fishing and sea-bed dredging (Mahiques et al.

1462   2016). Similar shelf mud deposits occur in the Bay of Biscay, in front of the Gironde estuary,

1463   SW France (Lesueur et al. 1996), where three mud-patches, totalling 630 km^2, occupy

1464   palaeo-valleys at depths of 30–75 m. The rhythmically laminated deposits there, which

1465   broadly represent storm layers, accumulated to a thickness of 1.8 m over the last 2000 years

1466   and the upper 0.2 m accumulated in <30 years, as shown by ^{14}C and pollen analyses. A

1467   marked increase in pollen from *Pinus pinaster* over the last century reflects extensive

1468   afforestation (Lesueur et al. 1996).

1469

1470   Estuaries and deltas are particular foci for neobiota (Wilkinson et al. 2014), often associated

1471   with marked declines in indigenous species. Widespread translocation of invasive species

1472   took place during the 19th and 20th centuries through the establishment of global shipping

1473   routes, and resultant transfer of species in ballast water and from hull fouling (Figure 8).

1474   Organisms such as diatoms, dinoflagellates, foraminifera and ostracods, are particularly

1475   susceptible to transportation in ballast water and hence are likely to produce novel signals

1476   within coastal sediments, especially close to major ports (McGann et al. 2000, Calvo-

1477   Marcilese and Langer 2010). The International Convention for the Control and Management

1478   of Ships' Ballast Water and Sediments, which came into force in September 2017, is aimed at

1479   reducing the rate of such biotic transfer.

1480

1481   Aquaculture of fish, shellfish and shrimps has become a growing feature of estuarine settings

1482   in the late 20th and early 21st century (Martinez-Porchas and Martinez-Cordova 2012). This

1483   has resulted in diverse biotic changes including the displacement of native species,

1484   competition for space and food, and the spread of pathogens and parasites, and impacts like

1485   these are likely to increase as this kind of fishery develops. In addition, destruction of natural

1486 ecosystems, most notably of mangroves along equatorial coastlines, which have seen a 25%

1487 decrease in 20 years to 150,000 km^2 in 2000 CE (Martinez-Porchas and Martinez-Cordova

1488 2012), has changed species presence/absence and abundance patterns. Aquaculture can

1489 also lead to eutrophication causing phytoplankton blooms, including red tides, the resultant

1490 anoxia and increased pathogens killing off benthic organisms (Martinez-Porchas and

1491 Martinez-Cordova 2012). The first arrival of many invasive species to local areas is commonly

1492 historically documented, but the fossil record of these changes as successive assemblages in

1493 recent well-dated sedimentary successions remains poorly studied.

1494

1495 'Bomb spike' calibration and AMS ^{14}C dating have been used to derive a detailed age-depth

1496 model for a 1-m long sediment column collected from a salt marsh in Poole Harbour,

1497 southern England (Marshall et al. 2007), enabling comparison with chronologies obtained

1498 from CRS ^{210}Pb analysis, ^{137}Cs age markers, pollen and spheroidal carbonaceous particles

1499 (SCPs). Little or no agreement was found between the ^{14}C 'bomb spike' dates, the ^{210}Pb

1500 chronology, and the ^{137}Cs data, the last of these being affected by local (non-fallout)

1501 discharges (Marshall et al. 2007). The study showed an acceleration in sedimentation rates

1502 during the last 100 years, and indicated that 'bomb spike' ^{14}C calibration dating may often

1503 better constrain salt-marsh sedimentation rates than ^{210}Pb dating (Marshall et al. 2007).

1504

1505 Table 6 summarises key advantages and disadvantages of hosting a potential GSSP within

1506 estuarine or deltaic deposits, where research has focused on impacts of anthropogenic

1507 pollution through geochemical signatures, especially heavy metals and POPs, and on

1508 microbiotic content such as foraminifera, diatoms and palynomorphs (Wilkinson et al. 2014).

1509 The examples provided below, for the Clyde Estuary (Scotland), Urola Estuary (northern

1510   Spain) and Indus Delta (Pakistan), demonstrate a range of signals. For a variety of reasons

1511   (Table 6) these types of environment seem unsuitable for hosting a GSSP.

1512

For:	Against:
• May be varved through seasonal variations in sediment flux • Independent dating using ^{210}Pb; ^{14}C more challenging • Radionuclides, no settling delay in water column; clear bomb spike • Micro- and macro-organisms reflect environmental change and commonly preserve as fossils (e.g. foraminifera, diatoms, palynomorphs, molluscs, fish) • Microplastics, direct source from effluents • Heavy metals, close to industrial sources • Persistent organic pollutants signal e.g. chlorinated pesticides, polychlorinated biphenyls • Modification of fluvial input to estuaries related to catchment modification • Samples relatively easy to procure	• Potential of bioturbation • Numerous omission surfaces (natural erosion and anthropogenic dredging) • Limited lateral continuity, but distinct systems may undergo similar histories • Strong modulation of signals by local processes • No GSSP precedent

1513   **Table 6.** Reasons for and against using an estuarine or deltaic deposit as a potential host for a GSSP.

1514

1515   ### 3.4.1 Clyde Estuary, Scotland (Pb and organic compounds)

1516   Lead concentrations in the Clyde Estuary were initially elevated early in industrial activity,

1517   peaking by about 1915 CE, with a prominent decline to historically low concentrations post-

1518   1980 CE (Vane et al. 2011, Figure 9a), as heavy industry declined and Pb use in gasoline was

1519   phased out. $^{207/206}$Pb isotope ratios of *Sphagnum* moss collected in Scotland from 1838 CE to

1520   the present record variation of atmospheric Pb aerosols (Farmer et al. 2002): a constant

1521   pattern during the 19th century until ~1915 CE reflects use of British lead coal-ore and coal-

1522   burning (Figure 9a); increased ratios from 1920 CE due to overseas Broken Hill-type Pb

1523 additives in gasoline and industrial lead, peaking in the 1980s; and then declining ratios

1524 following the banning of lead in gasoline (Vane et al. 2011).

1525

1526 Increased industrialization of the Clyde Estuary in west Scotland has led to elevated levels of

1527 sediment-hosted anthropogenic organic chemicals (Vane et al. 2011), including total

1528 petroleum hydrocarbons (TPHs), polycyclic aromatic hydrocarbons (PAHs), polychlorinated

1529 biphenyls (PCBs) and brominated flame-retardants (polybrominated diphenyl ethers, PBDEs)

1530 (Figure 9b). The PAHs are largely sourced from combustion of coal, petroleum or wood with

1531 peak concentrations in 1954 CE (Vane et al. 2011, Figure 9b). Increasing petroleum pollution

1532 mainly from shipping and petroleum refineries was recorded from about the 1950s by

1533 increasing TPH concentrations and a decline in PAHs that reflects decreasing coal use (Vane

1534 et al. 2011). This was followed by more modern pollution from the PCBs, which show a

1535 prominent onset (1950s), peak (1965–1977 CE) and decline (post-1980s).

1536

1537 The complexity of signals provides a very fine resolution chronometer of pollution in the

1538 Clyde Estuary. Although the Pb, TPHs and PAHs provide a local signal, the Pb isotopes and

1539 PCBs provide a more widespread and consistent, although not precisely coincident, global

1540 signal.

1541
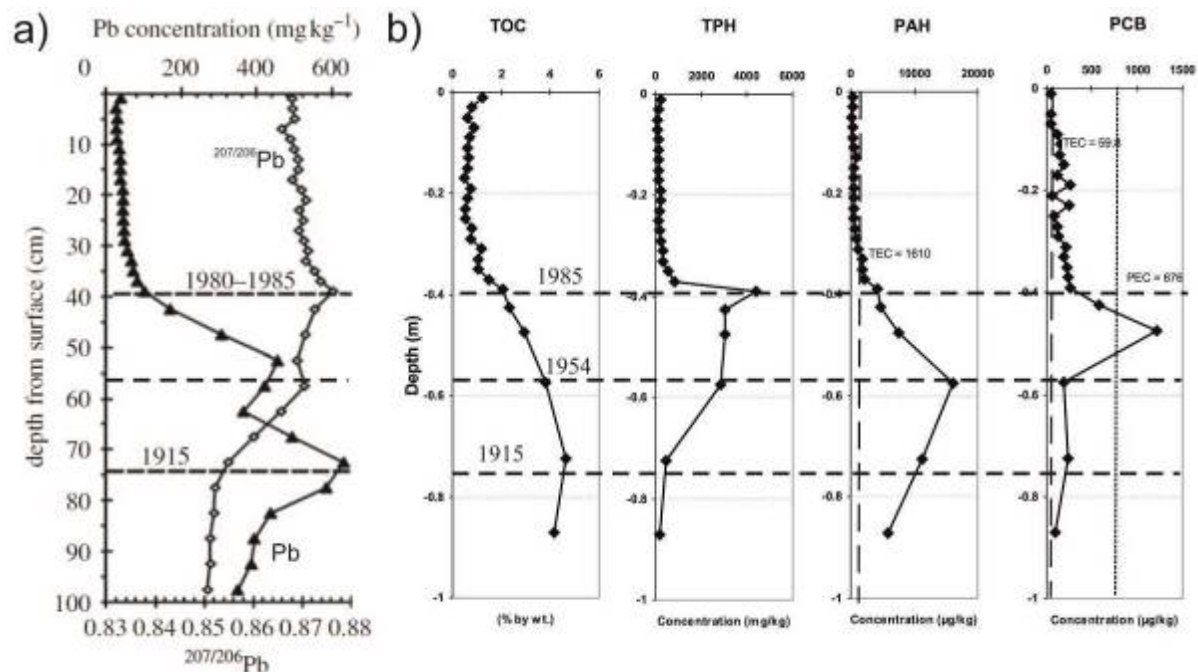
1542

Figure 9. Example of data from a single core from the Clyde Estuary showing a) Pb concentrations

and [207/206]Pb isotope ratios, and b) PAH, TPH and PCB organic chemical signatures (Vane et al. 2011).

Dates are interpreted.

3.4.2 Urola Estuary, Spain

The lower intertidal part of the Urola estuary (Basque coast, Spain) was studied in a 50 cm

core and dated using ^{210}Pb, the basal parts dated using ^{210}Pb to ~1850 CE (Goffard 2016).

From the 1960s to the 1980s the rate of sedimentation increased by >60% in response to

growing industrial activity, with further increase from the mid-1990s coinciding with nearby

dredging. Micropalaeontological analysis of benthic foraminiferal assemblages (FAs) (Goffard

2016) identified three assemblages (Fig. 10) that reflect a local cycle of biological

deterioration and reduced diversity followed by recovery. This biostratigraphic succession

has been correlated with changes in levels of industrially-derived metals in the sediment,

showing that chemical deterioration preceded biological deterioration. Longer-range

correlation is provided by: spheroidal carbonaceous particles, which occur mainly in the

1558 lower levels; iron spheroids, showing enrichment from the 1960s; and plastic microbeads,

1559 which increase from the 1980s (Goffard 2016).

1560
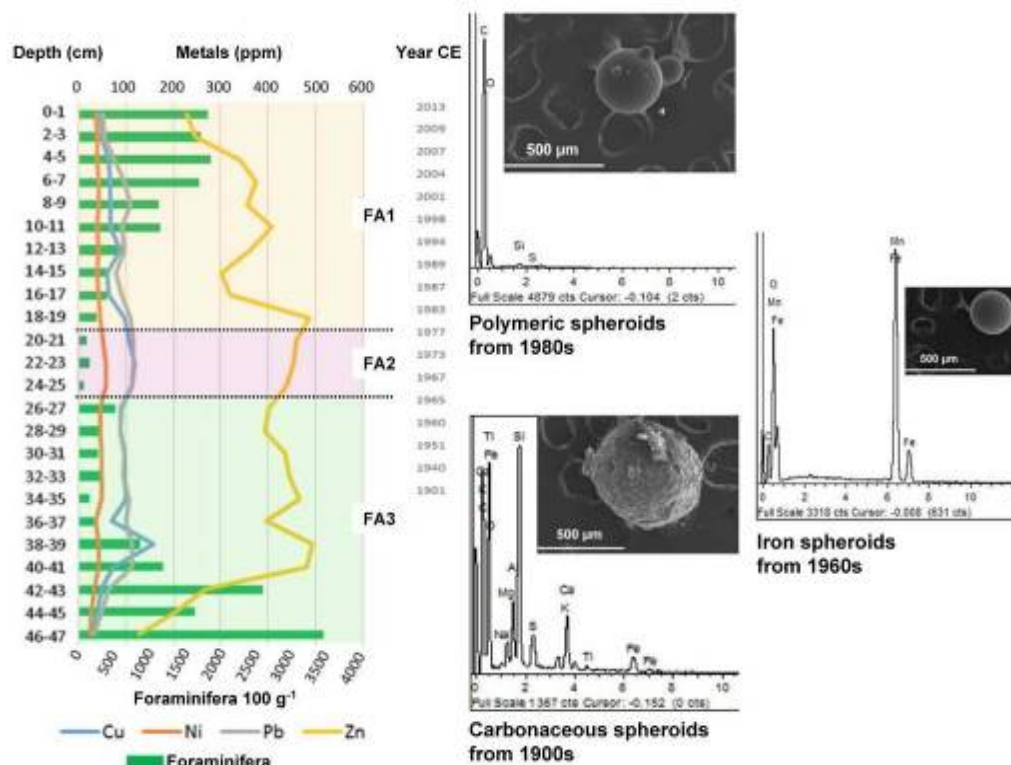
1561

1562 **Figure 10.** Metal concentrations (Cu, Ni, Pb, Zn) versus foraminiferal density in the Urola estuary

1563 (northern Spain). FA1–FA3 represent three distinct foraminiferal assemblages referred to in the text.

1564 Modified from Goffard (2016).

1565

1566 ### 3.4.3 San Francisco Bay, USA

1567 San Francisco Bay, with a well-documented history of invasive species (neobiota), is typical

1568 of the many coastal ecosystems around the world that are near shipping ports (Figure 8). In

1569 a seminal study by Cohen and Carlton (1998), some 234 neobiotic species were recognised,

1570 ranging from sponges to mammals. They noted an accelerating trend over 145 years, with

1571 about half the invasions occurring since 1960 CE. More recently, studies of shallow sub-tidal

1572   sediments in the bay have identified soft-sediment communities dominated by invasive

1573   species (Jimenez and Ruiz 2016). The presence of so many neobiotic species in San Francisco

1574   Bay suggests the potential for a high-resolution biostratigraphy using species invasions

1575   (Figure 11). Building such a stratigraphy would need to resolve the myriad complexities of a

1576   sedimentary succession heavily disturbed since the 19th century. Nevertheless, sediment

1577   cores with Pleistocene and Holocene micropalaeontology are well known (e.g. Sloan 1992,

1578   McGann et al. 2002), providing a pre-human influenced baseline for local coastal

1579   assemblages.
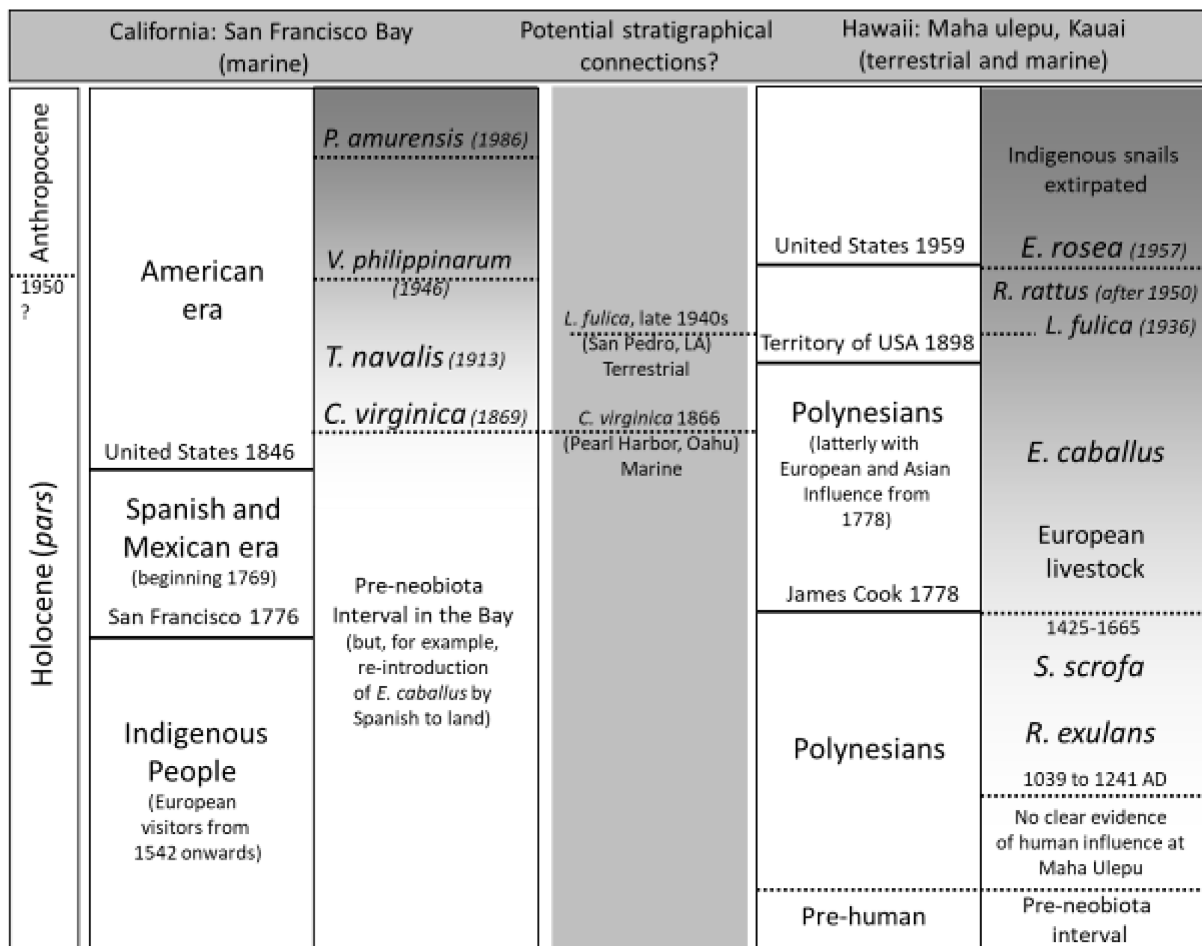
1580

1581   **Figure 11**. Chronology of selected invasive mollusc species into San Francisco Bay (for dates of

1582   invasion see: Carlton et al. 1990; Cohen 2004, 2011; Committee on Nonnative Oysters in the

1583   Chesapeake Bay, Fofonoff et al. 2017, National Research Council 2004), and terrestrial invasive

1584   species in the Maha'ulepu sinkhole succession of Kauai, Hawaii (Burney et al. 2001). In both

1585   successions, cultural human changes are indicated by the left-hand column, and neobiota in the

right-hand column. Although the two successions developed nearly 4000 km apart, and in warm temperate and tropical zones respectively, by the mid-19th century some taxa present on the California coast (e.g. the bivalve *Crassostrea virginica*, see DeFelice et al. 2001) were also present in Hawaii, suggesting the possibility of correlation between remote successions.

A focus of such analysis could be bivalves, which are commonly fossilized, widespread and readily recognisable neobiotic species. A biostratigraphic subdivision could begin with a pre-neobiotic interval that is characterised only by indigenous bivalve species, these persisting into the mid-19th century. A subsequent early neobiotic stage (see also Cohen and Carlton 1998) might be characterised by the first appearance of the oyster *Crassostrea virginica*, which entered the Bay in 1869 CE. A native to the Atlantic coast of North America, this species was introduced with the development of oyster fisheries. *Crassostrea virginica* was also introduced into the estuaries of the Hawaiian islands at about the same time (1866 CE), providing a potential biostratigraphic tie with a distant island succession (Figure 11).

The early phase of invasions into San Francisco Bay is followed by increasing indicators of pan-Pacific connections between North America and East Asia, signalled by, for example, the introduction of the East Asian bivalve *Venerupis philippinarum*, first recognised in San Francisco Bay in 1946 CE (Cohen 2011, Figure 11), although there are earlier records elsewhere on the Pacific coast of North America. Locally, this species occurs in abundances of 2000 individuals per m^2, and it has good preservation potential. It has also been widely introduced, from Hawaii (introduced in the 1880s, established by 1918 CE) to Europe. A later colonisation from East Asia was by the Amur Clam *Potamocorbula amurensis*, native to the waters of China, Siberia, Korea and Japan. It was introduced into San Francisco Bay in 1986 CE, likely through ships' ballast water (Figure 11) and then spread widely and rapidly. It now

1611 occurs in huge numbers in muddy substrates within the Bay: up to 48,000 individuals have

1612 been recorded per m^2 sediment (Cohen 2011).

1613 3.4.4 Indus Delta

1614 The Indus Delta, Pakistan, and its associated river system, is highly managed, with artificial

1615 levees, barrages, irrigation canals, upstream reservoir construction and inter-basin water

1616 diversions. It has also been affected by watershed deforestation. As a consequence, the river

1617 has changed radically, with a current sediment flux of ~13 Mt yr^{-1} to the tidal-dominated

1618 delta and its single active distributary, in contrast to the much larger flux >270 Mt yr^{-1} of

1619 mainly silt that was transported to the fluvial-dominated delta before these management

1620 schemes were implemented. The original delta system comprised 17 channels (which still

1621 avulsed naturally) in 1861 CE (Syvitski et al. 2014). Modifications started as early as 1762 CE,

1622 although constructed dams were all washed away in a flood in 1826 CE. The modern barrage

1623 system was initiated in 1859 CE (Syvitski et al. 2014). With rising sea-levels accompanied by

1624 tectonic subsidence, the abandoned distributary channels are being tidally reworked since

1625 1944 CE and the delta has lost 12.7 km^2 yr^{-1} of land and ~69 Mt yr^{-1} of sediment by erosion.

1626 The system is highly dynamic due to monsoon-driven floods, storm surges, tsunamis and

1627 earthquakes (Syvitski et al. 2014), and hence stratigraphic successions are beginning to

1628 emerge as complex backstepping packages of sediment with omission surfaces related to

1629 erosive events, in contrast to the pre-1869 CE delta, which was prograding at about 200 m

1630 yr^{-1}.

1631

1632 *3.5 Lake sediments*

1633 The planet has about 117 million lakes greater than 2000 m^2, covering about 3.7% of the ice-

1634 free land surface, with the highest concentration and area of lakes at boreal and arctic

latitudes between 45°N and 75°N (Verpoorter et al. 2014). The most suitable lake environment for hosting a potential GSSP is one where varves are present. Varves tend to occur in lakes in which a flat bottom profile limits sediment flow, and, ideally, where there is little or no bioturbation, water movement, or gas emission from buried organic material to disturb the laminae (Zolitschka et al. 2015). Many such features are common in glacial lakes, characterized by graded summer silt laminae alternating with winter clays, e.g. Holtgrieve et al. (2011) and Wolfe et al. (2013). Varves can also develop in hypoxic lakes (Figure 12), typically meromictic lakes with stratified water columns in which sediment is introduced through seasonal input of clastic or biogenic material. Saline lakes can develop varves in response to seasonal precipitation of evaporite minerals, within an environment commonly too hostile for benthic life, allowing preservation of the varves; however, these lakes are more likely to periodically dry out, thus tending to miss annual laminae. Lakes are already recognized as suitable locations for hosting a GSSP, having been used as the ancillary GSSP locations for the base of the Holocene (Walker et al. 2009).

Hypoxia has been recorded in sediments of 365 lakes worldwide (Figure 12). Of these, 71 (~20%) show hypoxia developed since the mid-19th century CE, much earlier than the widespread development of hypoxia in coastal zones during the mid-20th century (Jenny et al. 2016). This reflects the sensitivity of lakes to environmental change, where increasing human activities and nutrient release commonly lead to the onset of hypoxia. No correlations were found with changes in precipitation or temperature. There is no evidence for a post-1980s return to well-oxygenated lacustrine conditions in industrialized countries, despite the implementation of restoration programmes (Jenny et al. 2016). Hypoxia notably can change the behaviour of trace elements and radionuclides, by either increasing or reducing their mobility (e.g. Pavin Lake, France; Jeandel 1981).
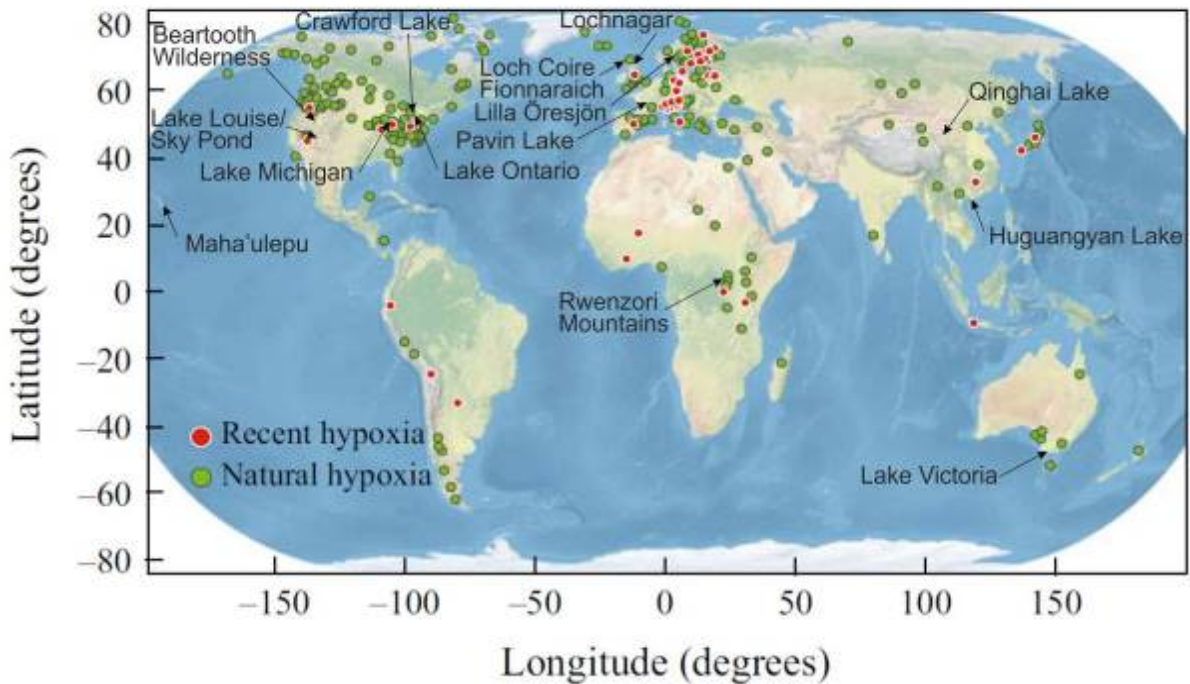
Figure 12. Location of the 365 sites recording lake hypoxia (Jenny et al. 2016). Recent hypoxia records onset of varves after 1700 CE, whereas naturally hypoxic lakes were taken to be those in which laminations persisted for at least 300 years.

The radiogenic fallout signature is commonly well expressed in unbioturbated lake sediments, especially as the mid-latitude Northern Hemisphere peak fallout distributions (Hancock et al. 2014, Waters et al. 2015) coincide with the greatest abundance of hypoxic lakes. Shallow lakes are advantageous in that they show little of the settling delay evident in the anoxic marine basins (see section 3.2). However, they may still be prone to reworking of fallout signals from catchment areas, such that the onset of the signal will probably be unaffected, but the bomb-peak may be broadened although still centred at ~1964 CE. Lake Victoria in Australia is an example of a lake with a large catchment. Despite showing the expected peak of the $^{239+240}$Pu and ^{137}Cs signals in 1964 CE (Figure 13), the Cs peak is broader and the post-1964 CE Pu decline is prolonged because of sedimentation associated with erosion within that catchment.

1678   Abundant organic and clay components in lake sediments enable sorption of the main long-

1679   lived radiogenic elements (plutonium and radiocarbon). Where plutonium concentrations

1680   are relatively high, α-spectroscopy effectively measures the combined activity of ^{239}Pu +

1681 ^{240}Pu and also measures ^{238}Pu activity (Figure 13), whereas mass spectrometric (MS)

1682   techniques are required where concentrations are low and to measure distinct ^{239}Pu

1683   concentrations (Hancock et al. 2014). However, plutonium (and caesium) can be mobilized

1684   under anoxic conditions in meromictic lakes, e.g. Pavin Lake, France (Jeandel 1981).
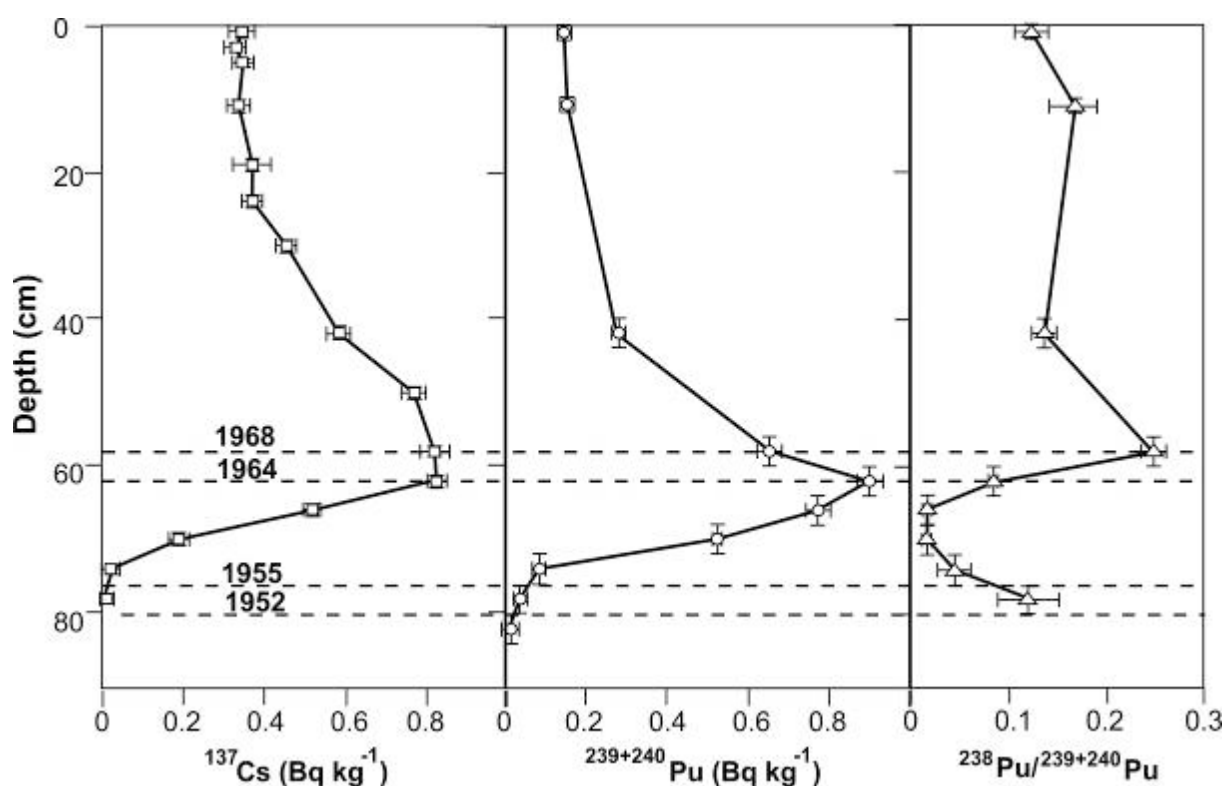
1686   **Figure 13.** Radiogenic signature from Lake Victoria, Australia (Hancock et al. 2011). Profiles of ^{137}Cs

1687   (closed squares), $^{239+240}$Pu (open circles) and ^{238}Pu/$^{239+240}$Pu (triangles).

1688

1689   The atmospheric transfer of reactive nitrogen (Nr) results in the deposition of NH_4^+, HNO_3,

1690   and NO_3^- even in remote lakes, as demonstrated in North America and the Arctic regions

1691   (Holtgrieve et al. 2011, Wolfe et al. 2013). Stable nitrogen isotope values from lake

1692   sediments of those regions show a consistent perturbation of δ^{15}N commencing after 1850

CE, typically at 1895 CE ± 10 years (Holtgrieve et al. 2011, Figure 14), but with a faster rate of

1694   depletion from 1950 to 1970 CE and after 1980 CE (Wolfe et al. 2013). This depletion is

1695   attributed to fossil fuel combustion and the production and use of fertilizers, both with

1696   depleted isotopic ratios compared with catchment and preindustrial atmospheric sources

1697   (Holtgrieve et al. 2011).
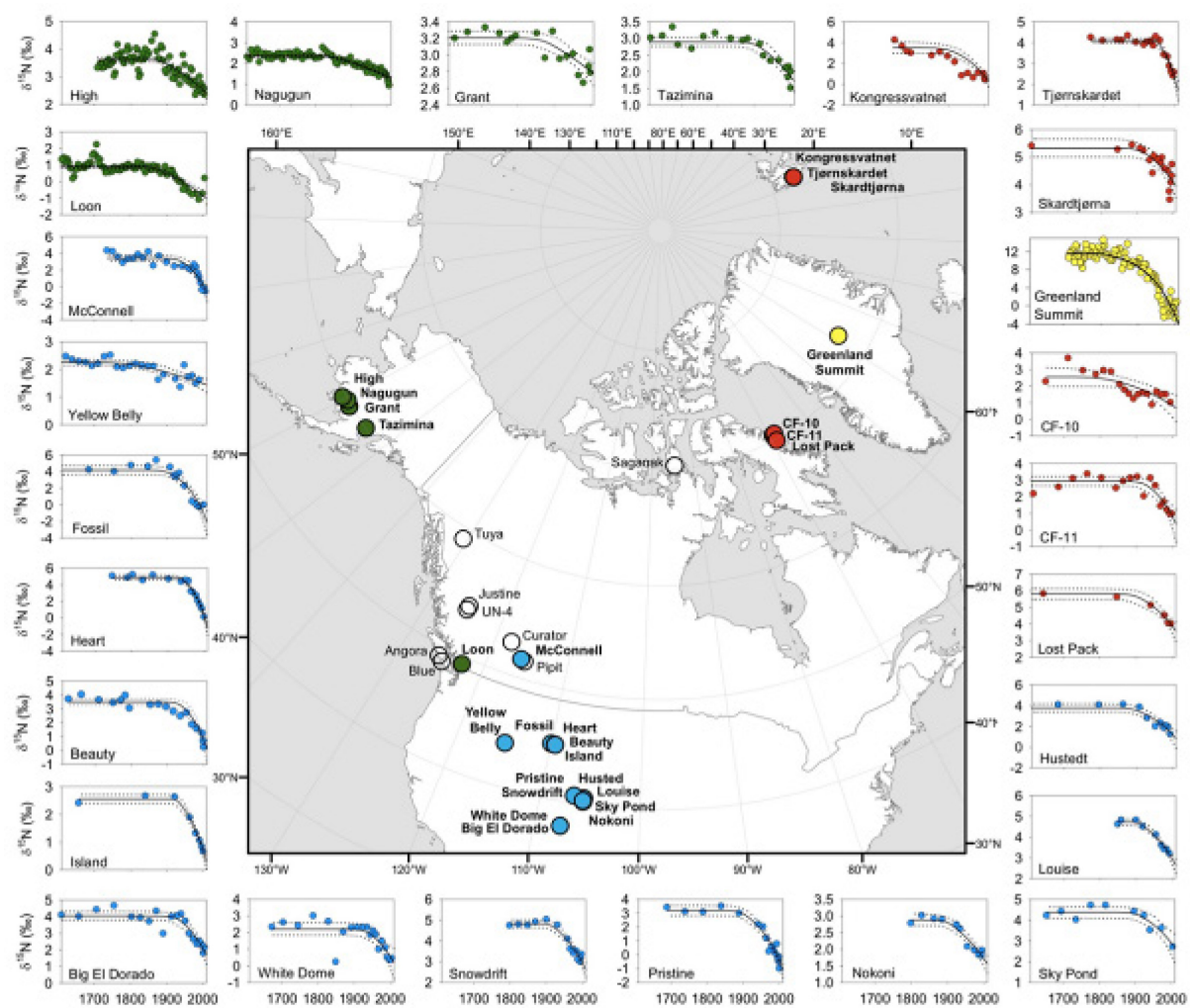
1700   **Figure 14.** Sediment δ^{15}N profiles from Northern Hemisphere lakes (from Holtgrieve et al. 2011).

1701   Lake ecotypes include: temperate/boreal (green circles), alpine (blue circles), and arctic (red circles),

1702   and the Greenland Summit ice core is indicated with a yellow circle. The solid lines are the median

1703   posterior fits to the observed data using the most parsimonious model, and the dotted lines are the

1704   2.5 and 97.5% credible limits.

1706   Although spheroidal carbonaceous particles (SCPs) are first recorded from strata dating to

1707   about 1830 CE, they show a near-synchronous global mid-20th century increase in

1708   abundance. This increase was driven by the introduction of fuel-oil combustion, in addition

1709   to coal, and coincided with increased abundance of large-scale power plants, with peak

1710   abundance in the 1970s to 1990s (Rose 2015). Black carbon, produced from the incomplete

1711   combustion of fossil fuels and vegetation, can accumulate in lakes from both atmospheric

1712   aerosols and riverine input, and is inert and resistant to degradation (Han et al. 2016). The

1713   atmospheric component, generally seen as a smaller size fraction (soot), is more widely

1714   transported and hence provides a more regional signal than coarser riverine char (Han et al.

1715   2016). Biomass burning typically produces higher char/soot ratios than fossil fuel

1716   combustion, especially motor vehicle emissions (Han et al. 2016). Polycyclic aromatic

1717   compounds (PACs) tend to be co-produced with black carbon during hydrocarbon

1718   combustion. These can include polycyclic aromatic hydrocarbons (PAHs) and derivatives such

1719   as oxygenated PAHs (OPAHs) and azaarenes (nitrogen heterocyclic PAHs, AZAs) (Han et al.

1720   2016). The relationship is demonstrated for Huguangyan Lake, eastern China (section 3.5.4).

1721

1722   Metal concentrations in lake sediments can be affected by variable factors such as the timing

1723   of local industrialisation, distinct sources of sediment supplied by river fluxes into the lake,

1724   and varying degrees of weathering of the source catchment areas. Anthropogenic Pb

1725   deposition in lakes typically shows elevated concentrations in modern sediments in response

1726   not only to local industrial sources, but also to regional to global scale Pb atmospheric

1727   release. In remote lakes, the supply of anthropogenic Pb is sourced via the atmosphere (e.g.

1728   Lake Qinghai, China; Jin et al. 2010), providing a wider and more consistent signal than Pb

1729   supplied via river-water influx from nearby industrial sources. In Lake Qinghai, elevated

1730   anthropogenic Pb concentrations from the 1960s to at least 2000 CE are considered

consistent with other remote Northern Hemisphere lakes (Jin et al. 2010). The lakes of the

Rwenzori Mountains of Uganda are distant from direct sources of Pb, and therefore the lake

sediments potentially contain reliable archives of long-range atmospheric pollution (Yang et

al. 2010). Hg concentrations in these high-altitude lakes show increased Hg burdens from the

1860s, with significantly elevated levels from 1930 ± 6 CE (Yang et al. 2010).

The Great Lakes of North America show widespread microplastic contamination, mainly in

surface waters and beach sediments, while plastic pellets have been recorded in bottom

sediments of Lake Ontario (Corcoran et al. 2015). Notably, high-density microplastics,

including mineral-polyethylene and mineral-polypropylene mixtures, sink to the lake bottom

rapidly and have been accumulating since at least 1977 CE (Corcoran et al. 2015).

Microplastics tend to concentrate in nearshore sediments, within low-energy environments

close to urban and industrial areas at concentrations of up to ~28,000 particles kg^{-1} dry

sediment and sediment depths of up to 15 cm (Ballent et al. 2016). Where microplastics are

deposited at water depths of <40 m, they are prone to reworking by storm events (Ballent et

al. 2016).

Persistent organic pollutants (POPs) are characterised by slow rates of environmental

degradation (years to decades), low solubility, high absorption to suspended particles and

efficient atmospheric transport. Chlorinated pesticides (e.g. DDT and its degradation

products), show a consistent worldwide rise from the 1950s (Muir and Rose 2007), and

subsequent decline in the youngest sediments reflecting the US banning of DDT in 1972 CE.

Temporal trends of input fluxes of polychlorinated biphenyls (PCBs), and the fire retardants

hexabromocyclododecanes (HBCD) and polybrominated diphenyl ethers (PBDEs) in sediment

cores from English lakes in urban settings show generally slow rises from ~1960 CE, which

1756   are less clearly developed in rural settings. In the case of HBCD, the rise may be delayed by

1757   some 35 years (Yang et al. 2016).

1758

1759   Invasive zebra mussels (*Dreissena polymorpha*) and quagga mussels (*Dreissena rostriformis*

1760   *bugensis*) represent novel species introduced into the North American Great Lakes in 1988

1761   and 1989 CE respectively (https://nas.er.usgs.gov/taxgroup/mollusks/ zebramussel/), both

1762   originating from southern Russia/Ukraine. As well as providing a novel biogenic signal, they

1763   also greatly modify the biotic content of the lakes. The trillions of quagga mussels in Lake

1764   Michigan (USA) can filter the equivalent of the entire lake volume in about 1 or 2 days. This

1765   has resulted in a shift in diatom composition, with significant reduction in the larger diatom

1766   genera, e.g. *Stephanodiscus* and *Aulacoseira*, leaving an impoverished algal community with

1767   mainly smaller genera, e.g. *Cyclotella* (Evans et al. 2011). Diatom assemblages in remote

1768   Northern Hemisphere lakes commonly show a consistent pattern. Typical Late Holocene

1769   benthic diatoms, such as *Staurosira* and *Achnanthidium* show declines concurrent with the

1770   rise of planktonic diatoms, first associated with an initially time-transgressive appearance of

1771   *Discostella stelligera*, attributed to climate warming (Wolfe et al. 2013). After 1950 CE, the

1772   planktonic diatoms *Asterionella formosa* and *Fragilaria crotonensis* became dominant (Saros

1773   et al. 2005, Figure 15; Wolfe et al. 2013 suggest 1980 CE). This later change may reflect

1774   elevated Nr availability (Wolfe et al. 2013, Figure 14) as well as rising temperatures. A

1775   comparable biotic change in the remote oligotrophic Scottish lake of Loch Coire Fionnaraich

1776   began in the 19th century following several hundred years of ecological stability (Pla et al.

1777   2009). Changes to diatom (mainly benthic) assemblages were strongly coincident with

1778   changes in spheroidal carbonaceous particle concentrations, and may result from

1779   atmospheric contamination, possibly Nr enrichment (Pla et al. 2009). Chrysophyte diatom

1780 cyst (mainly planktonic) assemblages changed in response to a combination of atmospheric

1781 pollution and regional climate warming (Pla et al. 2009).

1782

Beartooth Wilderness Montana-Wyoming

Rocky Mountains National Park Colorado
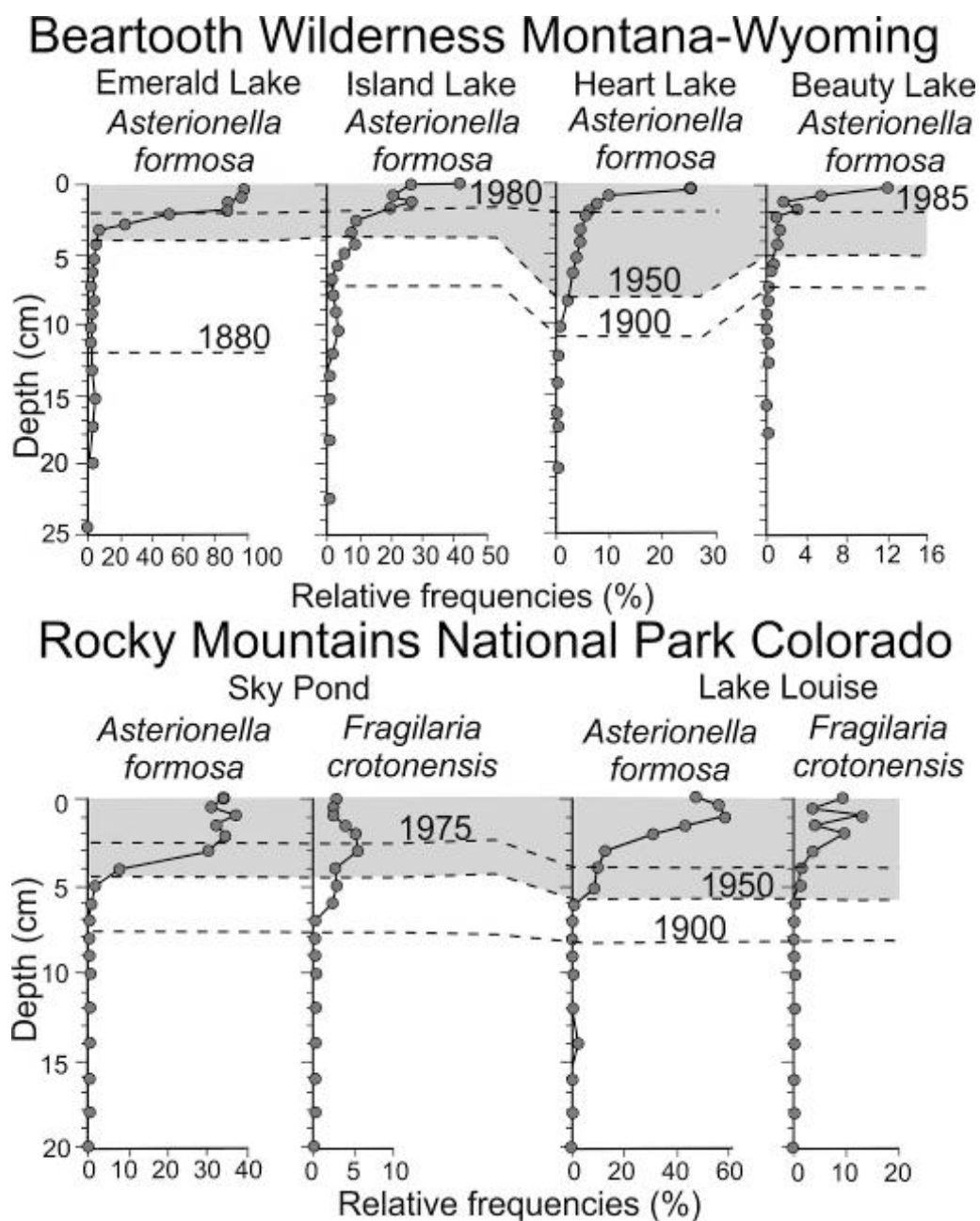
1783

1784 **Figure 15.** Replacement of Holocene diatom assemblages by *Asterionella formosa* and/or *Fragilaria*

1785 *crotonensis* mainly in lake cores from US high-altitude sites, since ~1950 CE (Saros et al. 2005).

1786 Location of lakes shown on Figure 14.

1787

1788 Table 7 summarises the key advantages and disadvantages of having a potential GSSP within

1789 lacustrine environments. Varved lake sediments can be strongly influenced by local

1790 variations in the geology, hydrology and land use present within catchments, and may be

1791 associated with distinct geochemical signals related to input from local industries.

1792 Correlation of varved successions within individual lakes may be limited to the extent of the

1793 water body, but widespread airborne contaminants, e.g. radiogenic fallout, nitrates, fly ash

1794 (Table 2), can show remarkably consistent patterns in lakes across diverse latitudes and be

1795 associated across continents. Crawford Lake (Ontario, Canada), Lochnagar (Scotland), Lilla

1796 Öresjön (Sweden), Huguangyan Lake (Guangdong, China) and Maha'ulepu Sinkhole (Kauai,

1797 Hawaii) are described as examples of potential trans-continental reference sections.

1798

For:	Against:
• May be varved; relatively few omission surfaces • Spatially extensive with regional–global coherent signals • Independent dating using ^{210}Pb and ^{14}C • May be correlatable with tephra stratigraphy • Microplastics and metals with direct source from effluents • Spheroidal carbonaceous particles show global upturn • δ^{15}N marked depletion from mid-20th century • Persistent organic pollutants, e.g. chlorinated pesticides • Radionuclides, no settling delay in water column; clear bomb spike • Microfossils responsive to environmental change e.g. diatoms, ostracods, palynomorphs • Cores relatively easy to procure	• Commonly low sediment accumulation rates (though typically greater than for marine anoxic basins) • Strong modulation of signals by local processes, except for upland or remote lakes • Pu and Cs are mobile under anoxic conditions at the bottom of meromictic lakes • No precedent as GSSP candidate; although 4 of 5 auxiliary stratotypes for the Holocene GSSP are lacustrine

1799 **Table 7.** Reasons for and against using a lake deposit as a potential host for a GSSP.

1800

1801   ### 3.5.1 Crawford Lake, Canada

1802   Crawford Lake (Ontario, Canada) is a small (surface area 2.5 ha), deep (24 m), meromictic

1803   lake located close to industrial pollution sources, although it lacks any significant urban

1804   development within the lake catchment area. It has a sediment record spanning eight

1805   centuries, with a varve chronology dating to 1867 CE and ^{14}C dating for older lamina (Ekdahl

1806   et al. 2004). Maize (*Zea mays*) pollen and corn smut spores (*Ustilago maydis*) are irregularly

1807   distributed through an interval greater than 200 years, termed the Iroquoian, reflecting

1808   sporadic occupation by pre-European indigenous peoples (Ekdahl et al. 2004, 2007, Figure

1809   16). This occupation is associated with increased numbers of the planktonic diatoms

1810   *Asterionella formosa, Fragilaria crotonensis* and *Synedra nana*, depleted numbers of

1811   *Cyclotella michiganiana*, and the loss of *Cyclotella bodanica*. These changes are attributed to

1812   increased nutrient input, which raised lake productivity, causing bottom-water anoxia and

1813   altering diatom assemblages (Ekdahl et al. 2004, 2007). Additional stratigraphic proxies

1814   record marked changes in the late-19th century (starting 1867 CE) due to introduction of a

1815   new agricultural regime by European settlers, and again in the mid- and late-20th century,

1816   driven by regional land-use changes of comparable magnitude to the earlier changes by

1817   indigenous peoples.
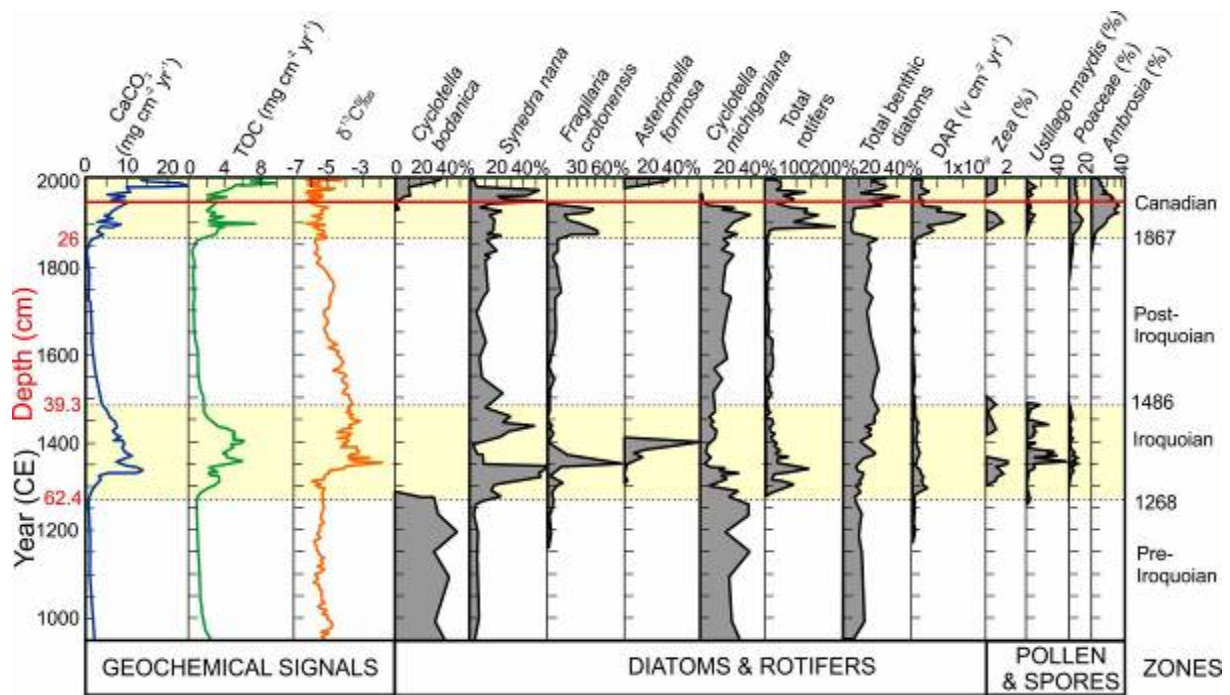
Figure 16. Stratigraphic signals of the last millennium in Crawford Lake, Canada. The horizontal red line near the top is the ~1950 CE level, marked by both lithological and biostratigraphic changes in available data. From Zalasiewicz et al. (2017a), modified after Ekdahl et al. (2004). DAR is diatom accumulation rate.

3.5.2 Lochnagar, Scotland

Lochnagar is a small (surface area 9.8 ha), deep (26.4 m), high altitude (788 m a.s.l) corrie lake in the Grampian Mountains of Scotland. As with many upland and mountain lakes, there are no direct sources of contamination in the catchment so all pollutants are originally from atmospheric deposition. However, the legacy of centuries of atmospheric inputs from industrial sources has resulted in a considerable store in the sparse peat soils which are now being remobilised to constitute a major pollution source to the loch (Yang et al. 2002a).

Lochnagar exhibits a full Holocene record contained within a sedimentary succession <2 m thick. These deposits, neither laminated nor varved but dated by [14]C (Dalton et al. 2005), show catchment-driven changes due to the development and degradation of soils (e.g. post-

1835 Little Ice Age soil erosion) and human interference on terrestrial vegetation via 'fire

1836 management' over the last ~1000 years. Due to the steep morphology of the loch basin,

1837 accumulation of sediments varies across the loch with recent accumulations (Rose 2007)

1838 being higher than earlier sedimentation rates, as is the case with many European lakes (Rose

1839 et al. 2011). Recent sediments are readily dated by ^{210}Pb, independently supported by 1963

1840 CE nuclear weapons testing signals of ^{137}Cs and ^{241}Am and the Chernobyl ^{137}Cs peak in 1986

1841 CE.

1842

1843 The diatom-inferred pH reconstruction for the last 9500 years shows a stable pH of 6.0–6.5

1844 until the 19th century (Monteith et al. 2007) when pH started to decline with the resultant

1845 loss of acid-sensitive diatom taxa (*Achnanthes minutissima*, *Achnanthes scotica* and

1846 *Fragilaria virescens* var. *exigua*) and an increase in those which are more acid-tolerant

1847 (*Achnanthes marginulata* and *Aulacoseira distans* var. *nivalis*) (Battarbee et al. 2014). The pH

1848 eventually reached a low of 5.5 in the 1970s before starting to recover in the 1980s,

1849 although the trajectory for diatom recovery is not a straightforward reversal (Battarbee et al.

1850 2014). Alongside the 19th century decline in pH were: a) the start of spheroidal carbonaceous

1851 particle deposition, which elevated markedly in the mid-20th century (Rose and Yang 2007,

1852 Figure 17a); b) increases in the concentrations of trace metals (Figure 17b) such as Pb (from

1853 1860s) and Hg (from the early-20th century), becoming elevated over long-term base-lines

1854 (Yang et al. 2002a), and also an increase in Cd, Cu and Zn concentrations (Yang et al. 2002b);

1855 and c) a decline in δ^{15}N starting in the late-19th century (Curtis and Simpson 2011, Figure

1856 17c). All of these signals indicate contamination via atmospheric deposition of long-range

1857 industrial pollutants.
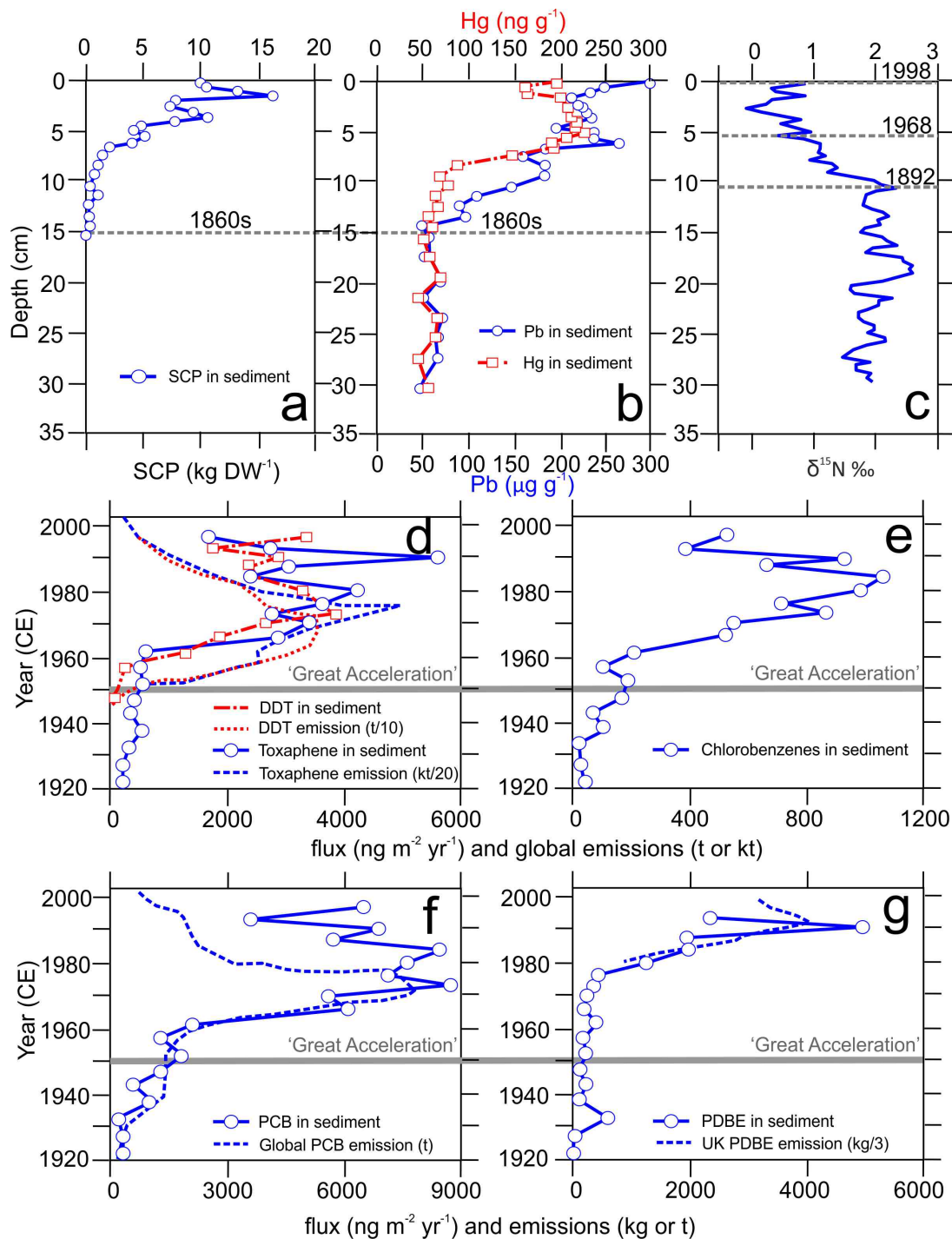
Figure 17. Contamination record in Lochnagar sediments (Scotland) demonstrating appearances as post-mid-20th century markers: (a) Spheroidal carbonaceous particles (SCPs) (from Yang et al. 2002a); (b) Hg and Pb (from Yang et al. 2002a); (c) δ^{15}N (from Curtis and Simpson 2011); (d) the chlorinated pesticides DDT and toxaphene from core collected in 1997 CE related to emission data (from Muir and Rose 2007); (e) chlorobenzenes (from Muir and Rose 2007); (f) total PCBs related to global emissions (from Muir and Rose 2007); and (g) PDBEs related to UK emissions (from Muir and Rose 2007).

1866

1867 Mercury, Pb and SCPs show a further and more significant increase in concentration in the

1868 mid-20th century (Figure 17a and b), primarily from fossil-fuel combustion. This period is also

1869 accompanied by significant increases in a range of POPs such as organochlorine pesticides,

1870 including DDT, although the accumulation in Lochnagar sediments lags about a decade

1871 behind emission figures (Muir and Rose 2007, Figure 17d). The organochlorine pesticide

1872 toxaphene was never used or produced in the UK (Muir and Rose 2007, Rose et al. 2001),

1873 but global emission was greatest in the 1970s with high accumulation rates in Lochnagar

1874 sediments in the 1980s and 1990s (Figure 17d). Industrial chemicals including

1875 chlorobenzenes and PCBs show elevated values from ~1960 CE and, later, brominated flame

1876 retardants such as PBDEs show elevated concentrations from ~1980 CE (Muir and Rose

1877 2007) (Figure 17e–g). The lake sediment records of trace metals and SCPs are matched by

1878 records of these same contaminants in the catchment peats of Lochnagar (Yang et al. 2001)

1879 with both mid-19th and mid-20th century increases observable.

1880

1881 While the sediment and peat cores of Lochnagar faithfully reflect the temporal trends in

1882 contaminant deposition through most of the industrial period, there is evidence that this is

1883 not now the case. Temporally-resolved full-basin inventories of Hg and Pb (Yang et al. 2002a)

1884 show no decline in inputs to lake sediments in recent decades (Figure 17b) even though

1885 emissions of these metals to the atmosphere have declined by 80–90% since the 1970s

1886 (NAEI 2017). This 'additional' input of metals can only come from the store of legacy

1887 contaminants in catchment soils as a result of increased soil erosion, possibly in part a result

1888 of a changing climate. This hypothesis is supported by work at other upland lakes in Scotland

1889 for a suite of trace metals and also for SCPs (Rose et al. 2012). The implication of this is that

1890 even while upland lake sediments are no longer reliably recording changes in atmospheric

1891 deposition (Yang and Smyntek 2014), by being a sink for reworked anthropogenic deposition

1892 on land, they are concentrating and temporally extending an anthropogenic signal. This

1893 would not affect a mid-20th century GSSP from among such sites.

1894 3.5.3 Lilla Öresjön, Sweden

1895 A lake core from Lilla Öresjön (SW Sweden), a high-sulphate deposition area, records marked

1896 physical, chemical and biological trends since 1800 CE (Renberg and Battarbee 1990). Areas

1897 of acute lake acidification tend to be associated with atmospheric pollutants including heavy

1898 metals, sulphur, fly-ash (spheroidal carbonaceous particles) and PAH, related to fossil-fuel

1899 combustion. However, anthropogenic Pb signals have a much longer record in lake

1900 sediments in Sweden, initiating 3500 to 4000 years ago, with a small, but clear Roman Pb

1901 peak at about 1 CE, a major and unreversed increase at ~1000 CE, markedly elevated levels

1902 during the Industrial Revolution, but most prominently after World War II, with peak

1903 concentrations at ~1970 CE (Renberg et al. 2000). The record of increased Pb concentration

1904 is associated with concomitant declines in the Pb isotope ratio (Renberg et al. 2000).

1905

1906 At Lilla Öresjön atmospheric pollution is evident with an increase in Pb, Zn, and

1907 benzo(a)pyrene at about 1900 CE (dated by ^{210}Pb) and a more pronounced increase of these

1908 signals along with sulphur and SCPs during the 1960s (Renberg and Battarbee 1990, Figure

1909 18). Heavy metal and sulphur signals peaked in the 1960s and 1970s, and SCPs and PAH in

1910 the 1970s. Analysis of diatoms, chrysophytes, cladocerans and pollen show a succession of

1911 changes reflecting decreasing lake pH, with a distinct post-mid 20th interval discernable

1912 (Figure 18 herein; Renberg and Battarbee 1990).
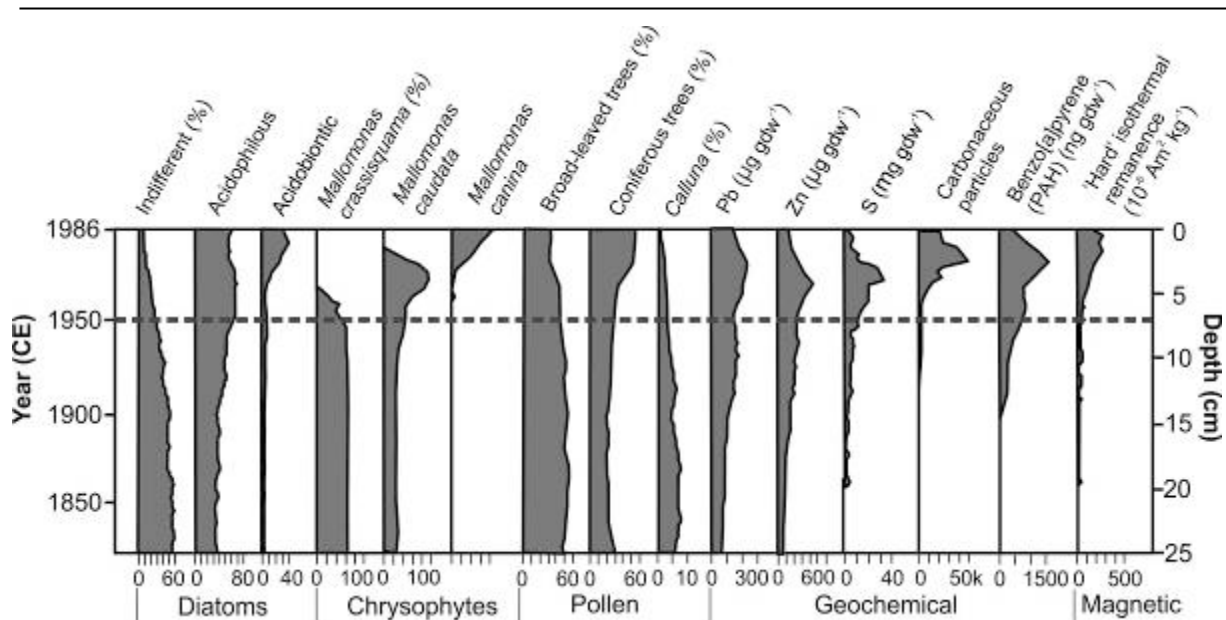
Figure 18. Physical, chemical and biological trends from Lilla Öresjön (SW Sweden), a high-sulphate deposition area (from Renberg and Battarbee 1990).

3.5.4 Huguangyan Maar Lake, Guangdong, China

Huguangyan Lake, eastern China, receives little sediment input from rivers or from soil erosion, hence its records of black carbon (BC) and polycyclic aromatic compounds (PACs) reflect atmospheric deposition (Han et al. 2016). The sediment record covers the past 350 years and has been dated reliably for the last 150 years using ^{210}Pb and ^{137}Cs activities (Han et al. 2016). Concentrations of BC, PAH, oxygenated PAHs (OPAH) and azaarenes (AZAs) increased sharply during the late-1940s to early-1950s, and again in the late-1970s (Han et al. 2016, Figure 19). The BC record peaks from 2004 to 2006 CE, with subsequent rapid decrease, whereas the PAC record has continued to rise (Han et al. 2016).
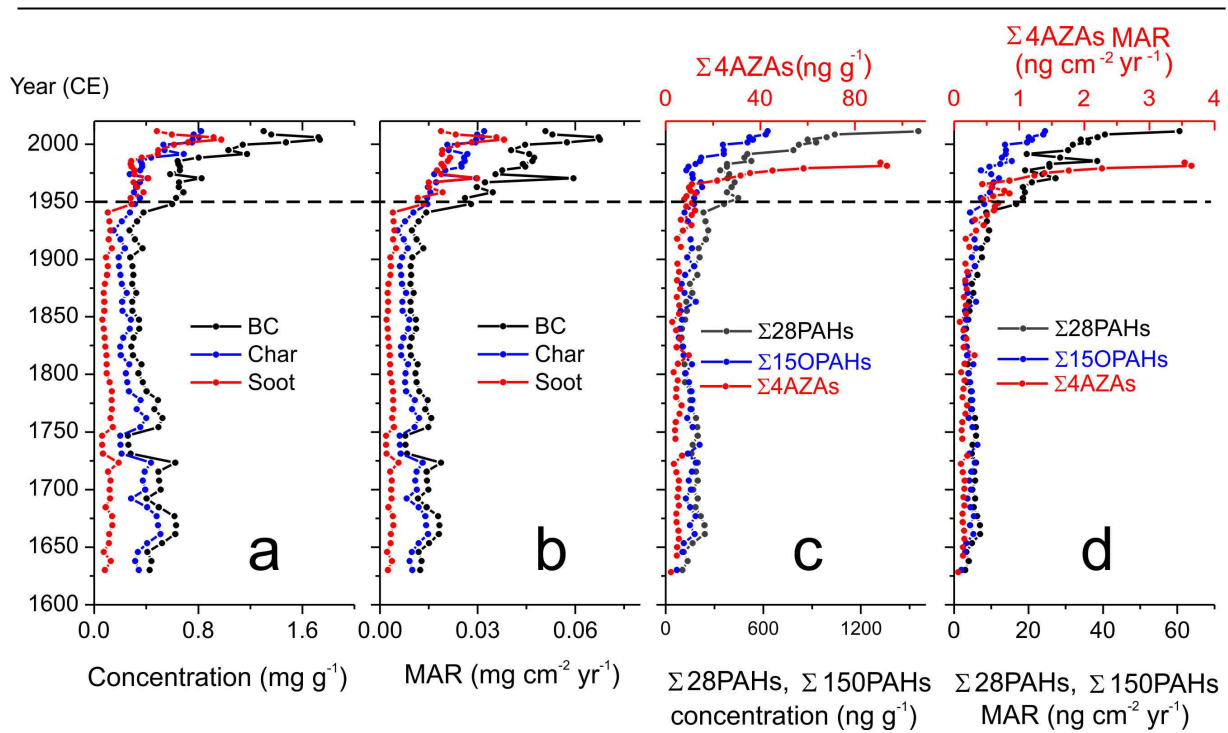
Figure 19. Historical variations of concentrations and mass accumulation rates (MARs) of black carbon (BC), char, and soot, parent-PAHs, oxygenated PAHs (OPAHs), and azaarenes (AZAs) in the Huguangyan Maar Lake (from Han et al. 2016).

The sedimentary record of char, soot, and PACs in this lake reflects the start of the rapid industrialization in China after the 1950s, associated with a change in dominant energy sources from mainly wood burning in the pre-1950s to fossil fuels in the post-1950s (Han et al. 2016).

3.5.5 Maha'ulepu Lake of Kauai, Hawaii

The sedimentary successions of the Maha'ulepu Sinkhole and caves of Kauai, Hawaii (Burney et al. 2001) show a record of extirpation of geographically local taxa and biotic invasions of rats and other fauna. The sinkhole succession extends over the past 9500 years that accumulated in a freshwater to brackish lake, with periodic marine incursions, and which includes diatoms, land snails and bivalves. The diatoms, coupled with ^{14}C dates, provide a

1941 detailed stratigraphy for the sinkhole and cave succession, which records step changes in

1942 anthropogenic influence through Polynesian and European colonisation of the island.

1943

1944 Human impact in the Maha'ulepu Sinkhole (Figure 11) is first seen as an introduced Pacific

1945 rat dated to between 1039 and 1241 CE (Burney et al. 2001). Changes in land snail species

1946 indicate the impact firstly of Polynesian and latterly European colonisers and their associated

1947 neobiota. Declines in several species coincide with Polynesian activity, whilst all indigenous

1948 snail taxa, with the exception of *Cookeconcha* cf. *psaucicostrata*, became extinct during the

1949 19th and early-20th centuries. In the 20th century, *Lissachatina fulica* (in 1936 CE) – the Giant

1950 African Snail - and *Euglandina rosea* (in 1957 CE) – the Cannibal Snail of Central America -

1951 were introduced (Figure 11). Anecdotal evidence suggests a 20th century extinction for the

1952 last indigenous snail population of *C.* cf. *psaucicostrata*. These changes provide a detailed

1953 and unfolding biostratigraphical record of human impact on the local biota that is supported

1954 by diatom, bird, pollen, and other fossil data (Burney et al. 2001). Furthermore, in the

1955 marine succession, neobiotic marine bivalves such as *C. virginica* on Oahu, offer potential for

1956 inter-regional correlation (Figure 11).

1957

1958 *3.6 Peat and peatlands (mires)*

1959 Peatlands (mires) may be defined as wetlands in which at least 40 cm of peat has

1960 accumulated; peat is partially-decomposed, sub-fossil plant material containing less than

1961 25% by weight mineral matter (Shotyk 1992). Swamps and fens are "minerotrophic"

1962 wetlands, that is, plants growing there receive mineral nutrients primarily from surface

1963 waters and groundwaters. Fens are almost always peatlands, but swamps may be either

1964 mineral wetlands or peatlands, depending on the thickness of peat accumulation (Shotyk

1965 1992). In contrast, the surface layers in bogs are beyond the influence of these waters, and

1966 the plants growing there receive their nutrients solely from atmospheric inputs (termed

1967 "ombrotrophic"). Because bog plants are fed exclusively by rain and dust, the peats which

1968 accumulate in bogs have naturally low concentrations of mineral matter and trace metals,

1969 providing low background values against which anthropogenic inputs may be compared.

1970 Note that wetlands are not necessarily peatlands, and that most peatlands are not

1971 ombrotrophic bogs.

1972

1973 Northern (boreal and subarctic) peatlands are by far the most extensive development of

1974 peat, covering some 4 million km^2, whereas the equivalent southern peatlands, mainly in

1975 Patagonia, South America cover only 45,000 km^2 (Yu et al. 2010, Figure 20). Tropical

1976 peatlands cover an area of ~370,000 km^2 (Yu et al. 2010), the most extensive area being the

1977 ~145,000 km^2 of the Congo Basin (Dargie et al. 2017). In the case of the Congo Basin,

1978 however, peat was defined as having <35 % mineral matter, and a thickness of >30 cm

1979 (Dargie et al. 2017), this differing from the conventional definition cited earlier. Tropical

1980 peats mainly occur along major river systems, and in SE Asia are associated with mangrove

1981 development along coastal zones (Yu et al. 2010). Peak accumulation rates for these peats

1982 are in the Middle Holocene for the tropical peats, Early Holocene for the northern peatlands,

1983 and Late Pleistocene for the southern peats (Yu et al. 2010).
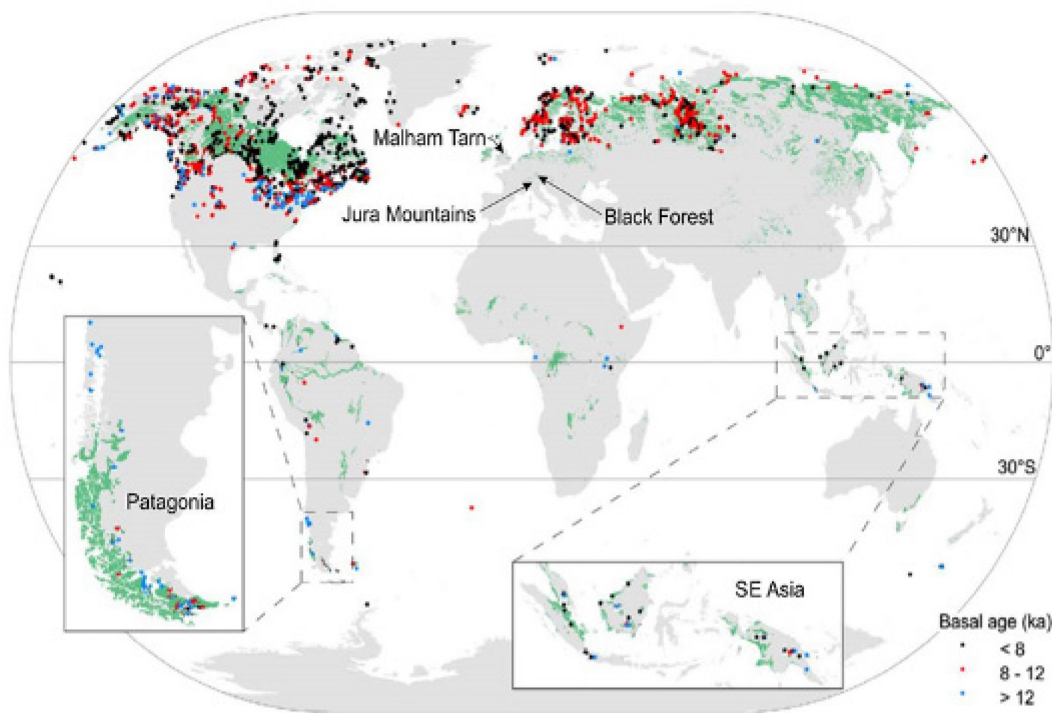
1984

1985   Figure 20. Global map of peatland regions with basal peat ages (black <8 ka, red 8–12 ka, and blue

1986   >12 ka) (from Yu et al. 2010).

1987

1988   Surface waters and groundwaters contain carbonate alkalinity from the chemical weathering

1989   of carbonate and silicate minerals, so the waters in fens and swamps tend to be neutral to

1990   alkaline in pH. Rainwater, on the other hand, contains very little alkalinity. In consequence,

1991   the organic acids generated during the decay of organic matter quickly render bog surface

1992   waters acidic (pH 4). Bog surface waters are also oligotrophic, so only specialized plant

1993   communities are able to thrive. Finally, the depth to water table in bogs will vary seasonally,

1994   resulting in redox conditions varying from oxic to anoxic. Seen from this perspective, the

1995   peat and corresponding porewaters in bogs represent a complex chemical milieu for the

1996   compounds that are continually being supplied by the atmosphere.

1997

1998   As peat accumulates over time, fens and swamps can evolve into bogs, as the surface layers

1999   become increasingly removed from the basal mineral sediments and plants gradually

2000   become deprived of nutrients. Thus, it is very common to find ombrotrophic bog peats

2001   overlying minerotrophic fen and swamp peats (Shotyk 1988). To use peat cores from bogs as

2002   archives of atmospheric deposition, it is crucial to clearly distinguish between the

2003   ombrotrophic versus minerotrophic sections: this can be done using a broad array of

2004   chemical indicators in either the solid or aqueous phases, such as ash or Ca content of the

2005   peat, or pH and Ca content of the porewaters (Shotyk 1996).

2006

2007   Peat cores from bogs have been used to study atmospheric change over time using the

2008   broad range of parameters listed in Table 8. This list of proxies of environmental change

2009   does not imply their fidelity in the peat bog archive. Rather, it should be viewed as an

2010   illustration of the broad potential and number of opportunities represented by bogs to study

2011   environmental change. While most of these proxies have been impacted by human

2012   activities, few provide truly global signals, mainly because of the varying chronology and

2013   intensity of anthropogenic emissions throughout the industrial world (mineral dusts,

2014   spheroidal particles), biogeochemical transformations within the peatland (N and S

2015   compounds) and the size of the host aerosol which is crucial for long-range atmospheric

2016   transport (metals and organic contaminants). Radionuclides from nuclear weapons testing

2017   are exceptional in that they reached the stratosphere, are found in the sub-micrometre

2018   aerosol fraction, and therefore their fallout was dispersed globally (Junge 1963).

2019

2020

2021

2022

2023

2024

Proxy	Type of environmental change	Example
Plant macrofossils	Climate change, human-induced changes in vegetation caused by impacts to watershed hydrology	Magnan et al. (2014)
Pollen	Landscape evolution in response to climate change, forest clearing and agriculture	Markgraf and Huber (2010)
Soil-derived mineral dusts	Wind erosion of soils due to climate change, or caused by forest clearing for agriculture and soil tillage	Chapman (1964); Vuorela (1983)
Volcanic ash	Natural, episodic inputs that may mask anthropogenic inputs of other inorganic constituents	Zoltai (1989)
Trace elements (Ag, As, Cd, Cr, Cu, Ni, Pb, Sb, Se, Sn, V, Tl, Zn)	Derived mainly from mining, smelting and refining of base metals as well as ferrous metallurgical processing and coal combustion. The chlor-alkali industry was a significant source of atmospheric Hg in the past, and artisanal gold mining is an important source of Hg today	As, Cu, Zn: Küttner et al. (2014); Cr, V; Allan et al. (2014); Hg: Enrico et al. (2016); Pb: Veron et al. (2014); Sb: Rothwell et al. (2010); Sn: Meharg et al. (2012)
Lithophile elements (Al, Sc, Th, Ti, Y and the REE)	Wind erosion of soils due to climate change, or caused by forest clearing for agriculture and soil tillage	Vanneste et al. (2015); Kylander et al. (2016); Pratte et al. (2017)
Platinum group elements (PGE)	From automobile catalytic converters	Rauch et al. (2004, 2010)
Fallout radionuclides (including ^{137}Cs, ^{241}Am; also isotopes of U and Pu)	From atmospheric nuclear weapons testing, plus accidental releases from nuclear reactors	Quinto et al. (2013a, b)
Organic contaminants	Polycyclic aromatic hydrocarbons (PAHs) from both natural (prairie and forest fires) and anthropogenic (fossil fuel combustion, petroleum refining) sources	Zhang et al. (2016)
Organometallic compounds	Tetraethyl-lead and tetramethyl lead, from leaded gasoline	Shotyk et al. (2002)
Nitrogen and sulphur (including stable isotopes)	Atmospheric emissions of nitrogen oxides from fossil fuel combustion; sulphur oxides from this plus sulphide mineral roasting	Wieder et al. (2016a, b)
Spheroidal carbonaceous particles	From fossil fuel combustion	Rose (2015); Swindles et al. (2015)
Inorganic ash spheres	From fossil fuel combustion and nuclear explosions	Fialkiewicz-Kozieł et al. (2016)

Table 8. Selected examples of the use of proxies for various types of atmospherically sourced environmental change.

The preservation over time of some of the constituents supplied by the atmosphere may be constrained by the low pH, abundance of complex-forming organic acids, range in redox potentials, and advective flow in response to water table drawdown. The extent of preservation ranges from near-perfect (plant macrofossils are extremely well preserved in anoxic water) to very poor (^{137}Cs is very mobile in ombrotrophic peat, simply because monovalent cations are poorly retained; it is far better retained in minerotrophic peat because of the abundance of phyllosilicates which fix Cs within their siloxane cavities). Some trace metals are very well preserved (e.g. Ti and Zr because of the stability of their host minerals in acidic waters), others not at all (e.g. Mn and Fe which form soluble, mobile cations under anoxic conditions). While there may be hundreds of publications employing bogs as environmental archives, there are remarkably few studies of chemical diagenesis of atmospheric contaminants, and the possible importance of post-depositional migration. Diagenesis of organic contaminants in peat is discussed at length by Thuens et al. (2013), using the example of PAHs, fallout radionuclides using the examples of U and Pu by Quinto et al. (2013a, b), and trace metals using the example of Pb by Shotyk et al. (2016).

Age-dating of peat profiles presents many challenges; peat bogs are not varved, but can have high (annual) growth rates, although these can be very variable. In Switzerland, 1 m peat cores ranged from ~ 1000 to 7000 years of peat accumulation (Shotyk et al. 2000). The most robust age-depth models use a combination of approaches, including ^{14}C (which is physically incorporated within the organic molecules making up the peat) and ^{210}Pb (which is

2049 supplied to the peatland surface by the sub-micrometre aerosol fraction and, apparently,

2050 becomes adsorbed to the peat).

2051

2052 Table 9 summarises the key advantages and disadvantages of hosting a potential GSSP

2053 within peatlands. Examples of geochemical records from peat bogs are provided from the

2054 Jura Mountains of Switzerland and Malham Tarn in England.

For:	Against:
• Widely distributed and studied in northern and southern latitudes; extensive deposits in the tropics are beginning to receive attention • Relatively rapid rates of accumulation of organic matter provide reasonable temporal resolution of atmospheric change • Readily amenable to ^{14}C age dating (including the post-1950 CE atmospheric bomb pulse) • Dating of recent peat accumulation (past ~150 years) possible using ^{210}Pb • Ombrotrophic bogs receive inputs directly and exclusively from the atmosphere with no settling delay • Wide variety of indicators of industrial activities are easily measured: soil-derived dust particles, N and S compounds, fallout radionuclides, heavy metals, organic contaminants, spheroidal carbonaceous particles (SCP) and inorganic ash spheres (IAS)	• In many industrialized regions most bogs have been damaged, altered or destroyed due to drainage for agriculture, development, forestry, or exploited for fuel or horticultural peat • Peat accumulation rates vary over time depending on climate, hydrology, fire and inputs of mineral matter from wind erosion of soils, or volcanic ash; they are not varved • ^{210}Pb age dating requires independent confirmation using chronostratigraphic markers including: other fallout radionuclides (such as ^{241}Am), pollen, tephrochronology, or contaminants of known emission history (e.g. DDT) • Pb is immobile in undisturbed peat profiles but can be mobilized by bog water acidification (from acid rain) or peatland drainage (which promotes leaching) • Minerotrophic peatlands are influenced and commonly dominated by aquatic inputs (surface and groundwater). Atmospheric signals may be discernible in minerotrophic systems provided that aquatic inputs are insignificant (e.g. fallout radionuclides) • With acidic bog waters and seasonal variations in water table depth (and therefore varying thickness of the oxic surface layer), each proxy may be subjected to chemical diagenesis; the possible importance of post-depositional migration (or chemical transformation) of each proxy must be evaluated

2055 **Table 9.** Reasons for and against using a peat deposit as a potential host for a GSSP.

3.6.1 Pb, organic contaminants and radionuclide fallout deposition at Etang de la Gruère, Jura Mountains, Switzerland

The protected ombrotrophic *Sphagnum* bog of Etang de la Gruère has the longest record of peat accumulation (6.5 m accumulated in ~15,000 years) in the Northern Hemisphere (Shotyk et al. 1998). Traces of atmospheric lead appear in this Swiss peat bog from 12,370 ^{14}C yr BP (Shotyk et al. 1998). Climate-controlled enhanced Pb fluxes derived from soil dust are recorded with maxima at 10,590 and 8230 ^{14}C yr BP, the latter coinciding with the start of the Middle Holocene (Shotyk et al. 1998). The first anthropogenically-controlled increase in Pb deposition starting at 5320 ^{14}C yr BP is thought to be due to forest clearing and the introduction of agriculture (Shotyk et al. 1998). The first influence of Pb pollution from mining and smelting started at 3000 ^{14}C yr BP and occurs at a depth of 1.4–1.5 m, seen as increased Pb enrichment and decreased ^{206}Pb/^{207}Pb ratios (Shotyk et al. 1998). However, by far the greatest Pb flux occurred in the late 20th century (Figure 21a), reaching 1570 times the background value by 1979 CE (Shotyk et al. 1998), associated with greatly decreased ^{206}Pb/^{207}Pb ratios (Figure 21b). Subsequently, reduced Pb contents and increasing Pb isotope ratios in the later decades of the 20th century appear to record the introduction of unleaded gasoline and a reduction in industrial sources of Pb in the region (Shotyk et al. 1998). The Pb signals in peat at this locality are consistent with Pb levels in the Greenland GRIP ice core over the past 3000 years (Shotyk et al. 1998) and can be compared with the Greenland ACT2 core (Figure 26).
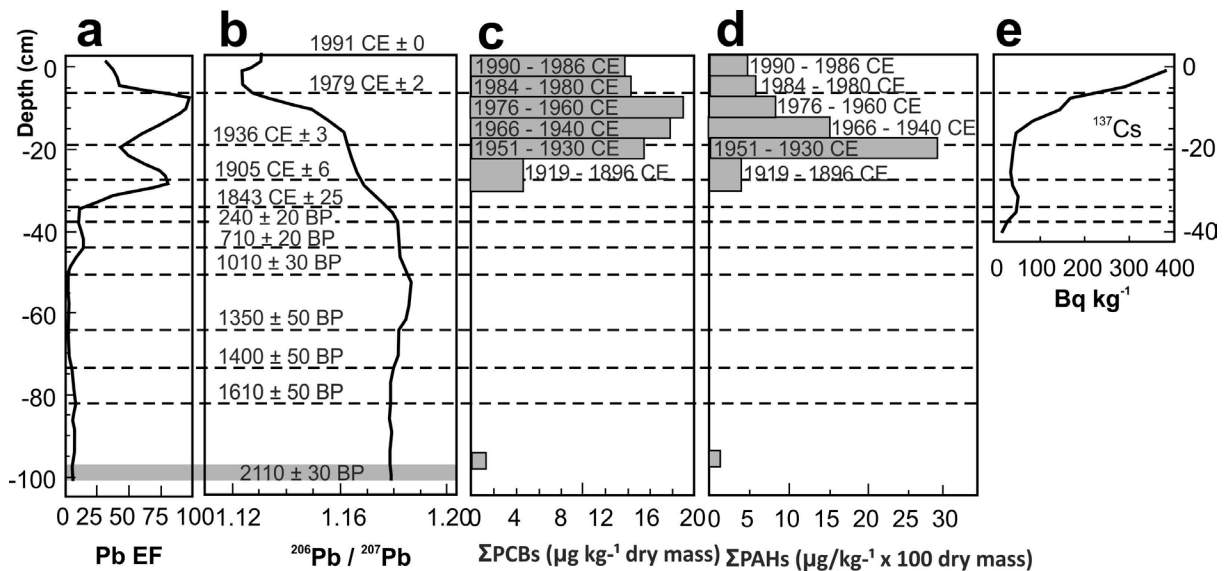
Figure 21. Core from Etang de la Gruère, Switzerland, collected in 1991 CE: a) Pb Enrichment Factor (EF) calculated as the ratio of Pb/Sc in the peats, normalized to the background value (from Shotyk et al. 1998); b) Pb isotopic values (from Shotyk et al. 1998); c) ΣPCBs (from Berset et al. 2001); d) ΣPAHs (from Berset et al. 2001); e) [137]Cs (from Appleby et al. 1997). Succession dated using ^{210}Pb to 35 cm depth (Appleby et al. 1997) and ^{14}C yr BP from 35 cm to base (Shotyk et al. 1998).

The highest concentrations of PCBs occurred at a depth of 10–15 cm (dating from 1976 to 1960 CE; Figure 21c) while PAHs reached a maximum at a depth of 20–25 cm (1951 to 1930 CE; Figure 21d), with post-depositional downward migration of these compounds unlikely (Berset et al. 2001). The maximum PAH values coincide with greatest use of coal in Switzerland, after which fuel oil dominated (Berset et al. 2001).

The same core has records of [241]Am activity limited to 12–15 cm depth (Appleby et al. 1997), marking the early 1950s to early 1960s bomb-spike. [137]Cs activity is at a maximum in the living part of the profile in the upper 3 cm (Appleby et al. 1997; Figure 21e), inferred to be sourced by the Chernobyl disaster of 1986 CE. [137]Cs is also recorded below the level of the [241]Am signal, probably because it has been remobilized downwards.

3.6.2 Spheroidal carbonaceous particles and Pb in Malham Tarn Moss, England

2093   Spheroidal carbonaceous particles (SCPs) first appear in the peat succession adjacent to an

2094   upland lake at Malham, England, at a level deposited in the 1850s, but there is a marked

2095   increase in their abundance in the 1950s (represented by less than 10 cm of peat), with a

2096   peak in the 1970s (Figure 22, Swindles et al. 2015). Atmospheric lead pollution from local

2097   industrial activity and additives in petrol, and increased soil erosion (reflected in the Fe and

2098   loss-on-ignition data), show comparable upturns in the mid-20th century.
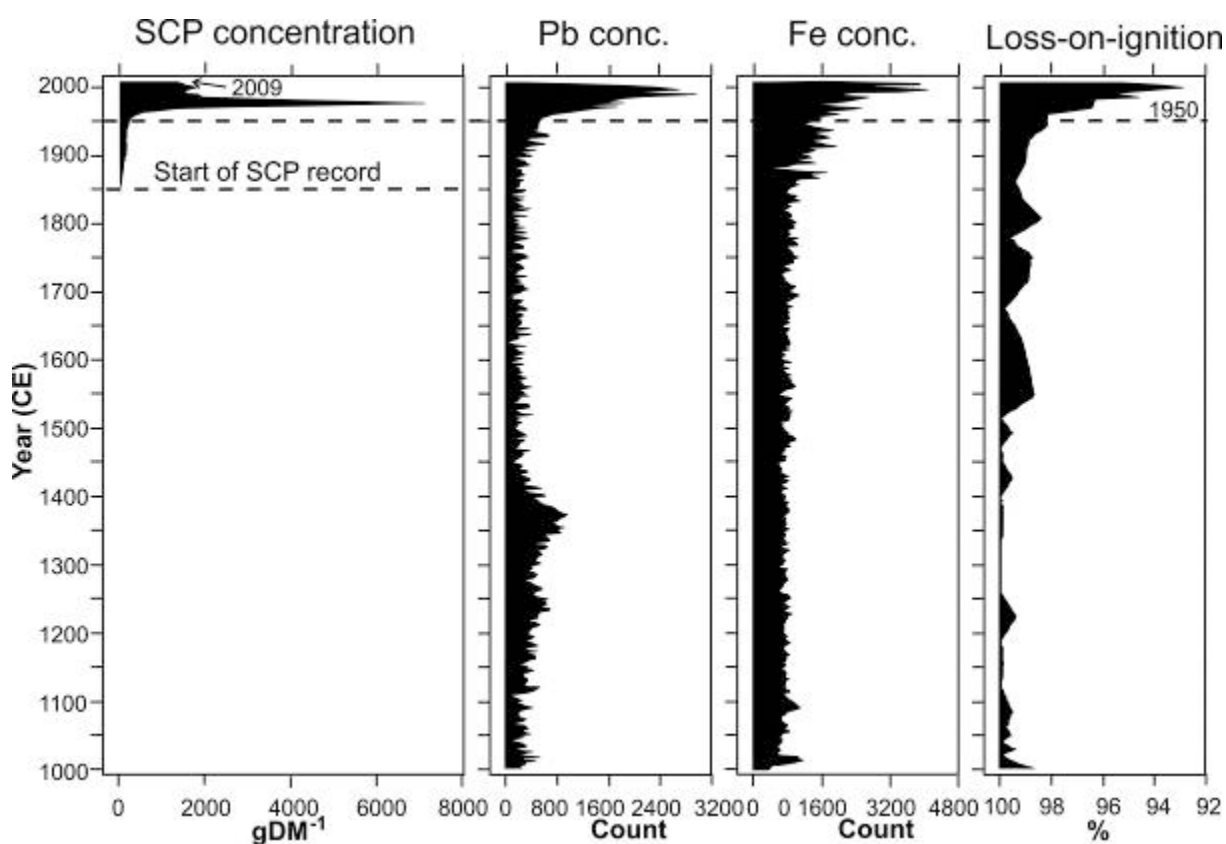
2099

2100   **Figure 22.** Spheroidal carbonaceous particles (SCPs), lead and iron concentrations from Malham Tarn

2101   Moss, England (from Swindles et al. 2015).

2102

3.7 Ice

Continental ice sheets including those of Antarctica, covering about 13 million km^2, and Greenland, covering about 1.7 million km^2 (UNEP 2007), are together equivalent to about 9.4% of the total land surface area (Figure 23). Ice from glaciers occurring both marginal to the ice sheets and in high-altitude regions makes up a further ~0.5% of the Earth's land surface, a coverage of 726,800 ± 34,000 km^2 (Pfeffer et al. 2014) (Davies, B. Mapping the World's Glaciers http://www.antarcticglaciers.org/glaciers-and-climate/mapping-worlds-glaciers/ Last updated 22/06/2017). Sea ice fluctuates in extent seasonally and does not form a permanent ice record for consideration as a potential GSSP site. Although ice sheets and glaciers have significant extents, what little permanent ice remains in Africa and Australasia (Figure 23) is rapidly being lost. Alpine glaciers from high altitudes may be suitable as potential GSSPs, but those from lower elevations are prone to significant seasonal melting and potential loss of laminae. Land glaciers in tropical regions are now melting from the top down and losing their younger layers (e.g. in Peru). Within alpine glaciers, unlike on polar ice sheets, meltwater processes can mobilize or remove solutes, attenuating or complicating the environmental signal (Schuster et al. 2002). In contrast, polar land ice is a more permanent record. The Greenland ice sheet shows the effects of greater local contamination from Northern Hemisphere industrial activities, while Antarctic land ice is more pristine.
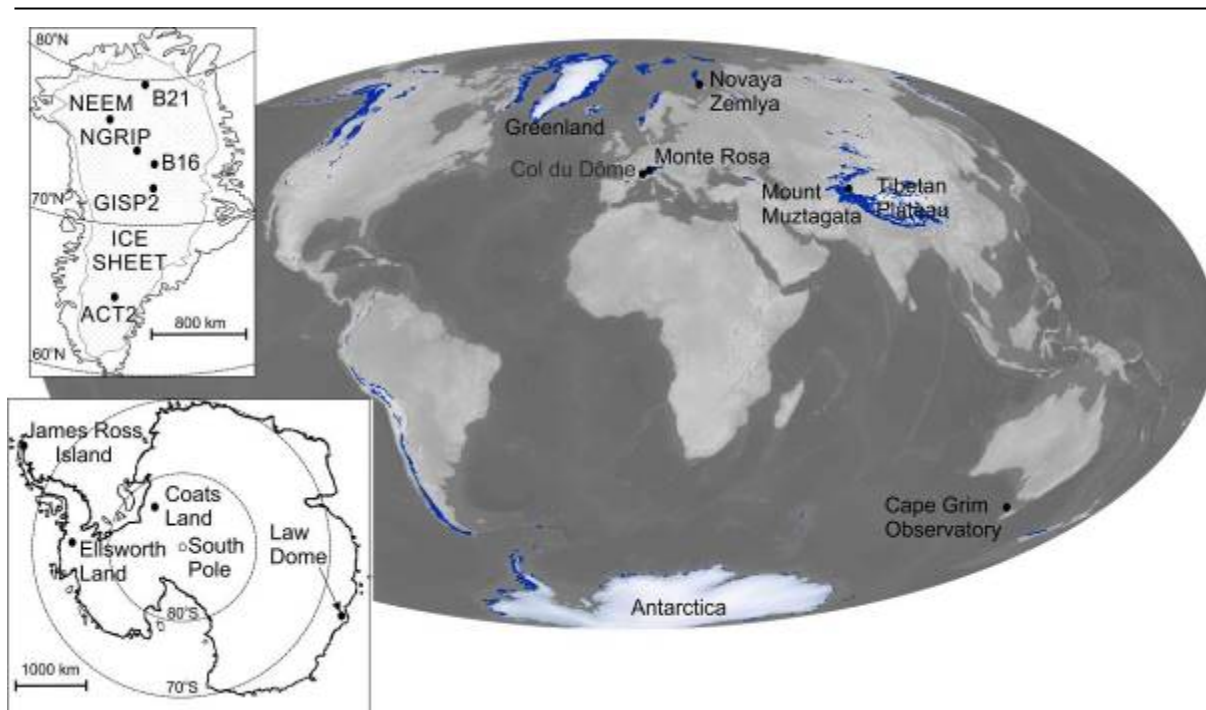
2123

Figure 23. Distribution of ice caps and glaciers (blue) and ice sheets (white) from NASA Earth Observatory Randall Glacier Inventory in 2014 CE http://earthobservatory.nasa.gov/IOTD/ view.php?id=83918 (acquired 7th May 2014; produced by Jesse Allen and Robert Simmon). Inset maps showing the main polar drilling sites in Antarctica and Greenland mentioned in the text.

Quaternary stratigraphy is closely linked to climatic variations during the ~2.6 million years of bipolar glaciation. Ice cores provide the best record of climate-related data for up to 800 ka, including isotopic ratios for $\delta^{18}O$ and δD, variations in CO_2 and CH_4 concentrations and dust, and S concentrations related to distinct volcanic events. The use of a Greenland ice core for the Holocene GSSP (Walker et al. 2009) provides a precedent that may be considered for the Anthropocene. Atmospheric CO_2 and CH_4 concentrations and novel compounds such as sulphur hexafluoride SF_6 can be detected in ice-core air bubbles (Wolff 2014). The ice record also captures anthropogenic signals derived from aerosols, including radionuclide signals from nuclear bomb testing (e.g. ^{239}Pu, ^{14}C), unprecedented increases in black carbon (BC) and metals such as Pb from industrial activity and automobile emissions, sulphate especially from coal combustion, and nitrate from fertilisers. These signals occur

2140 within annually resolvable laminae, the ages of which are typically determined by counting

2141 or from seasonal cycles in $\delta^{18}O$, and then verified using known volcanic eruption signals,

2142 which can be identified from electrical conductivity measurements in Greenland (e.g.

2143 Masson-Delmotte et al. 2015), and at Law Dome, Antarctica (Etheridge et al. 1996). Silicate

2144 dust concentrations in polar snow are exceedingly small, a mean of 2 ppb in Antarctica and

2145 35 ppb in Greenland, with the latter showing no systematic trends over two centuries from

2146 1750 CE (Murozumi et al. 1969).

2147

2148 The upper part of an ice sheet or glacier, which includes the succession that covers the mid-

2149 20th century interval, comprises firn (partially compacted snow that is not yet fully ice),

2150 where bubbles are not yet closed from connection to the atmosphere. For most signals that

2151 are trapped directly in the solid ice this does not represent a problem, but CO_2, CH_4 and N_2O

2152 are contained in trapped air bubbles. These air bubbles and their environmental signals are

2153 therefore always younger than the enclosing ice, and this effect is significant over the short

2154 timescales considered for the Anthropocene. However, recent work shows that the nitrogen

2155 isotopes in air bubbles can be used to estimate their ages correctly, enabling direct

2156 comparison with ice of the same age (Parrenin et al. 2013). The depth and hence timing of

2157 the firn-to-ice transition is dependent upon the accumulation rate, and so sites with rapid

2158 accumulation rates are preferable. At the South Pole, where the accumulation rate is only 8

2159 cm yr^{-1} the firn-to-ice transition depth is at about 123 m (Rubino et al. 2013).

2160

2161 Over the past 350 years in East Antarctica, δD proxy values show a long-term warming trend

2162 of about 1 ± 0.2 °C, with a marked colder period from 1750 to 1860 CE corresponding to the

2163 end of the "Little Ice Age (LIA)" (Ekaykin et al. 2017). This is consistent with James Ross Island

2164 and other parts of the Antarctic Peninsula, these areas warming significantly from about

2165 1950 CE onwards (Quayle et al. 2002, Abram et al. 2013). In north Greenland, $\delta^{18}O$ shows

2166 multi-decadal increasing trends in the late-19th century and since the 1980s, whereas the

2167 early-19th century had the lowest signals, associated with the Little Ice Age. Overall,

2168 Greenland δD and (laterally variable) $\delta^{18}O$ show no significant variation across the mid-20th

2169 century, with the most prominent climatically linked changes occurring about 1850 CE

2170 (Masson-Delmotte et al. 2015, Ekaykin et al. 2017, Figure 24 herein).
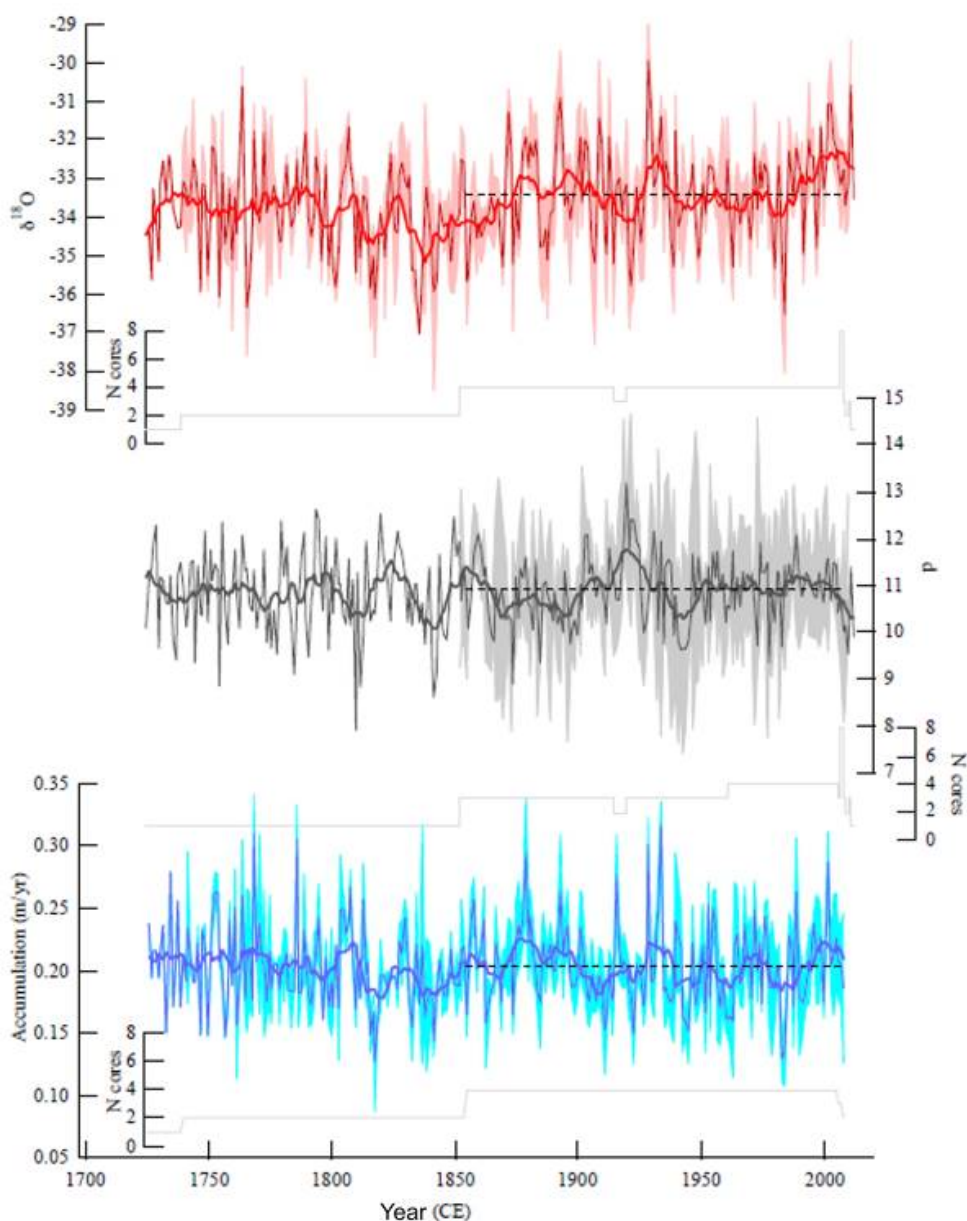
2171

2172 **Figure 24.** $\delta^{18}O$, δD and accumulation rates for the North Greenland Eemian Ice Drilling site (NEEM)

2173 (Masson-Delmotte et al. 2015).

2174

2175   One of the main climate-related signals evident in ice sheets is the increase in CO_2

2176   concentration (Figure 25), now 30% above the highest level of the last 800 ka (Wolff 2014),

2177   and the $\delta^{13}C$ change to more depleted values, both occurring at about 1960 CE in Law Dome

2178   ice core (Rubino et al. 2013) and discussed below. This may reflect the divergence of fossil

2179   fuel use (which has accelerated) and land use as independent sources of atmospheric CO_2

2180   and hence of the $\delta^{13}C$ signal (Rubino et al. 2013). CH_4 is now at ~1800 ppb (Figure 25),

2181   double the highest level of the last 800 ka (Wolff 2014).
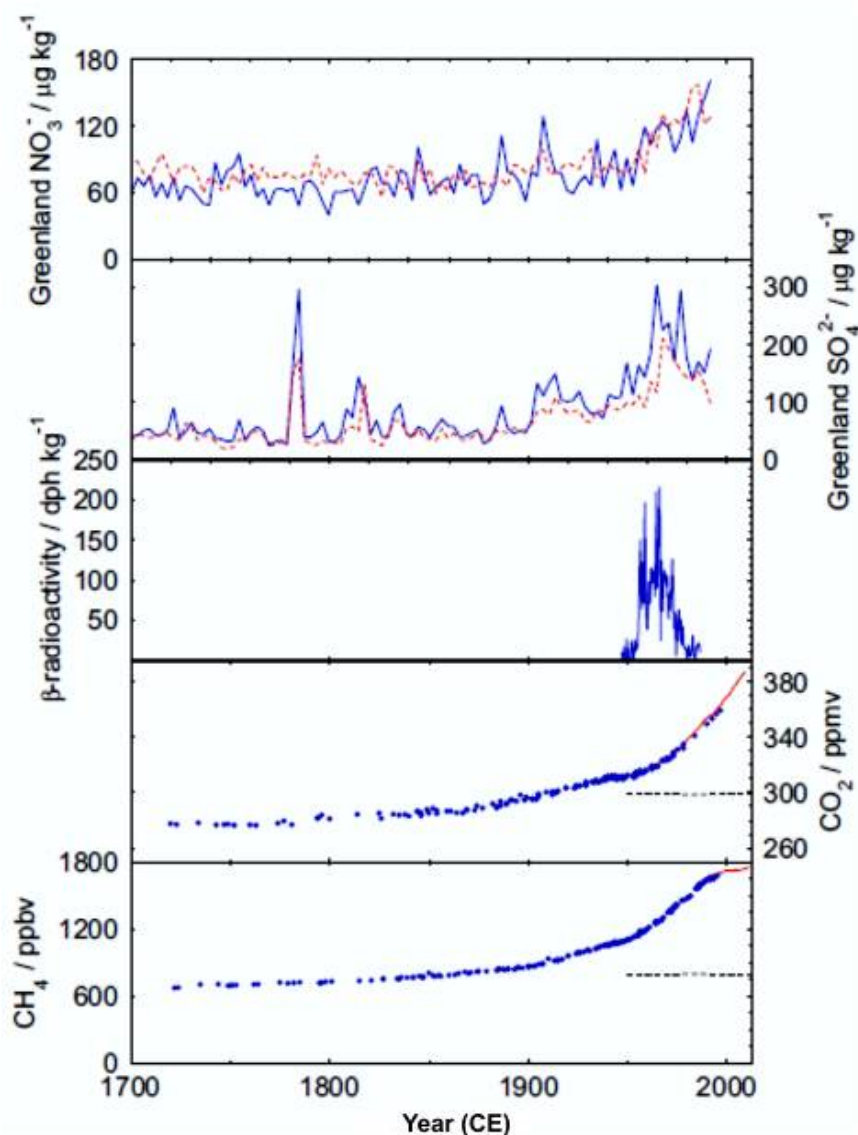
2182

Figure 25. Ice core signals since 1700 CE (from Wolff 2014). CH_4 and CO_2 ice-core data (blue dots) are from Law Dome, Antarctica (MacFarling Meure et al. 2006), and recent atmospheric data (red lines) from Mauna Loa (CO_2) and Cape Grim (CH_4) observatories. The horizontal dashed lines are the highest values observed in ice cores of the last 800,000 years prior to the period shown. Beta radioactivity is from Coats Land, Antarctica (Wolff et al. 1999). Sulphate and nitrate are shown for two cores from Greenland: B16 (dashed red) and B21 (solid blue) (Fischer et al. 1998). The 18th- and 19th-century spikes in sulphate are signals of volcanic eruptions.

The most abrupt anthropogenic signal in ice is radioactive fallout from the atmospheric testing of nuclear devices. This is clearly evident in ice core as a marked increase in beta radioactivity initially in 1954 CE and subsequently in 1964 CE to form a bomb-spike peak in 1966 CE (Figure 25), followed by slow decay towards natural background levels (Wolff et al. 1999, Wolff 2014) after testing went underground following the Partial Test Ban Treaty in 1963 CE and essentially ceased following the Comprehensive Test Ban Treaty in 1996 CE (see Waters et al. 2015). The beta radiation is from several radioactive isotopes, some with short half-lives, e.g. ^{90}Sr and tritium. The long-lived radionuclide ^{239}Pu in polar ice has been transferred primarily via the stratosphere, with atmospheric residence times of up to 5 years and with seasonal transfer to the troposphere occurring in late winter and spring in the Northern Hemisphere (Arienzo et al. 2016). The accumulation rate of ^{239}Pu is typically greater in ice, and shows less post-depositional alteration or mixing, than in corals and lake sediments (Arienzo et al. 2016). Analysis for ^{239}Pu using traditional accelerator mass spectrometry (AMS) requires large sample size, typically reducing the resolution to about 3 years (Arienzo et al. 2016). A high-resolution (0.5–1.5 years) ^{239}Pu profile from Monte Rosa on the Italian-Swiss border, using ICP-SFMS, shows an initial peak from 1954–1955 to 1958 CE (Gabrieli et al. 2011). Following a temporary halt of testing in 1959–1960 CE, in which the Pu concentration decreased by half with respect to the 1958 CE peak, in 1961–1962 CE Pu

concentrations increased rapidly to a peak in 1963 CE (Gabrieli et al. 2011). Following the Partial Test Ban Treaty, Pu deposition decreased sharply to a minimum in 1967 CE (Gabrieli et al. 2011). The interval 1967–1975 CE is characterized by small irregular Pu smaller peaks likely due to the deposition of Saharan dust contaminated by French nuclear tests of the 1960s, this effect diminishing after 1975 CE (Gabrieli et al. 2011). Arctic ice typically has a higher [239]Pu activity (differing by about a factor of three) than Antarctic ice (Arienzo et al. 2016) and, despite the first significant atmospheric thermonuclear detonations occurring in 1952 CE, the first detection of [239]Pu in polar ice was in 1953 CE (Arienzo et al. 2016). The post-moratorium [239]Pu bomb-spike (peak signal) occurs in the 1962 CE ice laminae in the Arctic, but is not strongly resolved in the Antarctic, mainly because the principal testing occurred in Novaya Zemlya (northern Russia), and little of this fallout crossed into the Southern Hemisphere (Arienzo et al. 2016).

Ice cores provide the most straightforward archives of sulphur, both as a record of global volcanic events (Schuster et al. 2002), but also in documenting the long-range effects of pollution unaffected by the local pollution seen in tree rings and speleothems (Fairchild et al. 2009). In Greenland ice, sulphate (SO_4^{2-}) concentrations increased markedly from 1900 to 1920 CE and 1940 to 1980 CE (Figures 24 and 25), and by 1980 CE concentrations were a factor of 2–5 above pre-industrial peak values (Fischer et al. 1998), but did not exceed concentrations linked to large volcanic eruptions or during the Last Glacial Maximum (Wolff 2014). In central Asia, in ice on Mount Muztagata (China), the steep rise in sulphate concentrations that started after the mid-1970s and decreased in the 1990s is associated with changes in industrial activity (Zhao et al. 2011). No equivalent signature is recorded in Antarctic ice, which is more remote from the main sources of sulphate pollution (Wolff 2014).

2234

2235 N_2O, a greenhouse gas, has an atmospheric lifetime of about 120 years, so any changes

2236   recorded in ice cores reflect global changes, thought to mainly reflect increased application

2237   of agricultural fertilizers (Wolff 2013). N_2O concentrations recorded in air bubbles within the

2238   ice have risen by about 20% in the last 200 years (see Law Dome example below) and are at

2239   levels higher than recorded for the last 800 ka (Wolff 2013). In contrast, ammonium (NH_4^+),

2240   mainly deposited as aerosol, and nitrate (NO_3^-), deposited as an aerosol or as nitric acid,

2241   have much shorter atmospheric residence times, and changes in their concentrations reflect

2242   local changes in source areas (Wolff 2013). Mid-latitude glaciers, such as Mount Muztagata

2243   in China, show an approximately three-fold increase in ammonium concentrations between

2244   1960 and 1990 CE, probably as a consequence of agricultural emissions (Zhao et al. 2011).

2245   However, there is no significant recent trend at either pole (Wolff 2013). Whereas

2246   ammonium is permanently fixed in the snow, nitrate can be re-emitted back to the

2247   atmosphere (Fischer et al. 1998, Wolff 2013). Increased nitrate concentrations evident in the

2248   Northern Hemisphere (Figure 25) are mainly due to NO_x emissions from fossil fuel

2249   combustion (Wolff 2013, 2014), including automobiles and coal-fired power stations. In

2250   Greenland ice the main phase of nitrate increase, which has risen by a factor of 2–3,

2251   occurred from 1950 to 1980 CE (Fischer et al. 1998, Wolff 2013); by 1980 CE levels were

2252   higher than over the past 100 kyr (Wolff 2014). In the French Alps, at the Col du Dôme, high

2253   snow accumulation rates allow distinction between summer and winter snow, with higher

2254   summer nitrate values showing a fivefold increase during the 20th century, most markedly

2255   between 1960 and 1980 CE and sourced by emissions within 1000 km of the glacier

2256   (Preunkert et al. 2003). However, nitrate does not provide a consistent global signal. In

2257   central Asia, at Mount Muztagata, the steep rise in nitrate concentrations, which increased

2258 by a factor of two, started after the late-1970s and had already peaked by 2000 CE (Zhao et

2259 al. 2011), whereas no significant increase occurs then in Antarctic ice (Wolff 2013).

2260

2261 A shallow (100 m) GISP2 ice core from Summit (Greenland), ranging in age from 1718 to

2262 2006 CE, shows a clear decreasing $\delta^{15}N$ trend in atmospheric nitrate, from pre-industrial

2263 values around 11 to -1‰ in the early 21st century (Hastings et al. 2009). The $\delta^{15}N$ trend

2264 began about 1850 CE, whereas the increase in nitrate from the same core rises in about

2265 1890 CE (Hastings et al. 2009). The greatest rate of change in $\delta^{15}N$ occurred from 1950 to

2266 1980 CE, coincident with a rapid rise in fossil fuel emissions (Hastings et al. 2009).

2267

2268 During pre-industrial times, about half the lead in the troposphere was associated with soil

2269 dust and half with volcanic gases (Patterson and Settle 1987). Pb, As, Sb, Bi, Cu, and Zn

2270 enrichments in Arctic ice cores started at around 3300–3000 yr BP, with an additional

2271 significant Roman phase (Hong et al. 1994, Krachler et al. 2008, 2009). Further increases of

2272 Pb, TI, and Cd in response to the Industrial Revolution are more significant, with elevated

2273 concentrations from the 1860s, accelerated concentrations from 1887 to 1889 CE and peaks

2274 in the early 20th century (TI in 1911–1915 CE, Cd in 1906 CE, Pb in 1915 CE) (McConnell and

2275 Edwards 2008, Figure 26). This early peak is considered to reflect increased coal burning in

2276 North America and Europe (McConnell and Edwards 2008). However, the greatest rises in Pb

2277 concentrations are from the 1950s, peaking in the 1960s, associated with emissions of Pb

2278 used in alkyl-leaded gasoline (Murozumi et al. 1969, Boutron et al. 1991, McConnell and

2279 Edwards 2008). TI shows no equivalent mid-20th century peak, whereas Cd has a 1946 CE

2280 peak concentration (Figure 26). At its peak, Pb levels in Greenland ice were above Holocene

2281 background levels by a factor of 200 and exceeded concentrations seen during the last

2282 glacial maximum (Murozumi et al. 1969); in Antarctic ice they were a factor of five above

2283   pre-Industrial levels (Patterson and Settle 1987, Wolff and Suttie 1994). Use of lead additives

2284   in gasoline became limited in the USA and other Northern Hemisphere countries from about

2285   1970 CE, and concentrations decreased in Greenland by a factor of 7.5 between 1970 and

2286   1990 CE, with Cd (Figure 26) and Zn sourced from industrial processes showing a decrease by

2287   a factor of 2.5 over the same interval (Boutron et al. 1991, McConnell and Edwards 2008). In

2288   Antarctica, by 1920 CE anthropogenic Pb (mainly from metal processing) dominated

2289   concentrations that were 2 to 4 times higher than pre-Industrial levels (Wolff and Suttie

2290   1994). Lower concentrations in the 1930s to mid-1940s are followed by a marked upturn in

2291   concentrations by a factor of >2 from 1950 to 1980 CE, with subsequent decline (Wolff and

2292   Suttie 1994). The first use of unleaded gasoline in many Southern Hemisphere countries

2293   started as late as the 1980s and 1990s (Wolff and Suttie 1994). Because most combustion of

2294   gasoline occurred in the Northern Hemisphere, it is in Greenland that the rise and

2295   subsequent fall of Pb signals is greatest. Lead aerosols have a 10-day residence time in the

2296   atmosphere resulting in little inter-hemispheric interchange (Patterson and Settle 1987).

2297
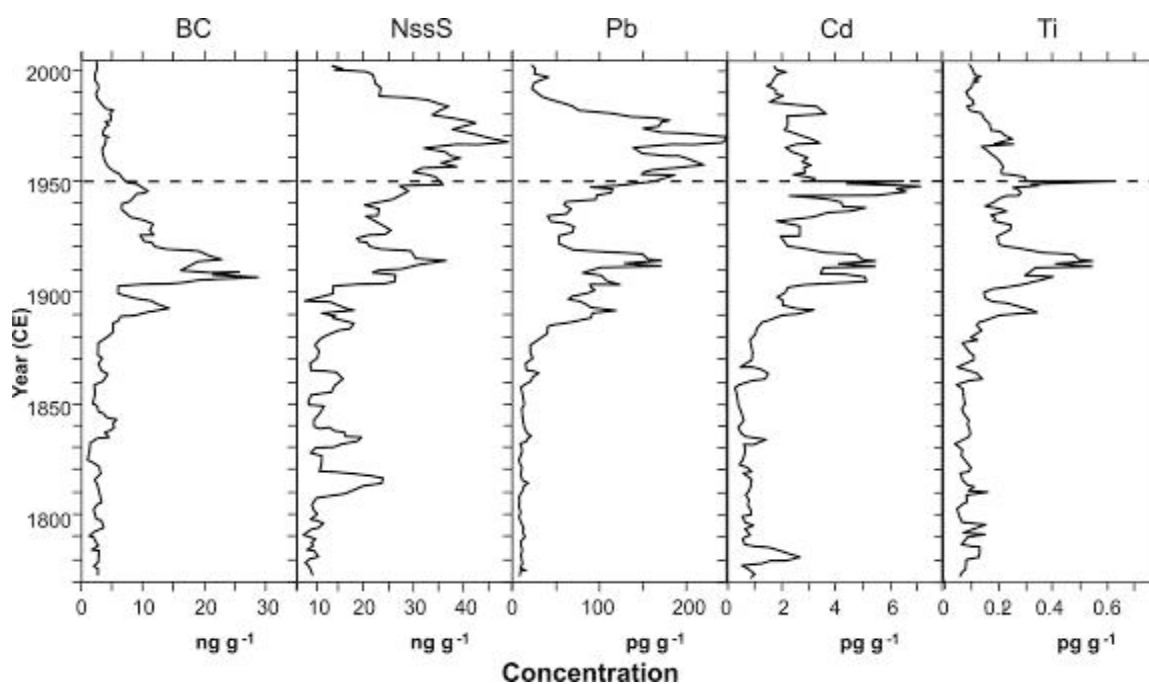
2298

Figure 26. Concentrations (5-year running means) in Greenland ACT2 ice core from 1772 to 2003 CE of sulphur (NssS), thallium (Tl), cadmium (Cd) and lead (Pb), compared to black carbon (BC), from McConnell and Edwards (2008). Sulphur peaks in 1817 and 1883 CE relate to the Tambora and Krakatoa volcanic eruptions, respectively. © (2008) National Academy of Sciences, U.S.A.

Atmospheric Hg contamination in a glacier in Wyoming (USA) from ~1720 to 1993 CE shows a twenty-fold increase from pre-1840 CE levels to a ~1984 CE peak (Schuster et al. 2002). Early spikes include both volcanic sources from Tambora (1815 CE) and Krakatoa (1883 CE), showing cross-hemispheric transfer of Hg, and an anthropogenic source with a double peak and elevated values from ~1850 to 1884 CE associated with the California Gold Rush in western USA (Schuster et al. 2002).

In Greenland, black carbon is attributed by McConnell and Edwards (2008) as: Preindustrial (1772–1860 CE), coal-dominated industrial (1860–1940 CE), and oil-dominated industrial (1940–2003 CE), with peak concentrations in the first decade of the 20th century (Figure 26). However, peak combustion of coal is later in Asia. Black carbon and organic carbon concentrations in Tibetan ice cores show a marked high during the 1950s and 1960s, attributed to the inflows of industrial emissions, mainly from Europe, with a decline during the 1970s and 1980s (Xu et al. 2009). Glaciers in the southern part of the plateau show black and organic carbon increases after the 1990s, from a southern source (Xu et al. 2009). Increased black carbon on glacial ice reduces surface reflectivity and increases melting (Xu et al. 2009), potentially causing significant hiatuses in modern laminae.

Microplastics have been reported in Arctic sea-ice (Obbard et al. 2014) from contaminated surface sea-water that has been frozen. However, there is no record of microplastics in polar

continental ice sheets or glaciers. The potential for airborne transfer of microfibres (Dris et

al. 2016) suggests that microplastic fallout in glacial ice might occur, especially where

glaciers are close to urban areas.

Table 10 summarises the key advantages and disadvantages of having a potential GSSP

within glacial ice, as is the case for the base of the Holocene. The Law Dome ice core from

Antarctica has a high-resolution multi-proxy record for the last 1000–2000 years and shows

many characteristics that make it suitable for hosting a potential GSSP. Other similarly

suitable ice cores are available elsewhere in both Antarctica and Greenland (Figure 23),

although many of the sites are unsuitable because the rate of accumulation is too low (e.g.

Dome C, Antarctica).

For:	Against:
• Annual layers, high resolution • Extensive distribution, but only Greenland and Antarctic ice sheets likely to persist • Independent dating using ^{210}Pb, but not ^{14}C • Major volcanic eruption events provide clear S spikes • SO_4^{2-} clear spike starts mid-20th century, but diachronous • NO_3^- increase and δ^{15}N depletion from ~1950 CE • Increased lead accumulation from 1950s, especially from gasoline source • Increased Zn, Cd, and Cu concentrations • Radionuclides, clearly resolved bomb spike • Holocene GSSP precedent in Greenland	• Surficial laminae (recent decades) are more prone to melting by global warming than deeper laminae (Holocene), especially in alpine glaciers and coastal ice sheets • Alpine glaciers melting at rapid rate • Lag between age of ice and younger age of air bubbles (100 years in Greenland, possibly up to 1000 years in Antarctica) • δD and δ^{18}O no significant variation across mid-20th century • Increased dust flux not consistently evident • Mid-20th century increased CO_2 and CH_4 concentrations and δ^{13}C depletion signal not fixed in air bubbles • Core difficult/expensive to procure and to store safely

Table 10. Reasons for and against using an ice core as a potential host for a GSSP.

3.7.1 Law Dome Ice Core, East Antarctica

A high-precision 1000–2000 year history of CO_2, CH_4, N_2O and $\delta^{13}C$ has been acquired from the Law Dome site in East Antarctica (Etheridge et al. 1996, Francey et al. 1999, Ferretti et al. 2005, MacFarling Meure et al. 2006, Rubino et al. 2013). As regards hosting a potential GSSP site, the high snow accumulation rates, low temperatures, and small quantities of impurities at Law Dome make this record particularly suitable, especially for recognising a high-resolution $\delta^{13}C$ signal (Rubino et al. 2013). The Law Dome site comprises three cores drilled between 1987 and 1993 CE, (Etheridge et al. 1996, Rubino et al. 2013), dated by counting annual layers in oxygen isotope ratios ($\delta^{18}0$), ice electroconductivity measurements and hydrogen peroxide (H_2O_2) concentrations (Etheridge et al. 1996), with a gas-age/ice-age difference of between ~31 and ~55 years for CO_2 (Rubino et al. 2013).

Between 1000 and 1600 CE, the CO_2 concentration varies between 278 and 284 ppm (Figure 27a), and between 1000 and 1500 CE, the $\delta^{13}C$ values remained constant at about -6.55‰ (Rubino et al. 2013). The brief decrease in concentration of CO_2 in the Law Dome ice core around 1600 CE (Etheridge et al. 1996, MacFarling Meure et al. 2006) was used by Lewis and Maslin (2015) as their "Orbis Event" which they regarded as sufficiently important to be a candidate for defining the beginning of the Anthropocene. Analysis of changes in atmospheric carbonyl sulphide concentration, which is linked to changes in gross primary production of terrestrial ecosystems, shows that temperature change, rather than vegetation re-growth, was the main cause of the increased terrestrial storage and hence drop in atmospheric CO_2 around 1600 CE (Rubino et al. 2016). After a recovery, CO_2 maintained comparatively low concentrations and elevated $\delta^{13}C$ through to 1750 CE (Rubino et al. 2013). Over the past 200 years, atmospheric CO_2 concentrations at Law Dome have increased by 29% (MacFarling Meure et al. 2006). Following the Industrial Revolution,

2364   Rubino et al. (2013) show two inflexion points in the 20th century δ¹³C signal: from 1915 CE,

2365   and from 1955 CE. There is stabilization of atmospheric CO₂ concentrations at 310–312 ppm

2366   from ~1940 to 1955 CE (Figure 25) (MacFarling Meure et al. 2006). The subsequent increase

2367   appears to coincide with increase in fossil fuel use at about 1950 CE (Rubino et al. 2013). The

2368   Francey et al. (1999) high-precision record of atmospheric δ¹³C based on Antarctic ice cores

2369   shows two straight segments: one between 1850 and 1961 CE, and a steeper segment

2370   between 1962 and 1980 CE.

2371

C

N₂O (ppbv) vs. age of air (Year CE)
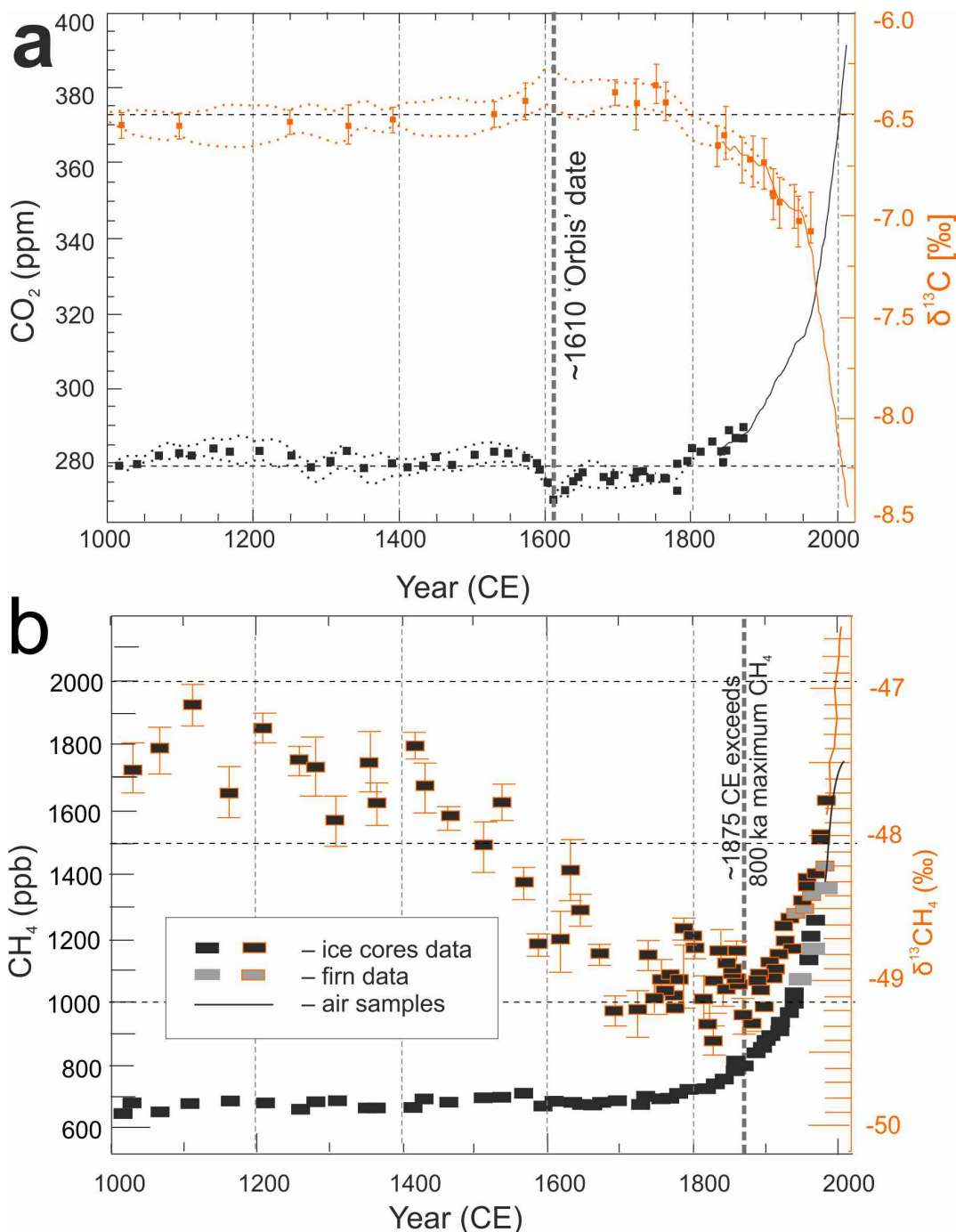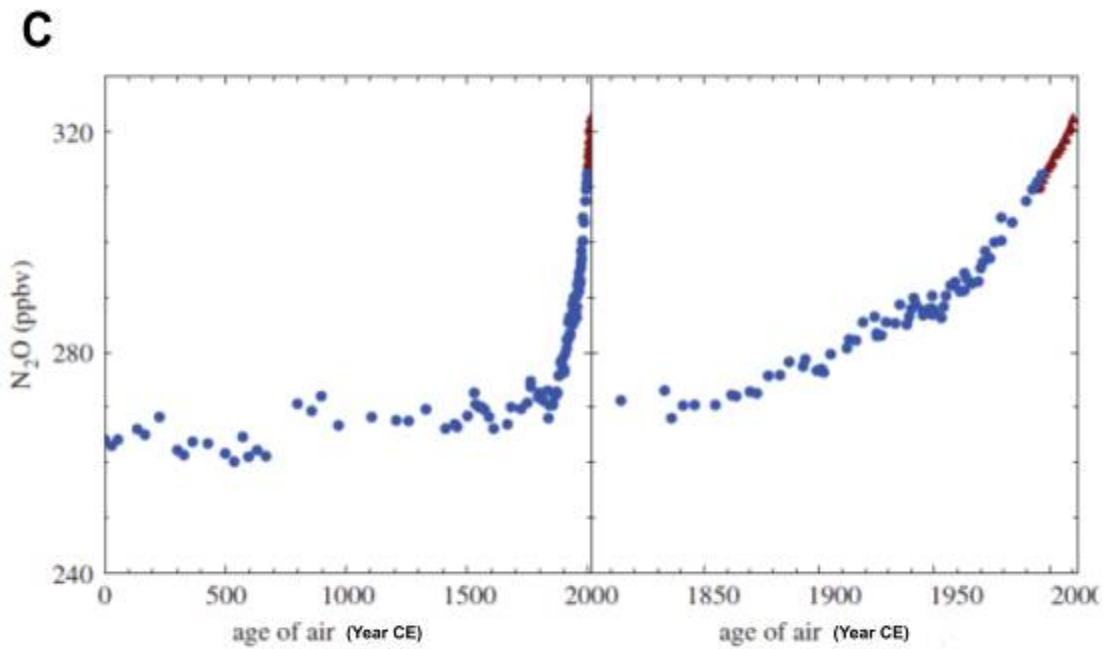
2372

2373 **Figure 27.** a) Law Dome ice core and firn records for CO_2 concentration and $\delta^{13}C$ for atmospheric CO_2

2374 for the past 1000 years (from Rubino et al. 2013); b) Law Dome ice core and firn records for CH_4

2375 concentration and $\delta^{13}C$ for atmospheric CH_4 for the past 1000 years (from Ferretti et al. 2005); c) N_2O

2376 concentrations in the Law Dome ice core over the past 2000 years and 200 years (Wolff 2013).

2377

2378 The Law Dome ice core records also show atmospheric methane (CH_4) concentrations

2379 ranging from 590 to 760 parts per billion (ppb) through much of the Holocene, up to 1700

2380 CE, with as little as ~55 ppb difference from 1000 to 1700 CE (Ferretti et al. 2005). This is

2381 followed by an unprecedented increase to 1700 ppb by 2004 CE (Ferretti et al. 2005, Figure

2382 27a), an increase of 150% over 200 years (MacFarling Meure et al. 2006). Growth rates in

2383 CH_4 decreased during ~1940–1955 CE (MacFarling Meure et al. 2006). The $\delta^{13}C$ curve for CH_4

2384 shows a marked decrease of ~2‰ from ~1000 to 1700 CE, perhaps in response to reduced

2385 biomass burning, and a subsequent abrupt rise from ~1875 CE to the present value of ~-

2386 47‰, reflecting increasing pyrogenic emissions (Ferretti et al. 2005, Figure 27a).

2387

2388 Over the past 200 years, atmospheric N_2O concentrations at Law Dome increased by 21%

2389 (MacFarling Meure et al. 2006). N_2O concentrations ranged from 260 to 270 ppb between 1

2390 and 1850 CE, followed by a steady rise to 290 ppb by 1950 CE, from when there was a rapid

2391 rise to 320 ppb by 2000 CE (Wolff 2013, Figure 27b). The $\delta^{15}N$ signal in firn ice at Law Dome

2392 is more scattered than would be expected, most probably due to random analytical noise

2393 (Rubino et al. 2013).

2394

2395 *3.8 Speleothems*

2396 Annually laminated calcareous speleothems (typically stalagmites) occur within natural cave

2397 systems, typical of karst environments, or within artificial tunnels where either the adjacent

2398 bedrock or the degradation of mortar in concrete linings of the tunnel contributes the

2399 calcium carbonate. Karst landscapes occur across extensive parts of Eurasia, Australasia and

2400 the Americas, in total about 10% of the Earth's land mass (Figure 28). There is precedent in

2401 using speleothems for the location of a GSSP, as Walker et al. (2012) used a stalagmite from

2402 Mawmluh Cave, India, as the proposed GSSP for the Upper Holocene Subseries (= proposed

2403 Meghalayan Stage) at 4.2 ka.

2404

2405 In addition to lamina counting, the age of older speleothems is typically determined by ^{234}U-

2406 ^{230}Th dating, although this is unsuitable for carbonates precipitated over the past century.

2407 Independent dating using ^{210}Pb–^{226}Ra has been undertaken at a few locations (e.g. by

2408 Condomines and Rihs 2006 at St. Nectaire, France, and Bonotto et al. 2012 at Santana Cave

2409 in Brazil). Radiocarbon has quite commonly been used to confirm an age model from annual

2410 laminae, but does not provide annually resolved dates. If Pu is chosen as a primary tool for

2411 correlation, the lack of Pu isotope determination would rule out a speleothem as GSSP for

2412 the Anthropocene (Fairchild 2017), but one could be chosen as an auxiliary site.

2413
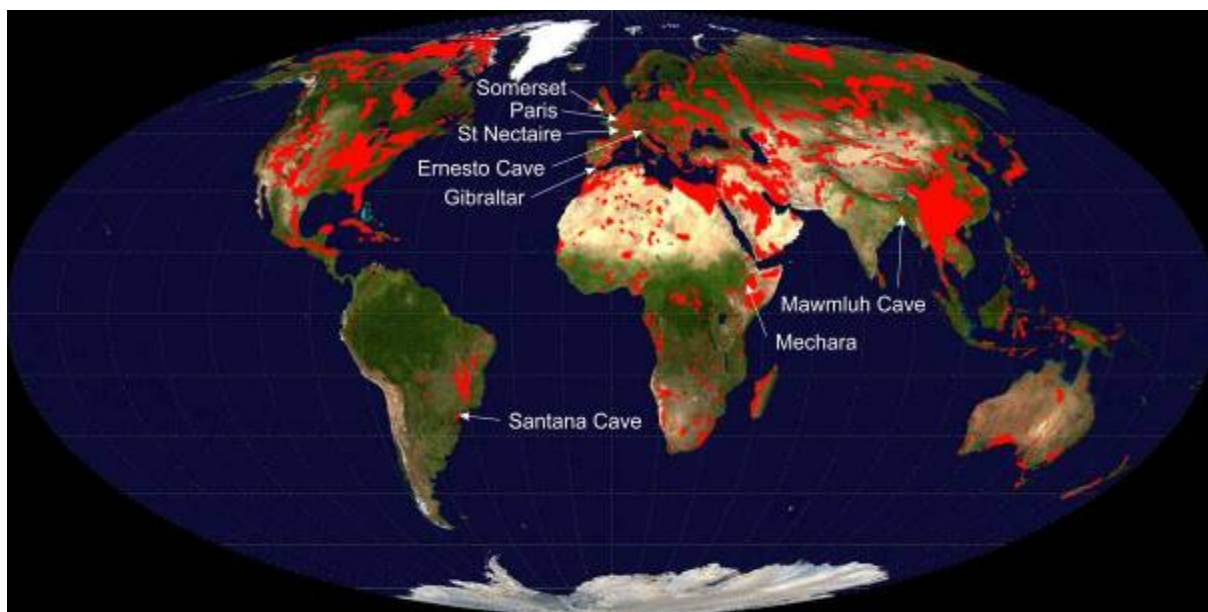
2414

2415 **Figure 28**. Extent of carbonate outcrops present across global land mass by Ulrichstill

2416 https://commons.wikimedia.org/w/index.php?curid=9412430 Created 6th February 2010. Karst

2417 landscapes and speleothems occur within these regions, and locations mentioned in the text are

2418 indicated.

2419

2420 Natural speleothem growth is typically slow, on the order of tens to hundreds of

2421 micrometres per year. In contrast, speleothems related to hyperalkaline groundwaters,

2422 commonly from anthropogenic sources, can grow at a rate of 10 mm per year (Baker et al.

2423 1998), hence potentially permitting fine-scale resolution of environmental changes, although

2424 the chemistry will be strongly kinetically modified (Hartland et al. 2014, Newton et al. 2015).

2425 ^{210}Pb dating of stalactites in Santana Cave (Brazil) shows a longitudinal growth rate of 1.3

2426 mm yr^{-1} and lateral rate of 0.01 mm yr^{-1} (Bonotto et al. 2012). A study of hydrothermal

2427 stalagmites at St Nectaire (France) using ^{210}Pb/^{226}Ra ratios showed growth rates varying from

2428 5.3 ± 0.5 mm to 2.6 ± 0.2 mm yr^{-1} (Condomines and Rihs 2006).

2429

2430 Speleothems record changing environmental conditions in the atmosphere, soil and

2431 ecosystem through geochemical signals transmitted from the ground surface, through rock,

2432 to the subterranean void. The processes of speleothem formation and their chemistry are

2433 detailed by Fairchild and Baker (2012), and their relevance to recognition of Anthropocene

2434 signals is given in Fairchild and Frisia (2014) and Fairchild (2017). Principal signals that may

2435 be used to recognise a potential Holocene–Anthropocene boundary (Table 2) include shifts

2436 in atmospheric ^{14}C and sulphur (sulphate concentration and δ^{34}S), which relate to global-

2437 scale changes to atmospheric chemistry (Fairchild and Frisia 2014, Figure 29). Local signals

2438 include: 1) variations in growth rates of laminae and δ^{18}O which relate to air temperature

2439 and humidity, 2) δ^{13}C as an indicator of deforestation and/or introduction of C4 plants, 3)

2440 development of biomarkers such as a reduction in the ratio of C_{27}/C_{31} n-alkanes and increase

2441 in n-alkanols as observed at Mechara (Ethiopia) reflecting the local introduction of

2442 agriculture about 1935 CE (Blyth et al. 2016), and 4) shifts in trace elements and isotope

2443 ratios (Fairchild 2017). Although of local source and probably diachronous in nature, such

2444 signals may link to global patterns of environmental change and so contribute to

2445 characterising a potential GSSP site. For example, Pb anomalies have been recorded in

2446 speleothems in Somerset, UK near mines active in pre-Roman, Roman and mediaeval times

2447 (McFarlane et al. 2013). Sulphur pollution from coal combustion increased during the

2448 Industrial Revolution and culminated in peak S concentrations and depleted δ^{34}S values in

2449 the mid- to late-20th century in developed countries (Wynn et al. 2010, Figure 29d).

2450 However, speleothems are insensitive to the significant increases in atmospheric CO_2

2451 concentrations and depletion in δ^{13}C over the past century (Fairchild and Frisia 2014).

Changes in the nitrogen cycle via N abundance or isotopic fractionation related to fertiliser use have not been investigated in speleothems (Fairchild 2017). Phosphorus is strongly modulated by seasonal vegetational die-back and changed infiltration rates (Fairchild and Frisia 2014) rather than by fertiliser application.

Transport of solutes via plants, soil and rock commonly results in signals being variably attenuated and delayed (Fairchild and Frisia 2014, Fairchild 2017). For example, speleothems in SW France and Gibraltar show ^{14}C concentrations with differing degrees of attenuation and delay of the peak signal, but the initial rise was consistent at 1958 CE and coincides with changes in atmospheric concentrations (Fairchild and Frisia 2014). The timing of onset of the ^{14}C rise in speleothems is typically within 1–2 years of the atmospheric change (Genty and Massault 1999).

Table 11 summarises the key advantages and disadvantages of such a potential GSSP for the Anthropocene. As examples, the Ernesto Cave in Italy has multi-proxy studies of speleothem laminae within a natural cave system, but urban speleothems may show greater tuning to modified anthropogenic signals.

For:	Against:
• Annual lamination • Undisturbed locations • Independent ^{14}C markers • S, δ^{34}S, ^{14}C reflect atmospheric composition, but modified by soil-ecosystem • Solid samples easier to handle than unconsolidated sediment • Precedent of Mawmluh Cave, India, for the proposed Upper Holocene GSSP	• The atmospheric Suess effect on δ^{13}C is smaller than fractionation effects in the soil-ecosystem so an inflection corresponding to atmospheric change is not normally present • Although S, δ^{34}S, ^{14}C may show initial rise as atmosphere changes, the peak is delayed because of storage in soil/ecosystem • Changes in trace pollutant metals (e.g. Pb, Zn, REE) are strongly linked to organic matter from soil and increases tend to reflect soil disturbance/deforestation effects • Not able to reliably detect signals usable elsewhere, e.g. Pu, anthropogenic detritus

2469 **Table 11.** Reasons for and against using a speleothem as a potential host for a GSSP.

2470

2471 ### 3.8.1 Ernesto Cave, Italy

2472 Ernesto Cave, northern Italy, closely studied for >20 years, has supplied various proxy data

2473 series from annually-laminated speleothems independently dated using U-Th series (Frisia et

2474 al. 2003). These show a strong annual signal of fluorescent laminae associated with a range

2475 of colloid-transported elements (Fairchild and Frisia 2014). A pronounced change is

2476 recognised since about 1840 CE, from open and impurity-rich crystals within relatively thin

2477 laminae to thicker laminae of clean calcite (Figure 29a), representing higher growth rates,

2478 closely correlated with temperature increases (Frisia et al. 2003, Fairchild and Frisia 2014)

2479 associated with the local ending of the Little Ice Age. This pattern broadly coincides with the

2480 initial increase in sulphate concentrations within speleothems in this cave at about 1880 CE

2481 (Frisia et al. 2005), associated with the initiation of atmospheric pollution in response to the

2482 Industrial Revolution.

2483

2484 No appreciable change in stable isotopes has occurred across the mid-20th century (Figure

2485 29b), the most significant change in δ^{13}C being a marked positive excursion at ~1840 CE

2486 (Scholz et al. 2012).

2487
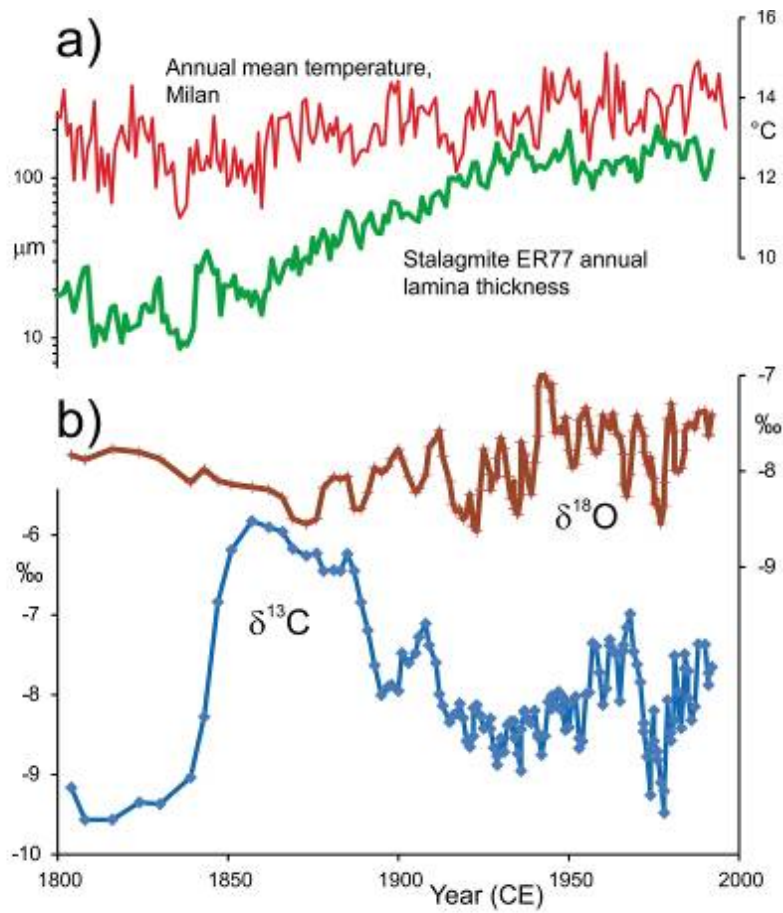
2488
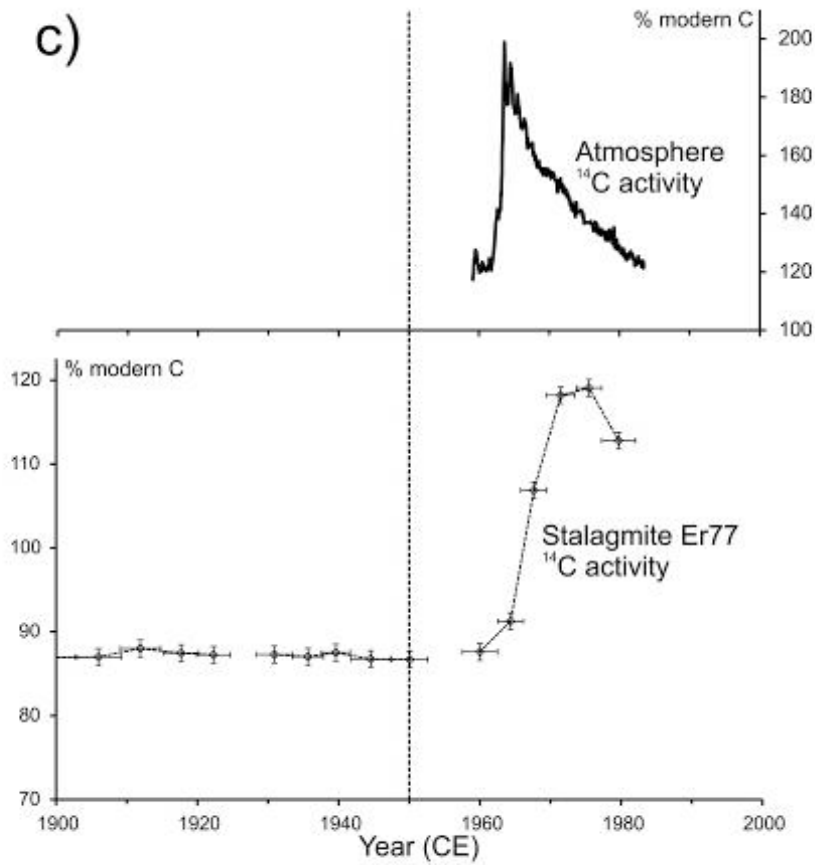
2489
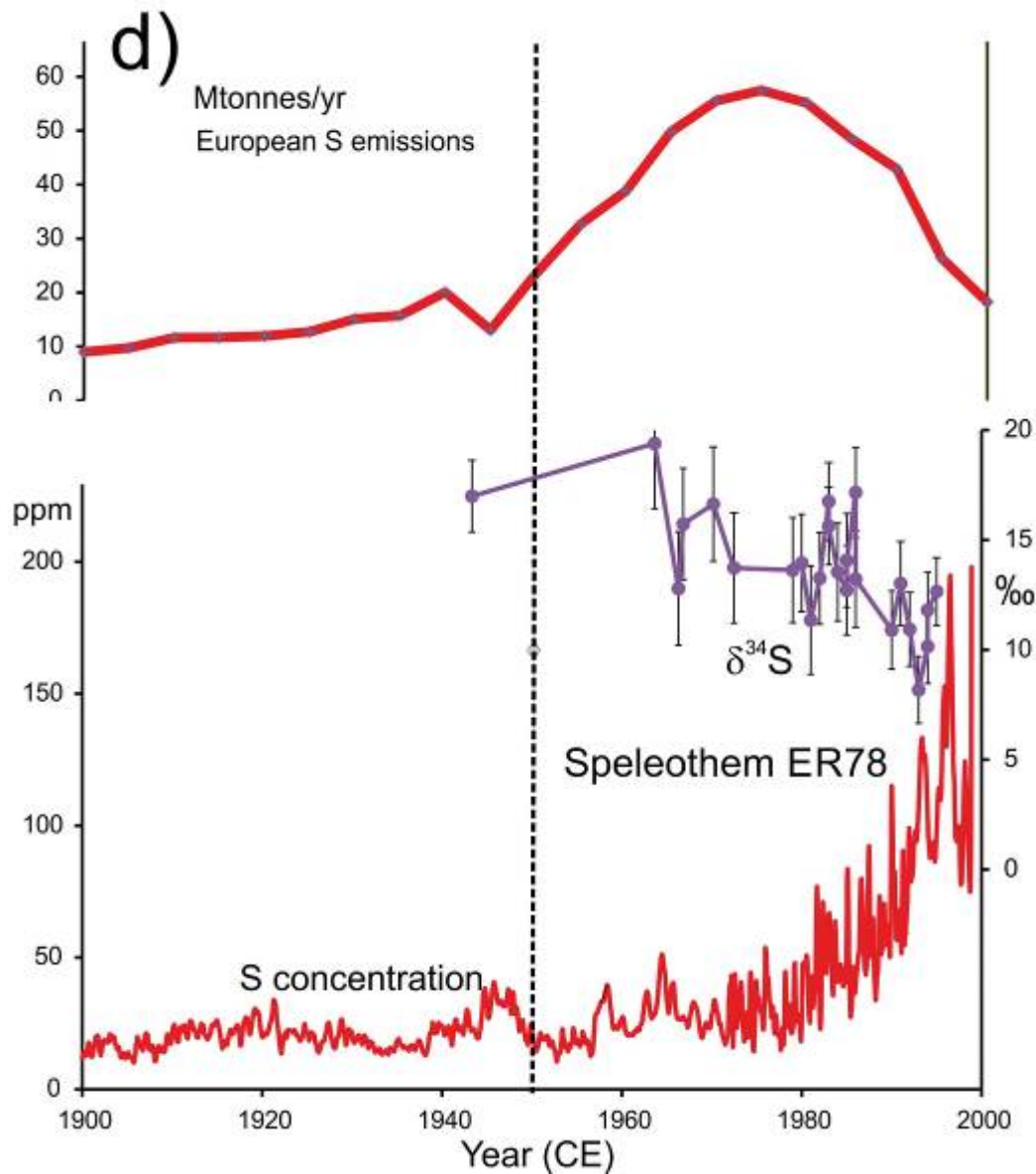
Figure 29. Ernesto Cave, Italy: a) Age model based on lamina counting related to local mean air temperature (Frisia et al. 2003); b) $\delta^{18}O$ and $\delta^{13}C$ profiles (Scholz et al. 2012); c) Radiocarbon profile and comparable European atmospheric emissions (Fohlmeister et al. 2011); d) S concentration and $\delta^{34}S$ (Frisia et al. 2005, Wynn et al. 2010).

The ^{14}C bomb-spike has been recorded from the cave (Figure 29c), but with a decade lag compared with atmospheric signals (Fohlmeister et al. 2011). Records of sulphur loading and lowering of $\delta^{34}S$ in both speleothem and tree rings show a similar lag in the speleothems of about 15–20 years (Figure 29c), such that in 2000 CE the speleothem was still recording peak atmospheric loading (Wynn et al. 2010, 2014) that was locally experienced in the 1980s

2501 (Fohlmeister et al. 2011), but which is now declining (Borsato et al. 2015). Trace element

2502 concentrations increased greatly during the early-20th century, a time of deforestation in the

2503 area (Borsato et al. 2007).

2504 3.8.2 Urban speleothem, Paris

2505 Rises in several trace metals and rare earth elements are found in urban speleothems in an

2506 underground aqueduct beneath Paris that have grown over 300 years with a record of two

2507 laminae per year, independently dated using U-Th series (Pons-Branchu et al. 2015). Two

2508 distinct phases of heavy metal pollution are recognised: a) 18th century metal contamination

2509 resulting from use of urban waste (night soil) as fertilizer; and b) since 1900 CE elevated Pb,

2510 Mn, V, Cu, Cd and Al concentrations, attributed to urbanisation, with a more marked

2511 increase since 1960–1970 CE (Pons-Branchu et al. 2015). ^{206}Pb/^{207}Pb isotope ratios show no

2512 consistent pattern in these speleothems. The dominant value of 1.181 ± 0.003, is typical of

2513 values associated with lead from northern Europe (Pons-Branchu et al. 2015), though one

2514 speleothem showed a change after the mid-19th century, suggesting a new contribution

2515 from coal burning or from Pb from Spain. Pb ratios typical of leaded gasoline are not

2516 discriminated (Pons-Branchu et al. 2015).

2517

2518 *3.9 Trees*

2519 Forest coverage in 2005 CE was about 39 million km^2, or ~30% of the world's land area (FAO

2520 2006) and there are an estimated 3 trillion trees (Crowther et al. 2015). Forests are extensive

2521 on all continents except Antarctica, and include the boreal forests of North America and

2522 Eurasia and tropical forests of South America, central Africa and south-east Asia (Figure 30).

2523 Tropical trees from aseasonal tropical regions lack reliable annual rings, so trees from

2524 temperate or boreal environments would be most suitable for a GSSP as the tree rings

2525 themselves can provide a precise annually-resolved chronology.

2526
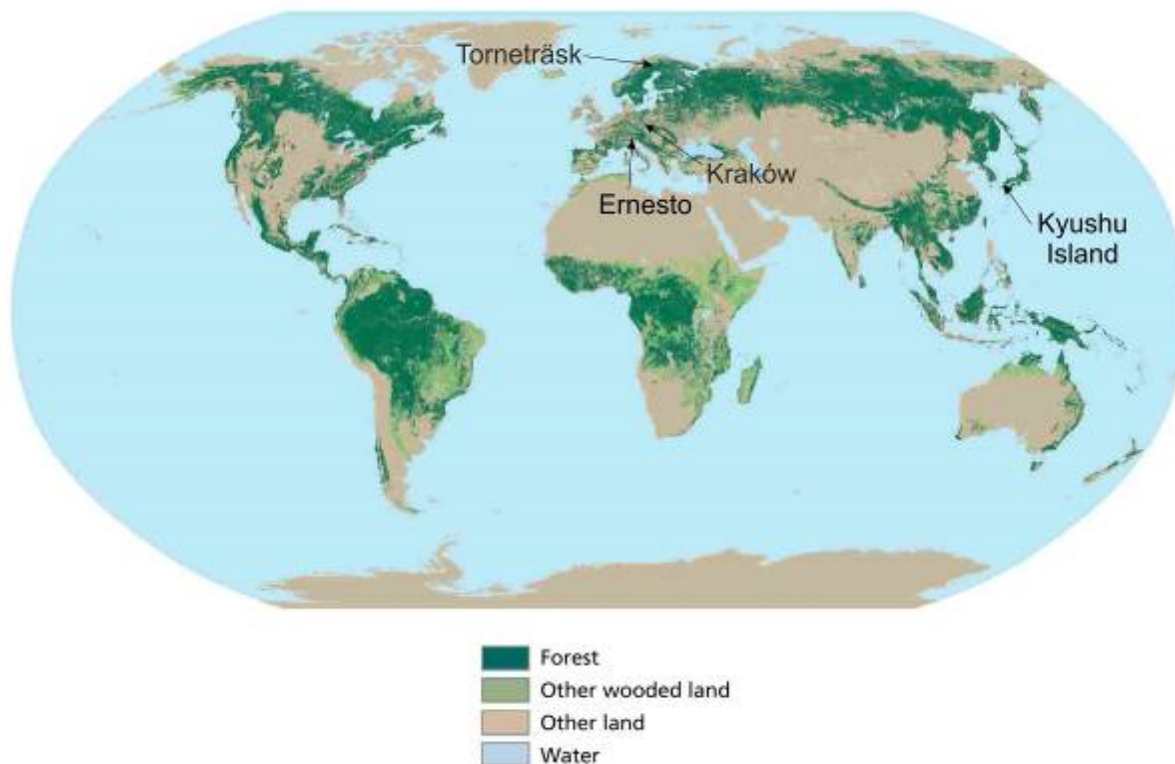
2528 **Figure 30.** Forest map of the world with key locations mentioned in the text. © (2006)FAO.]

2529

2530 Tree rings provide a perfect annually-resolved chronology, and within this an annually

2531 resolved archive of environmental change, most notably palaeoclimate, at local to global

2532 scales. This signal can be evident in the physical properties of the tree ring (width, density,

2533 reflectance) or chemical indicators such as the stable isotopic ratios of carbon (sourced from

2534 atmospheric CO_2), and hydrogen and oxygen (sourced from precipitation, soil or ground

2535 water) (Fritts 1976, Speer 2010, McCarroll and Loader 2004). In many species, the tree rings

2536 may be further divided into early wood (formed during the spring) and late wood (formed

2537 during the summer, primarily from photosynthates fixed during the growth year). Rings from

2538 living trees can provide environmental information spanning both the mid-20th century

2539 putative boundary for the Anthropocene and the late-18th century transition from pre-

2540 industrial times through the development of the Industrial Revolution. Similar records can

2541 also be found in preserved dead trees that accumulated in bogs or lakes, and also in building

2542 timbers. Where trees co-existed in time they will co-record a shared environmental signal

2543 that may therefore be cross-dated to assign chronology or to provide independent

2544 replication between trees or across study regions.

2545

2546 Table 12 summarises the key advantages and disadvantages of having a potential GSSP

2547 within tree rings. Proxy signals associated with palaeoclimate, stable carbon isotopes,

2548 sulphur concentrations and isotopic ratios, radiocarbon fallout and heavy metal

2549 concentrations are discussed below.

2550

For:	Against:
• Global expression and distribution; widespread terrestrial extent • Bi-annual layers • Precise dating through dendrochronology • Independent ^{14}C dating possible • Environmental signals preserved in deadwood • δ^{18}O and δD: record source water, which contains a climate signal • δ^{13}C is highly sensitive to the Suess effect on atmospheric CO_2 • Sulphur and δ^{34}S signal commencing mid-20th century • ^{14}C bomb spike clearly defined • High potential for independent replication • Tangible, stable and archivable	• Growth ring width may not be suitable for picking mid-20th century climate signal (due to local effects or 'divergence') • Complex record of local signals in physical and chemical proxies • δ^{13}C can be affected by local modifications • Heavy metal concentrations may be unsuitable proxy for pollution events due to radial mobility • No precedent of using a living/deceased organism for GSSP

2551 **Table 12.** Reasons for and against using a tree as a potential host for a GSSP.

3.9.1 Tree rings and palaeoclimate signals

Dendrochronology relies upon the counting and statistical synchronisation of annual changes in tree ring widths, and their assignment to a calendrical or relative timescale. This is possible because the variability in tree growth driving this signal is related to regional climatic changes. Trees growing at the same time in history, and experiencing a similar climate history, will in the absence of external disturbances yield similar patterns of wide and narrow growth rings that may be cross-dated by dendrochronology to develop a precise timescale. Due to the physical increase in the diameter of a tree as it grows, tree-rings show a characteristic decline in width with increasing tree age (size). Where a climatic signal is to be extracted from the ring width data, statistical techniques are required to remove this growth or age-related trend. This statistical processing may cause climate signals of frequency longer or equal to the age-span of the tree to be lost, reducing the value of tree-ring widths in recording long-term climate change (Cook et al. 1995, Esper et al. 2002). However, this effect can be significantly reduced/removed by using more complex detrending protocols and numerous multi-centennial records of temperature changes from 800 to 1990 CE have been determined from high-elevation and high-latitude locations across the Northern Hemisphere using Regional Curve-based Standardization techniques (Esper et al. 2002, Melvin and Briffa 2008). These data contain evidence for a Northern Hemisphere Medieval Climatic Anomaly (MCA) between about 900 and 1200 CE, and for below average temperatures typical of the Little Ice Age (LIA) from 1200 to 1850 CE, and for warming since 1850 CE comparable in scale to that of the MCA (Wilson et al. 2016, Esper et al. 2002, Figure 31a).

The suitability of using tree rings to establish the temperature profile post-1950 CE has been questioned due to a conspicuous increase in the statistical uncertainty in reconstructions

2577 after 1975 CE, which may reflect an anomalous reduction in growth performance at some

2578 high northern latitude conifer sites, but is also often coincident with a decrease in the

2579 replication of the composite record (Esper et al. 2002). This "divergence" between growth-

2580 based reconstructions and observed climate has been the subject of significant attention by

2581 dendroclimatologists and many potential causes, from unbalanced replication and signal

2582 processing effects to changes in seasonality and CO_2 fertilisation, have been considered

2583 (D'Arrigo et al. 2007). Whilst this may reduce current confidence in the use of ringwidth-

2584 based reconstructions to define climatic changes attributed to the start of the

2585 Anthropocene, maximum late wood density appears to be less impacted upon by such

2586 divergence issues and density-based reconstructions of past climate remain some of the best

2587 records of past climatic variability currently available to climate scientists. There are few

2588 palaeoclimate proxies other than tree-rings capable of providing the same precisely dated,

2589 annually-resolved palaeoclimate reconstructions with the same capacity for independent

2590 verification through replication, capable of being objectively calibrated against instrumental

2591 observations and independently verified.

800   1000   1200   1400   1600   1800   2000
Year (CE)
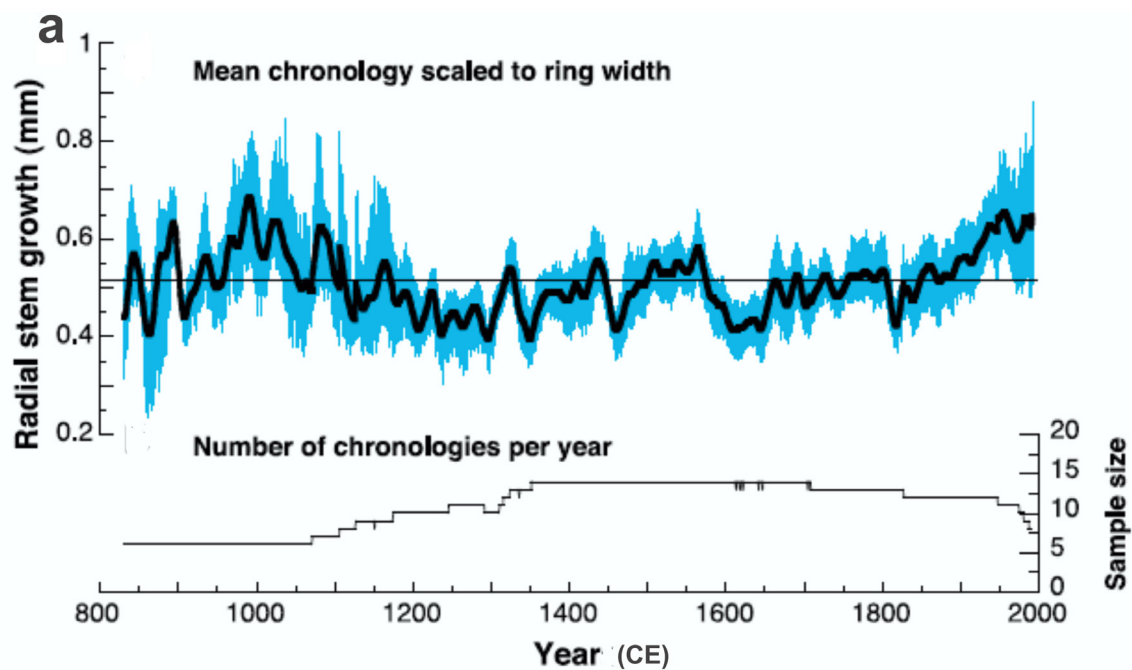
2592
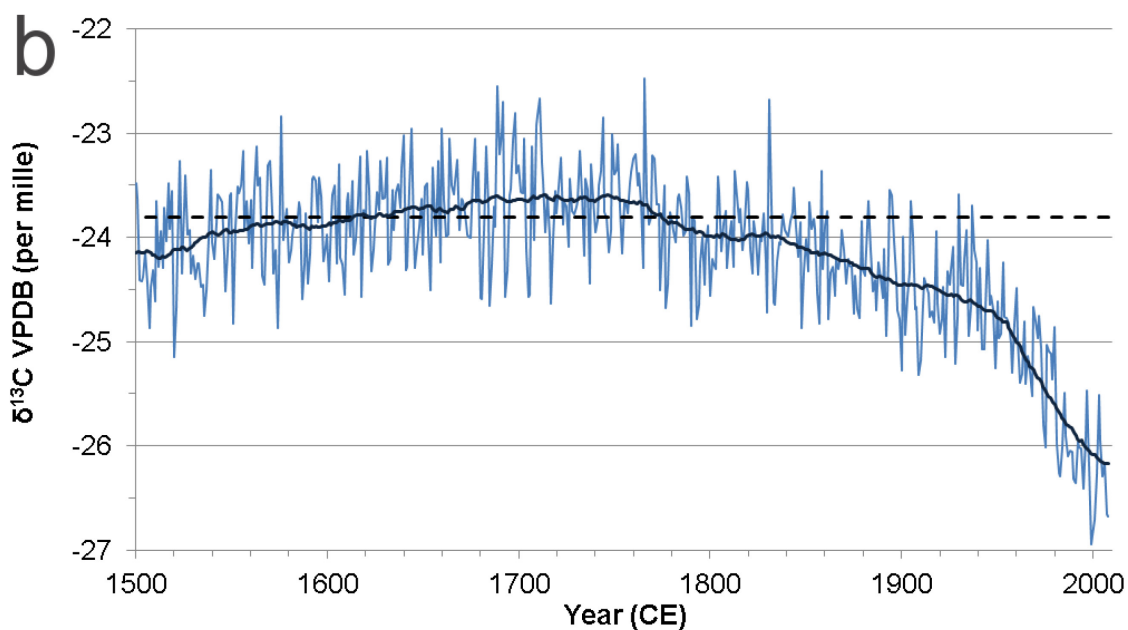
2593

Figure 31. a) The 20-year smoothed Northern Hemisphere extratropics reconstruction of radial stem

productivity in high elevation and high latitude forest environments since 800 CE (black) and two-

tailed 95% bootstrap confidence intervals (blue) (from Esper et al. 2002); b) $\delta^{13}C$ variability from

Loader et al. (2013a) for the period 1500–2008 CE measured in tree-ring cellulose for a composite

tree ring stable isotope chronology developed using *Pinus sylvestris* trees from northern

Fennoscandia. Fine line represents annually-resolved $\delta^{13}C$ variability, thick solid line presents the

132

2600   annual data smoothed with a centrally-weighted 51-year moving average. Dashed line represents the

2601   mean $\delta^{13}C$ value for the "pre-industrial" period 1500–1799 CE. Mean annual replication for the

2602   record is >13 trees. Analytical precision σ_{n-1} = 0.12 per mille n=951 which compares favourably with

2603   the analytical precision of the method typically reported (σ_{n-1} = 0.10 n=10) (Boettger et al. 2007,

2604   McCarroll and Loader 2004, Loader et al. 2013a).

2605

2606   ## 3.9.2 Stable carbon isotopic signal

2607   Stable isotope variability in tree rings appears to be less affected by non-climatic age-related

2608   tendencies (Young et al. 2011). Long-term trends of stable carbon isotopic data in tree rings

2609   may therefore mark the start of the Anthropocene in the tree ring archive. The stable carbon

2610   isotopes in tree rings record primarily the stable isotopic composition of the source CO_2

2611   sampled by the tree during photosynthesis. This signal is further imprinted upon by the

2612   tree's physiological response to climatic change (the balance between stomatal conductance

2613   and photosynthetic rate), photosynthetic and respiratory processes (Farquhar et al. 1982,

2614   McCarroll and Loader 2004, and references therein). Inter-annually, $\delta^{13}C$ values will vary in

2615   response to changes in irradiance, soil moisture, precipitation and relative humidity and this

2616   has allowed the tree rings to be used as a record of past climate variability. As a biological

2617   system, tree ring stable carbon isotopic ratios will also vary depending upon the species of

2618   tree (angiosperm versus gymnosperm) and their individual environmental history. In

2619   addition, factors such as leaf morphology, ecological amplitude, pollution, forest

2620   management history, disturbance and nutrient availability, can all influence the resulting

2621   tree ring isotopic record, but at all times, the basic physiological response of the tree will

2622   remain the same. This natural inter-tree variability has been characterised in resampling

2623   experiments (Loader et al. 2013b), and although extreme cases have been reported (Li et al.

2624 2005), natural intra-site variability falls within reasonable limits defined by current analytical

2625 uncertainties.

2626

2627 When viewed over a long (centennial-millennial) timescale, trees have the capacity to record

2628 and contextualise the unprecedented anthropogenic changes in atmospheric δ^{13}C associated

2629 with global industrialisation and land-use change. By combining records from different

2630 geographical regions, location-specific year-to-year climatic variability and the effect of

2631 random disturbances may be reduced to yield a regionally relevant record of carbon isotopic

2632 variability in atmospheric CO_2. A reduction of atmospheric δ^{13}C values by ~2‰ has occurred

2633 since the start of the global Industrial Revolution ~1820 CE (the δ^{13}C Suess effect), which is

2634 among the dates proposed as a start for the Anthropocene (Figure 31b). This effect is

2635 observed in tree rings worldwide and is also clearly observable in ringless trees from the

2636 aseasonal tropics (Loader et al. 2011).

2637

2638 The δ^{13}C Suess effect is commonly removed in tree ring carbon isotope series through

2639 mathematical detrending without loss of low-frequency climatic information (McCarroll and

2640 Loader 2004). This makes the data suitable for numerical calibration against instrumental

2641 climate data, but prevents its use as an arbiter of atmospheric δ^{13}C changes. To assess the

2642 potential base of the Anthropocene using δ^{13}C changes, raw carbon isotope data are

2643 required.

2644

2645 A further consideration when assessing the candidature of tree ring δ^{13}C as a marker for the

2646 Anthropocene is the influence of increased atmospheric CO_2 concentration on

2647 photosynthesis. This "fertilisation" or "greening" effect has been widely reported and in the

2648 context of stable carbon isotopic variability is seen as a change in the intrinsic water-use

2649   efficiency of the tree (Seibt et al. 2008, Saurer et al. 2014, Frank et al. 2015). Methods have

2650   been developed to quantify and to correct for this effect, which will vary from tree to tree

2651   (Treydte et al. 2009, McCarroll et al. 2009). Several studies have also identified a limit to the

2652   degree to which trees can adapt to higher atmospheric CO_2 concentrations. This

2653   "fertilisation" effect does not negate the use of $\delta^{13}C$ as a potential marker, but it should be

2654   taken into consideration.

2655

2656   A large-scale/global composite of global carbon isotope time-series from tree rings could

2657   help locate the boundary of the Anthropocene, as individual records are affected by local

2658   climate, forest disturbance, or the local impact of atmospheric pollution on stomatal

2659   conductance and disease (McCarroll and Loader 2004 and references therein, Bukata and

2660   Kyser 2007, Treydte et al. 2007, 2009, Loader et al. 2013b, Boettger et al. 2014, Saurer et al.

2661   2014, Frank et al. 2015), all of which could potentially obscure the true expression of the

2662   global $\delta^{13}C$ Suess effect in tree rings. Nevertheless, the change in tree ring carbon isotopic

2663   values resulting from global industrialisation is far greater than anything observed in the tree

2664   ring isotope record during the last 1100 years. The combination of a temporally stable proxy

2665   preserved within a precisely constrained chronology for the tree rings represents an

2666   opportunity to constrain a boundary to the Anthropocene.

2667   ### 3.9.3 Sulphur concentrations and isotopic ratios

2668   Bulk analyses of the conifer *Abies alba* from near the Ernesto cave site, NE Italy, show that S

2669   concentrations within annual rings reflect atmospheric SO_2 pollution (Figure 32b), with

2670   significantly higher values in the second half of the 20th century (Fairchild et al. 2009). Both

2671   the trees and the nearby stalagmite record the overall increasing trend in the 20th century,

2672   from the 1960s onwards, with the trees showing a more immediate (earlier) response to the

2673 high S emissions of the 1960s and 1970s (Fairchild et al. 2009, Wynn et al. 2014). The *Abies*

2674 samples show considerable noise, including variation between individual trees (Fairchild et

2675 al. 2009). Furthermore, the S is mainly sourced from soil-waters rather than directly from the

2676 atmosphere, and the S is stored both in soil and biomass, which means that the original

2677 atmospheric signal is necessarily modified (Fairchild et al. 2009). These trees also show a

2678 trend in $\delta^{34}S$ towards lighter isotopes in recent rings, with pre-industrial values of +7.5‰

2679 and modern values of +0.7‰, with no significant signature corresponding to the mid-20th

2680 century (Wynn et al. 2014, Figure 32b).

2681

2682 $\delta^{34}S$ is potentially a useful chronological proxy for past atmospheric S pollution, particularly

2683 as there is limited fractionation during incorporation into the tree (Kawamura et al. 2006).

2684 Three conifers studied from Kyushu Island, Japan provide a significant record from 1945 CE,

2685 where a dominant organically-bound sulphur (OBS) fraction and a minor water-soluble

2686 sulphur (WSS) fraction were discriminated (Kawamura et al. 2006). These showed a general

2687 increase, then decrease, in the second part of the 20th century, with higher values and a

2688 greater range seen in urban as compared with rural areas. Increased atmospheric S

2689 emissions from petroleum combustion with negative $\delta^{34}S$ values were mainly sourced from

2690 the Middle East since the 1950s, until legislation was introduced in 1968 CE. There is a ~5

2691 year delay in $\delta^{34}S_{OBS}$ tree ring values compared with maximum atmospheric S concentrations,

2692 probably reflecting the time taken for sulphur deposited in soil to mobilise to the roots, and

2693 for the metabolism of sulphur after absorption (Kawamura et al. 2006).
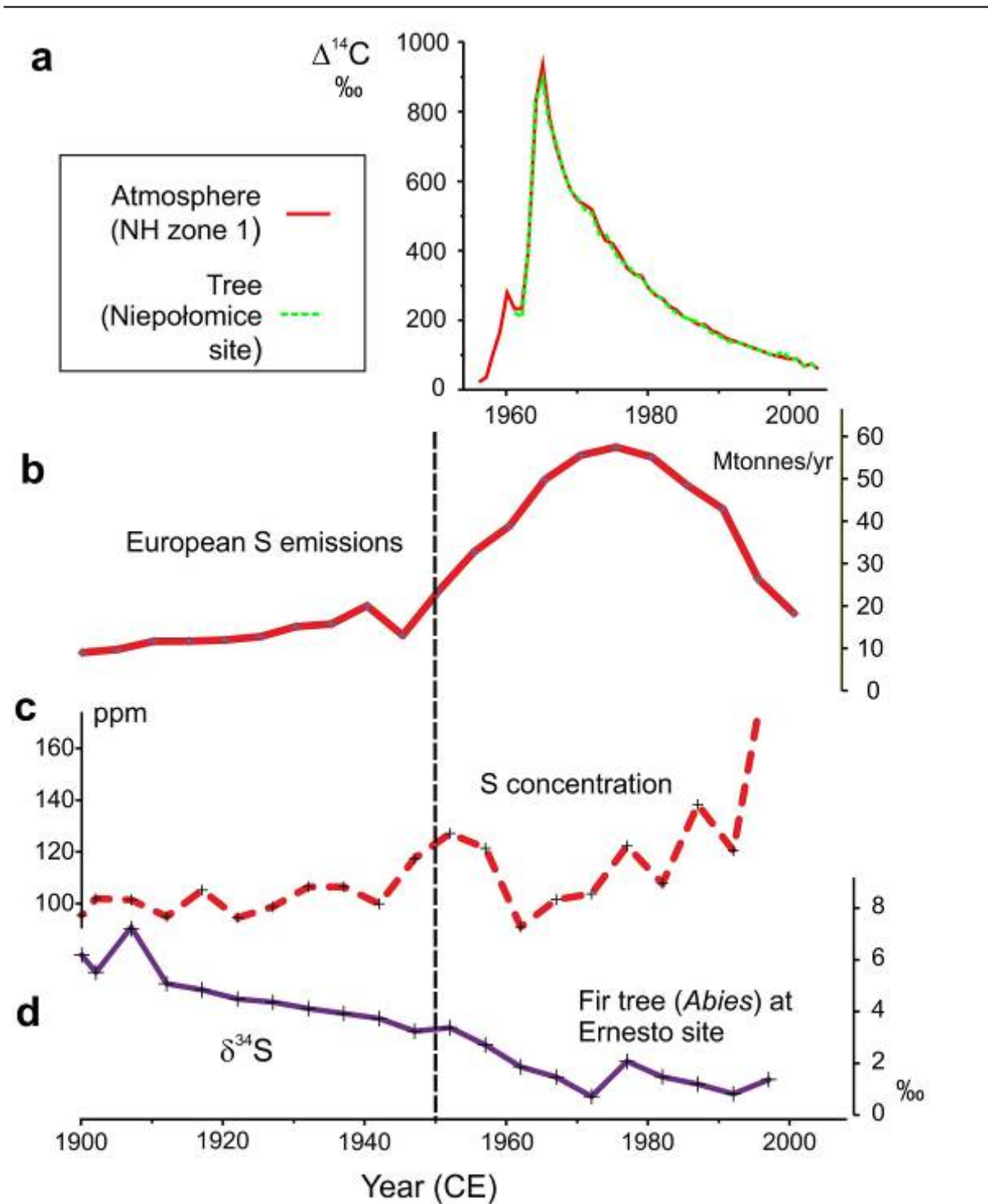
Figure 32. a) Tree rings (*Pinus sylvestris*) samples from 1960 to 2003 CE at Niepołomice (Poland) showing changes of radiocarbon concentration (from Rakowski et al. 2013) compared with Northern Hemisphere (Zone 1) atmospheric values (from Hua and Barbetti 2004); b) European S emissions; c) S concentrations; and d) δ^{34}S in *Abies alba* from NE Italy compared with European S emissions (Wynn et al. 2014).

3.9.4 The radiocarbon bomb spike and heavy metal concentrations

2701

2702 Atmospheric $\Delta^{14}C$ decreased by about 20.0‰ between 1890 and 1950 CE in response to the

2703 Suess effect of adding low-activity fossil carbon, punctuated by a marked bomb spike in

2704 response to nuclear weapons testing, peaking in ~1963 CE that led to a level two times

2705 higher than that of pre-1850 CE times (Rakowski et al. 2013). Annual rings of a pine tree

2706 (*Pinus sylvestris*) taken in the Niepołomice area, near Kraków, Poland from 1960 to 2003 CE

2707 show a clear $\Delta^{14}C$ bomb-spike in 1964 CE (Rakowski et al. 2013, Figure 32a). A suitable GSSP

2708 candidate should have a data set of both $\Delta^{14}C$ and $\delta^{13}C$ extending back to pre-industrial

2709 times; the data in the tree analysed by Rakowski et al. (2013) began close to the peak bomb-

2710 spike interval, so lack an adequate record of the transition across a potential Holocene–

2711 Anthropocene boundary. $^{239+240}Pu$ records in tree rings are less studied, but the distribution

2712 of Pu in tree rings and in lake sediment cores seems to show similar trends (Mahara and

2713 Kudo 1995) suggesting Pu as a potentially suitable signal.

2714

2715 Historical changes in trace metal levels can be recognised in some tree ring records,

2716 although there may well be a time lag between metal deposition and the passage through

2717 soils and root system. Element concentrations in tree rings for a given year may differ

2718 markedly between trees from a single location (Watmough 1999). Studies on the sugar

2719 maple (*Acer saccharum*) suggest that there is both a rapid uptake of trace metals (e.g. Cu, Ni,

2720 Cr, Zn, Cd, Co and As) and a minimal lateral movement between rings (Watmough 1999),

2721 although radial movement of trace elements has been reported in other studies (Hietz et al.

2722 2014).

2723

4 Summary

2725 Many of the signals described above are highly resolved, widespread and correlatable.

2726 Notably, heavy metals, $\delta^{13}C$ and radiogenic fallout signals tend to be recorded in most

2727 environments that might conceivably be suitable for hosting a GSSP (Table 2). Other airborne

2728 signals, such as fly ash, nitrates and $\delta^{15}N$, and to a lesser extent sulphur and sulphates, CO_2

2729 and CH_4 concentrations and $\delta^{18}O$ occur in many environments and provide additional means

2730 of correlation. Biotic assemblages have been demonstrated to respond rapidly to local

2731 environmental changes and can provide useful secondary and local markers, but seem on

2732 current evidence unlikely to provide a globally correlatable and synchronous marker that is

2733 as temporally well-resolved as $\delta^{13}C$ and radiogenic fallout or other airborne signals.

2734

2735 These more nearly synchronous and widespread signals, combined with the possibility of

2736 directly dating successions by such means as lamina counting, show that a well-chosen GSSP

2737 level might be precisely dated to the nearest year (or season) and might be correlated to

2738 other well-studied high-resolution sections with a resolution of a year or a few years. In less

2739 well-studied sections, or those lacking annual lamination, use of the very wide range of

2740 available proxy signals should still be able to provide correlative resolution of a few to

2741 several years, sufficient to widely locate a practically effective Holocene–Anthropocene

2742 boundary, even in apparently unpromising geological settings. For instance, Smith et al.

2743 (2016) identified what would be regarded as an Anthropocene succession of sub-ice shelf

2744 deposits at Pine Island in West Antarctica, by identifying bomb-derived plutonium within the

2745 deposits.

2746

2747 The location of such a Holocene–Anthropocene boundary within relatively recent

2748 successions – of the last few centuries – we regard as having use beyond the formal value of

2749 the establishment of chronostratigraphic divisions. An extensive, variably interconnected

2750 suite of physical, chemical and biological changes to the Earth System has been taking place,

2751 some local, some global, many of which leave stratigraphically detectable traces. These

2752 include phenomena such as the spread of various kinds of industrially related pollutants and

2753 their biotic effects, changes to the atmosphere and hence to the Earth's radiative properties,

2754 a complex pattern of species extinctions, extirpations and invasions, and the emergence and

2755 evolution of technological systems on a planetary scale. For practical analysis of these

2756 changes – many of which are ongoing, or accelerating – placing them in an effective

2757 framework of space and time is a prerequisite. We suggest that a chronostratigraphic

2758 Holocene–Anthropocene boundary could make a significant contribution to this analytical

2759 process, not least in that this time interval is emerging as a critical transition in the geological

2760 history of this planet (e.g. Steffen et al. 2016). The survey we provide here suggests that such

2761 a boundary would be workable in practice, across the range of the environments we survey

2762 here and likely more widely. Table 13 surveys the range of chemostratigraphic signals

2763 recorded here and provides their onset and peak date for key environments. This shows the

2764 wide range of potential proxies that could be used to mark a mid-20th century boundary.

2765

Environment	Black Carbon	Fly ash	Lead	PCBs	Pesticides (DDT)	NO_3^-	$\delta^{15}N$	Sulphur	SO_4^{2-}	CO_2	CH_4	$\delta^{13}C$	$\delta^{18}O$	D &/or dust	^{239}Pu	^{14}C
Marine anoxic basins (1)	?	?	1965 (1970s)	1945 (1967)	1952 (1967)	?	x	x	x	x	x	?	?	x	1950-54 (1970s)	?
Coral bioherms & marine bivalves (2) (3)	?	?	Late 1940s (1970s) (2)	?	x	~1970 (3)	~1950 (3)	x	x	x	x	1955 (2)	~1950 (2)	x	1952 (1964) (2)	1958 (1972) (3)
Estuaries/ Deltas (4) (5)	?	1900s (5)	(1915) (4)	1950s (1965-1977) (4)	?	?	x	x	x	x	x	?	?	x	?	?
Lakes (6) (7) (8) (9) (10)	1940s-1950s (2004-6) (8)	~1950 (1970-1990)	1960s (Post-2000) (8)	~1960 (9)	1950s (9)	?	~1950 (7)	~1950 (10)	x	x	x	?	?	x	~1955 (1964) (6)	?
Peat & peat-lands (11) (12)	x	1950s (1970s) (11)	1810 (1979) (12)	(1960-1976) (12)	x	x	x	x	x	x	x	?	x	x	x	x
Ice (13) (14)	~1880 (~1910) (14)	?	~1940 (~1970) (14)	?	?	~1950 (14)	~1950 (1980) (14)	~1940 (~1970) (14)	~1940 (14)	~1950 (13)	~1950 (13)	1955 (13)	1980s (2010) (14)	~1850 (13)	1953 (1962) (13)	1954 (1966) (13)
Speleothems (15)	x	x	?	?	?	?	?	1980 (2000)	1880 (15)	x	x	~1840 (1860)	1875 (1940)	x	x	~1965 (~1975)
Trees (16) (17) (18)	x	x	?	?	?	?	1945 (18)	1960s (15)	?	x	x	1940 (1750) (16)	?	1960	?	1956 (1964) (17)

2766 **Table 13.** Summary of key mid-20th century proxy signals and potential palaeoenvironments for a

2767 GSSP. The initial date represents the marked onset of the signal; the peak signal is shown in brackets.

2768 Key signals and environments are shown in boxes. Reference numbers relate to main geographical

2769 locations mentioned in the text: (1) Santa Barbara, USA; (2) Caribbean; (3) Nova Scotia, Canada; (4)

2770 Clyde Estuary, Scotland; (5) Urola Estuary, Spain; (6) Lake Victoria, Australia; (7) North America; (8)

2771 China; (9) Lochnagar, Scotland; (10) Lilla Öresjön, Sweden; (11) Northern England; (12) Switzerland;

2772 (13) Antarctica; (14) Greenland; (15) Ernesto Cave, Italy; (16) Fenno-Scandinavia; (17) Poland; (18)

2773 Ontario, Canada.

2774

2775 With regard to the environments most suitable for seeking a candidate GSSP, we offer the

2776 following guidance:

2777

2778 • Anthropogenic deposits are common in terrestrial environments. They may be

2779 relatively thick (up to tens of metres), contain signals that closely reflect human influence,

2780 and are readily datable, particularly using technofossils. They tend to lack lateral continuity,

2781 may contain omission surfaces, are not annually laminated, and may lack 'preservability', all

2782 of which are likely to discount many such deposits as hosts for primary or auxiliary GSSP

2783 candidates. However, much the same criticisms also apply to many Holocene deposits.

2784 Suitable potential GSSP candidates may well exist within anthropogenic deposits, or perhaps

2785 at the interface between anthropogenic and non-anthropogenic strata, although none have

2786 yet been identified or described. More work is required in this area of investigation.

2787

2788 • Marine anoxic basins tend to display undisturbed annually resolved laminae that can

2789 be independently dated. The radionuclide fallout signal may show some smearing due to

2790 processes affecting the settling of radioisotopes through the water column, which can inhibit

2791 development of a sharp bomb spike. Even so, the early 1950s start of the signal (Table 13) is

2792   typically robust. In these environments, heavy metals including Pb, organic compounds, such

2793   as PCBs and pesticides (Table 13), microplastics and biotic signals, including planktonic

2794   foraminifera and diatoms (and their stable isotope patterns), tend to be controlled by local

2795   environmental variations. Although they broadly display changes in the mid- to late-20th

2796   century, the onset of their signal can vary by decades between regions. Low sedimentation

2797   rates may reduce the thickness of Anthropocene strata to a few centimetres. Even so, the

2798   signals of change may still be clearly resolved and laterally extensive. This environment has

2799   potential for hosting an Anthropocene GSSP, provided that the fallout signal, especially

2800 ^{239}Pu, is not significantly smeared by slow settling rates or by bioturbation.

2801

2802   •   Coral growth bands can exhibit very-high resolution records, which, along with rapid

2803   growth rates commonly exceeding sediment accumulation rates, provide a potentially

2804   suitable medium for hosting a GSSP. The onset of the ^{239}Pu signal is particularly robust as an

2805   early 1950s marker (Table 13), with no concerns about the influence of settling rates through

2806   the water column; peak signals are more variable between localities. However, reefs that are

2807   distal to nuclear detonation test sites might be more suitable so as to more clearly show the

2808   global pattern, rather than including some residues of the early, pre-1952 CE tests that only

2809   left a local signal. The Caribbean, Red Sea, western and northern Indian Ocean are distant

2810   from the main testing grounds (Waters et al. 2015) and are more likely to most clearly show

2811   the global atmospheric signal. Radiocarbon tends to have latitudinal diachroneity and shows

2812   a delayed signal in shallow-water corals of about a decade compared with atmospheric ^{14}C

2813   and the ^{239}Pu signal (Table 13), with increased lags also associated with greater water depth

2814   of coral growth. The decline of δ^{13}C in corals is most marked in Atlantic corals from 1957 CE

2815   (Table 13), with the accumulation rate being more variable and of much smaller magnitude

2816   in the Indian and Pacific oceans. δ^{15}N values are complex, related to source areas of ocean

2817   currents and types of anthropogenic sources. Heavy metals can be concentrated within

2818   certain species of coral, but they tend to record only local contamination events.

2819   Temperature records are a mix of local and global factors and a single core would probably

2820   not be suitable as a GSSP. If corals are to be considered as a potential host for a GSSP,

2821   examples from the Caribbean, using ^{239}Pu as the primary signal, may be most suitable.

2822

2823   •   Estuaries and deltas are typically responsive to anthropogenic influence, whether

2824   biotic change in response to environmental modifications and widespread introduction of

2825   neobiota, changes to sediment flux through alteration of catchment erosion rates or

2826   impounding sediments through dam construction, or through contamination by fly ash,

2827   heavy metals such as Pb, organic chemicals such as PCBs (Table 13), or microplastics. These

2828   environments, while offering good potential for hosting a candidate GSSP, may suffer from

2829   strong modulation by local influences, a lack of lateral continuity, and the common presence

2830   of omission surfaces.

2831

2832   •   Lakes, despite being laterally disconnected, are found across large parts of the planet

2833   and, although commonly strongly modulated by local processes, also display numerous

2834   globally coherent signals. As with estuaries and deltas, lakes tend to be responsive to

2835   anthropogenic influence, resulting in a spectrum of highly resolved signals, including black

2836   carbon, fly ash, organic compounds, δ^{15}N, S and ^{239}Pu which provide potential 1950s markers

2837   (Table 13). Despite the Anthropocene successions being typically thin, shallow perennial

2838   lakes are advantageous for hosting a potential GSSP given that settling rates of radiogenic

2839   fallout and heavy metals will be minimal and at the same time there should be few omission

2840   surfaces. The latter issue limits the suitability of many arid saline lakes, but numerous

2841   Northern Hemisphere meromictic lakes could host suitable candidate GSSP or auxiliary

144

2842 sections. Lake sediments have been accepted as hosts for global auxiliary stratotypes for the

2843 base of the Holocene.

2844

2845 • Ombrotrophic peat bogs provide widespread local archives that faithfully record

2846 aerosol distribution from local, regional and global sources. The range of potential suitable

2847 signals are diverse (Table 8), with fly ash providing the most robust 1950s marker (Table 13).

2848 The behaviour of trace elements may be influenced by changing redox conditions and has to

2849 be carefully documented. As there is no varved sedimentation, and as some signals such as

2850 the Pu bomb spike show redistribution effects, hosting a primary GSSP in peat bogs seems

2851 not appropriate, but this environment may provide a useful auxiliary GSSP section.

2852

2853 • Glacial ice provides a broad spectrum of annually resolvable atmospheric signals

2854 including radionuclides, $\delta^{18}O$, sulphates, nitrates, $\delta^{15}N$, Pb and other metals, and so may

2855 provide a suitable mid-20th century marker (Table 13). Given the precedent of locating the

2856 Holocene GSSP in glacial ice, there is a strong argument for locating in an ice sheet at least

2857 an auxiliary stratotype GSSP section for the base of the Anthropocene, not least to show

2858 how its signals contrast with those at the base of the Holocene. A significant issue for the

2859 temporal resolution required for the Anthropocene is the significant time lag between the

2860 age of the ice and the included air bubbles. This lag affects CO_2, CH_4, $\delta^{13}C$ and N_2O values,

2861 which are consistently younger than the enclosing ice. This effect is most pronounced where

2862 snow accumulation is slowest, so is typically more of an issue in Antarctica than Greenland.

2863 Even so, it has been recently demonstrated that the age of air bubbles can be matched to

2864 that of the associated ice through the use of nitrogen isotopes (Parrenin et al. 2013), which

2865 may circumvent what until recently appeared to be a significant problem. Slowly

2866 accumulating Antarctic ice tends to show only the more global signals, whereas Greenland

2867 ice can reveal many regional Northern Hemisphere influences. Nevertheless, Antarctic

2868 coastal ice cores do accumulate at high rates (e.g. Law Dome) and may provide an

2869 appropriate GSSP candidate section. Care would have to be taken to locate such a

2870 prospective GSSP in a region where the danger of calving of significant areas of ice from ice

2871 shelves and ice loss due to global climate change is less imminent, given the shallow depths

2872 at which the signal would be evident. Ellsworth Land, at the base of the Antarctic Peninsula

2873 might provide a suitable location, since the observed increase in snow accumulation there

2874 during the late 20th century is unprecedented in the context of the past 300 years (Thomas

2875 et al. 2015).

2876

2877 • Speleothems suffer from modulation of environmental signals by the soil ecosystem,

2878 making the interpretation of signal variation complex. Sulphur loading, the depletion of δ^{34}S

2879 and the ^{14}C (but importantly not ^{239}Pu) bomb-spike can be clearly resolved in speleothems,

2880 with an onset close to the atmospheric signal, although the peak tends to show a decadal-

2881 scale lag (Table 13). These environments also tend to lack mid-20th century δ^{13}C, δ^{18}O and

2882 heavy metal shifts as potential environmental markers.

2883

2884 • Tree rings, compared with speleothems, are more responsive to and provide a

2885 clearer archive of changing atmospheric chemistries. They benefit from a global distribution

2886 and are capable of precise calendrical dating through dendrochronology without reliance

2887 upon external dating methods. Stable carbon isotopes provide the strongest "candidate"

2888 measure from tree rings as they have been demonstrated to record worldwide the change in

2889 atmospheric δ^{13}C since the onset of global industrialisation. Such a uniformly expressed,

2890 well-characterised ~1940 CE departure (Table 13) has not been observed in the older tree-

2891 ring record, and the co-recorded chronology enables this trend to be clearly recognised.

2892   Sulphur loading and depletion of $\delta^{34}S$ is evident in developed countries, starting in the

2893   1960s, with enrichment of excess ^{14}C from the early 1950s to a 1964 CE peak (Table 13), but

2894   this signal is a terrestrial marker only. Although certainly widespread, tree-ring signals can be

2895   influenced by complex local environmental processes, yet these may be resolved through a

2896   capacity for large-scale independent replication. There is no precedent for using a living or

2897   deceased organism (such as a tree) as the host for a GSSP, but as an archive containing a

2898   signal of atmospheric carbon isotope variability and precise timescale there are close

2899   parallels to the use of the North Greenland ice core (NGRIP) for establishing the base of the

2900   Holocene.

2901

2902   To summarize, the information provided here is a first overall appraisal of suitable

2903   palaeoenvironments as regards their overall potentials for hosting an Anthropocene GSSP

2904   and a range of auxiliary sections. Clearly, many candidates that are geologically suitable

2905   exist, and are found in a range of different depositional settings. The review presented here

2906   is a critical prelude to help guide the necessary next steps, which involve selecting a small

2907   number of maximally suitable sites from the most appropriate geological facies, and

2908   subjecting them to multi-proxy analysis in order to assess changes in stratigraphically-

2909   relevant proxies from pre-industrial times through to the present.

2910

5 Conclusions

2912   • Many widespread, correlatable, and highly resolved signals could be used as the

2913   primary marker and as secondary markers for the base of an Anthropocene Series.

2914 $\delta^{13}C$ and radionuclide fallout signals are applicable across most environments. The

2915   latter provides the most abrupt signal, with a marked upturn in abundance of

2916   radioisotopes of ^{239}Pu or ^{14}C, in 1952 and 1954 CE respectively, appearing to provide

2917   a consistent horizon for correlation, whereas the peak 'bomb-signals' appear

2918   diachronous.

2919   • Varved deposits, such as those accumulating in marine anoxic basins, meromictic

2920   lakes, and estuaries and deltas, along with layers in glacial ice and growth rings, such

2921   as developed in corals, marine bivalves, speleothems and trees, represent those

2922   palaeoenvironments yielding highest resolution 'stratigraphy' at annual or even

2923   seasonal scale, and are hence preferred targets for searching for a likely GSSP

2924   section. The use of lamina or layer counting to determine ages can be verified,

2925   precisely in the case of tree rings, or radiometrically via ^{210}Pb (marine anoxic basins,

2926   corals and bivalves, lakes, ice) and ^{14}C (marine anoxic basins, corals and bivalves,

2927   lakes, speleothems and trees) dating.

2928   • Ombrotrophic peat bogs and some anthropogenic deposits provide clear expression

2929   of numerous key stratigraphical markers and can show high stratal accumulation

2930   rates, but lack the annual lamination seen in other environments.

2931   • Preservation of continuous laminated successions without missing 'strata' is

2932   essential. Estuaries and deltas are prone to missing laminae through erosive events,

2933   ice laminae from high-altitude glaciers through melting events, and speleothems

2934   through periods of aridity.

2935   • Time lags between signal generation and recording within varves or laminae on

2936   decadal scales represents a significant correlatory problem in speleothems.

2937   • A lag between the age of ice and the younger age of air bubbles within the ice limits

2938   the potential use of atmospheric CO_2 and CH_4 signals from ice cores, but close

2939   examination of sites of rapid accumulation on the Antarctic Peninsula may be

2940 suitable, as well as sites in other coastal regions (Law Dome in Antarctica), or in

2941 Greenland).

2942 • Deep marine environments can display a significant settling delay that affects

2943 radioisotopes and heavy metal signals, though this effect mainly delays the peak

2944 signal rather than onset. Except for some marine anoxic basins and perhaps cold-

2945 water corals, the rates of sedimentation are too low and the rates of bioturbation are

2946 too high for the development of suitable sections for a GSSP.

2947 • Proximity to the source of signals can result in local discrepancies in the timing of

2948 their initial onset within successions. In the search for a GSSP, there is advantage in

2949 looking at locations that are distant from such perturbations and provide a global

2950 signal, e.g. Antarctica for glacial ice, or the Caribbean for corals.

2951 • Overall, the range of high-resolution stratigraphic proxy signals, and the varied and

2952 widespread nature of the palaeoenvironments where they can be systematically

2953 preserved in strata, suggests that there is excellent potential for locating an effective

2954 candidate Anthropocene GSSP together with auxiliary stratotypes.

2955 ## Acknowledgements

2960 ## Declaration of Interest

References

Abram, N.J., Mulvaney, R., Wolff, E.W., Triest, J., Kipfstuhl, S., Trusel, L.D., Vimeux, F, Fleet, L., Arrowsmith, C. 2013. Acceleration of snow melt in an Antarctic Peninsula ice core during the twentieth century. Nature Geoscience, v. 6, 404–411.

Abram, N.J., McGregor, H.V., Tierney, J.E., Evans, M.N., McKay, N.P., Kaufman, D.S. & the PAGES 2k Consortium, 2016, Early onset of industrial-era warming across the oceans and continents. Nature, v. 536, 411–418.

Ahmad, S.M., Padmakumari, V.M., Raza, W., 2011. High-resolution carbon and oxygen isotope records from scleractinian (*Porites*) coral of Lakshadweep Archipelago, Quaternary International, v. 238, 107–114.

Allan, M., Le Roux, G., De Vleeschouwer, F., Bindler, R., Blaauw, M., Piotrowska, N., Sikorski, J., Fagel, N., 2013. High-resolution reconstruction of atmospheric deposition of trace metals and metalloids since AD 1400 recorded by ombrotrophic peat cores in Hautes-Fagnes, Belgium. Environmental Pollution, v. 178, 381–394.

Alldredge, A.L., Gotschalk, C. 1988. In situ settling behavior of marine snow. Limnology and Oceanography, v. 33(3). 339–351.

Anderson, R.F., LeHuray, A.P., Fleisher, M.Q., Murray, J.W., 1989. Uranium deposition in Saanich Inlet sediments, Vancouver Island. Geochimica et Cosmochimica Acta, v. 53, 2205–2213.

Appleby, P.G., Shotyk, W., Fankhauser, A., 1997. 210Pb age dating of three peat cores in the Jura Mountains, Switzerland. Water Air and Soil Pollution, v. 100 (3/4), 223–231.

Archer, D., Eby, M., Brovkin, V., Ridgwell, A., Long Cao, Mikolajewicz, U., Caldeira, K., Matsumoto, K., Munhoven, G., Montenegro, A., Tokos, K., 2009. Atmospheric lifetime of fossil fuel carbon dioxide. Annual Review of Earth and Planetary Science, v.37, 117–34.

Arienzo, M.M., McConnell, J.R., Chellman, N., Criscitiello, A.S., Curran, M., Fritzsche, D., Kipfstuhl, S., Mulvaney, R., Nolan, M., Opel, T., Sigl, M., Steffensen, J.P., 2016. A method for continuous

2988 [239]Pu determinations in Arctic and Antarctic ice cores. Environmental Science and

2989 Technology, v. 50 (13), 7066–7073.

2990 Arthur, M.A., Dean, W.E., Neff, E.D., Hay, B.J., King, J., Jones, G., 1994. Varve calibrated records of

2991 carbonate and organic carbon accumulation over the last 2000 years in the Black Sea. Glob.

2992 Biogeochem. Cycles, v. 8, 195–217.

2993 Baker, A., Genty, D., Dreybrodt, W. Barnes, W.L., Mockler, N.J., Grapes, J., 1998. Testing theoretically

2994 predicted stalagmite growth rate with recent annually laminated samples: Implications for

2995 past stalagmite deposition. Geochimica et Cosmochimica Acta, v. 62(3), 393–404.

2996 Ballent, A., Corcoran, P.L., Madden, O., Helm, P.A., Longstaff, F.J., 2016. Sources and sinks of

2997 microplastics in Canadian Lake Ontario nearshore, tributary and beach sediments. Marine

2998 Pollution Bulletin, v .110, 383–395.

2999 Bamber, R.N., 1980. Properties of fly ash as a marine sediment. Marine Pollution Bulletin, v. 11, 323–

3000 326.

3001 Barnosky, A.D., Hadly, E.A, Gonzalez, P., Head, J., Polly, P.D., Lawing, A.M., Eronen, J.T., Ackerly, D.D.,

3002 Alex, K., Biber, E., Blois, J., Brashares, J., Ceballos, G., Davis, E., Dietl, G.P., Dirzo, R., Doremus,

3003 H., Fortelius, M., Greene, H.W., Hellmann, J., Hickler, T., Jackson, S.T., Kemp, M., Koch, P.L,.

3004 Kremen, C., Lindsey, E.L., Looy, C., Marshall, C.R., Mendenhall, C., Mulch, A., Mychajliw, A.M.,

3005 Nowak, C., Ramakrishnan, U., Schnitzler, J., Das Shrestha, K., Solari, K., Stegner, L., Stegner,

3006 M.A., Stenseth, N.C., Wake, M.H., Zhibin Zhang, 2017. Merging paleobiology with

3007 conservation biology to guide the future of terrestrial ecosystems. Science, v. 355(6325),

3008 eaah4787

3009 Barron, J.A., Bukry, D., Hendy, I.L., 2015, High-resolution paleoclimatology of the Santa Barbara Basin

3010 during the Medieval Climate Anomaly and early Little Ice Age based on diatom and

3011 silicoflagellate assemblages in Kasten core SPR0901-02KC, Quaternary International, v. 387,

3012 13–22.

3013 Battarbee, R.W., Simpson, G.L., Shilland, E.M., Flower, R.J., Kreiser, A., Yang, H., Clarke, G., 2014.

3014   Recovery of UK lakes from acidification: An assessment using combined palaeoecological and

3015   contemporary diatom assemblage data. Ecological Indicators, v. 37, 365–380.

3016 Benninger L.K., Dodge R.E., 1986, Fallout plutonium and natural radionuclides in annual bands of the

3017   coral *Montastrea annularis*, St. Croix, U.S. Virgin Islands, Geochimica Cosmochimica Acta, v.

3018   50, 2785–2797.

3019 Berry, K.L.E., Seemann, J., Dellwig, O., Struck, U., Wild, C., Leinfelder, R.R., 2013. Sources and spatial

3020   distribution of heavy metals in scleractinian coral tissues and sediments from the Bocas del

3021   Toro Archipelago, Panama. Environmental Monitoring and Assessment, v. 185, 9089–9099.

3022 Berset, J.-D., Kuehne, P., Shotyk, W., 2001. Concentrations and distribution of some polychlorinated

3023   biphenyls (PCBs) and polycyclic aromatic hydrocarbons (PAHs) in an ombrotrophic peat bog

3024   profile of Switzerland. Science of the Total Environment, v. 267, 76–85.

3025 Bindler, R., Renberg, I., Klaminder, J., Emteryd, O., 2004. Tree rings as Pb pollution archives? A

3026   comparison of 206 Pb/207 Pb isotope ratios in pine and other environmental media. Science

3027   of the Total Environment, v. 319(1), 173–183.

3028 Blyth, A.J., Hartland, A., Baker, A. 2016. Organic proxies in speleothems: New developments,

3029   advantages and limitations. Quaternary Science Reviews, v. 149, 1–17.

3030 Boettger, T., Haupt, M., Knöller, K., Weise, S.M., Waterhouse, J.S., Rinne, K.T., Loader, N.J., Sonninen,

3031   E., Jungner, H., Masson-Delmotte, V., Stievenard, M., Guillemin, M.-T., Pierre, M., Pazdur, A.,

3032   Leuenberger, M., Filot, M., Saurer, M., Reynolds, C.E., Helle, G., Schleser, G.H., 2007. Wood

3033   cellulose preparation methods and mass spectrometric analyses of $\delta^{13}C$, $\delta^{18}O$, and

3034   nonexchangeable δ^2H values in cellulose, sugar, and starch: An interlaboratory comparison.

3035   Analytical Chemistry, v. 79, 4603–4612.

3036 Boettger, T., Haupt, M., Friedrich, M, Waterhouse, J.S., 2014. Reduced climate sensitivity of carbon,

3037   oxygen and hydrogen stable isotope ratios in tree-ring cellulose of silver fir (*Abies alba* Mill.)

3038   influenced by background SO_2 in Franconia (Germany, Central Europe). Environmental

3039   Pollution, v. 185, 281–294.

3040   Bollhöfer, A., Rosman, K.J.R. 2001. Isotopic source signatures for atmospheric lead: the Northern

3041   Hemisphere. *Geochimica et Cosmochimica Acta*, v. *65*(11), 1727–1740.

3042   Bond, T.C., Bhardwaj, E., Dong, R., Jogani, R., Jung, S.K., Roden, C., Streets, D.G., Trautmann, N.M.

3043   2007. Historical emissions of black and organic carbon aerosol from energy-related

3044   combustion, 1850–2000. Global Biogeochem Cycles, v. 21(2). DOI: 10.1029/2006GB002840.

3045   Bonotto, D.M., Karmann, I., Baskaran, M.M., 2012. Growth rates in modern speleothems from

3046   Santana Cave, Brazil, by the ^{210}Pb-method. Radiation Measurements, v. 47, 168–177.

3047   Borsato, A., Frisia, S., Fairchild, I. J., Somogyi, A., Susini, J., 2007. Trace element distribution in annual

3048   stalagmite laminae mapped by micrometer-resolution X-ray fluorescence: implications for

3049   incorporation of environmentally significant species. Geochimica et Cosmochimica Acta, v.71,

3050   1494–1512.

3051   Borsato, A., Frisia, S., Wynn, P., Fairchild, I.J., Miorandi, R., 2015. Sulphate concentration in cave

3052   dripwater and speleothems: long-term trends and overview of its significance as proxy of

3053   environmental processes and climate forcing. Quaternary Science Reviews, v. 127, 48–60.

3054   Boutron, C.F., Görlach, U., Candelone, J.-P., Bolshov, M. A., Delmas, R.J., 1991. Decrease in

3055   anthropogenic lead, cadmium and zinc in Greenland snows since the late 1960s. Nature, v.

3056   353, 153–156.

3057   Boyle, E.A., Lee, J.-M., Echegoyen, Y., Noble, A. Moos, S. Carrasco, G. Zhao, N., Kayser, R., Zhang, J.

3058   Gamo, T. Obata, H., Norisuye, K., 2014. Anthropogenic lead emissions in the ocean: The

3059   evolving global experiment, Oceanography, v. 27(1), 69–75.

3060   Brown, A.G., Tooth, S., Bullard, J.E., Thomas, D.S.G., Chiverrell, R.C., Plater, A.J., Murton, J.,

3061   Thorndycraft, V.R., Tarolli, P., Rose, J., Wainwright, J., Downs, P., Aalto, R., 2017. The

3062   Geomorphology of the Anthropocene: Emergence, Status and Implications. Earth Surface

3063   Processes and Landforms, v. 42, 71–90.

3064   Bukata, A.R., Kyser T.K., 2007. Carbon and nitrogen isotope variations in tree-rings as records of

3065   perturbations in regional carbon and nitrogen cycles. Environmental Science and Technology,

3066   v. 41 (4), 1331–1338.

3067   Burney D.A., James H.F., Burney L.P., Olson S.L., Kikuchi W., Wagner W.L., Burney M., McCloskey D.,

3068   Kikuchi D., Grady F.V., Gage R. and Nishek R. 2001. Fossil evidence for a diverse biota from

3069   Kaua'i and its transformation since human arrival. Ecological Monographs, v. 7, 615–641.

3070   Calvo-Marcilese, L., Langer, M.R., 2010. Breaching biogeographic barriers: the invasion of *Haynesina*

3071   *germanica* (Foraminifera, Protista) in the Bahía Blanca estuary, Argentina. Biological

3072   Invasions, v. 12, 3299–3306.

3073   Campana, S.E., 1997. Use of radiocarbon from nuclear fallout as a dated marker in the otoliths of

3074   haddock *Melanogrammus aeglefinus*. Marine Ecology Progress Series, v. 150, 49–56.

3075   Carlton, J.T., Thompson, J.K., Schemel, L.E., Nichols, F.H., 1990. Remarkable invasion of San Francisco

3076   Bay (California, USA) by the Asian clam *Potamocorbula amurensis*. Marine Ecology Progress

3077   Series, v. 66, 81–94.

3078   Ceballos, G., Ehrlich, P.R., Barnosky, A.D., García, A., Pringle, R.M., Palmer, T.M., 2015. Accelerated

3079   modern human–induced species losses: Entering the sixth mass extinction. Science

3080   Advances, v. 1(5), e1400253, DOI: 10.1126/sciadv.1400253.

3081   Chapman, S.B., 1964. The ecology of Coom Rigg Moss, Northumberland, II. The chemistry of peat

3082   profiles and the development of the bog system. Journal of Ecology, v. 52, 315–321.

3083   Ciais, P., Sabine, C., Bala, G., Bopp, L., Brovkin, V., Canadell, J., Chhabra, A., DeFries, R., Galloway, J.,

3084   Heimann, M., Jones, C., Le Quéré, C., Myneni , R.B., Piao, S., Thornton, P., 2013. Carbon and

3085   Other Biogeochemical Cycles. In: Climate Change 2013: The Physical Science Basis.

3086   Contribution of Working Group I to the Fifth Assessment Report of the Intergovernmental

3087   Panel on Climate Change [Stocker, T.F., D. Qin, G.-K. Plattner, M. Tignor, S.K. Allen, J.

3088   Boschung, A. Nauels, Y. Xia, V. Bex and P.M. Midgley (eds.)]. Cambridge University Press,

3089   Cambridge, United Kingdom and New York, NY, USA, pp. 465–570.

3090   doi:10.1017/CBO9781107415324.015.

3091   Cocroft W., Schofield, G. 2012. The Secret Hill: Cold War Archaeology of the Teufelsberg. British

3092   Archaeology, v. 126, 38–43.

3093   Cohen, A.N., 2004. Invasions in the sea. Park Science, v. 22, 37–41.

3094 Cohen, A.N., 2011. The Exotics Guide: Non-native Marine Species of the North American Pacific
3095   Coast. Center for Research on Aquatic Bioinvasions, Richmond, CA, and San Francisco Estuary
3096   Institute, Oakland, CA. Revised September 2011. http://www.exoticsguide.org

3097 Cohen, A.N., Carlton, J.T., 1998. Accelerating invasion rate in a highly invaded estuary. Science, v.
3098   279, 555–557.

3099 Cole, J.E., 1996, Coral records of climate change: understanding past variability in the Tropical Ocean-
3100   Atmosphere, *In:* Jones, P. D., Bradley, R. S. and Jouzel, J. (eds.) Climatic Fluctuations and
3101   Forcing: Mechanisms of the Last 2000 Years, (Springer, Berlin), pp. 333–355.

3102 Cole, M., Lindeque, P., Fileman, E., Halsband, C., Goodhead, R., Moger, J., Galloway, T.S., 2013,
3103   Microplastic Ingestion by Zooplankton, Environ. Sci. Technol., v. 47, 6646–6655.

3104 Colonna, M., Casanova, J., Dullo, W.-C., Camoin, G., 1996. Sea-level changes and $\delta^{18}O$ record for the
3105   past 34,000 yr from Mayotte Reef, Indian Ocean. Quaternary Research, v. 46, 335–339.

3106 Committee on Nonnative Oysters in the Chesapeake Bay, National Research Council. 2004.
3107   Nonnative Oysters in the Chesapeake Bay. 344 pp.

3108 Condomines, M., Rihs, S., 2006. First ^{226}Ra–^{210}Pb dating of a young speleothem. Earth and Planetary
3109   Science Letters, v. 250, 4–10.

3110 Cook, E.R., Briffa, K.R., Meko, D.M., Graybill, D.A., Funkhouser, G., 1995. The 'segment length curse'
3111   in long tree-ring chronology development for palæoclimatic studies. The Holocene, v. 5 229–
3112   237.

3113 Corcoran, P.L., Norris, T., Ceccanese, T., Walzak, M.J., Helm, P.A., Marvin, C.H., 2015. Hidden plastics
3114   of Lake Ontario: Canada and their potential preservation in the sediment record.
3115   Environmental Pollution, v. 204, 17–25.

3116 Crowther, T.W., Glick, H.B., Covey, K.R., Bettigole, C., Maynard, D.S., Thomas, S.M., Smith, J.R.,
3117   Hintler, G., Duguid, M.C., Amatulli, G., Tuanmu, M.-N., Jetz, W., Salas, C., Stam, C., Piotto, D.,
3118   Tavani, R., Green, S., Bruce, G., Williams, S.J., Wiser, S.K., Huber, M.O., Hengeveld, G.M.,
3119   Nabuurs, G.-J., Tikhonova, E., Borchardt, P., Li, C.-F., Powrie, L.W., Fischer, M., Hemp, A.,
3120   Homeier, J., Cho, P., Vibrans, A.C., Umunay, P.M., Piao, S.L., Rowe, C.W., Ashton, M.S., Crane,

3121   P.R., Bradford, M.A., 2015. Mapping tree density at a global scale. Nature, v. 515, 201 [doi:

3122   10.1038/nature 14967]

3123 Crutzen, P.J., Stoermer, E.F., 2000. The Anthropocene, Global Change Newsletters, v. 41, 17–18.

3124 Curtis, C.J. and Simpson, G.L. (Eds.) (2011). Freshwater Umbrella – the effects of nitrogen deposition

3125   on freshwaters in the UK. Report to DEFRA under contract AQ0803. ECRC Research Report

3126   No 152. University College London, UK. 204 pp.

3127 Dalton, C., Birks, H.J.B., Brooks, S.J., Cameron, N.G., Evershed, R.P., Peglar, S.M., Scott, J.A.,

3128   Thompson, R., 2005. A multi-proxy study of lake-development in response to catchment

3129   changes during the Holocene at Lochnagar, north-east Scotland. Palaeogeography,

3130   Palaeoclimatology, Palaeoecology, v. 221(3-4), 175–201.

3131 Dargie, G.C., Lewis, S.L., Lawson, I.T., Mitchard, E.T., Page, S.E., Bocko, Y.E., Ifo, S.A., 2017. Age,

3132   extent and carbon storage of the central Congo Basin peatland complex. Nature, v. 542, 86–

3133   90.

3134 D'Arrigo, R., Wilson, R., Liepert, B., Cherubini, P., 2007. On the 'divergence problem' in northern

3135   forests: a review of the tree-ring evidence and possible causes. Global Planetary Change, v.

3136   60(3–4), 289–305.

3137 Dean, J.M., Kemp, A.E.S., 2004. A 2100 year BP record of the Pacific Decadal Oscillation, El Niño

3138   Southern Oscillation and Quasi-Biennial Oscillation in marine production and fluvial input

3139   from Saanich Inlet, British Columbia. Palaeogeography, Palaeoclimatology, Palaeoecology, v.

3140   213, 207– 229.

3141 Dean, J.M., Kemp, A.E.S., Pearce, R.B., 2001. Palaeo-flux records from electron microscope studies of

3142   Holocene laminated sediments, Saanich Inlet, British Columbia. Marine Geology, v. 174, 139–

3143   158.

3144 Dearing, J.A., Xiangdong Yang, Xuhui Dong, Enlou Zhang, Xu Chen, Langdon, P.G., Ke Zhang, Weiguo

3145   Zhang, Dawson, T.P., 2012. Extending the timescale and range of ecosystem services through

3146   paleoenvironmental analyses, exemplified in the lower Yangtze basin. Proceedings of the

3147   National Academy of Science, U.S.A., v. 109, E1111–E1120.

3148   De'ath, G., Lough, J.M., Fabricius, K.E., 2009. Declining coral calcification on the Great Barrier Reef.

3149   Science, v. 323, 116–119.

3150   DeFelice, R.C., Eldredge, L.G., Carlton, J.T., 2001. Nonindigenous invertebrates. In: Eldredge, L.G. &

3151   Smith, C.M. (eds). A guidebook of introduced marine species in Hawaii. Bishop Museum

3152   Technical Report 21.

3153   DeLong, K.L., Maupin, C.R., Flannery, J.A., Quinn, T.M., Shen, C.-C., 2016. Refining temperature

3154   reconstructions with the Atlantic coral Siderastrea siderea, Palaeogeography,

3155   Palaeoclimatology, Palaeoecology, v. 462, 1–15.

3156   Diaz, R.J., Rosenberg, R., 2008, Spreading Dead Zones and Consequences for Marine Ecosystems,

3157   *Science*, v. 321, 926–929.

3158   Dris, R., Gasperi, J., Saad, M., Mirande, C., Tassin, B., 2016. Synthetic fibers in atmospheric fallout: A

3159   source of microplastics in the environment? Marine Pollution Bulletin, v. 104, 290–293.

3160   Druffel, E.R.M., 1996. Post-bomb radiocarbon records of surface corals from the tropical Atlantic

3161   Ocean. Radiocarbon, v. 38(3), 563–572.

3162   Edgeworth, M., Richter D. deB., Waters, C.N., Haff, P., Neal, C., Price, S.J., 2015. Diachronous

3163   beginnings of the Anthropocene: The lower bounding surface of anthropogenic deposits,

3164   Anthropocene Review, v. 2(1), 1–26.

3165   Ekaykin, A.A., Vladimirova, D.O., Lipenkov, V.Y., Masson-Delmotte, V., 2017. Climatic variability in

3166   Princess Elizabeth Land (East Antarctica) over the last 350 years, Climate of the Past

3167   Discussions, 13(1), 61–71..

3168   Ekdahl, E.J., Teranes, J.L., Guilderson, T.P., Turton, C.L., McAndrews, J.H., Wittkop, C.A., Stoermer,

3169   E.F., 2004. Prehistorical record of cultural eutrophication from Crawford Lake, Canada,

3170   Geology, v. 32, 745–748.

3171   Ekdahl, E.J., Teranes, J.L., Wittkop, C.A., Stoermer, E.F., Reavie, E.D., Smol, J.P., 2007. Diatom

3172   assemblage response to Iroquoian and Euro-Canadian eutrophication of Crawford Lake,

3173   Ontario, Canada, Journal of Paleolimnology, v. 37, 233–246.

3174 Ellis, E.C., Antill, E.C., Kreft, H., 2012. All is not loss: Plant biodiversity in the Anthropocene. PLoS ONE,

3175   v. 7(1), e30535. doi:10.1371/journal.pone.0030535

3176 Enrico, M., Le Roux, G., Marusczak, N., Heimbürger, L., Claustres, A., Fu, X., Sun, R., Sonke, J.E., 2016.

3177   Atmospheric mercury transfer to peat bogs dominated by gaseous elemental mercury dry

3178   deposition. Environmental Science & Technology, v. 50, 2405–2412.

3179 Erisman, J.W., Galloway, J.N., Seitzinger, S., Bleeker, A., Dise, N.B., Petrescu, A.M.R., Leach, A.M., de

3180   Vries, W., 2013. Consequences of human modification of the global nitrogen cycle.

3181   Philosophical Transactions of the Royal Society B, v. 368: 20130116.

3182 Esper, J., Cook, E.R., Schweingruber, F.H., 2002. Low-frequency signals in long tree ring chronologies

3183   for reconstructing past temperature variability. Science, v. 295, 2250–2253.

3184 Etheridge, D.M., Steele, L.P., Langenfelds, R.L., Francey, R.J., Barnola, J.M., Morgan, V.I., 1996.

3185   Natural and anthropogenic changes in atmospheric CO_2 over the last 1000 years from air in

3186   Antarctic ice and firn. J. Geophys. Res., v. 101(D2), 4115–4128.

3187 Evans, M.A., Fahnenstiel, G., Scavia, D., 2011. Incidental Oligotrophication of North American Great

3188   Lakes. Environmental Science & Technology, v. 45(8), 3297–3303.

3189 Fairchild, I.J., 2017. Geochemical records in Speleothems. *In:* Elias, S. (ed.) Encyclopedia of the

3190   Anthropocene, Elsevier Reference Modules. DOI10.1016/B978-0-12-409548-9.10006-5.

3191 Fairchild, I.J., Baker, A., 2012. Speleothem Science. From Process to Past Environment. Wiley-

3192   Blackwell, Chichester.

3193 Fairchild, I.J., Frisia, S., 2014. Definition of the Anthropocene: a view from the underworld. In:

3194   Waters, C., Zalasiewicz, J., Williams, M., Ellis, M.A., and Snelling A. (eds.) A Stratigraphical

3195   Basis for the Anthropocene. Geological Society Special Publication, v. 395, 239–254.

3196 Fairchild, I.J., Loader, N.J., Wynn, P.M., Frisia, S., Thomas, P.A., Lageard, J.G.A., De Momi, A.,

3197   Hartland, A., Borsato, A., La Porta, N., Susini, J., 2009. Sulfur fixation in wood mapped by

3198   synchrotron X-ray studies: implications for environmental archives, Environmental Science

3199   and Technology, v. 43, 1310–1315.

3200 FAO (Food and Agriculture Organization of the United Nations) (2006). Global Forest Resources Assessment 2005: Progress towards sustainable forest management. FAO Forestry Paper 147. Published January 2006.

3203 Farmer, J.G., Eades, L.J., Atkins, H., Chamberlain, D.F., 2002, Historical trends in the lead isotopic composition of archival Sphagnum mosses from Scotland (1838–2000). Environmental Science & Technology, v. 36, 152–157.

3206 Farquhar, G.D., O'Leary, M.H., Berry, J.A., 1982 On the relationship between carbon dioxide discrimination and the intercellular carbon dioxide concentration in leaves. Australian Journal of Plant Physiology, v. 9, 121–137.

3209 Ferretti, D.F., Miller, J.B., White, J.W.C., Etheridge, D.M., Lassey, K.R., Lowe, D.C., MacFarling Meure, C., Dreier, M.F., Trudinger, C.M., van Ommen, D., 2005. Unexpected changes to the global methane budget over the last 2,000 years. Science, v. 309, 1714–1717.

3212 Fiałkiewicz-Kozieł, B., Smieja-Król, B., Frontasyeva, M., Słowiński, M., Marcisz, K., Lapshina, E., Gilbert, D., Buttler, A., Jassey, V E J., Kaliszan, Laggoun-Défarge, K.F., Kołaczek, P. Lamentowicz, M., 2016. Anthropogenic- and natural sources of dust in peatland during the Anthropocene. Scientific Reports, v. 6, 38731. DOI: 10.1038/srep38731.

3216 Field, D.B., Baumgartner, T.R., Charles, C.D., Ferreira-Bartrina, V., Ohman, M.D., 2006. Planktonic foraminifera of the California Current reflect 20th-century warming. Science, v. 311, 63–66.

3218 Fischer, H., Wagenbach, D., Kipfstuhl, J. 1998. Sulfate and nitrate firn concentrations on the Greenland ice sheet. 2. Temporal anthropogenic deposition changes. Journal of Geophysical Research, v. 103, 21 935–21 942.

3221 Florea, N., Cristache, C., Oaie, G., Duliu, O.G., 2011. Concordant ^{210}Pb and ^{137}Cs ages of black sea anoxic unconsolidated sediments. Geochronometria, v. 38, 101–106.

3223 Fofonoff, P.W., Ruiz, G.M., Steves, B., Simkanin, C., Carlton, J.T. 2017. National Exotic Marine and Estuarine Species Information System. http://invasions.si.edu/nemesis/.

3225 Fohlmeister, J., Kromer, B., Mangini, A., 2011. The influence of soil organic matter age spectrum on the reconstruction of atmospheric ^{14}C levels via stalagmites, Radiocarbon, v. 53, 99–115.

3227   Ford, J.R., Price, S.J., Cooper, A.H., Waters, C.N., 2014, An assessment of lithostratigraphy for

3228   anthropogenic deposits, *In*: Waters, C.N., Zalasiewicz, J., Williams, M., Ellis, M.A., and Snelling

3229   A. (eds.) A Stratigraphical Basis for the Anthropocene. Geological Society, London, Special

3230   Publications v. 395, 55–89.

3231   Fowler D, Coyle M, Skiba U, Sutton, M.A., Cape, J.N., Reis, S., Sheppard, L.J., 2013. The global

3232   nitrogen cycle in the 21st century. Philosophical Transactions of the Royal Society B, v.

3233   368(1621), 1–13.

3234   Francey, R.J., Allison, C.E., Etheridge, D.M., Trudinger, C.M., Enting, I.G., Leuenberger, M.,

3235   Langenfelds, R.L., Michel, E., Steele, L.P., 1999. A 1000-year high precision record of $\delta13C$ in

3236   atmospheric CO_2. Tellus, v. 51B, 170–193.

3237   Frank, D.C., Poulter, B., Saurer, M., Esper, J., Huntingford, C., Helle, G., Treydte, K., Zimmermann,

3238   N.E., Schleser, G.H., Ahlström, A., Ciais, P., Friedlingstein, P., Levis, S., Lomas, M., Sitch, S.,

3239   Viovy, N., Andreu-Hayles, L., Bednarz, Z., Berninger, F., Boettger, T., D'Alessandro, C.M.,

3240   Daux, V., Filot, M., Grabner, M., Gutierrez, E., Haupt, M., Hilasvuori, E., Jungner, H., Kalela-

3241   Brundin, M., Krapiec, M., Leuenberger, M., Loader, N.J., Marah, H., Masson-Delmotte, V.,

3242   Pazdur, A., Pawelczyk, S., Pierre, M., Planells, O., Pukiene, R., Reynolds-Henne, C.E., Rinne,

3243   K.T., Saracino, A., Sonninen, E., Stievenard, M., Switsur, V.R., Szczepanek, M., Szychowska-

3244   Krapiec, E., Todaro, L., Waterhouse, J.S., Weigl, M., 2015. Water-use efficiency and

3245   transpiration across European forests during the Anthropocene. Nature Climate Change, v.5,

3246   579–583.

3247   Freiwald, A., Rogers, A., Hall-Spencer, J., Guinotte, J.M., Davies, A.J., Yesson, C., Martin, C.S.,

3248   Weatherdon, L.V., 2017. Global distribution of cold-water corals (version 3.0). Second update

3249   to the dataset in Freiwald, A., Fosså, J.H., Grehan, A., Koslow, T., Roberts, J.M. (2004) Cold-

3250   water coral reefs: out of sight – no longer out of mind. Biodiversity Series 22. Cambridge

3251   (UK): UNEP World Conservation Monitoring Centre. 86 pp. URL: http://data.unep-

3252   wcmc.org/datasets/3

3253 Frisia, S., Borsato, A., Preto, N., McDermott, F., 2003, Late Holocene annual growth in three Alpine

3254   stalagmites records the influence of solar activity and the North Atlantic Oscillation on winter

3255   climate, Earth and Planetary Science Letters, v. 216, 411–424.

3256 Frisia, S., Borsato, A., Fairchild, I. J., Susini, J., 2005. Variations in atmospheric sulphate recorded in

3257   stalagmites by synchrotron micro-XRF and XANES analyses. Earth and Planetary Science

3258   Letters, v.235, 729–740.

3259 Fritts, H.C., 1976. Tree Rings and Climate. Academic Press, USA

3260 Gabrieli, J., Cozzi, G. Vallelonga, P., Schwikowski, M., Sigl, M., Eickenberg, J., Wacker, L., Boutron, C.,

3261   Gäggeler, H., Cescon, P., Barbante, C., 2011. Contamination of Alpine snow and ice at Colle

3262   Gnifetti, Swiss/Italian Alps, from nuclear weapons tests. Atmospheric Environment, v. 45,

3263   587–593.

3264 Gagnon, C., Pelletier, É., Mucci, A., 1997. Behaviour of anthropogenic mercury in coastal marine

3265   sediments. Marine Chemistry, v. 59, 159–176.

3266 Genty, D., Massault, M., 1999. Carbon transfer dynamics from bomb-^{14}C and ^{13}C time series of a

3267   laminated stalagmite from SW France: modelling and comparison with other stalagmite

3268   records. Geochimica et Cosmochimica Acta, v. 63, 1537–1548.

3269 Geyer, R., Jambeck, J.R. Lavender Law, K. 2017. Production, use, and fate of all plastics ever made.

3270   Science Advances, v. 3, e1700782. DOI: 10.1126/sciadv.1700782

3271 Giosan, L., Syvitski, J., Constantinescu, S., Day, J., 2014, Climate Change: Protect the world's deltas.

3272   Nature, v. 516, 31–33.

3273 Goffard, A., 2016. Registro geológico del impacto humano en el estuario del Urola (Geoparque de la

3274   Costa Vasca) durante el Antropoceno. CKQ Estudios de Cuaternario, v. 6, 43–60.

3275 Gradstein, F.M., Ogg, J.G, Schmitz, M., Ogg, G. (eds) A Geological Time Scale 2012. Elsevier, 1144 pp.

3276 Grudd, H., 2008. Torneträsk tree-ring width and density AD 500–2004: A test of climatic sensitivity

3277   and a new 1500-year reconstruction of north Fennoscandian summers. Climate Dynamics, v.

3278   31, 843–857.

3279 Hall, N.M, Berry, K.L.E., Rintoul, L., Hoogenboom, M.O., 2015. Microplastic ingestion by scleractinian

3280   corals, Marine Biology, v. 162, 725–732.

3281 Han, Y.M., Wei, C., Huang, R.J., Bandowe, B.A.M., Ho, S.S.H., Cao, J.J., Jin, Z.D., Xu, B.Q., Gao, S.P., Tie,

3282   X.X., An, Z.S., Wilcke, W. 2016. Reconstruction of atmospheric soot history in inland regions

3283   from lake sediments over the past 150 years. Scientific Reports, v. 6, 19151.

3284 Han, Y.M., An, Z.S. and Cao, J.J., 2017. The Anthropocene—A potential stratigraphic definition based

3285   on black carbon, char, and soot records. Encyclopedia of the Anthropocene.

3286   DOI:10.1016/B978-0-12-409548-9.10001-6.

3287 Hancock, G.J., Leslie, C., Everett, S.E., Tims, S.G., Brunskill, G.J., and Haese, R., 2011, Plutonium as a

3288   chronomarker in Australian and New Zealand sediments: a comparison with ^{137}Cs, Journal of

3289   Environmental Radioactivity, v. 102, 919–929.

3290 Hancock, G.J., Tims, S.G., Fifield, L.K., Webster, I.T., 2014. The release and persistence of radioactive

3291   Anthropogenic nuclides. In: Waters, C.N., Zalasiewicz, J., Williams, M., Ellis, M.A., Snelling, A.

3292   (eds) A Stratigraphical Basis for the Anthropocene. Geological Society, London, Special

3293   Publications, v. 395, 265–281.

3294 Hanebuth, T.J.J., Lantzsch, H., Nizou, J., 2015. Mud depocenters on continental shelves—appearance,

3295   initiation times, and growth dynamics. Geo-Marine Letters, v. 35(6), 487–503.

3296 Hartland, A., Fairchild, I.J., Müller, W., Domínguez-Villar, D., 2014. Preservation of colloid-metal

3297   complexes in a modern hyperalkaline stalagmite: implications for speleothem trace element

3298   geochemistry. Geochimica et Cosmochimica Acta, v. 128, 29–43.

3299 Hastings, M.G., Jarvis, J.C., Steig, E.J., 2009. Anthropogenic impacts on nitrogen isotopes of ice-core

3300   nitrate. Science, v. 324, 1288.

3301 Hazen, R.M., Grew, E.S., Origlieri, M.J., Downs, R.T., 2017. On the mineralogy of the "Anthropocene

3302   Epoch". American Mineralogist, v. 102, 596–611.

3303 Head, M.J., Gibbard, P.L., 2015. Formal subdivision of the Quaternary System/Period: Past, present,

3304   and future. Quaternary International, v. 383, 4–35.

3305 Heikoop, J.M., Risk, M.J, Lazier, A.V., Edinger, E.N., Jompa, J., Limmon, G.V., Dunn, J.J., Browne, D.R.,

3306   Schwarcz, H.P., 2000. Nitrogen-15 signals of anthropogenic nutrient loading in reef corals.

3307   Marine Pollution Bulletin, v. 40(7), 628–636.

3308 Hendy, I.L., Dunn, L., Schimmelmann, A., Pak D.K., 2013. Resolving varve and radiocarbon chronology

3309   differences during the last 2000 years in the Santa Barbara Basin sedimentary record,

3310   California. Quaternary International, v. 310, 155–168.

3311 Hendy, I.L., Napier, T.J., Schimmelmann, A., 2015. From extreme rainfall to drought: 250 years of

3312   annually resolved sediment deposition in Santa Barbara Basin, California. Quaternary

3313   International, v. 387, 3–12.

3314 Hetzinger, S., Pfeiffer, M., Dullo, W.-C., Garbe-Schönberg, D., Halfar, J., 2010. Rapid 20th century

3315   warming in the Caribbean and impact of remote forcing on climate in the northern tropical

3316   Atlantic as recorded in a Guadeloupe coral. Palaeogeography, Palaeoclimatology,

3317   Palaeoecology, v. 296, 111–124.

3318 Hietz, P., Horsky, M., Prohaska, T., Lang, I., Grabner, M., 2015. High-resolution densitometry and

3319   elemental analysis of tropical wood. Trees, v. 29, 487–497.

3320 Hoegh-Guldberg, O., 2014. Coral reefs in the Anthropocene: persistence or the end of the line? *In:*

3321   Waters, C.N., Zalasiewicz, J., Williams, M., Ellis, M.A., and Snelling A. (eds.) A Stratigraphical

3322   Basis for the Anthropocene. Geological Society, London, Special Publications, v. 395, 167–

3323   183.

3324 Holtgrieve, G.W., Schindler, D.E., Hobbs, W.O., Leavitt, P.R., Ward, E.J., Bunting, L., Chen, G., Finney,

3325   B.P., Gregory-Eaves, I., Holmgren, S., Lisac, M.J., Lisi, P.J., Nydick, K., Rogers, L.A., Saros, J.E.,

3326   Selbie, D.T., Shapley, M.D., Walsh, P.B., Wolfe, A.P., 2011. A Coherent Signature of

3327   Anthropogenic Nitrogen Deposition to Remote Watersheds of the Northern Hemisphere,

3328   Science, v. 334, 1545–1548.

3329 Hom, W., Risebrough, R.W., Soutar, A., Young, D.R., 1974. Deposition of DDE and Polychlorinated

3330   Biphenyls in Dated Sediments of the Santa Barbara Basin. Science, v. 184 (4142), 1197-1199.

3331   Hong, S., Candelone, J.P., Patterson, C.C., Boutron, C.F., 1994. Greenland ice evidences of

3332   hemispheric pollution for lead two millennia ago by Greek and Roman civilizations. Science,

3333   v. 265, 1841–1843.

3334   Hua, Q., Barbetti, M., 2004. Review of tropospheric bomb ^{14}C data for carbon cycle modeling and age

3335   calibration purposes. Radiocarbon, v. 46(3) 1273–1298.

3336   Hughen, K.A., Overpeck, J.T., Peterson, L.C., Anderson, R.F., 1996. The nature of varved

3337   sedimentation in the Cariaco Basin, Venezuela, and its palaeoclimatic significance. In: Kemp,

3338   A.E.S. (Ed.), Palaeoclimatology and palaeoceanography from laminated sediments. Geol. Soc.

3339   London Spec. Pub., v. 116, 171–183.

3340   Hughes T.P. Kerry J.T., Álvarez-Noriega M., Álvarez-Romero J.G., Anderson K.D., Baird A.H., Babcock

3341   R.C., Beger M., Bellwood D.R., Berkelmans R., Bridge T.C., Butler I.R., Byrne M., Cantin N.E.,

3342   Comeau S., Connolly S.R., Cumming G.S., Dalton S.J., Diaz-Pulido G., Eakin C.M., Figueira W.F.,

3343   Gilmour J.P., Harrison H.B., Heron S.F., Hoey A.S., Hobbs J.-P.A., Hoogenboom M.O., Kennedy

3344   E.V., Chao-yang Kuo, Lough J.M., Lowe R.J., Gang Liu, McCulloch M.T., Malcolm H.A.,

3345   McWilliam M.J., Pandolfi J.M., Pears R.J., Pratchett M.S., Schoepf V., Simpson T., Skirving

3346   W.J., Sommer B., Torda G., Wachenfeld D.R., Willis B.L. and Wilson S.K., 2017. Global

3347   warming and recurrent mass bleaching of corals. Nature, v. 543, 373–377.

3348   Irabien, M.J. García-Artola, A., Cearreta, A., Leorri, E., 2015. Chemostratigraphic and

3349   lithostratigraphic signatures of the Anthropocene in estuarine areas from the eastern

3350   Cantabrian coast (N. Spain), Quaternary International, v. 364, 196–205.

3351   Isdale, P., 1984. Fluorescent bands in massive coral record centuries of coastal rainfall, Nature, v.

3352   310, 578–579.

3353   Ivar do Sul, J.A., Costa, M.F., 2014. The present and future of microplastic pollution in the marine

3354   environment, Environmental Pollution, v. 185, p. 352–364.

3355   Jambeck, J.R., Geyer, R., Wilcox, C., Siegler, T.R., Perryman, M., Andrady, A., Narayan, R, Law, K.L.,

3356   2015. Plastic waste inputs from land into the ocean. Science, v. 347, 768–771.

3357 Jeandel C., 1981. Comportement du Plutonium dans les mileux naturels (Lacustre, Fluvial et

3358   Estuarien). Thèse 3° Cycle, Université de Paris VII, 280 p.

3359 Jenny, J-P, Francus, P., Normandeau, A., Lapointe, F., Perga, M-E., Ojala, A., Schimmelmann, A.,

3360   Zolitschka, B., 2016, Global spread of hypoxia in freshwater ecosystems during the last three

3361   centuries is caused by rising local human pressure Global Change Biology, v. 22, 1481–1489.

3362 Jimenez, H., Ruiz, G.M., 2016. Contribution of non-native species to soft-sediment marine

3363   community structure of San Francisco Bay, California. Biological Invasions, v. 18 (7), 2007–

3364   2016.

3365 Jin, Z., Han, Y., Chen, L., 2010. Past atmospheric Pb deposition in Lake Qinghai, northeastern Tibetan

3366   Plateau. Journal of Paleolimnology, v. 43, 551–563.

3367 Junge, C.E., 1963. Air Chemistry and Radioactivity. Academic Press, New York, 382pp.

3368 Kawamura, H., Matusoka, N., Momoshima, N., Koike, M., Takashima, T., 2006. Isotopic evidence in

3369   tree rings for historical changes in atmospheric sulfur sources. Environ. Sci. Technol., v. 40,

3370   5750–5754.

3371 Kelly, A.E., Reuer, M.K. Goodkin, N.F., Boyle, E.A., 2009. Lead concentrations and isotopes in corals

3372   and water near Bermuda, 1780–2000. Earth and Planetary Science Letters, v. 283, 93–100.

3373   http://dx.doi.org/10.1016/j.epsl.2009.03.045.

3374 Key, R.M., Kozyr, A., Sabine, C.L., Lee, K., Wanninkhof, R., Bullister, J.L., Feely, R.A., Millero, F.J.,

3375   Mordy, C., Peng, T.-H., 2004. A global ocean carbon climatology: Results from Global Data

3376   Analysis Project (GLODAP), Global Biogeochem. Cycles, v. 18, GB4031,

3377   doi:10.1029/2004GB002247.

3378 Koide, M., Griffin, J.J., Goldberg, E.D., 1975. Records of Plutonium Fallout in Marine and Terrestrial

3379   Samples, Journal of Geophysical Research, v. 80, 4153–4162.

3380 Kowalski, N., Reichardt, A.M., Waniek, J.J., 2016. Sinking rates of microplastics and potential

3381   implications of their alteration by physical, biological, and chemical factors. Marine Pollution

3382   Bulletin, v. 109, 310–319.

3383   Krachler, M., Zheng, J., Fisher, D., Shotyk, W., 2008. Atmospheric Sb in the Arctic during the past

3384   16,000 years: Responses to climate change and human impacts, Global Biogeochemical

3385   Cycles, v. 22, GB1015. doi:10.1029/2007GB002998

3386   Krachler, M., Zheng, J., Fisher, D., Shotyk, W., 2009, Global atmospheric As and Bi contamination

3387   preserved in 3000 year old Arctic ice, Global Biogeochemical Cycles. v. 23, GB3011.

3388   Krishnaswami, S., Lal, D., Amin, B.S., Soutar, A., 1973, Geochronological studies in Santa Barbara

3389   Basin: 55Fe as a unique tracer for particulate settling, Limnology and Oceanography, v. 18

3390   (5), 763–770.

3391   Küttner, A., Mighall, T.M., De Vleeschouwer, F., Mauquoy, D., Martínez Cortizas, A., Foster, I.D.L.,

3392   Krupp, E.A., 2014. 3300-year atmospheric metal contamination record from Raeburn Flow

3393   raised bog, south west Scotland. Journal of Archaeological Science, v. 44, 1–11.

3394   Kylander, M.E., Martínez-Cortizas, A., Bindler, R., Greenwood, S.L., Mörth, C.-M., Rauch, S., 2016.

3395   Potentials and problems of building detailed dust records using peat archives: An example

3396   from Store Mosse (the "Great Bog"), Sweden. Geochimica Cosmochimica Acta, v. 190, 156–

3397   174.

3398   Lee, J-M., Boyle, E.A., Nurhati, I.S., Pfeiffer, M., Meltzner, A.J., Suwargadi, B., 2014. Coral-based

3399   history of lead and lead isotopes of the surface Indian Ocean since the mid-20th century.

3400   Earth and Planetary Science Letters, v. 398, 37–47.

3401   Lee, J-M., Eltgroth, S.F., Boyle, E.A., Adkins, J.F., 2017. The transfer of bomb radiocarbon and

3402   anthropogenic lead to the deep North Atlantic Ocean observed from a deep sea coral. Earth

3403   and Planetary Science Letters, v. 458, 223–232.

3404   Le Quéré, C., Andrew, R.M., Canadell, J.G., Sitch, S., Korsbakken, J.I., Peters, G.P., Manning, A.C.,

3405   Boden, T.A., Tans, P.P., Houghton, R.A., Keeling, R.F., Alin, S., Andrews, O.D., Anthoni, P.,

3406   Barbero, L., Bopp, L., Chevallier, F., Chini, L.P., Ciais, P., Currie, K., Delire, C., Doney, S.C.

3407   Friedlingstein, P., Gkritzalis, T., Harris, I., Hauck, J., Haverd, V., Hoppema, M., Klein Goldewijk,

3408   K., Jain, A.K., Kato, E., Körtzinger, A., Landschützer, P., Lefèvre, N., Lenton, A. Lienert, S.,

3409   Lombardozzi, D., Melton, J.R., Metzl, N., Millero, F., Monteiro, P.M.S., Munro, D.R., Nabel,

3410   J.M.S., Nakaoka, S-I., O'Brien, K., Olsen, A., Omar, A.M., Ono, Pierrot, T.D.,Poulter, B.,

3411   Rödenbeck, C., Salisbury, J., Schuster, U., Schwinger, J., Séférian, R., Skjelvan, I., Stocker, B.D.,

3412   Sutton, A.J., Takahashi, T., Tian, H., Tilbrook, B., van der Laan-Luijkx, I.T., van der Werf, G.R.,

3413   Viovy, N., Walker, A.P., Wiltshire, A.J. and Zaehle, S. (2016) Global Carbon Budget 2016. Earth

3414   System. Science Data, v. 8, 605–649.

3415 Lesueur, P., Tastet, J.P., Marambat, L., 1996. Shelf mud fields formation within historical times:

3416   examples from offshore the Gironde estuary, France. Continental Shelf Research, v. 16(14),

3417   1849–1870.

3418 Lewis, S.L., Maslin, M.A., 2015. Defining the Anthropocene, Nature, v. 519, 171–180.

3419 Lindahl, P., Asami, R., Iryu, Y., Worsfold, P., Keith-Roach, M, Choi, M.-S., 2011. Sources of plutonium

3420   to the tropical Northwest Pacific Ocean (1943–1999) identified using a natural coral archive,

3421   Geochemica et Cosmochimica Acta, v. 75, 1346–1356.

3422 Lindberg, S., Bullock, R., Ebinghaus, R., Engstrom, D., Xinbin, Feng, Fitzgerald, W., Pirrone, N.,

3423   Prestbo, E., Seigneur, C., 2007. A synthesis of progress and uncertainties in attributing the

3424   sources of mercury in deposition. Ambio, v. 36(1), 19–32.

3425 Livingston, H.D., Povinec, P.P., Ito, T., Togawa, O.., 2001. The behaviour of plutonium in the Pacific

3426   Ocean. In: Kudo A (ed.) Radioactivity in the Environment. Volume 1, Plutonium in the

3427   Environment. Amsterdam: Elsevier, pp. 267–292.

3428 Loader, N.J., Walsh, R.P.D, Robertson, I., Bidin, K., Ong, R.C., Reynolds, G., McCarroll, D., Gagen, M.,

3429   Young, G.H.F.., 2011. Recent trends in the intrinsic water-use efficiency of ringless rainforest

3430   trees in Borneo. Philosophical Transactions of the Royal Society B, v. 366, 3330–3339.

3431 Loader, N.J., Young, G.H.F., Grudd, H., McCarroll, D., 2013a. Stable carbon isotopes from Torneträsk,

3432   northern Sweden provide a millennial length reconstruction of summer sunshine and its

3433   relationship to Arctic circulation. Quaternary Science Reviews, v. 62, 97–113.

3434 Loader, N.J., Young, G.H.F., McCarroll, D., Wilson. R.J.S., 2013b. Quantifying uncertainty in isotope

3435   dendroclimatology. The Holocene, v. 23, 1221 – 1226. 10.1177/0959683613486945

Lough, J.M., Barnes, D.J., 2000. Environmental controls on growth of the massive coral *Porites*, Journal of Experimental Marine Biology and Ecology, v. 245 (2), 225–243.

Loring, D.H., Rantala, R.T.T., Smith, J.N., 1983. Response time of Saguenay Fjord sediments to metal contamination. In: Hallberg, R. (ed.) Environtal Biogeochemistry Ecological Bulletins (Stockholm) v. 35, 59–72.

MacFarling Meure, C., Etheridge, D. E., Trudinger, C., Steele, P., Langenfelds, R., van Ommen, T., Smith, A., Elkins, J., 2006. Law Dome CO_2, CH_4 and N_2O ice core records extended to 2000 years BP, Geophys. Res. Lett., v. 33(14), L14810, doi:10.1029/2006GL026152.

McCarroll, D., Loader, N.J., 2004. Stable isotopes in tree rings. Quaternary Science Reviews, v. 23, 771–801.

McCarroll, D., Gagen, M.H., Loader, N.J., Robertson, I., Anchukaitis, K.J., Los, S., Young, G.H.F., Jalkanen, R., Kirchhefer, A., Waterhouse, J.S., 2009. Correction of tree ring stable carbon isotope chronologies for changes in the carbon dioxide content of the atmosphere. Geochimica et Cosmochimica Acta, v. 73, 1539–1547.

McConnell, J.R., Edwards, R., 2008. Coal burning leaves toxic heavy metal legacy in the Arctic. Proceedings of the National Academy of Sciences, v. 105(34), 12140–12144.

McFarlane, D. A., Lundberg, J., Neff, H., 2013. A speleothem record of early British and Roman mining at Charterhouse, Mendip, England. Archaeometry http://dx.doi.org/10.1111/arcm.12025

McGann, M., Sloan, D., Cohen, A.N., 2000. Invasion by a Japanese marine microorganism in western North America. Hydrobiologia, v. 421, 25–30.

McGann, M., Sloan, D., Wan, E., 2002. Biostratigraphy beneath central San Francisco Bay along the San Francisco-Oakland Bay Bridge transect. pp. 11–28 in: Crustal structure of the coastal and marine San Francisco Bay region, California.

McQuoid, M.R., Hobson, L.A., 1997. A 91-year record of seasonal and inter-annual variability of diatoms from laminated sediments in Saanich Inlet, British Columbia. J. Plankton. Res., v. 19(1), 173–194.

3463   Magnan, G., Garneau, M., Payette, S., 2014. Holocene development of maritime ombrotrophic

3464   peatlands of the St. Lawrence North Shore in eastern Canada. Quaternary Research, v. 82 (1),

3465   96–106.

3466   Mahara, Y., Kudo, A., 1995. Plutonium released by the Nagasaki A-bomb: mobility in the

3467   environment. Applied Radiation and Isotopes, v. 46(11), 1191–1201.

3468   Mahiques, M.M., Hanebuth, T.J.J., Martins, C.C., Montoya-Montes, Alcántara-Carrió, J., Figueira,

3469   R.C.L, Bícego, M.C., 2016. Mud depocentres on the continental shelf: a neglected sink for

3470   anthropogenic contaminants from the coastal zone. Environmental Earth Sciences, v. 75(44).

3471   doi: 10.1007/s12665-015-4782-z.

3472   Markgraf, V., Huber, U.M., 2010. Late and postglacial vegetation and fire history in Southern

3473   Patagonia and Tierra del Fuego. Palaeogeography Palaeoclimatology Palaeoecology, v. 297,

3474   351–366.

3475   Marshall, W.A., Gehrels, W.R., Garnett, M.H., Freeman, S.P.H.T., Maden, C., Xu, S., 2007. The use of

3476   'bomb pike' calibration and high-precision AMS ^{14}C analyses to date salt marsh sediments

3477   deposited during the last three centuries. Quaternary Research, v. 68, 325–337.

3478   Martin J., Puig, P., Palanques, A., Giamportone, A., 2015. Commercial bottom trawling as a driver of

3479   sediment dynamics and deep seascape evolution in the Anthropocene, Anthropocene, v. 7,

3480   1–15.

3481   Martínez-García, B., Pascual, A., Baceta, J.I., Murelaga, X., 2013. Estudio de los foraminíferos

3482   bentónicos del "beach-rock" de Azkorri (Getxo, Bizkaia). Geogaceta, v. 53, 29–32.

3483   Martinez-Porchas, M., Martinez-Cordova, L.R., 2012. World Aquaculture: Environmental Impacts and

3484   Troubleshooting Alternatives. The Scientific World Journal, v. 2012, Article ID 389623, 9 p.

3485   doi:10.1100/2012/389623

3486   Masson-Delmotte, V., Steen-Larsen, H.C., Ortega, P., Swingedouw, D., Popp, T., Vinther, B.M., Oerter,

3487   H., Sveinbjornsdottir, A.E., Gudlaugsdottir, H., Box, J.E., Falourd, S., Fettweis, X., Gallée, H.,

3488   Garnier, E., Gkinis, V., Jouzel, J., Landais, A., Minster, B., Paradis, N., Orsi, A., Risi, C., Werner

3489   M., White, J.W.C., 2015. Recent changes in north-west Greenland climate documented by

3490   NEEM shallow ice core data and simulations, and implications for past-temperature

3491   reconstructions. The Cryosphere, v. 9, 1481–1504.

3492 Matsuguma, Y., Takada, H., Kumata, H, Kanke, H., Sakurai, S., Suzuki, T., Itoh, M., Okazaki, Y.,

3493   Boonyatumanond, R., Zakaria, M.P., Weerts, S., Newman, B., 2017. Microplastics in sediment

3494   cores from Asia and Africa as indicators of temporal trends in plastic pollution. Archives of

3495   Environmental Contamination and Toxicology, v. 73, 230–239.

3496 Matsumoto, E., Wong, C.S., 1977. Heavy metal sedimentation in Saanich Inlet measured with [210]Pb

3497   technique. J. Geophys. Res., v. 82, 5477–5482..

3498 Meharg, A.A., Edwards, K.J., Schofield, J.E., Raab, A., Feldmann, J., Moran, A., Bryant, C.L., Thornton,

3499   B., Dawson, J.J.-C., 2012. First comprehensive peat depositional records for tin, lead and

3500   copper associated with the antiquity of Europe's largest cassiterite deposits. Journal of

3501   Archaeological Science, v. 39, 717–727.

3502 Melosi, M.V., 2016. Fresh Kills: The Making and Unmaking of a Wastescape, *in* Mauch, C. (ed.), Out of

3503   Sight, Out of Mind: The Politics and Culture of Waste. RCC Perspectives: Transformations in

3504   Environment and Society, v. 1, 59–65.

3505 Melvin, T.M., Briffa, K.R., 2008. A ''signal-free'' approach to dendroclimatic standardisation.

3506   Dendrochronologia, v. 26, 71–86.

3507 Mielke, H.-J., 2011. Wald und Politik: Die unendliche Geschichte des Berliner Teufelsberges. 48 pp,

3508   Berlin, (Projekte-Verlag Cornelius GmbH).

3509 Miller, K.G., Wright, J.D., 2017. Success and failure in Cenozoic global correlations using golden

3510   spikes: A geochemical and magnetostratigraphic perspective. Episodes, v. 40, 8–21.

3511 Monteith, D.T., Evans, C.D., Dalton, C., 2007. Acidification of Lochnagar and prospects for recovery.

3512   In: Rose, N.L. (ed.). Lochnagar: The natural history of a mountain lake. Developments in

3513   Paleoenvironmental Research, v. 12, 317–344. Springer, Dordrecht.

3514 Muir, D.C.G., Rose, N.L., 2005. Lake sediments as records of Arctic and Antarctic pollution. In: Pienitz,

3515   R., Douglas, M.S.V., Smol, J.P. (eds.) Long-term Environmental Change in Arctic and Antarctic

3516   Lakes. Developments in Paleoenvironmental Research, v. 8, 209–239. Kluwer Academic

3517   Publishers, Dordrecht, The Netherlands.

3518 Muir, D.C.G., Rose, N.L., 2007. Persistent organic pollutants in the sediments of Lochnagar. *In* Rose,

3519   N.L. (ed.), Lochnagar: The Natural History of a Mountain Lake, Developments in

3520   Paleoenvironmental Research, v. 12, 375–402. Springer, Dordrecht.

3521 Murozumi, M., Chow, T.J., Patterson, C.C., 1969. Geochemical concentrations of pollutant lead

3522   aerosols, terrestrial dusts and sea salts in Greenland and Antarctic snow data. Geochimica et

3523   Cosmochimica Acta, v. 33, 1247–1294.

3524 Nagle, R., 2008. To love a Landfill. The History and Future of Fresh Kills, *in* France, R.L. (ed.) Handbook

3525   of Regenerative and Landscape Design. CRC Press, Boca Raton, p. 3–16.

3526 National Atmospheric Emissions Inventory (NAEI), 2017. Overview of air pollutants.

3527   http://naei.defra.gov.uk/overview/ap-overview Accessed 12th April 2017

3528 Newton, K.E., Fairchild, I.J., Gunn, J., 2015. Rates of calcite precipitation from hyperalkaline waters,

3529   Poole's Cavern, Derbyshire. Cave and Karst Science, v. 42, 116–124.

3530 Nisbet, E.G., Dlugokencky, E.J., Manning, M.R., Lowry, D., Fisher, R.E., France, J.L., Michel, S.E., Miller,

3531   J.B., White, J.W.C., Vaughn, B., Bousquet, P., Pyle, J.A., Warwick, N.J., Cain, M., Brownlow, R.,

3532   Zazzeri, G., Lanoisellé, M., Manning, A.C., Gloor, E., Worthy, D.E.J., Brunke, E.-G.,

3533   Labuschagne, C., Wolff, E.W., Ganesan A.L., 2016. Rising atmospheric methane: 2007–2014

3534   growth and isotopic shift. Global Biogeochemical Cycles, v. 30, 1356–1370.

3535 Noller, J.S., 2000. Lead-210 Geochronology, Quaternary Geochronology: Methods and Applications,

3536   AGU Reference Shelf 4.

3537 Obbard, R.W., Sadri, S. Wong, Y.Q., Khitun, A.A. Baker, I., Thompson, R.C., 2014, Global warming

3538   releases microplastic legacy frozen in Arctic Sea ice, Earth's Future, v. 2, 315–320.

3539 Oldfield, F., 2014. Can the magnetic signatures from inorganic fly ash be used to mark the onset of

3540   the Anthropocene? Anthropocene Review, v. 2(1), 3–13.

3541 Pandolfi, J.M., Bradbury, R.H., Sala, E., Hughes, T.P., Bjorndal, K.A., Cooke, R.G., McArdle, D.,

3542   McClenachan, L., Newman, M.J., Paredes, G., Warner, R.R., 2003. Global trajectories of the

3543   long-term decline of coral reef ecosystems. Science, v. 301(5635), 955–958.

3544 Parrenin, F., Masson-Delmotte, V., Köhler, P., Raynaud, D., Paillard, D., Schwander, J., Barbante, C.,

3545   Landais, A., Wegner, A., Jouzel, J., 2013. Synchronous change of atmospheric CO_2 and

3546   Antarctic temperature during the last deglacial warming. Science, v. 339, 1060–1063.

3547 Patterson, C.C., Settle, D.M., 1987. Review of data on eolian fluxes of industrial and natural lead to

3548   the lands and seas in remote regions on a global scale. Mar. Chem., v. 22, 137–162.

3549 Paull, C.K., Ussler III, W., Mitts, P.J., Caress, D.W., West, G.J., 2006. Discordant ^{14}C-stratigraphies in

3550   upper Monterey Canyon: A signal of anthropogenic disturbance. Marine Geology. v. 233, 21–

3551   36.

3552 Pfeffer, W.T., Arendt, A.A., Bliss, A., Bolch, T., 2014. The Randolph Glacier Inventory: a globally

3553   complete inventory of glaciers. Journal of Glaciology, v. 60(221), 537–552.

3554 Pilskaln, C.H., Pike, J., 2001. Formation of Holocene sedimentary laminae in the Black Sea and the

3555   role of the benthic flocculent layer. Paleoceanography, v. 16, 1–19.

3556   http://dx.doi.org/10.1029/1999PA000469.

3557 Pla, S., Monteith, D., Flower, R., Rose, N., 2009. The recent palaeolimnology of a remote Scottish loch

3558   with special reference to the relative impacts of regional warming and atmospheric

3559   contamination. Freshwater Biology, v. 54, 505–523.

3560 Poirier, C., Chaumillon, E., Arnaud, F., 2011. Siltation of river-influenced coastal environments:

3561   Respective impact of late Holocene land use and high-frequency climate changes, Marine

3562   Geology, v. 290, 51–62.

3563 Pons-Branchu, E., Ayrault, S., Roy-Barman, M., Bordier, L., Borst, W., Branchu, P., Douville, E.,

3564   Dumont, E., 2015. Three centuries of heavy metal pollution in Paris (France) recorded by

3565   urban spelelothems. Science of the Total Environment, v. 518-519, 85–96.

3566 Pratte, S., Garneau, M., De Vleeschouwer, F., 2017. Late-Holocene atmospheric dust deposition in

3567   eastern Canada. The Holocene, v. 27, 12–25.

3568 Preunkert S, Wagenbach D, Legrand M., 2003. A seasonally resolved alpine ice core record of nitrate:

3569 comparison with anthropogenic inventories and estimation of preindustrial emissions of NO

3570 in Europe. J. Geophys. Res., v. 108, 4861. doi:10.1029/2003JD003475.

3571 Quayle, W.C., Peck, L.S., Peat, H., Ellis-Evans, J.C., Harrigan, P.R., 2002. Extreme responses to climate

3572 change in Antarctic lakes. Science, v. 295, 645.

3573 Quinto, F., Hrnecek, E., Krachler, M., Shotyk, W., Steier, P., Winkler, S.R., 2013a. Determination of

3574 ^{239}Pu, ^{240}Pu, ^{241}Pu and ^{242}Pu at femtogram and attogram levels - evidence for the migration of

3575 fallout plutonium in an ombrotrophic peat bog profile. Environmental Science Processes and

3576 Impacts, v. 15(4), 839–847.

3577 Quinto, F., Hrnecek, E., Krachler, M., Shotyk, W, Steier, P., Winkler, S.R., 2013b. Measurements of

3578 ^{236}U in ancient and modern peat samples and implications for post depositional migration of

3579 fallout radionuclides. Environmental Sciemce & Technology, v. 47, 5243–5250.

3580 Rakowski, A.Z., Nadeau, M-J, Nakamura, T., Pazdur, A., Pawełczyk, S., Piotrowska, N., 2013.

3581 Radiocarbon method in environmental monitoring of CO_2 emission. Nuclear Instruments and

3582 Methods in Physics Research B, v. 294, 503–507.

3583 Ramirez-Llodra, E., Tyler, P.A., Baker, M.C., Bergstad, O.A., Clark, M.R., Escobar, E., Levin, L.A. Menot,

3584 L., Rowden, A.A., Smith, C.R., Van Dover, C.L., 2011. Man and the Last Great Wilderness:

3585 Human Impact on the Deep Sea. Plos One, v. 6(8), e22588, 1–25.

3586 Rauch, S., Hemond, H.F, and Peucker-Ehrenbrink, B., 2004. Source characterisation of atmospheric

3587 platinum group element deposition into an ombrotrophic peat bog. Journal of Environmental

3588 Monitoring, v. 6, 335–343.

3589 Rauch, S., Peucker-Ehrenbrink, B., Kylander, M., Weiss, D.J., Martinez-Cortizas, A., Heslop, D., Olid, C,

3590 Mighall, T.M. and Hemond, H.F., 2010. Anthropogenic Forcings on the Surficial Osmium Cycle

3591 Environmental Science & Technology, v. 44, 881–887.

3592 Remane, J., Bassett, M.G., Cowie, J.W., Gohrbandt, K.H., Lane, H.R., Michelsen, O., Wang, N., with the

3593 cooperation of members of ICS, 1996. Revised guidelines for the establishment of global

3594   chronostratigraphic standards by the International Commision on Stratigraphy (ICS).

3595   Episodes, v. 19, 77–81.

3596   Remane, J., 1997. Foreword: chronostratigraphic standards: how are they defined and when should

3597   they be changed? Quaternary International, v. 40, 3–4.

3598   Remane, J., 2003. Chronostratigraphic correlations: their importance for the definition of

3599   geochronologic units, Palaeogeography, Palaeoclimatology, Palaeoecology, v. 196, 7–18.

3600   Renberg, I., Battarbee, R.W., 1990. The SWAP Palaeolimnology Programme: A synthesis. In Mason,

3601   B.J (ed) The Surface Waters Acidification Programme. Cambridge University Press,

3602   Cambridge, 281–300.

3603   Renberg, I., Brännvall, M-L., Bindler, R., Emteryd, O., 2000. Atmospheric lead pollution history during

3604   four millennia (2000 BC to 2000 AD) in Sweden. Ambio, v. 29(3), 150–156.

3605   Ren, H., Chen, Y-C., Wang, X.T., Wong, G.T.F., Cohen, A.L., DeCarlo, T.M., Weigand, M.A., Mii, H-S.,

3606   Sigman, D.M., 2017. Atmospheric deposition of anthropogenic nitrogen has become a major

3607   nitrogen source in the South China Sea. Science, v. 356, 749–752.

3608   Reuer, M.K. and Weiss, D.J. 2002, Anthropogenic lead dynamics in the terrestrial and marine

3609   environment. Philosophical Transactions of the Royal Society London A, v. 360, 2889–2904.

3610   Reynolds, D.J., Scourse, J.D., Halloran, P.R., Nederbragt, A.J., Wanamaker, A.D., Butler, P.G.,

3611   Richardson, C.A. Heinemeier, J., Eiríksson, J., Knudsen, K.L., Hall, I.R., 2016. Annually resolved

3612   North Atlantic marine climate over the last millennium. Nature Communications, v. 7, 13502.

3613   doi: 10.1038/ncomms13502.

3614   Roemmich, D., McGowan, J., 1995. Climatic warming and the decline of zooplankton in the California

3615   Current, Science, v. 267, 1324.

3616   Rose, N.L., 2007. The sediments of Lochnagar: Distribution, accumulation and composition. In: Rose,

3617   N.L. (ed.). Lochnagar: The natural history of a mountain lake. Developments in

3618   Paleoenvironmental Research, v. 12, 155–175. Springer, Dordrecht.

3619 Rose, N.L., 2015. Spheroidal carbonaceous fly ash particles provide a globally synchronous

3620   stratigraphic marker for the Anthropocene, Environmental Science and Technology, v. 49(7),

3621   4155–4162.

3622 Rose, N.L., Yang, H., 2007. Temporal and spatial patterns of spheroidal carbonaceous particles (SCPs)

3623   in sediments, soils and deposition at Lochnagar. In: Rose, N.L. (ed.). Lochnagar: The natural

3624   history of a mountain lake. Developments in Paleoenvironmental Research, v. 12, 403–423.

3625   Springer, Dordrecht.

3626 Rose, N.L., Backus, S., Karlsson, H., Muir, D.C.G., 2001. An historical record of toxaphene and its

3627   congeners in a remote lake in western Europe. Environmental Science & Technology, v. 35(7),

3628   1312–1319.

3629 Rose, N.L., Morley, D., Appleby, P.G., Battarbee, R.W., Alliksaar, T., Guilizzoni, P., Jeppesen, E.,

3630   Korhola, A., Punning, J.M., 2011. Sediment accumulation rates in European lakes since

3631   AD1850: trends, reference conditions and exceedence. Journal of Paleolimnology, v. 45, 447–

3632   468.

3633 Rose, N.L., Yang, H., Turner, S.D., Simpson, G.L., 2012. An assessment of the mechanisms for the

3634   transfer of lead and mercury from atmospherically contaminated organic soils to lake

3635   sediments with particular reference to Scotland, UK. Geochimica et Cosmochimica Acta, v.

3636   82, 113–135.

3637 Rothwell, J.J., Taylor, K.G., Chenery, S.R.N., Cundy, A.B., Evans, M.G., Allott, T.E.H., 2010. Storage and

3638   behavior of As, Sb, Pb, and Cu in ombrotrophic peat bogs under contrasting water table

3639   conditions. Environtal Science & Technology, v. 44, 8497–8502.

3640 Rubino, M., Etheridge, D.M. Trudinger, C.M. Allison, C.E. Battle, M.O. Langenfelds, R.L. Steele, L.P.

3641   Curran, M. Bender, M. White, J.W.C., Jenk, T.M. Blunier, T., Francey., R.J., 2013. A revised

3642   1000 year atmospheric δ^{13}C-CO_2 record from Law Dome and South Pole, Antarctica. Journal

3643   of Geophysical Research Atmospheres, v. 118, 8482–8499.

3644 Rubino, M., Etheridge, D.M., Trudinger, C.M., Allison, C.E., Rayner, P.J., Enting, I., Mulvaney, R.,

3645   Steele, L.P., Langenfelds, R.L., Sturges, W.T., Curran, M.A.J., Smith, A.M., 2016. Low

3646   atmospheric CO_2 levels during the Little Ice Age due to cooling-induced terrestrial uptake.

3647   Nature Geoscience v. 9, 691–694.

3648 Saros, J.E., Michel, T.J., Interlandi, S.J., Wolfe, A.P., 2005. Resource requirements of *Asterionella*

3649   *formosa* and *Fragilaria crotonensis* in oligotrophic alpine lakes: implications for recent

3650   phytoplankton community reorganizations. Canadian Journal of Fisheries and Aquatic

3651   Sciences, v. 62(7), 1681–1689.

3652 Saurer, M., Spahni, R., Frank, D.C., Joos, F., Leuenberger, M., Loader, N.J., McCarroll, D., Gagen, M.,

3653   Poulter, B., Siegwolf, R.T.W., Andreu-Hayles, L., Boettger, T., Liñán, I.D., Fairchild, I.J.,

3654   Friedrich, M., Gutierrez, E., Haupt, M., Hilasvuori, E., Heinrich, I., Helle, G., Grudd, H.,

3655   Jalkanen, R., Levanič, T., Linderholm, H.W., Robertson, I., Sonninen, E., Treydte, K.,

3656   Waterhouse, J.S., Woodley, E.J., Wynn, P.M., Young, G.H.F., 2014. Spatial variability and

3657   temporal trends in water-use efficiency of European forests. Global Change Biology, v. 20,

3658   3700–3712.

3659 Sax, D.F., Gaines, S.D., 2008. Species invasions and extinction: the future of native biodiversity on

3660   islands. Proceedings of the National Academy of Sciences, v. 105, Supplement 1, 11490–

3661   11497.

3662 Schimmelmann, A., Hendy, I.L., Dunn, L., Pak D.K., Lange, C.B., 2013. Revised ~2000-year

3663   chronostratigraphy of partially varved marine sediment in Santa Barbara Basin, California,

3664   GFF, v. 135(3–4), 258–264.

3665 Schimmelmann, A., Lange, C.B., Schieber, J., Francus, P., Ojala, A.E.K., Zolitschka, B., 2016. Varves in

3666   marine sediments: A review. Earth-Science Reviews, v. 159, 215–246.

3667 Schmidt, H., Reimers, C.E., 1991. The Recent History of Trace Metal Accumulation in the Santa

3668   Barbara Basin, Southern California Borderland, Estuarine, Coastal and Shelf Science, v. 33,

3669   485–500.

3670 Scholz, D., Frisia, S., Borsato, A., Spötl, C., Fohlmeister, J., Mudelsee, M., Miorandi, R., Mangini, A.,

3671   2012. Holocene climate variability in north-eastern Italy: potential influence of the NAO and

3672   solar activity recorded by speleothem data. Climate of the Past, v. 8, 1367–1383.

Schuster, P.F., Krabbenhoft, D.P., Naftz, D.L., Cecil, L.D., Olson, M.L., De Wild, J.F., Susong, D.D., Green, J.R., Abbott, M.L., 2002. Atmospheric mercury deposition during the last 270 years: A glacial ice core record of natural and anthropogenic sources. Environmental Science & Technology, v. 36(11), 2303–2310.

Scourse, J.D., Wanamaker Jr, A.D., Weidman, C., Heinemeier, J., Reimer, P.J., Butler, P.G., Witbaard, R., Richardson, C.A., 2012. The marine radiocarbon bomb pulse across the temperate north Atlantic: a compilation of Δ^{14}C time histories from *Arctica Islandica* growth increments. Radiocarbon, v. 54(2), 165–186.

Seibt, U., Rajabi, A., Griffiths, H., Berry, J.A., 2008. Carbon isotopes and water use efficiency: sense and sensitivity. Oecologia, v. 155, 441–454.

Sherwood, O.A., Scott, D.B., Risk, M.J., Guilderson, T.P. 2005a. Radiocarbon evidence for annual growth rings in a deep sea octocoral (*Primnoa resedaeformis*). Marine Ecology Progress Series, v. 301, 129–134.

Sherwood, O.A., Heikoop, J.M., Scott, D.B., Risk, M.J., Guilderson, T.P., McKinney, R.A., 2005b. Stable isotopic composition of deep-sea gorgonian corals *Primnoa* spp.: a new archive of surface processes. Marine Ecology Progress Series, v. 301, 135–148.

Sherwood, O.A., Lehmann, M.F., Schubert, C.J., Scott, D.B., McCarthy, M.D., 2011. Nutrient regime shift in the western North Atlantic indicated by compound-specific δ^{15}N of deep-sea gorgonian corals, PNAS, v. 108(3), 1011–1015.

Shotyk, W., 1988. Review of the inorganic geochemistry of peats and peatland waters. Earth-Science Reviews, v. 25(2), 95–176.

Shotyk, W., 1992. Organic soils. Ch. 13 in Martini, I.P. and Chesworth, W. (eds.) Weathering, Soils, and Paleosols. Elsevier, Amsterdam, 203–224.

Shotyk, W., 1996. Peat bog archives of atmospheric metal deposition: Geochemical assessment of peat profiles, natural variations in metal concentrations, and metal enrichment factors. Environmental Reviews, v. 4(2), 149–183.

3699   Shotyk, W., Weiss, D., Appleby, P.G., Cheburkin, A.K., Frei, R., Gloor, M., Kramers, J.D., Reese, S., van

3700   der Knaap, W.O., 1998. History of atmospheric lead deposition since 12,370 14C yr BP from a

3701   peat   bog,   Jura   Mountains,   Switzerland.   Science,   v.   281,   1635–1640.

3702   http://dx.doi.org/10.1126/science.281.5383.1635.

3703   Shotyk, W., Blaser, P., Grünig, A., Cheburkin, A.K., 2000. A new approach for quantifying cumulative,

3704   anthropogenic, atmospheric lead deposition using peat cores from bogs: Pb in eight Swiss

3705   peat bog profiles. Science of the Total Environment, v. 249, 281–295.

3706   Shotyk, W., Weiss, D., Heisterkamp, M., Cheburkin, A.K., Adams, F.C., 2002. A new peat bog record of

3707   atmospheric lead pollution in Switzerland: Pb concentrations, enrichment factors, isotopic

3708   composition, and organolead species Environmental Science and Technology, v. 36(18),

3709   3893–3900.

3710   Shotyk, W., Appleby, P.G., Bicalho, B., Davies, L, Froese, D., Grant-Weaver, I., Krachler, M., Magnan,

3711   G., Mullan-Boudreau, G., Noernberg, T., Pelletier, R., Shannon, B, van Bellen, S., and Zaccone,

3712   C., 2016. Peat bogs in northern Alberta, Canada reveal decades of declining atmospheric Pb

3713   contamination. Geophysical Research Letters, v. 43, 9964–9974.

3714   Sloan, D., 1992. The Yerba Buena mud: record of the last-interglacial predecessor of San Francisco

3715   Bay, California. GSA Bulletin, v. 104, 716–727.

3716   Smith, A.G. Barry, T., Bown, P., Cope, J., Gale, A., Gibbard, P., Gregory, J., Hounslow, M., Kemp, D.,

3717   Knox, R., Marshall, J., Oates, M., Rawson, P., Waters, C., 2014. GSSPs, global stratigraphy and

3718   correlation, in Smith, D.G., Bailey, R.J., Burgess, P.M., and Fraser, A.J. eds., Strata and Time:

3719   Probing the Gaps in Our Understanding. Geological Society, London, Special Publications, v.

3720   404, 37–67.

3721   Smith, D.M., Zalasiewicz, J.A., Williams, M., Wilkinson, I., Redding, M., Begg, C., 2010. Holocene

3722   drainage of the English Fenland: roddons and their environmental significance. Proceedings

3723   of the Geologists' Association, v. 121, 256–269.

3724   Smith, J.A., Andersen, T.J., Shortt, M., Gaffney, A.M., Truffer, M., Stanton, T.P., Bindschadler, R.,

3725   Dutrieux, P., Jenkins, A., Hillenbrand, C.-D., Ehrmann, W., Corr, H.F.J., Farley, N., Crowhurst,

3726 S., Vaughan, D.G. 2016. Sub-ice-shelf sediments record twentieth century retreat of Pine

3727 Island Glacier. Nature, v. 541, 77–80.

3728 Smith, J.N., Levy, E.M., 1990. Geochronology for Polycyclic Aromatic Hydrocarbon contamination in

3729 sediments of the Saguenay Fjord. Environ. Sci. Technol., v. 24, 874–879.

3730 Smith, J.N., Walton, A., 1980. Sediment accumulation rates and geochronolgies measured in the

3731 Saguenay Fiord using the Pb-210 dating method. Geochimica et Cosmochimica Acta, v. 46,

3732 941–954.

3733 Smol, J.P., 2008. Pollution of lakes and rivers: A palaeoenvironmental perspective (2nd Ed.). Wiley-

3734 Blackwell, 396 pp.

3735 Speer, J.H., 2010. Fundamentals of Tree-Ring Research. The University of Arizona Press. USA.

3736 Steffen, W., Leinfelder, R., Zalasiewicz, J., Waters, C.N., Williams, M., Summerhayes, C., Barnosky,

3737 A.D., Cearreta, A., Crutzen, P.J., Edgeworth, M., Ellis, E.C., Fairchild, I.J., Gałuszka, A.,

3738 Grinevald, J., Haywood, A., Ivar Do Sul, J., Jeandel, C., McNeill, J.R., Odada, E., Oreskes, N.,

3739 Revkin, A., Richter, D. DeB., Syvitski, J., Vidas, D., Wagreich, M., Wing, S.L., Wolfe, A.P.,

3740 Schellnhuber, H.J., 2016. Stratigraphic and Earth System approaches in defining the

3741 Anthropocene. Earth's Future, v. 8, 324–345.

3742 Suess, E., 1862. Der Boden der Stadt Wien nach seiner Bildungsweise, Beschaffenheit und seinen

3743 Beziehungen zum Bürgerlichen Leben. Eine geologische Studie von Eduard Suess. Wilhelm

3744 Braumüller, 326 pp.

3745 Suess, E., 1897. Der Boden der Stadt Wien und sein Relief. Geschichte der Stadt Wien, Bd. 1, 26 pp.

3746 (Herausgegeben vom Alterthumsvereine zu Wien).

3747 Swart, P.K., Rubenstone, J.L., Charles, C., Reitner, J. 1998. Sclerosponges: a new proxy indicator of

3748 climate. National Oceanic and Atmospheric Administration (NOAA), Climate and Global

3749 Change Program, Special Report, v. 12, 21 pp.

3750 Swart, P.K., Greer, L., Rosenheim, B.E., Moses, C.S., Waite, A.J., Winter, A., Dodge, R.E., Helmle, K.,

3751 2010. The ^{13}C Suess effect in scleractinian corals mirror changes in the anthropogenic CO_2

3752 inventory of the surface oceans, Geophysical Research Letters, v. 37, L05604.

3753   Swindles, G. T., Watson, E., Turner, T. E., Galloway, J. M., Hadlari, T., Wheeler, J., Bacon, K. L., 2015.

3754   Spheroidal carbonaceous particles are a defining stratigraphic marker for the Anthropocene.

3755   Scientific Reports, v. 5(10264). doi:10.1038/srep10264.

3756   Syvitski, J.P.M., Kettner, A., 2011. Sediment flux and the Anthropocene, Philosophical Transactions of

3757   the Royal Society A, v. 369, 1938, 957–975.

3758   Syvitski, J.P.M., Kettner, A.J., Overeem, I., Hutton, E.W.H., Hannon, M.T., Brakenridge, G.R., Day, J.,

3759   Vörösmarty, C., Saito. Y., Giosan, L., Nicholls, R.J., 2009. Sinking deltas due to human

3760   activities. Nature Geoscience, v. 2, 681–686.

3761   Syvitski, J.P.M., Kettner, A.J., Overeem, I., Giosan, L., Brakenridge, G.R., Hannon, M., Bilham, R., 2014.

3762   Anthropocene metamorphosis of the Indus Delta and lower floodplain, Anthropocene, v. 3,

3763   24–35.

3764   Syvitski, J.P.M., Saito, Y., 2007. Morphodynamics of deltas under the influence of Humans. Global and

3765   Planetary Changes, v. 57, 261–182.

3766   Tessler, Z.D., Vörösmarty, C.J., Grossberg, M., Gladkova, I. Aizenman, H., Syvitski, J.P.M., Foufoula-

3767   Georgiou, E., 2015. Profiling risk and sustainability in coastal deltas of the world, Science, v.

3768   349 (6248), 638–643.

3769   Thomas, E.R., Hosking, J.S., Tuckwell, R.R., Warren, R.A., and Ludlow, E.C., 2015. Twentieth century

3770   increase in snowfall in coastal West Antarctica, Geophysical Research Letters, v. 42, 9387–

3771   9393. doi:10.1002/2015GL065750.

3772   Thuens, S., Blodau, C., Radke, M., 2013. How suitable are peat cores to study historical deposition of

3773   PAHs? Science of the Total Environment, v. 450-451, 271–279.

3774   Tierney, J.E., Abram, N.J., Anchukaitis, K.J., Evans, M.N., Giry, C., Kilbourne, J.H., Saenger, C.P., Wu,

3775   H.C., Zinke, J., 2015. Tropical sea surface temperatures for the past four centuries

3776   reconstructed from coral archives. Paleoceanography, v. 30, 226–252.

3777   Treydte, K., Frank, D., Esper, J., Andreu, L., Bednarz, Z., Berninger, F., Boettger, T., D'Alessandro, C.M.,

3778   Etien, N., Filot, M., Grabner, M., Guillemin, M.T., Gutierrez, E., Haupt, M., Helle, G.,

3779   Hilasvuori, E., Jungner, H., Kalela-Brundin, M., Krapiec, M., Leuenberger, M., Loader, N.J.,

Masson-Delmotte, V., Pazdur, A., Pawelczyk, S., Pierre, M., Planells, O., Pukiene, R., Reynolds-Henne, C.E., Rinne, K.T., Saracino, A., Saurer, M., Sonninen, E., Stievenard, M., Switsur, V.R., Szczepanek, M., Szychowska-Krapiec, E., Todaro, L., Waterhouse, J.S., Weigl, M., Schleser, G.H., 2007. Signal strength and climate calibration of a European tree-ring isotope network. Geophysical Research Letters, v. 34, L24302. doi:10.1029/2007GL031106.

Treydte, K.S., Frank, D.C., Saurer, M., Helle, G., Schleser, G.H., Esper, J., 2009. Impact of climate and CO_2 on a millennium-long tree-ring carbon isotope record. Geochim. Cosmochim. Acta, v. 73, 4635–4647.

Tyson, R.V., Pearson, T.H., 1991, Modern and ancient continental shelf anoxia: an overview *in* Tyson, R.V., and Pearson, T.H. (eds.) Modern and Ancient Continental ShelfAnoxia, Geological Society Special Publication, v. 58, 1–24.

UNEP, 2007. Global glacier changes: facts and figures. World Glacier Monitoring Service, pp.88.

UNSCEAR (United Nations Scientific Committee on the Effects of Atomic Radiation) (2000) Sources and Effects of Ionizing Radiation, 2000 Report, Volume 1. New York: United Nations. Available at: http://www.unscear.org/unscear/en/publications/2000_1.html

Vane, C.H., Chenery, S.R., Harrison, I., Kim, A.W. Moss-Hayes, V., Jones, D.G., 2011. Chemical signatures of the Anthropocene in the Clyde estuary, UK: sediment-hosted Pb, [207/206]Pb, total petroleum hydrocarbon, polyaromatic hydrocarbon and polychlorinated biphenyl pollution records, Philosophical Transactions of the Royal Society A, v. 369, 1085–1111.

Vanneste, H., Vleeschouwer, F. De, Martínez-Cortizas, A., von Scheffer, C., Piotrowska, N., Coronato, A., Le Roux, G., 2015. Late-glacial elevated dust deposition linked to westerly wind shifts in southern South America. Scientific Reports, v. 5, 11670. DOI:10.1038/srep11670.

Veron, A., Novak, M., Brizova, E., Stepanova, M., 2014. Environmental imprints of climate changes and anthropogenic activities in the Ore Mountains of Bohemia (Central Europe) since 13 cal. kyr BP. The Holocene, v. 24, 919–931.

Verpoorter, C., Kutser, T., Seekell D.A., Transvik, L.J., 2014. A global inventory of lakes based on high-resolution satellite imagery, Geophysical Research Letter, v. 41, 6396–6402.

3807   Vuorela, I., 1983. Field erosion by wind as indicated by fluctuations in the ash content of Sphagnum

3808   peat. Bulletin of the Geological Society of Finland, v. 55, 25–33.

3809   Walker, M., Johnsen, S., Rasmussen, S.O., Popp, T., Steffensen, J.-P., Gibbard, P., Hoek, W., Lowe, J.,

3810   Andrews, J., Björck, S., Cwynar, L.C., Hughen, K., Kershaw, P., Kromer, B., Litt, T., Lowe, D.J.,

3811   Nakagawa, T., Newnham, R., Schwander, J., 2009. Formal definition and dating of the GSSP

3812   (Global Stratotype Section and Point) for the base of the Holocene using the Greenland

3813   NGRIP ice core, and selected auxiliary records, Journal of Quaternary Science, v. 24, 3–17.

3814   Walker, M.J.C., Berkelhammer, M., Björck, S., Cwynar, L.C., Fisher, D.A., Long, A.J. Lowe, J.J.,

3815   Newnham, R.M., Rasmussen, S.O., Weiss, H., 2012. Formal subdivision of the Holocene

3816   Series/Epoch: a Discussion Paper by a Working Group of INTIMATE (Integration of ice-core,

3817   marine and terrestrial records) and the Subcommission on Quaternary Stratigraphy

3818   (International Commission on Stratigraphy). Journal of Quaternary Science, V. 27, 649–659.

3819   Walling, D.E., Fang, D., 2003. Recent trends in the suspended sediment loads of the world's rivers.

3820   Global Planetary Change, v. 39, 111–126.

3821   Waters, C.N., Zalasiewicz, J., 2017. Concrete: the most abundant novel rock type of the

3822   Anthropocene. In: Encyclopedia of the Anthropocene, D. DellaSala (Editor). Elsevier.

3823   Waters, C.N., Syvitski, J.P.M., Gałuszka, A. Hancock, G.J., Zalasiewicz, J., Cearreta, A., Grinevald, J.,

3824   Jeandel, C., McNeill, J.R., Summerhayes, C., Barnosky, A., 2015. Can nuclear weapons fallout

3825   mark the beginning of the Anthropocene Epoch? Bulletin of the Atomic Scientists, v. 71, 46–

3826   57.

3827   Waters, C.N., Zalasiewicz J., Summerhayes C., Barnosky, A.D., Poirier, C., Gałuszka, A., Cearreta, A.,

3828   Edgeworth, M., Ellis, E.C., Ellis, M., Jeandel, C., Leinfelder, R., McNeill, J.R., Richter, D. deB.,

3829   Steffen, W., Syvitski, J., Vidas, D., Wagreich, M., Williams, M., An Zhisheng, Grinevald, J.,

3830   Odada, E., Oreskes, N., Wolfe, A.P., 2016. The Anthropocene is functionally and

3831   stratigraphically distinct from the Holocene, Science, v. 351, 137,

3832   http://dx.doi.org/10.1126/science.aad2622.

3833 Watmough, S.A., 1999. Monitoring historical changes in soil and atmospheric trace metal levels by

3834   dendrochemical analysis. Environmental Pollution, v. 106, 391–403.

3835 Wei, G., McCulloch, M.T., Mortimer, G., Deng, W., Xie, L., 2009. Evidence for ocean acidification in

3836   the Great Barrier Reef of Australia. Geochimica et Cosmochimica Acta, v. 73, 2332–2346.

3837 Weidman, C.R., Jones, G.A., 1993. A shell-derived time history of bomb ^{14}C on Georges Bank and its

3838   Labrador Sea implications. Journal of Geophysical Research, v. 98(C8), 14577–14588.

3839 Wieder, R.K., Vile, M.A., Scott, K.D., Albright, C.M., McMillen, K.J., Vitt, D.H., Fenn, M.E., 2016.

3840   Differential effects of high atmospheric N and S deposition on bog plant/lichen tissue and

3841   porewater chemistry across the Athabasca oil sands region. Environmental Science &

3842   Technology, v. 50, 12630–12640.

3843 Wilkinson, I.P., Poirier, C, Head, M.J., Sayer, C.D., Tibby, J., 2014. Microbiotic signatures of the

3844   Anthropocene in marginal marine and freshwater palaeoenvironments, *in* Waters, C.N.,

3845   Zalasiewicz, J.A., Williams, M., Ellis, M.A., Snelling, A.M. eds., A Stratigraphical Basis for the

3846   Anthropocene. Geological Society, London, Special Publications, v. 395, 185–219.

3847 Willis, K.J., Bailey, R.M., Bhagwat, S.A., Birks, H.J.B., 2010. Biodiversity baselines, thresholds and

3848   resilience: Testing predictions and assumptions using palaeoecological data. Trends in

3849   Ecology and Evolution, v. 25, 583–591.

3850 Wilson, R. Anchukaitis, K., Briffa, K.R., Büntgen, U., Cook, E., D'Arrigo, R., Davi, N., Esper, J., Frank, D.,

3851   Gunnarson, B., Hegerl, G., Helama, S., Klesse, S., Krusic, P.J., Linderholm, H.W., Myglan, V.,

3852   Osborn, T.J., Rydval, M., Zorita., E., 2016. Last millennium northern hemisphere summer

3853   temperatures from tree rings: Part I: The long term context. Quaternary Science Reviews,

3854   v.134, 1–18.

3855 Wolfe, A.P., Hobbs, W.O., Birks, H.H., Briner, J.P., Holmgren, S.U., Ingólfsson, Ó., Kaushal, S.S., Miller,

3856   G.H., Pagani, M., Saros, J.E., Vinebrooke, R.D., 2013. Stratigraphic expressions of the

3857   Holocene–Anthropocene transition revealed in sediments from remote lakes. Earth Science

3858   Reviews, v. 116, 17–34.

3859 Wolff, E.W., 2013. Ice sheets and nitrogen. Philosophical Transactions of the Royal Society B, v. 368,

3860   20130127. http://dx.doi.org/10.1098/rstb.2013.0127.

3861 Wolff, E.W., 2014. Ice Sheets and the Anthropocene, *in* Waters, C.N., Zalasiewicz, J.A., Williams, M.,

3862   Ellis, M.A., and Snelling, A.M. eds., A Stratigraphical Basis for the Anthropocene. Geological

3863   Society, London, Special Publications, v. 395, 255–263.

3864 Wolff, E.W., Suttie, E.D. 1994. Antarctic snow record of southern hemisphere lead pollution.

3865   Geophysical Research Letters, v. 21, 781–784.

3866 Wolff, E.W., Suttie, E.D., Peel, D.A. 1999. Antarctic snow record of cadmium, copper, and zinc content

3867   during the twentieth century. Atmospheric Environment, v. 33, 1535–1541.

3868 Wynn, P.M., Fairchild, I.J. Frisia, S., Spötl, C., Baker, A., Borsato., A., 2010. High-resolution sulphur

3869   isotope analysis of speleothem carbonate by secondary ionisation mass spectrometry.

3870   Chemical Geology, v. 271, 101–107.

3871 Wynn, P.M., Loader, N.J., Fairchild, I.J., 2014. Interrogating trees for isotopic archives of atmospheric

3872   sulphur deposition and comparison to speleothem records. Environmental Pollution, v. 187,

3873   98–105.

3874 Xu, B.Q., Cao, J., Hansen, J, Yao, T., Joswia, D.R., Wang, N., Wu, G., Wang, M., Zhao, H., Yang, W., Liu,

3875   X, He, J., 2009. Black soot and the survival of Tibetan glaciers, Proceedings of the National

3876   Academy of Sciences (U.S.A.), v. 106(52), 22,114–22,118.

3877 Yang, C., Rose, N.L., Turner, S.D., Yang, H., Goldsmith, B., Losada, S., Barber, J.L., Harrad, S.., 2016.

3878   Hexabromocyclododecanes, polybrominated diphenyl ethers, and polychlorinated biphenyls

3879   in radiometrically dated sediment cores from English lakes, ~ 1950–present. Science of the

3880   Total Environment, v. 541, 721–728.

3881 Yang, H., Smyntek, P.M., 2014. Use of the mercury record in Red Tarn sediments to reveal air

3882   pollution history and the implications of catchment erosion. Environmental Science:

3883   Processes and Impacts, v. 16, 2554–2563.

Yang, H., Rose, N.L., Boyle, J.F., Battarbee, R.W., 2001. Storage and distribution of trace metals and spheroidal carbonaceous particles (SCPs) from atmospheric deposition in the catchment peats of Lochnagar, Scotland. Environmental Pollution, v. 115(2), 231–238.

Yang, H., Rose, N.L., Battarbee, R.W., Boyle, J.F., 2002a. Mercury and lead budgets for Lochnagar, a Scottish mountain lake and its catchment. Environmental Science & Technology, v. 36(7), 1383–1388.

Yang, H., Rose, N.L., Battarbee, R.W., 2002b. Distribution of some trace metals in Lochnagar, a Scottish mountain lake ecosystem and its catchment. Science of the Total Environment, v. 285, 197–208.

Yang, H., Engstrom, D.R., Rose, N.L., 2010. Recent changes in atmospheric mercury deposition recorded in the sediments of remote equatorial lakes in the Rwenzori Mountains, Uganda. Environmental Science & Technology, v. 44, 6570–6575.

Young, G.H.F., Demmler, J.C., Gunnarson, B.E., Kirchhefer, A.J., Loader, N.J., McCarroll, D., 2011. Age trends in tree-ring growth and isotopic archives: A case study of *Pinus sylvestris L.* from northwestern Norway. Global Biogeochemical Cycles, v. 25, GB2020. doi:10.1029/2010GB003913.

Yu, Z., Loisel, J., Brosseau, D.P., Beilman, D.W., 2010. Global peatland dynamics since the Last Glacial Maximum. Geophysical Research Letters, v. 37, L13402. doi:10.1029/2010GL043584.

Zaccone C., Cocozza, C., Cheburkin, A.K., Shotyk, W., Miano, T.M., 2007. Enrichment and depletion of major and trace elements, and radionuclides in ombrotrophic raw peat and corresponding humic acids. Geoderma, v. 141, 235–246.

Zalasiewicz, J., Williams, M., Waters, C.N., Barnosky, A.D., Haff, P., 2014a. The technofossil record of humans, Anthropocene Review, v. 1, 34–43.

Zalasiewicz, J., Waters, C.N., Williams, M., 2014b. Human bioturbation, and the subterranean landscape of the Anthropocene. Anthropocene, v. 6, 3–9.

Zalasiewicz, J., Williams, M., Waters, C.N., 2014c. Can an Anthropocene Series be defined and recognized? *In:* Waters, C.N., Zalasiewicz, J.A., Williams, M, Ellis, M.A., and Snelling, A.M.

3911   (eds.) A stratigraphical basis for the Anthropocene. Geological Society, London, Special

3912   Publication, v. 395, 39–54.

3913 Zalasiewicz, J., Waters, C.N., Barnosky, A.D., Cearreta, A., Edgeworth, M., Ellis, E.C., Gałuszka, A.,

3914   Gibbard, P.L., Grinevald, J., Hajdas, I., Ivar do Sul, J.A., Jeandel, C., Leinfelder, R., McNeill, J.R.,

3915   Poirier, C., Revkin, A., Richter, D. deB., Steffen, W., Summerhayes, C., Syvitski, J.P.M., Vidas,

3916   D., Wagreich, M., Williams, M., Wolfe, A.P., 2015. Colonization of the Americas, 'Little Ice

3917   Age' climate, and bomb-produced carbon: Their role in defining the Anthropocene. The

3918   Anthropocene Review, v. 2, 117–127.

3919 Zalasiewicz, J. Waters, C.N., Ivar do Sul, J., Corcoran, P.L., Barnosky, A.D., Cearreta, A., Edgeworth, M.,

3920   Galuszka, A., Jeandel, C., Leinfelder, R., McNeill, J.R., Steffen, W., Summerhayes, C., Wagreich,

3921   M., Williams, M., Wolfe, A.P., Yonan, Y., 2016a. The geological cycle of plastics and their use as

3922   a stratigraphic indicator of the Anthropocene, Anthropocene, v. 13, 4–17.

3923 Zalasiewicz, J., Waters, C.N., Wolfe, A.P., Barnosky, A.D., Cearreta, A., Edgeworth, M., Ellis, E.C.,

3924   Fairchild, I.J., Gradstein, F.M., Grinevald, J., Haff, P., Head, M.J., Ivar do Sul, J.A., Jeandel, C.,

3925   Leinfelder, R., McNeill, J.R., Oreskes, N., Poirier, C., Revkin, A., Richter, D. deB., Steffen, W.,

3926   Summerhayes, C., Syvitski, J.P.M., Vidas, D., Wagreich, M., Wing, S., Williams, M., 2017a.

3927   Making the case for a formal Anthropocene Epoch: an analysis of ongoing critiques.

3928   Newsletters on Stratigraphy, v. 50, 205–226.

3929 Zalasiewicz, J., Williams, M., Waters, C., Barnosky, T., Palmesino, J., Rönnskog, A.-S., Edgeworth, M.,

3930   Neal, C., Cearreta, A., Ellis, E.C., Grinevald, J., Haff, P., Ivar do Sul, J., Jeandel, C., Leinfelder,

3931   R., McNeill, J.R., Odada, E., Oreskes, N., Price, S.J., Revkin, A., Steffen, W., Summerhayes, C.,

3932   Vidas, D., Wing, S., Wolfe, A.P., 2017b. Scale and diversity of the physical technosphere: a

3933   geological perspective, The Anthropocene Review, v. 4, 9–22.

3934 Zalasiewicz, J., Waters, C.N., Summerhayes, C., Wolfe, A.P., Barnosky, A.D., Cearreta, A., Crutzen, P.,

3935   Ellis, E.C., Fairchild, I.J., Gałuszka, A., Haff, P., Hajdas, I., Head, M.J., Ivar do Sul, J., Jeandel, C.,

3936   Leinfelder, R., McNeill, J.R., Neal, C., Odada, E., Oreskes, N., Steffen, W., Syvitski, J.P.M.,

3937   Wagreich, M., Williams, M., 2017c. The Working Group on the 'Anthropocene': Summary of

3938   evidence and recommendations 2016. Anthropocene, v.19, 55–60.

3939   Zhang, Y., Shotyk, W., Zaccone, C., Noernberg, T., Pelletier, R., Bicalho, B., Froese, D.G., Davies, L.,

3940   Martin, J.W., 2016. Airborne petcoke dust is amajor source of polycyclic aromatic

3941   hydrocarbons in the Athabasca oil sands region. Environmental Science & Technology, v. 50,

3942   1711–1720.

3943   Zhao, H, Xu, B, Yao, T, Tian, L, Li, Z., 2011. Records of sulfate and nitrate in an ice core from Mount

3944   Muztagata, central Asia. Journal of Geophysical Research, v. 116, D13304.

3945   doi:10.1029/2011jd015735

3946   Zinke, J., Reuning, L., Pfeiffer, M., Wassenburg. J.A., Hardman, E., Jhangeer-Khan, R., Davies, G.R., Ng,

3947   C.K.G., Kroon, D., 2016. A sea surface temperature reconstruction for the southern Indian

3948   Ocean trade wind belt from corals in Rodrigues Island (19◦ S, 63◦ E), Biogeosciences, v. 13,

3949   5827–5847.

3950   Zolitschka, B., Francus, P., Ojala, A.E.K., Schimmelmann, A., 2015. Varves in lake sediments – a

3951   review. Quat. Sci. Rev., v. 117, 1–41.

3952   Zoltai, S.C., 1989. Late Quarternary volcanic ash in the peatlands of central Alberta. Canadian Journal

3953   of Earth Sciences, v.26, 207–214.